BOND BEHAVIOUR BETWEEN RECYCLED AGGREGATE CONCRETE AND DEFORMED STEEL BARS

Ph.D. THESIS

by

JOHN ROBERT PRINCE M

DEPARTMENT OF CIVIL ENGINEERING
INDIAN INSTITUTE OF TECHNOLOGY ROORKEE
ROORKEE - 247 667 (INDIA)
SEPTEMBER, 2015

BOND BEHAVIOUR BETWEEN RECYCLED AGGREGATE CONCRETE AND DEFORMED STEEL BARS

A THESIS

Submitted in partial fulfilment of the requirements for the award of the degree of

DOCTOR OF PHILOSOPHY

in

CIVIL ENGINEERING

by

JOHN ROBERT PRINCE M

DEPARTMENT OF CIVIL ENGINEERING
INDIAN INSTITUTE OF TECHNOLOGY ROORKEE
ROORKEE - 247 667 (INDIA)
SEPTEMBER, 2015

INDIAN INSTITUTE OF TECHNOLOGY ROORKEE
ROORKEE

CANDIDATE'S DECLARATION

I hereby certify that the work which is being presented in this thesis entitled **"BOND BEHAVIOUR BETWEEN RECYCLED AGGREGATE CONCRETE AND DEFORMED STEEL BARS"** in partial fulfilment of the requirements for the award of the Degree of Doctor of Philosophy and submitted in the Department of Civil Engineering of the Indian Institute of Technology Roorkee is an authentic record of my own work carried out during a period from December, 2010 to September, 2015 under the supervision of Dr. Bhupinder Singh, Associate Professor, Department of Civil Engineering, Indian Institute of Technology Roorkee.

The matter presented in this thesis has not been submitted by me for the award of any other degree of this or any other Institute.

(**JOHN ROBERT PRINCE M**)

This is to certify that the above statement made by the candidate is correct to the best of my knowledge.

Date: (BHUPINDER SINGH)

Supervisor

ABSTRACT

Bond of deformed steel bars, having diameters in the range of 8 mm – 25 mm, embedded in recycled aggregate concrete made with coarse recycled concrete aggregate has been investigated with the help of pullout and a selected number of splice beam tests. Three grades of recycled aggregate concrete corresponding to normal-strength, medium-strength and high-strength were studied in the pullout tests whereas in the splice beam tests only the behaviour of normal- and the high-strength concrete has been compared. Natural coarse aggregates in the control concrete mixtures were substituted with an equal weight of the coarse recycled concrete aggregates (in the saturated-surface-dry moisture condition) at replacement levels of 25 %, 50 %, 75 % and 100 % and the effect on the mechanical properties and bond behaviour was monitored. The 56-day compressive strength of the three concrete grades decreased by approximately 33 %, 30 % and 27 % respectively upon 100 % substitution of the natural coarse aggregates (NCA) with the recycled concrete aggregates (RCA). For the aforementioned condition, the 56-day splitting tensile strength however increased by about 18 %,13 % and 19 % for the normal-, the medium- and the high-strength concrete respectively. A bond strength predictive model for short rebar embedded lengths and which is valid for both NCA as well as RCA concretes (with cylinder crushing strengths of up to 70 MPa) has been proposed and validated. The predictive efficacy of the proposed model was better compared to that of the model in the *fib* Model Code 2010, which is widely referred to for short embedded lengths. In the proposed model, the effect of concrete properties on bond strength has been represented using the square root of the compressive strength. Across all the three concrete grades, the pullout specimens embedded with the 8 mm, the 10 mm and in some cases with the 12 mm bars, showed pullout failure and the normalised bond strengths in the case of these specimens increased with an increase in the amount of RCA in concrete. This trend in the normalised bond strength has been explained in terms of fracture toughness of concrete estimated using brittleness index, an analogous parameter from rock mechanics. The trend of increasing normalised bond strength with increasing RCA replacement levels was not clearly evident in the case of the pullout specimens embedded with the 16 mm, the 20 mm, the 25 mm and to some extent with the 12 mm bars, the observed failure mode in all these cases being pullout failure induced by through splitting. In all the three concrete grades, the measured bond stress-slip relationships for all the bar sizes under investigation were similar in the NCA and the RCA concretes and no significant difference was noted in the interfaces of the two concrete types. For the specimens failing in pullout, five distinct stages of bond behaviour could be identified whereas for the specimens failing in pullout induced by through splitting four stages of

bond behaviour were noted. The predictions of the proposed empirical model for the bond stress-slip relationship associated with two failure modes noted in this investigation were in good agreement with the measured data. Failure modes of the NCA and the RCA concrete specimens in the splice beam tests were similar and a bond strength predictive model for long embedded lengths typical in splice beam testing (and in actual construction) has been proposed for both NCA and RCA concrete in terms of parameters which are widely accepted to influence bond behaviour. This model, which is valid for cylindrical compressive strengths of up to 70 MPa, accounts for the effect of $\left(f_c^{'}\right)^{1/4}$. It was noted that the bond strength model in the ACI 408R-03, originally developed for NCA concrete, gave reasonably accurate predictions for the bond strengths measured in the splice beam tests.

ACKNOWLEDGEMENT

First and foremost, the author prays the Almighty God for his blessings and records his profound and sincere gratitude towards his worthy supervisor, Dr. Bhupinder Singh, Associate Professor, Department of Civil Engineering, Indian Institute of Technology Roorkee for his inspiring guidance, constant encouragement throughout the course of this research work and painstaking correction of the draft manuscript. It was an opportunity of a life time to be associated with him. Words would fail to record the invaluable moral and material support which the author was privileged to receive from him on numerous occasions.

The author owes his sincere gratitude to the Head, Department of Civil Engineering, the staff members of his office and the faculty members of the Department of Civil Engineering for the facilities and the cooperation received whenever needed.

The author expresses his special thanks to Student Research Committee (SRC) members Prof. Vipul Prakash, Prof. Akhil Upadhyay, Department of Civil Engineering and Prof. Pankaj Agarwal, Department of Earthquake Engineering, Indian Institute of Technology Roorkee for giving valuable suggestions and guidance for the right approach of the research problem.

The author expresses his gratefulness to Prof. Pradeep Bhargava, Department of Civil Engineering and Prof. V. Devadas, Department of Architecture and Planning, for their parental care, encouragement and support throughout the course of his study.

The financial support from Ministry of Human Resource Development (MHRD), Government of India is gratefully acknowledged.

Thanks are due to Mr. Surendra Sharma, Mr. Anil Kumar Sharma, Mr. Siddiqui, Mr. Chetan Chand and Mr. Pritam Singh of Civil Engineering Laboratory and all the casual workers including Mr. Dilshad Khan for their generous help in carrying out the experimental investigations.

The author wishes to record his sincere thanks and indebtedness to his colleagues and friends, Mr. A.B. Danie Roy, Mr. Franklin F.R. Frederick, Mr. K. Senthil, Mr. R. Siva Chidambaram, Mr. N. Prabhu,, Mr. G.B. Ramesh Kumar, Mr. C. Naveen Kumar, Mr. Shakeel, Mr. J. Venkatesan, Dr. Rajesh Kumar, Dr. Dipak Kumar Sahoo, Dr. Kranti Jain, Dr. Srinivasan Alavandar, Dr. Manju, Dr. Purushothaman, Dr. Thangaraj, Dr. Radha, Mrs. C. Shermi, Miss. Padma Priya, Miss. Malarkodi for their helping hands in needs.

The author expresses his thanks to his dear loving wife Dr. M. Germin Nisha, who stood behind him at every moment with care and affection. The author feels proud of his daughter J. Prisha and his son J. Jeffrey whose funny fights and laughter's provided him pleasant moments during the course of this work.

The author gratefully acknowledges the moral support of his father Mr. M. Maria Innasi, mother Mrs. M. Gnana Selvam, father-in-law Mr. V. Maria Francis, mother-in-law Mrs. I. Mary Retnam, brothers and sister-in-laws, whose prayers and blessings led a smooth path throughout this research work.

Finally, last but not the least, the author is grateful to God for bringing this day in his life.

(JOHN ROBERT PRINCE M)

CONTENTS

LIST OF FIGURES

LIST OF TABLES

NOTATION AND ABBREVIATIONS

Symbol	Description
A_b	Area of the reinforcing bar
A_b	Area of developed or spliced bar
A_s	Area of a single anchored bar with maximum bar diameter
A_{tr}	Area of transverse reinforcement normal to the plane of splitting through the anchored bars
b	Breadth of the beam
c	Minimum concrete cover (c_{so}, c_b)
C	Concrete grade
c_{min}	Smaller of minimum concrete cover or ½ of the clear spacing between bars
c_{min}	Minimum (c_{so}, c_b, $c_{si} + d_b/2$)
c_{med}	Median (c_{so}, c_b, $c_{si} + d_b/2$) [that is, middle value]
c_b	Bottom concrete cover for reinforcing bar being developed or spliced
c_c	Concrete cover measured to the centre of the bar
c_d	Minimum of clear spacing between spliced bars, side cover and, bottom cover
c_s	Minimum [c_{so}, c_{si} + 6.35 mm]
c_{si}	½ of the bar clear spacing
c_{so}	Side cover for reinforcing bar
d_{cs}	The smaller of (i) the distance from the closest concrete surface to the centre of the bar being developed, or (ii) two-thirds of the centre-to-centre spacing of the bars being developed
d_b	Nominal rebar diameter

dM	Differential moment
dT	Differential tension
f_{bd}	Design value of ultimate bond stress
f'_c	Cylinder compressive strength of concrete
f_{ck}	Characteristic compressive cylinder strength of concrete
f_{cm}	Mean value of concrete cylinder compressive strength
f_{ct}	Splitting tensile strength of concrete
f_{ctd}	Design value of concrete tensile strength
$f_{ctk,0.05}$	Concrete tensile strength with 5% fracture
f_{ctm}	Mean value of the axial tensile strength of concrete
f_s	Stress in reinforcing bar
f_{sy}	Yield strength of reinforcing steel
f_y	Yield strength of the longitudinal reinforcement
f_{yt}	Yield strength of transverse reinforcement
G	Replacement level of coarse RCA
h	Height of the beam
h_r	Rib height
jd	Lever arm
k_1	Bar location factor
k_2	Coating factor
k_3	Concrete density factor
k_4	Bar size factor

L_b	Design anchorage length
L_{bd}	Design anchorage length
$L_{b,min}$	Minimum anchorage length if no other limitation is applied
$L_{b,rqd}$	Basic required anchorage length
L_d	Bonded length
L_d	Development or spliced length
L_s	Splice length
$L_{sy.tb}$	Development length
M	Constant for the bond strength of bars
n	Number of bars developed or spliced at the same location
N	Number of transverse bars in the development or splice length
P_{max}	Peak load
P_{tr}	Mean compression stress perpendicular to the potential splitting failure surface at the ultimate limit state
R_r	Relative rib area
s	Slip at unloaded end
s	Spacing of transverse reinforcement
S	Replacement level of fine RCA
s_r	Rib spacing
T_b	Total bond force of a developed or spliced bar = $T_c + T_s$
T_c	Concrete contribution to total bond force
t_d	Term representing the effect of bar size on T_s
t_r	Term representing the effect of relative rib area on T_s

T_s	Steel contribution to total bond force
V	Shear force
$\sum o$	Total perimeter of the bars
α_1	Effect of form of the bars assuming adequate cover
α_2	Effect of concrete minimum cover
α_3	Effect of confinement by transverse reinforcement
α_4	Influence of one or more welded transverse bars
α_5	Effect of the pressure transverse to the plane of splitting along the design anchorage length
α_{ct}	Coefficient for taking into account long term effects on the tensile strength and of unfavourable effects resulting from the way the load is applied
γ_c	Partial safety factor for concrete
η_1	Coefficient related to the quality of the bond and the position of the bar during concreting
η_1	Bar surface factor
η_2	Term related to the bar diameter
η_2	Bar location factor
η_3	Bar size factor
η_4	Factor representing the characteristic strength of steel reinforcement being anchored or lapped
ϕ	Longitudinal bar diameter
τ_a	Anchorage bond stress
τ_{bd}	Design bond stress
τ_c	Average bond stress
$\tau_{\max}$	Peak bond strength

$\tau_{r,\max}$	Normalised bond strength
τ_f	Local bond stress
σ_{sd}	Design stress of the bar at the position starting where the anchorage is measured
λ	Modification factor reflecting the reduced mechanical properties of lightweight concrete
ψ_e	Coating factor
ψ_s	Bar size factor
ψ_t	Reinforcement location factor
ε_s	Strain in steel bar
ACV	Aggregate crushing value
BI	Brittleness index
COV	Coefficient of variation
DVR	Direct volume replacement
DWR	Direct weight replacement
EDG	Electric dial gauge
EMR	Equivalent mortar replacement
FA	Fine aggregate
HRWRA	High range water reducing admixture
LVDT	Linear variable differential transducer
OPC	Ordinary Portland cement
NAC	Natural aggregate concrete
NCA	Natural coarse aggregate
PO	Pullout

PS	Pullout-induced by through splitting
RA	Recycled aggregate
RAC	Recycled aggregate concrete
RCA	Recycled concrete aggregate
RM	Residual mortar
RNA	Recycled natural aggregate
SD	Standard deviation
SSD	Saturated surface-dry
TMT bars	Thermo-mechanically treated bars
UTM	Universal testing machine

Chapter 1

INTRODUCTION

1.1 INTRODUCTION

Bond in reinforced concrete refers to the adhesion between the reinforcing steel and the surrounding concrete which enables load to be transferred between the two materials. Bond therefore, provides strain compatibility and is responsible for 'composite action' of concrete and steel. It is only if the bond is effective that the plane-section assumption in flexure theory of reinforced concrete is valid. Therefore, bond is a fundamental characteristic of reinforced concrete and deserves attention. The following are the mechanisms of bond resistance in reinforced concrete:

(i) Chemical adhesion – This is due to adhesive action of hydration products.

(ii) Frictional resistance – This is due to surface roughness of the steel reinforcement bars and the grip exerted by shrinking concrete on the steel bars.

(iii) Mechanical interlock – This is the most significant mechanism in deformed steel bars and occurs due to interlock of their surface protrusions or 'ribs' with surrounding concrete.

In reinforced concrete, bond is characterised as:

(i) Flexural bond – This bond is developed in flexural members on account of variation of bending moment in the member which in turn causes a variation of axial tension along the length of the reinforcing bar.

(ii) Anchorage bond – This is also called as development bond and essentially it resists 'pulling out' if the bar is in tension and 'pushing in' if the bar is in compression. Anchorage bond is the bond developed over the length of anchorage provided in a bar or near the end or cut-off point of a reinforcing bar.

Since bond behaviour of plain and of deformed bars embedded in concrete made with natural aggregates has been extensively investigated and is well understood, design recommendations for bond in natural aggregate concrete are fairly well established in current design codes.

For the past several years, production of concrete using recycled materials is being increasingly encouraged so as to reduce the environmental impact of concrete construction (Dosho, 2007; Li, 2008; Nielsen and Glavind, 2007). Because of the dwindling supplies of natural aggregates in particular there is growing emphasis on identification of alternate and sustainable sources of this material. One of the alternate options which has been extensively explored as potential a source of aggregates is the

concrete in Construction and Demolishing Wastes (CDWs). According to the Environmental Protection Agency (EPA, 1998) CDW is waste material that is produced in the process of construction, renovation or demolition of structures which may be buildings of all types as well as roads and bridges. Typical components of CDW include concrete, asphalt, wood, metals, gypsum wall board, floor tile and roofing. This concrete in CDW can be recycled to obtain either fine or coarse recycled concrete aggregates. However, because of various reasons the use of Coarse Recycled Concrete Aggregates (RCA) rather than fine recycled concrete aggregates a substitute for natural coarse aggregates (NCA) in concrete has found greater acceptability with concrete technologists. The mechanical properties and structural behaviour of RCA concrete (concrete made with RCA as part or full replacement of NCA) in flexure, shear and to a limited extent in bond, has been extensively investigated though widely accepted code-based design recommendations for this concrete are yet to evolve. As a result, due to the gaps in knowledge about its properties and behaviour and the absence of support from current design codes, RCA concrete has been mostly used in non-structural applications. The lack of sufficient knowledge about structural behaviour, particularly in bond, is significant since only limited studies of bond behaviour of RCA concrete are available in the literature.

The investigation reported in this thesis has been planned and executed to contribute to the current knowledge base on bond behaviour of RCA concrete. Bond studies on deformed steel bars embedded in selected grades of concrete containing various levels of replacement of natural coarse aggregates with coarse recycled concrete aggregates have been carried out. It is the fond hope of the author that the results reported in this thesis will enable structural engineers to make more informed choices about RCA concrete. The use of RCA concrete for structural applications will contribute to the sustainability agenda by reducing the environmental impact of concrete construction.

1.2 CONSTRUCTION AGGREGATES SCENARIO IN INDIA

According to the Freedonia Group (2015), global demand for construction aggregates is expected to be 48.3 billion metric tons in the year 2015. It is estimated that aggregates for use in concrete construction typically constitute about 40% of the total product demand. Dhir and Paine (2010) has reported that India's share in the global aggregate demand is about 3 % which translates into an annual requirement of about 1.5 billion metric tons. This makes India the third biggest aggregate market in the Asia-Pacific region and the fourth largest market in the world after China, U.S.A and Japan. It is estimated that aggregate sales in India have risen an average 7.7 % annually over more than a decade, a figure which exceeds both regional and global averages. Most of the

aggregate supply in India is provided by small local quarry and pit operators and this supply is increasingly constrained due to environmental concerns about river-bed quarrying. It is not unusual to note that in some parts of the country good quality aggregates for use in concrete construction cost as much as, if not more, than cement. To address shortages in supply, efforts have been directed at identifying and tapping alternative sources of construction aggregates, with particular attention being paid to construction and demolition waste. There are no reliable figures for the amount of construction and demolition waste generated every year in India, though some estimates suggest that the total amount may be in the range of 12 to 15 million metric tons of which 7 – 8 million metric tons consist of waste concrete and brick. According to the Centre for Science and Environment (CSE, 2014), if on an average 50 kg of construction and demolition waste is generated every square metre of a newly constructed building then about 50 million tons of construction wastes would have been generated in the year 2013 from the 1 billion square metre of floor space added in that year. As per TIFAC (TIFAC, 2001), demolition and renovation/repair of the older building stock generates about 300 – 500 kg of waste per square metre of floor area. The Centre for Science and Environment Environment (CSE, 2014) estimates that even if only five percent of the existing building stock in India gets annually demolished and rebuilt completely, approximately 288 million tons of demolition waste mould have been produced in the country in the year 2013 above. Though it is difficult to verify the accuracy of the above quoted figures due to absence of any systematic survey, even causal observations indicate that a significant volume of CDW is generated in the country and this can be tapped as a potential source of aggregates for concrete. The key barriers to recycling of CDW, and in particular concrete, in India are lack of awareness, absence of standardization, inadequate policy push and uncertainty about availability and regular supply of aggregates sourced from CDW.

1.3 RESEARCH SIGNIFICANCE

With growing emphasis on sustainability, there is clearly a need to fill gaps in our understanding of the properties and behaviour of recycled aggregate concrete which will facilitate under structural application of this material. This investigation has been addressed towards increasing understanding of bond behaviour of recycled aggregate concrete towards a more rational design of structural elements made with this concrete. Bond characteristics of different sizes of high yield strength deformed steel bars embedded in different grades of RAC have been experimentally investigated and modelled numerically. Besides rebar diameter and concrete grade, the other parameter for investigation has been the amount of coarse recycled concrete aggregates in the total

aggregate content of concrete. The effect of the variables on average pullout bond strength, bond-slip relationship, toughness in bond and failure mode of the pullout specimens used in the majority of the experimental investigations and in the limited number of splice beam tests has been studied and the bond-slip relationship has been numerically modelled. Two bond strength predictive models for RCA concrete, one for short embedded lengths and the other for long embedded lengths have been proposed. In these models, the effect of concrete properties on bond strengths has been represented using $\left(f_c^{'}\right)^{1/2}$ and $\left(f_c^{'}\right)^{1/4}$ respectively. The results of this investigation show that bond behaviour of recycled aggregate concrete made with coarse recycled concrete aggregates in the saturated surface dry moisture condition are comparable or in many respects superior to that of concrete made with natural coarse aggregates. It is recommended that like concrete made with natural coarse aggregates, normalisation of the measured peak bond strengths with $\left(f_c^{'}\right)^{1/2}$ gives a better match with experimental data.

1.4 OBJECTIVES

The following are the objectives of this thesis:

(1) To investigate the effect of using coarse recycled concrete aggregates on the mechanical properties of concrete.

(2) To experimentally and numerically investigate bond behaviour of concrete made with coarse recycled aggregate concrete (For convenience, this concrete has been designated as RCA concrete in this thesis).

(3) Based on the investigations, recommend a broader scope for application of coarse recycled aggregate in structural concrete in the context of bond behaviour.

1.5 SCOPE

The following is the scope of this investigation:

(1) The coarse recycled concrete aggregate (RCA) was sourced from the waste concrete specimens (tested cubes, cylinders, beams, slab panels etc) obtained from the concrete laboratory of the author's host institute.

(2) In all the experimental investigations involving recycled concrete aggregate, the RCA was used in the saturated surface dry (SSD) moisture condition.

(3) In the investigations of mechanical and bond behaviour, the following four weight replacement levels of the natural coarse aggregate with the RCA were considered: 25 %, 50 %, 75 % and 100 %.

(4) The experimental investigations of mechanical and bond behaviour were carried out for three concrete grades corresponding to normal-strength, medium-strength and high-strength concrete.

(5) Investigation of only one-grade of deformed steel bars (having a nominal yield strength of 500 MPa) with diameters of 8 mm, 10 mm, 12 mm, 16 mm, 20 mm and 25 mm was investigated.

(6) In the splice beam tests, the c/d_b (c is the clear cover and d_b is the rebar diameter) was kept constant at 1.25 for both the 12 mm as well as 20 mm bars under investigation. One splice length was tested for each rebar diameter.

(7) In the numerical part of the investigations, empirical bond-slip relationships have been proposed and a bond strength predictive equation for RCA concrete has been suggested which takes into account the effect of concrete grade, clear cover, rebar diameter, bonded/splice length, rib height, rib spacing and replacement level of RCA in concrete. Predictions from the numerical models have been compared with results available in the literature.

1.6 METHODOLOGY

The following methodology was adopted in the experimental investigations:

(1) The RCA was obtained by crushing waste concrete specimens obtained from the Concrete Laboratory of the author's host institute in a jaw crusher.

(2) Saturated-surface-dry (SSD) moisture condition in the RCA in water for a period of 24 h before batching.

(3) A major part of the investigations focused on local bond behaviour which was studied with the help of cylindrical pullout specimens (100 mm diameter and 200 mm height) having short rebar embedded lengths (in order to pre-empt yielding of the embedded rebars during pullout). Towards ensuring repeatability of results, three nominally identical companion pullout specimens were tested for each parameter under investigation.

(4) Local bond stresses were investigated with selected number of splice beam tests carried out in singly reinforced simply supported beam specimens detailed with either 12 mm or 20 mm diameter longitudinally loaded to failure and local bond stresses were calculated on the basis of the tensile force in the spliced bars. The splices were so configured in the beam that bond failure would invariably pre-empt flexural failure.

1.7 ORGANISATION OF THE THESIS

This thesis has five chapters and one appendix. Introduction of the thesis is presented in Chapter 1. A review of the relevant literature has been carried out in Chapter 2 which starts with a discussion of bond of steel reinforcement in concrete. The literature on predictive models for bond strength and recommendations of design codes is briefly discussed. In the next part of Chapter 2, the bond of steel reinforcement in recycled aggregate concrete has been reviewed. The sources, classification and the properties like grading, water absorption, bulk density, specific gravity, abrasion resistance, aggregate crushing value, residual mortar content of recycled concrete aggregates is also discussed. A summary of the design code recommendations related to recycled concrete aggregates is presented along with the properties of concrete made with recycled concretes and this chapter concluded with an explanation of the need for this investigation.

The experimental programme is presented in Chapter 3 which starts with a compilation of the measured physical and mechanical properties of the materials used in this investigation. Mixture design of the normal-strength, medium-strength and high-strength concrete is briefly discussed next. The protocols for bond testing has been explained followed by a detailed discussion of the experimental programme including parameters, test setup and the variables used in this investigation.

The measured results have been presented, analysed and discussed in Chapter 4. Measured bond strengths have been compared with predictions of selected bond models available in the literature as well as the predictions of bond strength models which has been proposed from numerical analysis as a part of this investigation. Calibration of the proposed model has also been carried out with the help of selected experimental data from the literature.

Finally, Chapter 5 presents the conclusions drawn from this investigation.

1.8 CONCLUSION

The thesis has been introduced in this chapter which begins with a background of the proposed work. The research significance, objectives, scope and the methodology adopted in this investigation follows next and the chapter concludes with a brief discussion of the thesis layout. A review of the literature is presented in the next chapter.

Chapter 2

LITERATURE REVIEW

2.1 INTRODUCTION

This chapter presents a review of the literature on bond behaviour of reinforced concrete. Salient developments in understanding of bond in reinforced concrete have been discussed. Attention has been paid to state-of-the-art in bond behaviour of RCA concrete towards identification of knowledge gaps. Finally, Justification for the investigation reported in the thesis is presented.

2.2 BOND OF STEEL REINFORCEMENT IN CONCRETE

Traditionally, bond strength has been represented in terms of shear stress at the interface between a reinforcing bar and surrounding concrete. This approach effectively treats bond as a material property. Developments in our understanding of bond have shown that bond, anchorage, development, and splice strength are structural properties, dependent not only on the materials but also on the geometry of the reinforcing bar and the structural member itself (ACI, 2003). It is now accepted that besides serving to transfer axial force from a reinforcing bar to surrounding concrete, bond also serves a range of structural functions in reinforced concrete. At the serviceability limit state, bond serves to control crack widths and deflection. At the ultimate limit state, strength of laps and anchorages depend on bond. In addition, bond characteristics of flexural reinforcement will influence rotation capacity of plastic hinges. Extreme reductions in bond stiffness would affect the composite interaction between reinforcement and concrete and negate the usual assumptions of plane section behaviour (i.e., plane sections remain plane before and after bending). Bond of steel reinforcement in concrete is important to three aspect of structural performance namely (1) bond is used to anchor rebar ends, (2) bond transfers force into concrete under tension, reducing the average strain in flexural reinforcement and enhancing member stiffness, (3) bond is used to maintain composite interaction between rebar and concrete (*fib*, 2000).

2.2.1 Mechanisms of bond resistance

In reinforced concrete construction, efficient and reliable force transfer between reinforcement and concrete is required for optimal design. The transfer of forces from the reinforcement to the surrounding concrete occurs for a deformed bar (Figure 2.1) by:

- Chemical adhesion between the reinforcing bar and the surrounding concrete;
- Frictional forces arising from the roughness of the interface, forces transverse to the bar surface, and the relative slip between the bar and the surrounding concrete; and
- Mechanical anchorage or bearing of the ribs against the concrete surface (ACI, 2003).

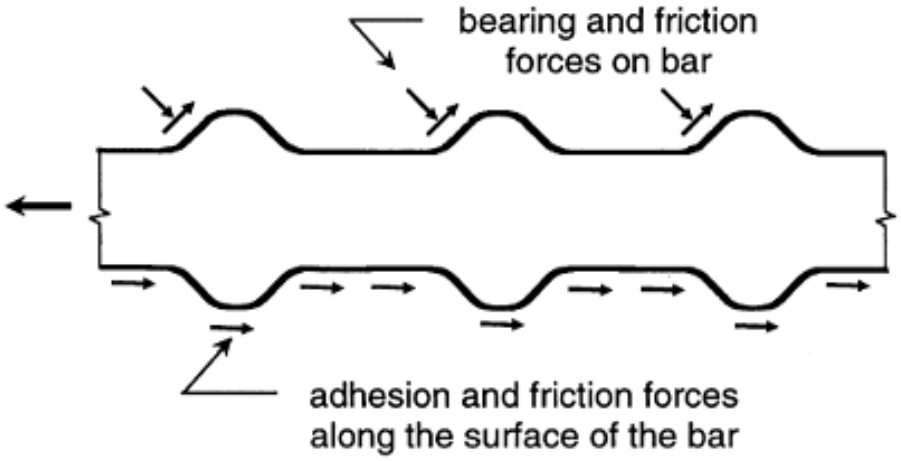

Figure 2.1 Bond force transfer mechanisms (ACI, 2003)

Bond resistance occurs due to development of tangential (shear) stresses components along the interface (contact surface) between the reinforcing bar and surrounding concrete. This stress is called as the bond stress and is expressed as the tangential force per unit surface area of the rebar.

According to the ACI Committee 408 (ACI, 2003), friction plays a major role in the bond resistance of plain bars. These slip-induced frictional forces come into play due to transverse stresses at the bar surface caused by small variations in bar shape and surface roughness of the bars. However, when a deformed bar moves with respect to the surrounding concrete chemical adhesion gets quickly lost and bearing forces on the ribs and friction forces on the ribs and barrel of the rebar are mobilised. With increase in slip, friction on the barrel of the reinforcing bar is reduced and the bearing forces remain the principal mechanism of bond resistance. The bearing forces can be resolved into tensile stresses acting in concrete which can result in cracking in planes that are both perpendicular and parallel to the reinforcement. The ACI Committee 408 (ACI, 2003) states that splitting cracks form if concrete cover or spacing between the bars is small whereas if the concrete cover, bar spacing or transverse reinforcement is sufficient to prevent or delay a splitting failure, then bond resistance will be lost by shearing of concrete along a surface at the top of the ribs around the bars resulting in what is called as a “pullout” failure.

The ACI Committee 408 (ACI, 2003) states that bond resistance is governed by the following factors:

(i) The mechanical properties of concrete, in particular its tensile and its bearing strength

(ii) The concrete volume surrounding the bar

(iii) Presence of confinement which can delay and control crack propagation

(iv) Surface condition of the bar

(v) Bar geometry in terms of deformation height, rib spacing, width and face angle

2.2.2 Types of bond

Depending on the loading situation, bond is characterised as:

- Flexural bond
- Anchorage or development bond.

2.2.2.1 Flexural bond

Flexural bond arises in flexural members on account of shear or a variation in bending moment. It causes a variation in axial tension along the length of a reinforcing bar (Figure 2.2(d)). Flexural bond is critical at locations where shear ($V=dM/dx$) is significant. The flexural stresses at two adjacent sections of a beam, dx apart, subjected to a differential moment dM, are depicted in Figure 2.2(b). The differential tension dT in the tension steel over the length dx is given by

$$dT = \frac{dM}{jd} \qquad (2.1)$$

where jd is the internal lever arm.

This unbalanced bar force is transferred to the surrounding concrete by means of 'flexural bond' developed along the interface. Assuming the flexural (local) bond stress τ_f to be uniformly distributed over the interface in the elemental length dx, equilibrium of forces gives:

$$\tau_f \left(\sum o\right) dx = dT \qquad (2.2)$$

Where $\sum o$ is the total perimeter of the bars at the beam section under consideration (Figure 2.2(c)).

From Equation 2.2, it is evident that the bond stress is directly proportional to the change in the bar force. Combining Equation 2.2 with Equation 2.1, the following expression for the local bond stress τ_f is obtained.

$$\tau_f = \frac{dM/dx}{(\sum o)jd} \qquad (2.3a)$$

Alternatively, in terms of the transverse shear force at the section $V = dM/dx$,

$$\tau_f = \frac{V}{(\sum o)jd} \qquad (2.3b)$$

The above discussion shows that flexural bond stress is high at locations of high shear, and that this bond stress can be effectively reduced by providing an increased number of bars of smaller diameter bars (to give the same required A_b). According to Pillai and Menon (2010) the actual bond stress will be influenced by flexural cracking, local slip, splitting and other secondary effects which are not accounted for in Equations 2.3a and 2.3b. In particular, flexural cracking significantly affects the magnitude and distribution of local bond stresses.

2.2.2.2 Anchorage bond

Anchorage bond (or development bond) arises over the length of anchorage provided for a bar or near the end (or cut-off point) of a reinforcing bar. At a conceptual level, this bond resists the 'pulling out' of the bar if it is in tension (Figure 2.2(e)), or conversely, the 'pushing in' of the bar if it is in compression. An example of anchorage bond is depicted in the cantilever beam of Figure 2.3, where it may be seen that the tensile stress in the bar segment varies from a maximum (f_s) at the continuous end D to practically zero at the discontinuous end C.

The bending moment, and the tensile stress f_s, are maximum at the section at D. Evidently, if a stress f_s is to be developed in the bar at D, the bar should not be terminated at D, but has to be extended ('anchored') into the column by a certain length CD. At the discontinuous end C of the bar, the stress is zero. The difference in force between C and D is transferred to the surrounding concrete through anchorage bond. According to Pillai and Menon (2010), the probable variation of the anchorage bond stress τ_a is as shown in Figure 2.3(b) with a maximum value at D and zero at C. It may be noted that a similar (but not identical) situation exists in the bar segment CD of the simply supported beam in Figure 2.2(e).

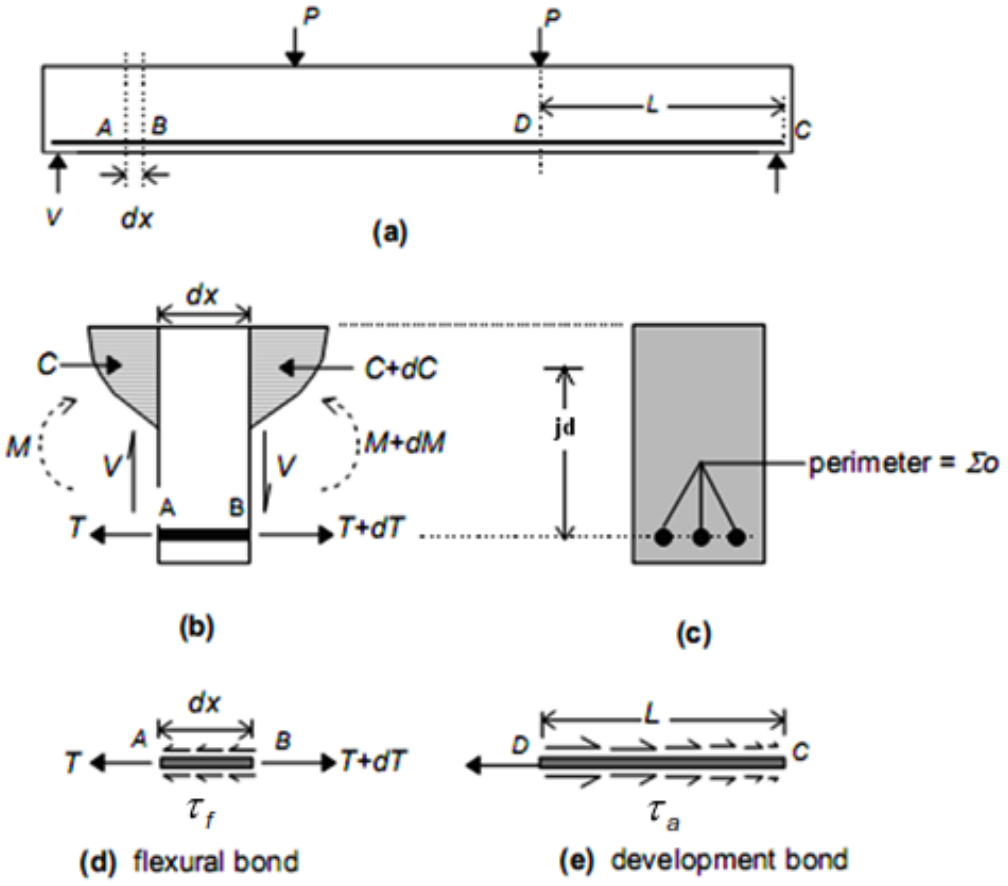

Figure 2.2 Bond stress in a beam (Pillai and Menon, 2010)

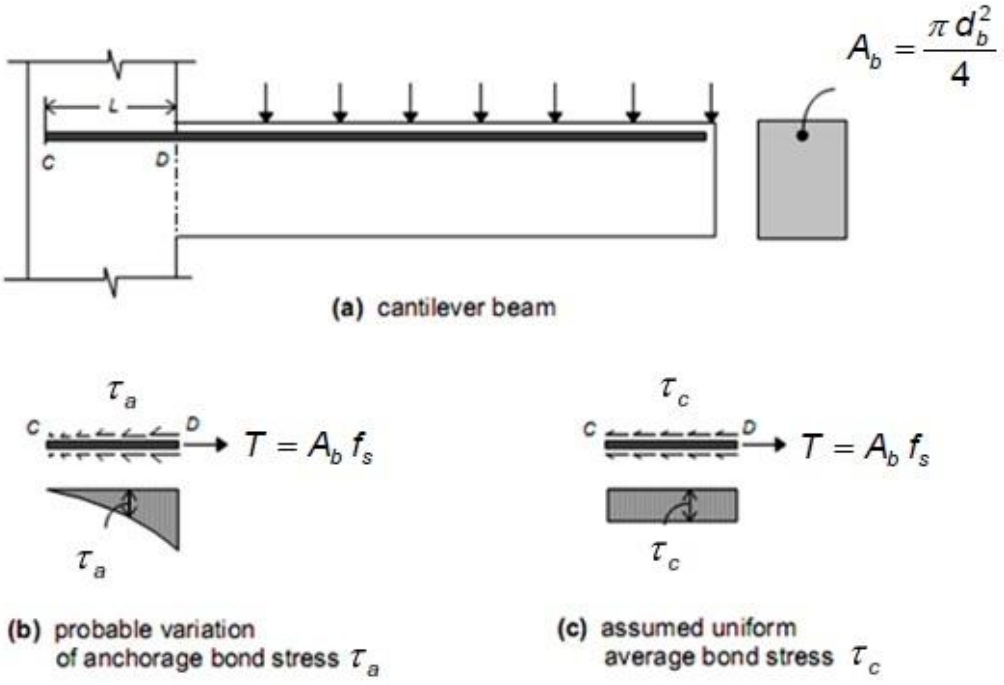

Figure 2.3 Anchorage bond stress (Pillai and Menon, 2010)

The average bond stress τ_c can be calculated by assuming a uniform bond stress distribution over the length L of the bar of diameter d_b (Figure 2.3(c)), and considering equilibrium of forces as given below:

$$(\pi d_b L)\tau_c = \left(\frac{\pi d_b^2}{4}\right) f_s \Rightarrow \tau_c = \frac{d_b f_s}{4L} \qquad (2.4)$$

The above bond stress may be viewed as the average bond stress generated over a length L in order to develop a maximum tensile (or compressive) stress f_s at a critical section. Therefore, this type of bond is referred to as 'development bond' or it may also be viewed as the bond required to provide anchorage for a critically stressed bar, hence the name anchorage bond.

2.2.3 Bond failure mechanisms

According to Pillai and Menon (2010), the mechanisms that initiate bond failure may be any one or a combination of the following:

- break-up of adhesion between the bar and the concrete;
- longitudinal splitting of the concrete around the bar;
- crushing of the concrete in front of the bar ribs (in deformed bars); and
- shearing of the concrete keyed between the ribs along a cylindrical surface surrounding the ribs (in deformed bars).

The most common type of bond failure is pulling loose of the reinforcement bar following the longitudinal splitting of the concrete along the bar embedment. In the case of plain bars placed with large cover, failure may occur due to the bar pulling out of concrete with little or no splitting of concrete. Such a failure may also occur with very small diameter deformed steel bars embedded in concrete with a large cover. However, for the usual sizes of deformed steel bars and concrete cover, longitudinal splitting of concrete is the most common bond failure mechanism.

2.3 FACTORS AFFECTING BOND

Although many factors are known to affect bond between reinforcing bars and concrete, only the major ones are reviewed here under three subject headings: structural characteristics, bar properties, and concrete properties.

2.3.1 Structural characteristics

2.3.1.1 Concrete cover and bar spacing

Bond failure mode depends on concrete cover and bar spacing (Untrauer, 1965; Tepfers, 1973; Orangun *et al*., 1977; Eligehausen, 1979; Darwin *et al*., 1996). Pullout failure occurs when the cover and bar spacing is large. This type of failure can occur with some splitting if the member has significant reinforcement to confine the anchored steel. If the cover and bar spacing is small, splitting failure will occur, resulting in lower bond strength. Splitting failures can occur between the bars, between the bars and the free surface, or both (ACI, 2003).

2.3.1.2 Bonded length

Although increase in the bonded length (development or splice length) of a reinforcing bar increases the bond strength, it is not proportional. As the bar moves (or slips) with respect to concrete, splitting may also be accompanied by crushing of the concrete in front of the ribs, especially in normal-strength concrete. Even at low embedded lengths, the bars will have measurable bond strength. This occurs because, in the tests, there is always at least one set of ribs that forces the concrete to split before failure. When failure occurs, a significant crack area is opened in the member due to splitting (Brown *et al*., 1993; Darwin *et al*., 1994; Tholen and Darwin, 1996). As the bonded length of the bar increases, crack surface at failure also increases in a linear but not proportional manner with respect to the bonded length. The total energy needed to form the crack and, in turn, the total bond force required to fail the member, increase at a rate that is less than the increase in bonded length. Therefore, the ACI Building Code (ACI, 2011) design practice of establishing a proportional relationship between bond force and development or splice length is conservative for short bonded lengths, but becomes progressively less conservative, and eventually unconservative, as the bonded length and stress in the developed or spliced bar increase (ACI, 2003). Bond-slip failure will occur due to inadequate bonded length of steel bars in concrete (Chugh and Menon, 2005; Girija and Menon, 2011).

2.3.1.3 Transverse reinforcement

The presence of transverse reinforcement confines the development and spliced bars by limiting the growth of splitting cracks, thus increasing the bond force required to cause failure (Tepfers, 1973; Orangun et al., 1977; Darwin and Graham 1993a, 1993b). By increasing the amount of transverse reinforcement, splitting failure mode may change to pullout failure due to increase in bond force. Orangun *et al*. (1977) concluded that there

no significant gain in bond strength is obtained if the amount of transverse reinforcement is more than that required.

2.3.1.4 Bar casting position

The bar casting position plays an important role in bond strength between concrete and reinforcing bar (Abrams, 1913). Bottom-cast bars develop higher bond strengths compared to top-cast bars (Clark, 1946, 1950; Collier, 1947; Larnach, 1952; Menzel, 1952; Menzel and Woods, 1952; Ferguson and Thompson, 1962, 1965; CUR, 1963; Untrauer, 1965; Welch and Patten, 1965; Untrauer and Warren, 1977; Thompson *et al*., 1975; Jirsa and Breen, 1981; Luke *et al*., 1981; Zekany *et al*., 1981; Donahey, 1984, 1985; Brettmann *et al*., 1984, 1986; Jeanty *et al*., 1988). As per ACI 318-11 (2011), a 30% increase in development length is required for top horizontal reinforcement when the fresh concrete depth exceeds 300mm. The reason for this recommendation is the settlement of fresh concrete and the accumulation of bleed water below the reinforcing steel. Ferguson and Thomson (1965) conducted beam tests to compare the ratio of top-cast to bottom-cast bar bond strength. These authors conclude that bond strength of top-cast bars decreased with slump and decreasing top cover (ACI, 2003).

2.3.2 Bar properties

2.3.2.1 Bar Size

Because of the following two reasons, there is no appreciable relationship between bar size and bond strength: (1) as the bar size increases, longer development or splice length is required, and (2) for a given development or splice length, larger bars achieve higher total bond forces than smaller bars for the same degree of confinement. The total force developed at bond failure is not only an increasing function of concrete cover, bar spacing, and bonded length, but also of bar area (Orangun *et al*., 1977; Darwin *et al*., 1992; 1966). The bond force at failure, however, increases more slowly than the bar area. If there are no space restrictions, it is advisable to use larger number of smaller bar diameters by replacing large bar diameters for the same area of reinforcement (ACI, 2003).

2.3.2.2 Bar geometry

Some studies indicate that bar geometry strongly influences bond strength, while other studies indicate that the influence is minor. Based on the bond studies of both plain and deformed bars, Abrams (1913) concluded that deformed bars produced higher bond strength than plain bars. Abrams (1913) observed that the ratio of the bearing area of the

projections (projected area measured perpendicular to the bar axis) to the entire surface area of the bar in the same length could be used as a criterion for evaluating bond resistance of deformed bars and suggested the ratio be not less than 0.2 (ACI, 2003). When the face angle is greater than 40º, slip occurs by crushing of concrete in front of the ribs, and for the face angle 30 to 40º, the crushed concrete acts as a wedge (Lutz et al., 1966; Lutz and Gergely, 1967).

To account for the effect of bar geometry on bond strength, ACI 408.3-01/408.3R-01 (2001a) recommends the use of the parameter called as the relative rib area, R_r, illustrated in Figure 2.4, which is the ratio of the bearing area of the bar deformation to the shearing area between the deformations. The definition of average rib width is illustrated in Figure 2.5, where h_r is the height of the rib and s_r is the spacing of the rib. For evaluating splice and development length of coated and uncoated reinforcing bars in tension having a high relative rib area ($R_r \geq 0.1$), ACI 408.3-01/408.3R-01 (2001a) provides the following restrictions:

(i) The relative rib area is at least 0.10, but no larger than 0.14

(ii) The ribs are at an angle of 45 to 65 degrees inclusive with respect to the axis of the bar

(iii) Ribs shall not cross. Use of X-patterns and diamond patterns for ribs is not permitted

(iv) The rib spacing is at least 0.44 of the nominal diameter d_b of the reinforcing bar

(v) The average rib width is less than or equal to one third of the average rib spacing

(vi) The diameter of the bar does not exceed 36 mm

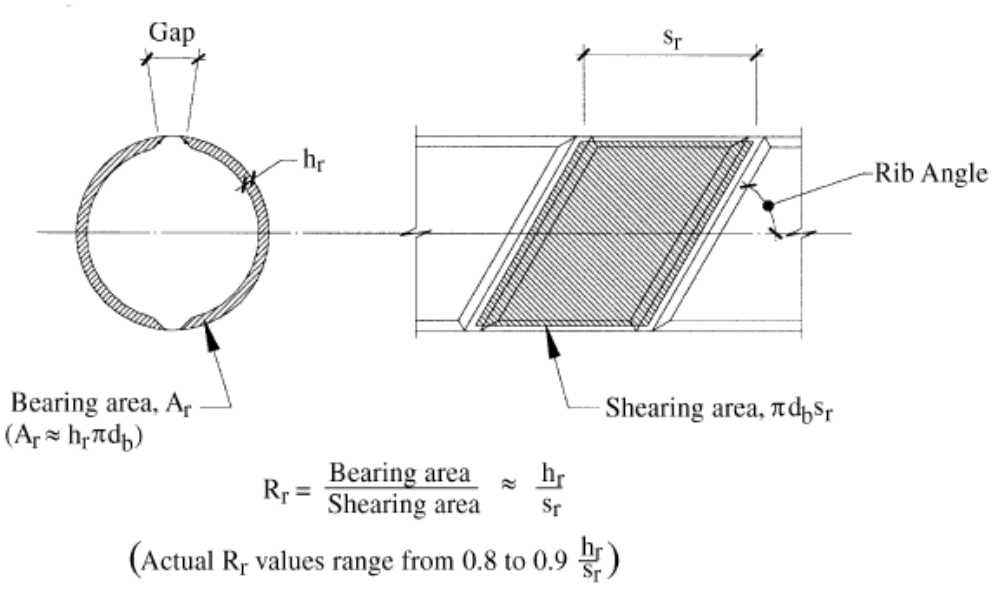

Figure 2.4 Definition of relative rib area, R_r (ACI, 2001a)

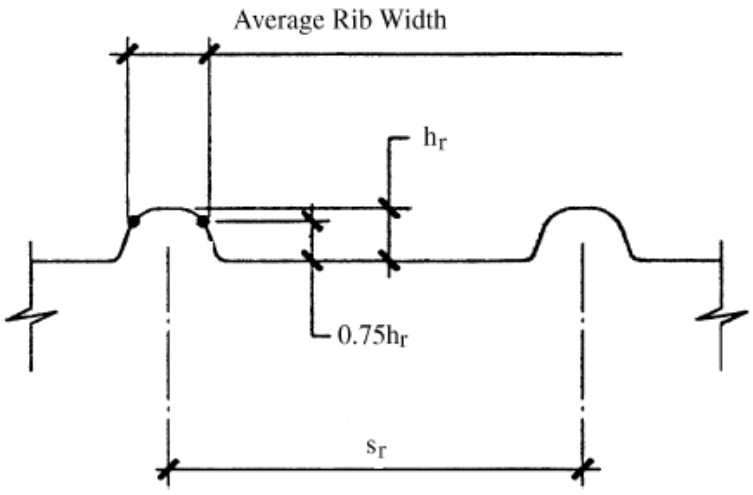

Figure 2.5 Definition of average rib width (ACI, 2001a)

Failure mechanisms at the ribs of deformed bars as a function of h_r/s_r are presented in Figure 2.6. This figure shows that when $h_r/s_r > 0.15$, shearing of concrete in front of the ribs occurs and when $h_r/s_r < 0.1$, crushing of concrete in front of the ribs occurs.

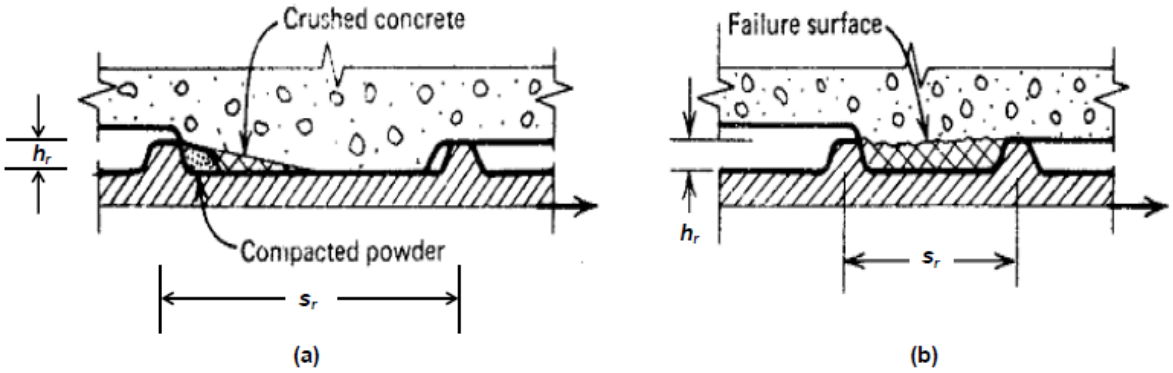

Figure 2.6 Failure mechanisms at the ribs of deformed bars: (a) h_r/s_r >0.15, (b) h_r/s_r < 0.1 (Park and Paulay, 1975)

2.3.2.3 Bar surface condition and strength

Bar surface condition is an important parameter which affects the bond strength because of its effect on friction and ability of the ribs to transfer force between the two materials. Bar surface condition is defined by the presence or absence of foreign and/or deleterious matter on the bar surface. This may include rust, epoxy coating, mud, oil, dirt and bar finish during manufacturing. The ACI 318-11 (2011) requires that the reinforcement must be free of mud, oil, and other nonmetallic coatings that decrease the bond. An epoxy coated bar is much smoother than the normal non-coated bar. Although

epoxy coating will not significantly affect the bond strength of deformed bars, in the case of plain bars (which rely on adhesion and friction) bond strength is likely to be significantly compromised by epoxy coating (*fib*, 2000). Reinforcement yield strength also influences bond strength. It has been observed that when high-strength steel is used, the concrete adjacent to the bars will have greater strains and cracks when compared to when normal strength steel is used, leading to a reduction in ultimate bond strength (ACI, 1973).

2.3.3 Concrete properties

2.3.3.1 Compressive strength

According to the ACI Committee 408 (ACI, 2003) bond strength between steel bars and NA concrete has been traditionally normalised to the square root of concrete compressive strength, f'_c (Tepfers, 1973; Orangun *et al*., 1977; Darwin *et al*., 1992; Esfahani and Rangan, 1998a, 1998b; Harajli, 2005; ACI, 2011) though this practice has not been universal. Zsutty (1985), on the other hand has found that $f'_c{}^{1/3}$ provided a better match with data compared to $f'_c{}^{1/2}$. On the basis of a review of a large number of bond test results of concretes with strengths between 17 MPa and 110 MPa, Darwin *et al*. (1996) and Zuo and Darwin (1998, 2000) have reported that the effect of concrete grade on splice strength for normal-strength as well as high-strength concrete is more accurately represented if the bond strength data are normalised to $f'_c{}^{1/4}$. Bond test results of Harajli and Al-Hajj (2002) show that as the compressive strength of concrete increased from about 28 MPa to about 55 MPa, the local splice strength increased in proportion to $f'_c{}^{p}$ where p is in excess of ½. These authors found that for all their parameters under investigation, whenever the local splice strengths were normalised to $f'_c{}^{1/2}$, the results of high-strength concrete were about 23% larger than those of normal-strength concrete. On the other hand, according to Azizinamini *et al*. (1993), normalised average bond strength at failure in high-strength concrete reduces relative to normal-strength concrete and this reduction in bond strength increases with an increase in splice length. In contrast to the results of Azizinamini *et al*. (1993), Esfahani and Rangan (1996) found that the average bond stress at failure normalised with respect to $f'_c{}^{1/2}$ is higher for high-strength concrete than for normal-strength concrete. According to the literature, $f'_c{}^{1/2}$ does not accurately represent the effect of concrete strength on bond and ACI 408R-03 (2003) states inter alia that 'when bond strengths are normalised with respect to $f'_c{}^{1/2}$, the effect of concrete strength is exaggerated resulting in an overestimation of bond strength for higher strength concretes'.

2.3.3.2 Tensile strength

According to the ACI Committee 408 (ACI, 2003), the observed effects of aggregate strength and quantity and of concrete compressive strength on bond strength strongly indicate that the tensile properties of concrete play a significant role in determining bond strength. The concrete contribution to total bond force increases approximately with $f'_c{}^{1/4}$. This contrasts with the relationship between compressive strength and tensile strength, where it is generally agreed that tensile strength increases approximately with $f'_c{}^{1/2}$. Some studies dealing with high-strength concrete, a power higher than ½ has been observed to relate f'_c to tensile strength (Ahmad and Shah, 1985; Kozul and Darwin, 1997). If tensile strength alone the key governing factor in bond strength, $f'_c{}^{1/2}$ should provide a good representation of the relationship between compressive strength and bond strength, and aggregate strength should have little effect on concrete contribution to total bond force (ACI, 2003).

2.3.3.3 Aggregate type

Zuo and Darwin (2000) concluded that under all conditions of confinement, stronger coarse aggregates provides higher splice strength and for splices confined by transverse reinforcement, the higher the quantity of coarse aggregate in the concrete, the greater the contribution of transverse reinforcement to splice strength. Among aggregate types, basalt gives higher fracture energy, increases resistance to crack propagation that delays splitting failure and hence increases splice strength (Zuo and Darwin, 2000).

2.3.3.4 Slump and workability

According to Darwin (1987), workability of concrete has a significant effect on bond strength. In higher slump concrete, the tendency for settling and bleeding will be more which in turn will reduce bond strength. In the case of reinforced concrete members with a concrete depth of more than 300 mm, the presence of bleed water accumulated below the top-cast bars produces voids. These voids affect the bond strength (ACI, 2003). By using hand-rodded concrete with slump ranging from 127 to 152 mm, Menzel (1952) observed a marked reduction in bond strength when the height of top-cast bars increased from 54 to 841 mm. ACI 408R-03 (2003) concluded that an increase in slump and the use of workability-enhancing admixtures tends to have a negative effect on bond strength.

2.3.3.5 Mineral admixtures

Mineral admixtures like silica fume, flyash and ground granulated blast furnace slag have been used by various researchers (Gettu *et al*., 1990; Gjorv et al., 1990; Olsen,

1990a, 1990b; Hwang et al. 1994; Hamad and Itani, 1998; Sivakumar and Santhanam, 2007a, 2007b; Bhaskar *et al*., 2008; Chidiac and Panesar, 2008; Bhaskar *et al*., 2012; Onuaguluchi and Panesar, 2014), to produce high-strength and high-performance concretes. According to the ACI Committee 408 (ACI, 2003), most studies of the effect of mineral admixtures on bond strength have been limited to the effects of silica fume and for this case bond strengths are normalised with respect to $f'_c{}^{1/2}$. Because this value overestimates the effect of compressive strength, the conclusion has often been made that silica fume has a negative effect on bond strength. If the test results are normalised with respect to $f'_c{}^{1/4}$, however, the apparent negative impact of silica fume on bond is significantly decreased (ACI, 2003). Gjorv *et al*. (1990) conducted pullout tests for concrete strengths ranging from 21 MPa to 83 MPa with silica fume replacements of 0 %, 8% and 16% by weight of cement and concluded that silica fume increases bond strength between concrete and reinforcing steel. An increase in bond strength by 10 % for concrete containing silica fume and 17 % for concrete containing fly ash has been reported by Olsen (1990a, 1990b). On the other hand, a 7-12% reduction in bond strength has been reported by Hwang *et al*. (1994). Hamad and Itani (1998) carried out 16 splice tests that included both top- and bottom-cast bars. The test strengths showed reductions in bond strength averaging 5 % for silica fume replacements of Portland cement between 5 and 20 % (ACI, 2003).

2.3.3.6 Fibre reinforcement

Fibre reinforcement has been used by various researchers (Banthia and Trottier, 1994; Harajli, 1994; Harajli et al., 1995; Harajli and Salloukh, 1997; Banthia et al., 2000; Bindiganavile and Banthia, 2002; Bindiganavile and Banthia, 2005; Baruah and Talukdar, 2007a; Mohammadi *et al*., 2008; Singh *et al*., 2010; Onuaguluchi *et al*., 2014; Singh *et al*., 2014), to enhance the performance of concrete. Addition of fibres in concrete improves the tensile strength of concrete, however the increase is small (ACI, 2003). Harajli *et al*. (1995) measured the local bond stress-slip behaviour for bars embedded in fibre reinforced concrete pullout specimens. These authors studied the effect of bar diameter (19 mm and 25 mm), mode of failure (pullout, splitting), type, volume fraction and aspect ratio of the bars. They reported a 20 % increase in bond strength when using 2 % fibres by volume. Bond strength of reinforcing bars embedded in both plain and fibre reinforced concrete using splice specimens were studied by Harajli *et al*. (2002). They investigated the effect of the ratio of concrete cover to bar diameter and fibre volume fraction. Harajli *et al*. (2002) reported a 26 % and a 33 % increase in bond strength for 1 and 2 % fibre volume fraction respectively.

2.4 BOND TEST SPECIMENS

Bond strength between reinforcing steel and concrete can be evaluated by using a variety of test specimen configurations. Only the most common configurations viz. pullout, beam-end, beam-anchorage and splice specimens are reviewed in the following sections. According to the ACI 408R-03 (2003) specimen configuration affects the measured bond strength and the nature of the bond response.

2.4.1 Pullout specimens

Pullout specimens are widely used for investigation of bond behaviour because of their ease of fabrication and the simplicity of the test and they provide a simple means of comparing normalized bond behaviour (Abrams, 1913; Menzel, 1952; Gjorv *et al.*, 1990; Harajli *et al.*, 1995; Esfahani and Rangan, 1998a; Ajdukiewicz and Kliszewicz, 2002; Xiao and Falkner, 2007; Choi and Kang, 2008; Corinaldesi and Moriconi, 2009; Harajli and Abouniaj, 2010; Bai *et al*., 2010; Bhaskar *et al*., 2012; Kim *et al*., 2012; Kim and Yun, 2013; Breccolotti and Materazzi, 2013; Seara-Paz *et al*., 2014; Metelli and Plizzari, 2014). However, these specimens are the least realistic because the stress fields in them do not accurately simulate bond conditions in actual construction. As the bar is placed in tension, the concrete is placed in compression unlike in actual construction wherein both the embedded bar and the surrounding concrete are in tension. Figure 2.7 shows a typical pullout specimen, wherein the pullout load is applied on the concentrically embedded steel bar.

Figure 2.7 Pullout specimen (ACI, 2003)

2.4.2 Beam-end specimens

A beam-end specimen, also sometimes called as a modified cantilever beam is shown in Figure 2.8 and has been used by a number of investigators for studying bond (Johnston and Zia, 1982; Brettmann *et al*., 1984, 1986; Zilveti *et al*., 1985; Darwin and

Graham, 1993a, 1993b; Darwin e*t al*., 1996; Tan *et al*., 1996; Zuo and Darwin, 1998, 2000; Butler *et al*., 2011; Butler, 2012; Fathifazl *et al*., 2012; Butler *et al*., 2014) Compared to pullout specimens, these specimens simulate more accurately the state of stress in actual construction with the reinforcing steel and the surrounding concrete being simultaneously placed in tension. The specimen consists of a reinforcing bar which is cast in a block of reinforcing concrete. According to the ACI Committee 408 (ACI, 2003), to achieve the desired state of stress, the compressive force must be located away from the reinforcing bar by a distance approximately equal to the embedded or the bonded length of the bar within the concrete.

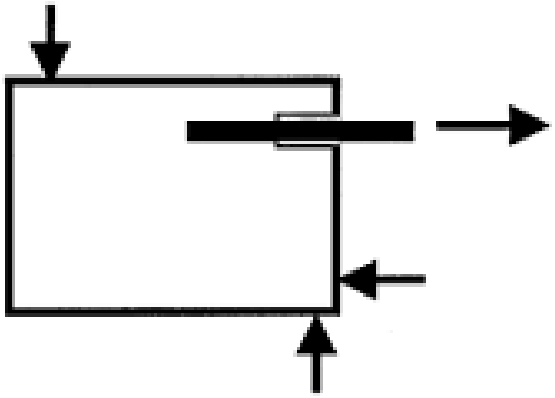

Figure 2.8 Beam-end specimen (ACI, 2003)

2.4.3 Beam anchorage specimens

Beam anchorage specimens are large specimens ideally suited to represent full-size and they provide realistic data on development and splice length. The anchorage specimen Figure 2.9 simulates a member with a flexural crack and a known bonded length. According to the ACI 408R-03 (2003), in order to minimise the effect of increased normal stresses caused by support reactions, it is desirable that the reactions are displaced laterally from the centre-line of the beam. Beam anchorage specimens have been used for example by Hamad *et al*., 2005.

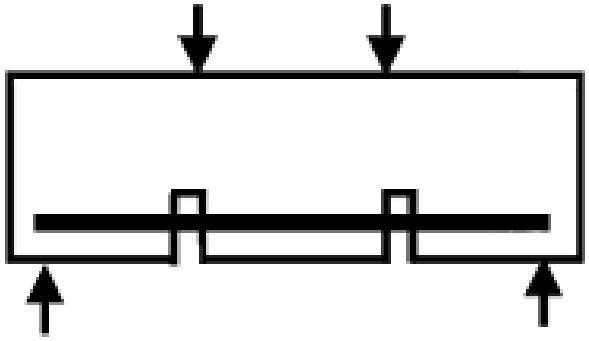

Figure 2.9 Beam anchorage specimen (ACI, 2003)

2.4.4 Splice specimens

Splice specimens are also large specimens and are representative of actual construction and like beam anchorage specimens they also provide realistic data on development and splice length. The splice specimen (Figure 2.10) is normally fabricated with the splice in a constant moment region and produces bond strengths similar to those obtained with the anchorage specimens. Their advantage over anchorage specimens is that they are easier to fabricate while at the same time they provide realistic stress-state in the vicinity of the bars. According to the ACI Committee 408 (ACI, 2003), the bulk data provided by these specimens has been used to establish design provisions for development length as well as splice length, in ACI 318-11 (2011) starting with ACI 318-95 (1995). Splice specimens have been used by researchers like Chinn et al. (1955), Chamberlin (1958), Zekany *et al.* (1981), Treece and Jirsa (1989), Hamad and Jirsa (1993), Darwin *et al*. (1996), Tan *et al*. (1996), Harajli and Salloukh (1997), Hamad and Itani (1998), Esfahani and Rangan (1998b), Zuo and Darwin (1998, 2000), Harajli *et al*. (2002), Morohashi *et al*. (2007), Harajli and Abouniaj (2010), Hassan *et al.* (2012), Pay *et al*. (2014).

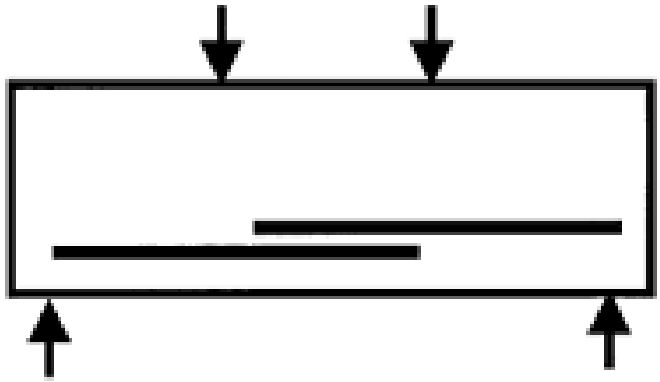

Figure 2.10 Splice specimen (ACI, 2003)

2.5 PREDICTIVE MODELS FOR BOND STRENGTH AND RECOMENDATIONS OF DESIGN CODES

2.5.1 Predictive models for bond strength

The following sections discuss selected bond strength predictive models in the literature. Although currently there is no widely accepted and accurate theory-based model for development and splice strength, a majority of the bond models in the literature are based on statistical comparison of experimental results and these models produce reasonably accurate predictions of bond strength.

2.5.1.1 Orangun, Jirsa and Breen

Based on a nonlinear regression analysis of test results of 62 beam-splice specimens, Orangun *et al*. (1975, 1977) developed equations (Equation 2.5 and 2.6), for bond strength of concrete not confined and confined by transverse reinforcement respectively. Equations 2.5 and 2.6 are applicable for only splitting failure with restriction given in Equation 2.7.

$$\frac{\tau_c}{\sqrt{f_c^{'}}} = 0.10 + 0.25\frac{c_{\min}}{d_b} + 4.15\frac{d_b}{L_d} \tag{2.5}$$

$$\frac{T_b}{\sqrt{f_c^{'}}} = \frac{T_c + T_s}{\sqrt{f_c^{'}}} = \frac{A_b f_s}{\sqrt{f_c^{'}}} = 0.25\pi L_d\left(c_{\min} + 0.4d_b\right) + 16.6A_b + \frac{\pi L_d A_{tr}}{41.5sn} f_{yt} \tag{2.6}$$

$$\frac{1}{d_b}\left(c_{\min} + 0.4d_b + \frac{A_{tr} f_{yt}}{10.34sn}\right) \leq 2.5 \tag{2.7}$$

where A_b = area of developed or spliced bar (mm^2), A_{tr} = area of transverse reinforcement normal to the plane of splitting through the anchored bars in (mm^2), c_{min} = smaller of minimum concrete cover or ½ of the clear spacing between bars = minimum (c_b, c_s) (mm), c_b = bottom concrete cover for reinforcing bar being developed or spliced (mm), c_s = minimum [c_{so}, c_{si} + 6.35 mm] (mm), c_{si} = ½ of the bar clear spacing (mm), c_{so} = side cover for reinforcing bar (mm), d_b = bar diameter (mm), $f_c^{'}$ = cylinder compressive strength of concrete (MPa), f_s = stress in reinforcing bar (MPa), f_{yt} = yield strength of transverse reinforcement (MPa), L_d = development or spliced length (mm), n = number of bars developed or spliced at the same location, s = spacing of transverse reinforcement (mm), T_b = total bond force of a developed or spliced bar = T_c + T_s (kN), T_c = concrete contribution to total bond force, the bond force that would be developed without transverse reinforcement (kN), T_s = steel contribution to total bond force, the additional bond strength provided by the transverse steel (kN), τ_c = average bond strength at failure (MPa).

2.5.1.2 Darwin *et al*.

Darwin *et al*. (1996) used a larger database of bottom-cast bars, consisting of 133 splice and development specimens without confined transverse reinforcement and 166 specimens with confined transverse reinforcement. They observed that $f'_c{}^{1/4}$ provided a better representation of concrete strength than the more traditional $f'_c{}^{1/2}$. For bars confined by transverse reinforcement, the relative rib area R_r shows a significant effect on bond

strength. Based on their studies, equations were developed for bars not confined and confined by transverse reinforcement and these are presented in Equations 2.8 and 2.9 respectively. Equations 2.8 and 2.9 are applicable for only splitting failure subject to restrictions given in Equation 2.10.

$$\frac{T_c}{f_c^{'1/4}} = \frac{A_b f_s}{f_c^{'1/4}} = \left[1.5L_d\left(c_{\min}+0.5d_b\right)+51A_b\right]\left(0.1\frac{c_{\max}}{c_{\min}}+0.9\right) \tag{2.8}$$

where $\left(0.1\frac{c_{\max}}{c_{\min}}+0.9\right)\leq 1.25$

$$\frac{T_b}{f_c^{'1/4}} = \frac{T_c+T_s}{f_c^{'1/4}} = \frac{A_b f_s}{f_c^{'1/4}} = \left[1.5L_d\left(c_{\min}+0.5d_b\right)+51A_b\right]\left(0.1\frac{c_{\max}}{c_{\min}}+0.9\right)+53.3t_r t_d\frac{NA_{tr}}{n}+1019 \tag{2.9}$$

where $t_r = 9.6R_r+0.28$ and, $t_d = 0.028d_b+0.28$

$$\frac{1}{d_b} = \left[\left(c_{\min}+0.5d_b\right)\left(0.1\frac{c_{\max}}{c_{\min}}+0.9\right)+\left(\frac{35.3t_r t_d A_{tr}}{sn}\right)\right]\leq 4.0 \tag{2.10}$$

where A_b, A_{tr}, c_{max}, c_{min}, c_b, c_s, c_{so}, c_{si}, d_b, $f_c^{'}$, f_s, L_d, n, s, T_b, T_c and T_s are defined in section 2.5.1.1, N = number of transverse bars in the development or splice length, R_r = relative rib area, t_d = term representing the effect of bar size on T_s, t_r = term representing the effect of relative rib area on T_s.

2.5.1.3 Zuo and Darwin

Zuo and Darwin (1998, 2000) expanded the work of Darwin *et al*. (1996) by increasing the database and adding substantially to the percentage of test specimens containing high-strength concrete (55 MPa). The database included 171 specimens containing bars not confined by transverse reinforcement and 196 specimens containing bars confined by transverse reinforcement. All bars were bottom cast. They concluded that $f'_c{}^{1/4}$ realistically represents the contribution of concrete strength to bond strength for bars not confined by transverse reinforcement, which supports the earlier observations. Their bond strength equations for bars not confined and confined by transverse reinforcement are presented as Equations 2.11 and 2.12 respectively. Equations 2.11 and 2.12 are applicable for splitting failure only subjected to restrictions given in Equation 2.13.

$$\frac{T_c}{f_c^{'1/4}} = \frac{A_b f_s}{f_c^{'1/4}} = \left[1.43 L_d \left(c_{\min} + 0.5 d_b\right) + 56.2 A_b\right] \left(0.1 \frac{c_{\max}}{c_{\min}} + 0.9\right) \quad (2.11)$$

$$\frac{T_b}{f_c^{'1/4}} = \frac{T_c + T_s}{f_c^{'1/4}} = \frac{A_b f_s}{f_c^{'1/4}} = \left[1.43 L_d \left(c_{\min} + 0.5 d_b\right) + 56.2 A_b\right] \left(0.1 \frac{c_{\max}}{c_{\min}} + 0.9\right)$$

$$+ \left(9 t_r t_d \frac{N A_{tr}}{n} + 744\right) f_c^{'1/2} \quad (2.12)$$

where $t_r = 9.6 R_r + 0.28$ and $t_d = 0.03 d_b + 0.22$

$$\frac{1}{d_b}\left[\left(c_{\min} + 0.5 d_b\right)\left(0.1 \frac{c_{\max}}{c_{\min}} + 0.9\right) + \left(\frac{6.26 t_r t_d A_{tr}}{sn}\right) f_c^{'1/2}\right] \leq 4.0 \quad (2.13)$$

where the notations are defined in sections 2.5.1.1 and 2.5.1.2.

2.5.1.4 Esfahani and Rangan

Esfahani and Rangan (1998a, 1998b), extended the local bond theory of Tepfers (1973) and developed expressions for bond strength of bars not confined by transverse reinforcement (Equations 2.14 and 2.15).

For f'_c < 50 MPa

$$\frac{T_c}{\sqrt{f_c^{'}}} = \frac{A_b f_s}{\sqrt{f_c^{'}}} = 2.7 \pi L_d \frac{\left(c_{\min} + 0.5 d_b\right)\left(1 + \frac{1}{M}\right)}{\left(\frac{c_{\min}}{d_b} + 3.6\right)\left(1.85 + 0.024\sqrt{M}\right)} \left(0.12 \frac{c_{med}}{c_{\min}} + 0.88\right) \quad (2.14)$$

where $M = \cosh\left(0.0022 L_d \sqrt{\frac{r f_c^{'}}{d_b}}\right)$

For f'_c ≥ 50 MPa

$$\frac{T_c}{\sqrt{f_c^{'}}} = \frac{A_b f_s}{\sqrt{f_c^{'}}} = 4.73 \pi L_d \frac{\left(c_{\min} + 0.5 d_b\right)\left(1 + \frac{1}{M}\right)}{\left(\frac{c_{\min}}{d_b} + 5.5\right)\left(1.85 + 0.024\sqrt{M}\right)} \left(0.12 \frac{c_{med}}{c_{\min}} + 0.88\right) \quad (2.15)$$

where A_b, d_b, L_d, f_s, $f_c^{'}$, T_c are defined in section 2.5.1.1, c_{min} = minimum (c_{so}, c_b, c_{si} + $d_b/2$) (mm), c_{med} = median (c_{so}, c_b, c_{si} + $d_b/2$) [that is, middle value] (mm), M = constant for the bond strength of bars. For conventional reinforcement ($R_r \approx 0.07$), r = 0.3. The hyperbolic cosine enters the relationship based on the assumed variation in bond stress along the developed or spliced length of a bar.

Esfahani and Rangan (1998a), also presented the following equations (Equations 2.16 and 2.17) for predicting peak bond strength in short length specimens.

For f'_c < 50 MPa

$$\tau_{\max} = 4.9\left(\frac{\frac{c}{d_b}+0.5}{\frac{c}{d_b}+3.6}\right)f_{ct} \qquad (2.16)$$

For $f'_c \geq 50$ MPa

$$\tau_{\max} = 8.6\left(\frac{\frac{c}{d_b}+0.5}{\frac{c}{d_b}+5.5}\right)f_{ct} \qquad (2.17)$$

where $\tau_{\max}$ = peak bond strength (MPa), c = minimum concrete cover (c_{so}, c_b) (mm), c_{so} = side cover, c_b = bottom cover, d_b = bar diameter, $f_{ct} = 0.55\sqrt{f_c^{'}}$ = splitting tensile strength of concrete (MPa), $f_c^{'}$ = cylinder compressive strength of concrete (MPa).

2.5.1.5 ACI 408R-03

Using the database 10-2001, the ACI Committee 408 (ACI, 2003) has updated the equations (Equations 2.11 and 2.12) developed by Zuo and Darwin (1998, 2000) with minor changes and these are presented below as Equations 2.18 and 2.19 respectively. The restriction in Equation 2.20 (same as Equation 2.13) applies to Equations 2.18 and 2.19 also.

$$\frac{T_c}{f_c^{'1/4}} = \frac{A_b f_s}{f_c^{'1/4}} = \left[1.43L_d\left(c_{\min}+0.5d_b\right)+57.4A_b\right]\left(0.1\frac{c_{\max}}{c_{\min}}+0.9\right) \qquad (2.18)$$

$$\frac{T_b}{f_c^{'1/4}} = \frac{T_c + T_s}{f_c^{'1/4}} = \frac{A_b f_s}{f_c^{'1/4}} = \left[1.43 L_d \left(c_{\min} + 0.5 d_b\right) + 57.4 A_b\right]\left(0.1\frac{c_{\max}}{c_{\min}} + 0.9\right)$$

$$+\left(8.9 t_r t_d \frac{N A_{tr}}{n} + 558\right) f_c^{'1/2} \qquad (2.19)$$

where $t_r = 9.6R_r + 0.28$ and $t_d = 0.03 d_b + 0.22$

$$\frac{1}{d_b}\left[\left(c_{\min} + 0.5 d_b\right)\left(0.1\frac{c_{\max}}{c_{\min}} + 0.9\right) + \left(\frac{6.26 t_r t_d A_{tr}}{sn}\right) f_c^{'1/2}\right] \leq 4.0 \qquad (2.20)$$

where the notations are defined in sections 2.5.1.1 and 2.5.1.2.

2.5.1.6 MacGregor

The following equation was presented by MacGregor (1997) for predicting the peak bond strength of concrete.

$$\tau_{\max} = 0.498\sqrt{f_c'}\left(\frac{c_b}{d_b} - \frac{1}{2}\right) \qquad (2.21)$$

where $\tau_{\max}$ = peak bond strength (MPa), c_b = concrete cover measured from the centre of the bar (mm), d_b = bar diameter, f_c' = cylinder compressive strength of concrete (MPa).

2.5.1.7 Kim *et al*.

Kim *et al*. (2012) modified the equation of MacGregor (1997) for predicting the bond strength of RCA concrete. The bond strength equation of MacGregor (1997) was suitably modified to take care of both fine and coarse RCA replacement levels and the following equation was obtained.

$$\tau_{\max} = \left[0.614\sqrt{f_c'}\left(\frac{c_c}{d_b} - 0.55\right)\right] - \left(0.4203 e^{0.0172 S} + 0.007 G\right) \qquad (2.22)$$

where $\tau_{\max}$ = peak bond strength (MPa), c_c = concrete cover measured to the centre of the bar (mm), d_b = bar diameter, f_c' = cylinder compressive strength of concrete (MPa), S = replacement level of fine RCA, G = replacement level of coarse RCA.

2.5.2 Development length provisions in design codes

In structural design, bond is of direct relevance for calculating the development lengths of rebars. Most current design codes give equations for calculating development lengths as a function of the allowable bond stress, besides many other parameters. In these predictive equations, the allowable bond stress is expressed as a function of the grade of concrete. A review of development length provisions in selected design codes is presented in the following sections.

2.5.2.1 ACI 318-11

ACI 318-11 (2011) provides the following equation, based on the expressions developed by Orangun, Jirsa, and Breen (1975, 1977), for calculating development and splice length. This equation is applicable to both confined as well as unconfined concretes.

$$L_d = \left(\frac{f_y}{1.1\lambda\sqrt{f_c^{'}}} \frac{\psi_t \psi_e \psi_s}{\left(\frac{c_b + K_{tr}}{d_b} \right)} \right) d_b \tag{2.23}$$

The peak bond strength for concrete according to ACI 318-11 (2011) is given by the equations (Equation 2.24 and 2.25).

For rebar diameter ≤ 20 mm

$$\tau_{\max} = \frac{0.34375 c_b \sqrt{f_c^{'}}}{d_b} \tag{2.24}$$

For rebar diameter > 25 mm

$$\tau_{\max} = \frac{0.275 c_b \sqrt{f_c^{'}}}{d_b} \tag{2.25}$$

where c_b = the factor that represents the smallest of the side cover, the cover over the bar or wire (in both cases measured to the centre of the bar or wire), or one-half the centre-to-centre spacing of the bars or wires, d_b = bar diameter, $f_c^{'}$ = cylinder compressive strength of concrete, f_y = yield strength of the longitudinal reinforcement, $K_{tr} = \frac{40A_{tr}}{sn}$ = the factor that represents the contribution of the confining transverse reinforcement across potential

splitting planes, A_{tr} = area of transverse reinforcement perpendicular to the plane of splitting, s = spacing of transverse reinforcement in the splice zone, n = number of bars or wires being spliced or developed along the plane of splitting, $\left(\frac{c_b + K_{tr}}{d_b}\right)$ = confinement term which shall not be taken greater than 2.5 to avoid pullout failure, L_d = development or spliced length, λ = modification factor reflecting the reduced mechanical properties of lightweight concrete, 0.75 for light weight concrete and, 1.0 for normal weight concrete, ψ_t = reinforcement location factor, 1.3 when the horizontal reinforcement is placed such that more than 300 mm of the fresh concrete is cast below the development length or splice and, 1.0 for other situations, ψ_e = coating factor, 1.0 for uncoated reinforcement, 1.5 for epoxy-coated bars or wires with cover less than $3d_b$ or clear spacing less than $6d_b$, 1.2 for epoxy-coated bars or wires, ψ_s = bar size factor, 0.8 for 19 mm and smaller bars and, 1.0 for 22 mm and larger bars, $\tau_{\max}$ = peak bond strength (MPa). The value of $\sqrt{f_c'}$ should not exceed 8.3 MPa.

2.5.2.2 Canadian standard CSA A23.3-04

Canadian Standards Association, CSA A23.3-04 (2004) recommends the following equation (Equation 2.26) for calculating development and splice length. This equation has been modelled on the expressions ACI 318-11 (2011) developed by Orangun, Jirsa, and Breen (1975, 1977). This equation is applicable to both confined as well as unconfined concretes.

$$L_d = 1.15 \frac{k_1 k_2 k_3 k_4}{(d_{cs} + K_{tr})} \frac{f_y}{\sqrt{f_c'}} A_b \qquad (2.26)$$

where A_b = cross-sectional area of the bar being developed or spliced, d_{cs} = the smaller of (i) the distance from the closest concrete surface to the centre of the bar being developed, or (ii) two-thirds of the centre-to-centre spacing of the bars being developed, f_y = yield strength of the longitudinal reinforcement, f_c' = cylinder compressive strength of concrete, $K_{tr} = \frac{A_{tr} f_{yt}}{10.5sn}$ = the factor that represents the contribution of the confining transverse reinforcement across potential splitting planes, A_{tr} = area of transverse reinforcement perpendicular to the plane of splitting, s = spacing of transverse reinforcement in the splice zone, n = number of bars or wires being spliced or developed along the potential plane of bond splitting, $(d_{cs} + K_{tr})$ = confinement term which shall not be taken greater

than 2.5d_b to avoid pullout failure, k_1 = bar location factor, 1.3 for horizontal reinforcement placed in such a way that more than 300 mm of fresh concrete is cast in the member below the development length or splice and, 1.0 for other cases, k_2 = coating factor, 1.5 for epoxy-coated reinforcement with clear cover less than 3d_b, or with clear spacing between bar being developed less than 6d_b 1.2 for all other epoxy-coated reinforcement and, 1.0 for uncoated reinforcement, k_3 = concrete density factor, 1.3 for structural low-density concrete, 1.2 for structural semi-low-density concrete and, 1.0 for normal-density concrete, k_4 = bar size factor, 0.8 for 20 mm and smaller bars and deformed wires and, 1.0 for 25 mm and larger bars. The product $k_1 k_2$ need not be taken greater than 1.7, L_d = development or spliced length.

2.5.2.3 Australian code AS 3600-2009

The development length for deformed bars in tension according to Australian code AS 3600-2009 (2009) is given by the following equation (Equation 2.27).

$$L_{sy.tb} = \frac{0.5 k_1 k_3 f_{sy} d_b}{k_2 \sqrt{f_c'}} \geq 29 k_1 d_b \tag{2.27}$$

where d_b = bar diameter, $L_{sy.tb}$ = development length, f_c' = cylinder compressive strength of concrete at 28 days which shall not be taken to exceed 65 MPa, f_{sy} = yield strength of reinforcing steel, k_1 = 1.3 for a horizontal bar with more than 300 mm of concrete cast below the bar, 1.0 for other cases, $k_2 = (132 - d_b)/100$, $k_3 = 1.0 - 0.15(c_d - d_b)/d_b$ subjected to $0.7 \leq k_3 \leq 1.0$, c_d = min of clear spacing between spliced bars, side cover and, bottom cover. It is worth nothing that the minimum value of 29$k_1 d_b$ is specified to ensure that the bar does not prematurely pullout prior to the mobilization of the concrete around the bar in providing an effective means of stress development.

In AS 3600-2009 (2009), the peak bond strength for concrete is given by Equation 2.28.

$$\tau_{\max} = 0.265 \sqrt{f_c'} \left(\frac{c}{d_b} - 0.5 \right) \tag{2.28}$$

where $\tau_{\max}$ = peak bond strength (MPa), c = concrete cover measured from the surface of the bar (mm), d_b = bar diameter, f_c' = cylinder compressive strength of concrete (MPa).

2.5.2.4 British standard Eurocode 2

The British standard, Eurocode 2 (2004), recommends the following equations for calculating the basic anchorage length (Equation 2.29) and the design anchorage length (Equation 2.30) for both confined and unconfined concretes.

$$L_{b,rqd} = \frac{\phi \sigma_{sd}}{4 f_{bd}} \tag{2.29}$$

$$L_{bd} = \alpha_1 \alpha_2 \alpha_3 \alpha_4 \alpha_5 L_{b,rqd} \geq L_{b,\min} \tag{2.30}$$

where $f_{bd} = 2.25 \eta_1 \eta_2 f_{ctd}$ = design value of ultimate bond stress, η_1 = coefficient related to the quality of the bond and the position of the bar during concreting, 1.0 for good conditions and, 0.7 for all other cases, η_2 = term related to the bar diameter, 1.0 for $\phi \leq 32mm$ and, $\eta_2 = \left(\frac{132 - \phi}{100}\right)$ for $\phi > 32mm$, $f_{ctd} = \frac{\alpha_{ct} f_{ctk,0.05}}{\gamma_c}$ = design value of concrete tensile strength, α_{ct} = coefficient for taking into account long term effects on the tensile strength and of unfavourable effects resulting from the way the load is applied recommended value is 1.0, γ_c = partial safety factor for concrete, 1.5 for persistent & transient and, 1.2 for accidental loads, $f_{ctk,0.05} = 0.7 f_{ctm}$=concrete tensile strength with 5% fracture, f_{ctm} = mean value of the axial tensile strength of concrete, $f_{ctm} = 0.30 f_{ck}^{(2/3)} \leq C50/60$, $f_{ctm} = 2.12 \ln\left(1 + \left(\frac{f_{cm}}{10}\right)\right) > C50/60$, C = concrete grade, f_{ck} = characteristic compressive cylinder strength of concrete at 28 days, f_{cm} = mean value of concrete cylinder compressive strength, $L_{b,rqd}$ = basic required anchorage length, σ_{sd} = design stress of the bar at the position starting where the anchorage is measured, ϕ = longitudinal bar diameter, L_{bd} = design anchorage length, α_1 = effect of form of the bars assuming adequate cover, 1.0 for straight bars, α_2 = effect of concrete minimum cover given by $\alpha_2 = 1 - 0.15(c_d - \phi)/\phi$ and $0.75 \geq \alpha_2 \leq 1.0$, c_d = minimum of clear spacing between spliced bars, side cover and, bottom cover, α_3 = effect of confinement by transverse reinforcement given by $\alpha_3 = 1 - K\lambda$ and $0.7 \geq \alpha_3 \leq 1.0$, $\lambda = \left(\sum A_{st} - \sum A_{st,\min}\right)/A_s$, $\sum A_{st}$ = cross-sectional area of the transverse reinforcement along the design anchorage length L_{bd} , $\sum A_{st,\min}$ = cross-sectional area of the minimum transverse reinforcement, $0.25A_s$ for beams and, 0 for slabs, A_s = area of a single anchored bar with maximum bar diameter, K = 0.1 for the beam, p = transverse pressure

at ultimate limit state along L_{bd} , α_4 = influence of one or more welded transverse bars $(\phi_t > 0.6\phi)$ along the design anchorage length L_{bd}, α_5 = effect of the pressure transverse to the plane of splitting along the design anchorage length, $L_{b,min}$ = minimum anchorage length if no other limitation is applied; for anchorage in tension: $l_{b,\min} \geq \max\{0.3l_{b,rqd}, 10\phi, 100mm\}$. The product $(\varepsilon_2 \alpha_3 \alpha_5) \geq 0.7$.

2.5.2.5 *fib* Model code 2010

In the *fib* Model code 2010 (2013), the design anchorage length for both confined and unconfined concrete is calculated from the following equation

$$L_b = \frac{\phi \sigma_{sd}}{4 f_{bd}} \geq L_{b,\min} \tag{2.31}$$

where $L_{b,min}$ = minimum anchorage length, $L_{b,\min} > \max\{0.3\phi f_{yd} / (4 f_{bd}); 10\phi; 100mm\}$, L_b = design anchorage length, σ_{sd} = steel stress to be anchored by bond over the distance L_b , ϕ = diameter of the anchored bar, f_{yd} = design yield strength of reinforcing steel in tension, $f_{bd} = \left((\alpha_2 + \alpha_3) f_{bd,0} - 2p_{tr} / \gamma_c\right) < \left(2.5 f_{bd,0} - 0.4 p_{tr} / \gamma_c\right) < \left(1.5\left(\sqrt{f_{ck}}\right) / \gamma_c\right)$, f_{bd} = design bond strength, α_2 = factor representing the influence of confinement due to concrete cover, may conservatively be taken as 1.0, α_3 = factor representing the influence of confinement due to transverse reinforcement, may conservatively be taken as 0, P_{tr} = mean compression stress perpendicular to the potential splitting failure surface at the ultimate limit state; where transverse compression perpendicular to the bar axis acts over a portion of the bond length, bond strength may be increased over that portion, negative when transverse stress is compressive, γ_c = partial safety factor for bond, taken as 1.5, $f_{bd,0}$ = basic bond strength, $f_{bd,0} = \eta_1 \eta_2 \eta_3 \eta_4 \left(f_{ck} / 25\right)^{0.5} / \gamma_c$, η_1 = bar surface factor, taken as 1.75 for ribbed bars (including galvanized and stainless reinforcement and, 1.4 for fusion bonded epoxy coated ribbed bars, η_2 = bar location factor, 1.0 for good bond condition and, 0.7 for all other cases, η_3 = bar size factor, 1.0 for $\phi \leq 25mm$ and, $(25/\phi)^{0.3}$ for $\phi \leq 25mm$, η_4 = factor representing the characteristic strength of steel reinforcement being anchored or lapped, η_4 = 1.0 for f_{yk} = 500 MPa, η_4 = 1.2 for f_{yk} = 400 MPa, η_4 = 0.85 for f_{yk} = 600 MPa, η_4 = 0.75 for f_{yk} = 700 MPa, η_4 = 0.68 for f_{yk} = 800 MPa, f_{yk} = characteristic value of yield strength of reinforcing steel in tension, f_{ck} = characteristic

cylinder compressive strength of concrete. Intermediate values for η_4 may be obtained by interpolation.

fib model code 2010 (2013) recommends the following equation for calculating the peak bond strength in short length specimens.

$$\tau_{\max} = 2.5\sqrt{f_c'} \tag{2.32}$$

where $\tau_{\max}$ = peak bond strength (MPa), f_c' = cylinder compressive strength of concrete (MPa).

2.5.2.6 Indian standard IS 456:2000

The following equation is included in the IS 456:2000 (2000) for calculating the development length for deformed steel bars in tension.

$$l_b = \frac{\phi \sigma_s}{4\tau_{bd}} \tag{2.33}$$

where ϕ = nominal diameter of the bar, σ_s = stress in bar at the section considered at design load, τ_{bd} = design bond stress, τ_{bd} = 1.92 for f_{ck} = 20 MPa, τ_{bd} = 2.24 for f_{ck} = 25 MPa, τ_{bd} = 2.4 for f_{ck} = 30 MPa, τ_{bd} = 2.72 for f_{ck} = 35 MPa, τ_{bd} = 3.04 for f_{ck} = 40 MPa and above, f_{ck} = characteristic cube compressive strength.

Equation 2.33 is also applicable for calculating the development length for deformed steel bars in compression. For bars in compression, the values of bond stress for bars in tension shall be increased by 25 %.

2.6 RECYCLED CONCRETE AGGREGATES

Growth of population, combined with overall growth of the country, has necessitated development of industries, residential accommodation and commercial offices. Concrete use will increase many-fold in the years to come. As concrete consumes non renewable natural resource of aggregates, in addition to emission of around 1 kg of carbon dioxide for every kg of cement produced, sustainability has to be seriously addressed (Ramalingam and Santhanam, 2012). A depletion in the availability of quality aggregates together with environmental, economic, and energy considerations is encouraging recycling of demolished concrete structures and pavements for use as aggregates in new concrete constructions (Bindra *et al*., 2003, 2007b). Recycling of concrete is the alternative for the sustainable development of construction industry.

2.6.1 Sources of recycled concrete aggregates

The main source of recycled concrete aggregates is the demolished concrete obtained from buildings, pavements and returned ready-mixed concrete. Recycling aggregate entails breaking old concrete, removing reinforcement and contaminants, and crushing the processed material to a specified size and gradation. Demolition can be carried out using any one or a combination of the following techniques: crushing, chopping, splitting, blasting, cutting/drilling, laser, electric heating, and microwaving. While selecting the appropriate technique, considerations like resources, safety, time constraints, quality of concrete, geometry of the demolished object, quantity of concrete to be demolished, location, aggregate hardness, concrete compressive strength, environment, specific risks, utility locations and adjoining construction should be evaluated (ACI, 2001b). Figure 2.11 outlines the production process of RCA recommended by ACI 555R-01 (2001b).

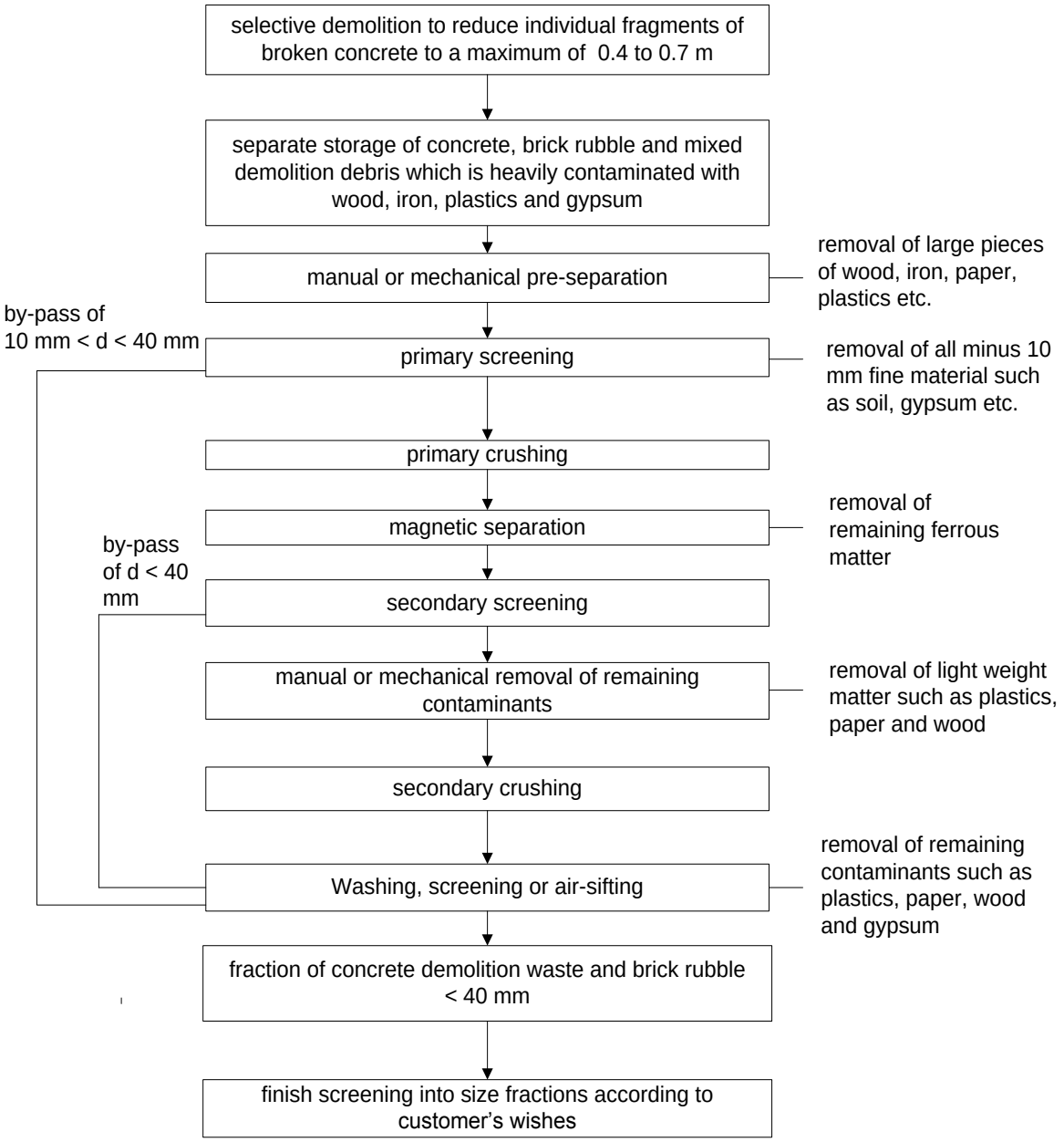

Figure 2.11 Flow chart for processing of building and demolition waste (ACI, 2001b)

2.6.2 Classification

RILEM (1984) classifies RCA of size greater than 4 mm as coarse RCA and particle with a size lesser than 4 mm as fine RCA and further classifies coarse RCA in the following three categories:

- **Type I** aggregates originated primarily from masonry rubble.
- **Type II** aggregates originated primarily from concrete rubble.
- **Type III** aggregates consist of a blend of recycled aggregates and natural aggregates.

The above classification of the materials is based on the mandatory requirements stated in Table 2.1. In addition, RILEM (1984) specifies that the composition of type III aggregates shall meet the following additional requirements:

- the minimum content of natural aggregates is at least 80 % (m/m)
- the maximum content of type I aggregates is 10 % (m/m)

Table 2.1 Classification of coarse recycled concrete aggregates for concrete (RILEM, 1994)

Mandatory requirements	Coarse RCA Type I	Coarse RCA Type II	Coarse RCA Type III
Min. dry particle density (kg/m^3)	1500	2000	2400
Max. water absorption (% m/m)	20	10	3
Max. content of material with SSD < 2200 kg/m^3 (% m/m)	-	10	10
Max. content of material with SSD < 1800 kg/m^3 (% m/m)[a]	10	1	1
Max. content of material with SSD < 1000 kg/m^3 (% m/m and % v/v)	1	0.5	0.5
Max. content of foreign materials (metals, glass, soft material, bitumen) (% m/m)	5	1	1
Max. content of metals (% m/m)	1	1	1
Max. content of organic material (% m/m)	1	0.5	0.5
Max. content of filler (< 0.063 mm) (% m/m)	3	2	2
Max. content of sand (< 4 mm) (% m/m)[b]	5	5	5
Max. content of sulphate (% m/m)[c]	1	1	1

[a] *Water saturated surface-dry condition (SSD)*
[b] *If the maximal allowable content of sand is exceeded, this part of the aggregates shall be considered together with the total sand fraction.*
[c] *Water soluble sulphate content calculated as SO_3.*

2.6.3 Grading

Grading is the particle-size distribution of an aggregate as determined by sieve analysis. Various investigations (Hansen and Narud, 1983; Kawamura *et al*., 1983; Fergus, 1981) of fine crusher products below 5 mm are compared in Figure 2.12. All gradings fall within the shaded area of the grading curve. All the investigated samples were produced by crushing old concretes in a jaw crusher. It may be seen that all the gradings in Figure 2.12 are somewhat coarser than the lower limit of ASTM grading requirements for fine aggregates. Fergus (1981) found that the material finer than 75 micron in 38 mm maximum size coarse aggregates ranged from 0.3 to 0.5 %. Also in the case of fine recycled aggregate (material finer than 4 mm maximum size) depending on

the quality of aggregate, the material finer than 75 micron ranged from 4.1 to 6.6% whereas Hansen and Narud (1983) found that the range was 0.8 to 3.5 %.

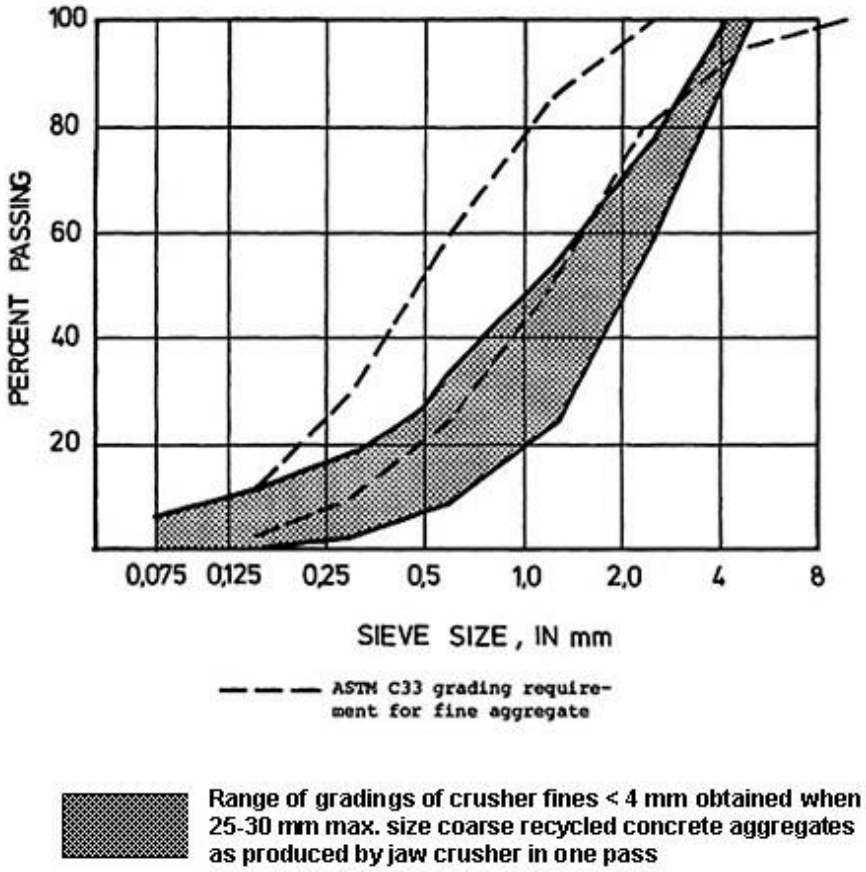

Figure 2.12 Range of gradings of crusher fines < 4 mm (fine aggregate) obtained when 25-30 mm max. size coarse recycled aggregates were produced by a jaw crusher in one pass (Hansen, 1986)

2.6.4 Water absorption

Water absorption capacity is defined as the total amount of water required to bring the aggregate to a saturated surface-dry condition. Aggregates may exist in several moisture states namely oven dry, air-dry, saturated surface-dry and moist and these are schematically illustrated in Figure 2.13. Neville (1997) stated that water absorption depends on the size and number of internal pores in the aggregates. Hasaba *et al*. (1981) found water absorption to be about 7 % for coarse RCA in the size range of 5 mm – 25mm and 11 % for fine recycled aggregate. When the water absorption is more than 7 % for coarse aggregates and more than 13 % for fine aggregates, the recycled aggregates should not be used for concrete production (BCSJ, 1977). In order to maintain uniform quality during concrete production, it is suggested to use presoaked aggregates (Hansen, 1986). Additional findings of earlier researchers on water absorption of coarse RCA are summarised in Table 2.2.

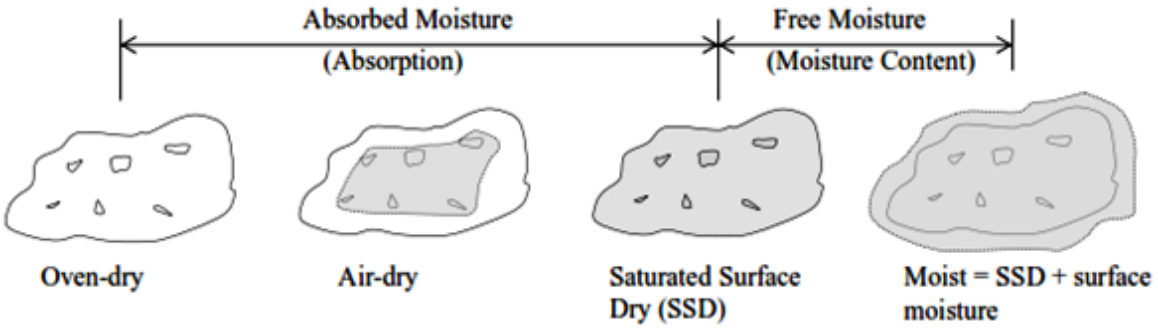

Figure 2.13 Various moisture states of aggregates (Neville, 1997)

Table 2.2 Summary of findings of various researchers on water absorption of coarse RCA (Butler, 2012)

Researcher(s)	Number of RCA sources studied	Water absorption
Bordelon *et al.* (2009)	1	5.3 %
Rahal (2007)	1	3.5 %
Tam and Tam (2007)	10	0.6 – 8.8 %
Lin *et al.* (2004)	1	7 %
Casuccio *et al.* (2008)**	2	3.9 %
Chen *et al.* (2003)	2	5 – 7.5 %
Padmini *et al.* (2009)**	3	3.6 – 4.9 %
Nagataki *et al.* (2004)*	3	4.9 – 6.3 %
Poon *et al.* (2004)	1	6.3 %
Movassaghi (2006)	2	5.2 – 11.6 %
Etxeberria *et al*. (2007)	1	4.5 %
Choi and Kang (2008)	3	2.7 – 6.3 %
Obla and Kim (2009)	4	4.3 – 5.9 %
Fathifazl *et al*. (2009)	2	3.3 – 5.4 %
Smith (2009)	1	4.3 %
Shayan and Xu (2003)	1	4.3 %
Gokce *et al*. (2004)	2	3.2 – 5.6 %
Hansen and Narud (1983)	3	5.7 – 6.0 %
Sagoe-Crentsil *et al*. (2001)	1	5.6 %
Xiao and Falkner (2007)	1	9.25 %

** Investigated a secondary crushing process which reduced the amount of adhered mortar and consequently, the absorption.*
***Used laboratory produced original concrete with nominal aggregate size of 20 mm.*

2.6.5 Bulk density

The bulk density of an aggregate is the mass of the aggregate divided by the volume of particles and the voids between particles. Independent of original concrete, Hansen and Narud (1983) found that the bulk densities of coarse RCA in SSD condition ranged from 2340 kg/m^3 (for 4 – 8 mm material) to 2490 kg/m^3 (for 16 – 32 mm material). The corresponding bulk densities of original coarse aggregates ranged from 2500 kg/m^3 to 2610 kg/m^3. Additional findings of earlier researchers on bulk density of coarse RCA are summarised in Table 2.3.

Table 2.3 Findings of selected researchers on bulk density of coarse RCA

Researcher(s)	Number of RCA sources studied	Bulk density (kg/m^3)
Belén *et al.* (2011)	4	2400 – 2580
Poon *et al*. (2009)	2	2330 – 2370
Etxeberria *et al.* (2007)	1	2430
Tam and Tam (2007)	10	2330 – 2580
Gokce et al. (2004)	2	2410 – 2500

2.6.6 Specific gravity

The specific gravity of an aggregate is the mass of the aggregate in air divided by the mass of an equal volume of water. Specific gravity of coarse RCA obtained by selected researchers are summarised in Table 2.4.

Table 2.4 Findings of selected researchers on specific gravity of coarse RCA

Researcher(s)	Number of RCA sources studied	Specific gravity (Bulk)	Specific gravity (SSD)	Specific gravity (Apparent)
Chen *et al*. (2003)	2	-	2.28 – 2.29	-
Obla and Kim (2009)	4	-	2.54 – 2.56	-
Smith (2009)	1	-	-	2.40
Tu *et al*. (2006)	1	-	2.48	2.35
Fathifazl *et al*. (2009)	2	2.31 - 2.42	2.42 - 2.50	2.64

2.6.7 Abrasion resistance

The abrasion resistance of an aggregate is a measure of its ability to resist being worn away by rubbing and friction or shattering upon impact. It is a general measure of aggregate quality and resistance to degradation due to handling, stockpiling, or mixing. According to Kosmatka *et al*. (2002), low abrasion resistance of an aggregate increases the quantity of fines in the concrete and increases water demand. Los Angeles abrasion test is the most common method for finding the abrasion resistance. BCSJ (1977) reported a Los Angeles abrasion loss of 12.5 to 35.1 % for coarse RCA sourced from 15 different countries and having a variety of strengths with the aggregate being obtained by different crushing methods. A selection of results on abrasion resistance of coarse RCA is presented in Table 2.5.

Table 2.5 Selected findings on abrasion resistance of coarse RCA (Butler, 2012)

Researcher(s)	Number of RCA sources studied	Los Angeles abrasion resistance	Micro-Deval abrasion resistance
Casuccio *et al.* (2008)	2	34 – 39 %	-
Obla and Kim (2009)*	4	23.8 – 26.0 %	-
Movassaghi (2006)	2	-	10.6 – 34.2 %
Hansen and Narud (1983)*	3	26.4 – 36.7 %	-
Shayan and Xu (2003)	1	32 %	-
Tu *et al.* (2006)	1	29.3 %	-
Smith (2009)	1	-	14.9 %

**Note: only 2 of the 4 RCA sources were derived from returned concrete*

2.6.8 Aggregate crushing value

The aggregate crushing value gives a relative measure of the resistance of an aggregate to crushing under a gradually applied compressive load. The compressive strength of concrete mainly depends on strength of the aggregate. Several codes like BS 812-110:1990 (1990) and IS 2386 (Part IV):1963 (1963a) provides guidelines for determining the aggregate crushing value (ACV). There is no direct correlation between ACV and aggregate compressive strength although values will sometimes be in agreement. It may be possible that the influence of aggregate on the strength of concrete is not only due to the mechanical properties of the aggregates, but also its absorption and bond characteristics (Neville, 1997). On the basis of tests on RCA derived from two different sources, Limbachiya (2010) concluded that the ACV for natural aggregate was

12.4 and for the RCAs it was 17.5 and 22.0 respectively. Table 2.6 shows some findings of researchers on aggregate crushing value of coarse RCA.

Table 2.6 Selected results on aggregate crushing value of coarse RCA (Butler, 2012)

Researcher(s)	Number of RCA sources studied	Aggregate crushing value
Padmini *et al.* (2009)*	3	23 – 26 %
Hansen and Narud (1983)	3	23.2 – 28.4 %
Sagoe-Crentsil et al. (2001)	1	23.1 %
Rakshvir and Barai (2006)	3	26.2 – 28.1 %
Shayan and Xu (2003)	1	24 %
Katz (2003)	1	24.3 %

**RCA was produced from laboratory concrete with nominal aggregate size of 20 mm*

2.6.9 Residual mortar content

The coarse RCA obtained after crushing process contains both natural aggregate and old hardened cement mortar attached to it to varying degrees. This hardened cement mortar is called as residual mortar. Though the amount of residual mortar may vary from sample to sample, it is estimated that residual mortar may constitute between 25 to 60 % of volume of the coarse aggregate particle. It is also reported that as the aggregate size decreases the residual mortar content increases (Hansen and Narud, 1983; Tu *et al*., 2006; Juan and Gutierrez, 2009). Properties like absorption, density, abrasion resistance and sulphate content are significantly affected by the residual mortar content. It is also reported that as the number of passes through the crushing cycle increases the amount of residual mortar decreases (Juan and Gutierrez, 2009; Nagataki *et al*., 2004). The amount of residual mortar can be determined by different methods. Hansen and Narud (1983) prepared RCA concrete cubes using various grades of RCA particles and red coloured cement. After hardening, the cubes were cut into slices and the slices polished. Mortar attached to natural gravel particles in recycled aggregates could be clearly distinguished both from the original gravel particles and from the red cement matrix. Chemical treatment is the most common method for determining residual mortar content. Hydrochloric acid method (Gokce *et al*., 2004, Nagataki *et al*., 2004, Poon *et al*., 2004), nitric acid method (Movassaghi, 2006), freeze-thaw method (Abbas et al., 2008) and thermal treatment method (Juan and Gutierrez, 2009) are the common methods adopted by the researchers. Findings of selected researchers on residual mortar content of coarse RCA are given in Table 2.7.

Table 2.7 Selected results on residual mortar content of coarse RCA (Butler, 2012)

Researcher(s)	Number of RCA sources studied	Method of residual mortar removal	Residual mortar content
Nagataki *et al*. (2004)	3	Hydrochloric acid dissolution	30.2 – 55.0 %
Gokce *et al*. (2004)	2	Hydrochloric acid dissolution	32.4 – 55.7 %
Fathifazl *et al*. (2009)	2	Freeze-thaw + sulphate attack	23 – 41 %
Movassaghi (2006)	2	Nitric acid dissolution	37.6 – 62.6 %
Liu *et al*. (2011)	2	Image analysis	42.2 – 46.5 %
Juan and Gutierrez (2009)**	1	Thermal treatment	40 – 55 %
Hansen and Narud (1983)	3	Linear traverse method	41 – 43 %

**Note: the linear traverse method is based on a percent volume of residual mortar.*
***The RCA sample came from one recylcing plant however, 15 separate samples were tested.*

2.6.10 Specifications of recycled concrete aggregates

In the following sections, a summary of design code recommendations related to RCA is presented.

2.6.10.1 American concrete institute (ACI)

The ACI 318-11 (2011) does not include specific provisions on using RCA concrete in building construction. The ACI 555R-01 (2001b) provides guidelines for the removal and reuse of hardened concrete. Guidance on production of concrete from recycled aggregate is given in section 5 which includes a discussion on aggregate production process, aggregate quality, effects of recycled aggregates on concrete properties and guidelines for mixture proportioning.

2.6.10.2 British standard

The British standard BS 8500-2:2002 (2002) allows the use of coarse RCA in concrete. Recycled aggregate is classified into two classes namely recycled concrete aggregate (RCA) and recycled aggregate (RA). The RCA should consist of more than 95 % of crushed concrete whereas the RA comprises less than 95 % of crushed concrete. The other requirements specified in BS 8500-2:2002 (2002) are compiled in Table 2.8.

Table 2.8 Requirements of BS 8500-2:2002 for RCA and RA (BSI, 2002)

Items	Recycled concrete aggregate [a, b]	Recycled aggregate
Max. masonry content, %	5	100
Max. fines, %	5	3
Max. lightweight material (density < 1000 kg/m^3), %	0.5	1
Max. asphalt, %	5	10
Max. other foreign materials, %	1	1
Max. acid-soluble sulphates, SO_3	1	-[c]

[a] *Where the material to be used is obtained by crushing hardened concrete of known composition and which has not been contaminated by use, the only requirements are those for grading and maximum fines.*
[b] *The provisions for recycled concrete aggregate may be applied to mixtures of natural coarse aggregate blended with the listed constituents.*
[c] *The appropriate limit needs to be determined on a case-by-case basis.*

2.6.10.3 Canadian standards association (CSA)

Currently there is no specific section on the use of RCA in Canadian standards. However in CSA A23.1-09 (2009) clause 4.2.3.1 reference is given for using recycled concrete as aggregate. It states that aggregates should be evaluated in a similar manner to normal density aggregates and the following parameters should be assessed: durability characteristics, deleterious materials, potential alkali-aggregate reactivity, chloride contamination, and workability characteristics of concrete made using the recycled aggregates.

2.6.10.4 European guidelines (RILEM)

RILEM (1994) provides detailed specifications for concrete made with recycled aggregates. Based on the nature of the aggregates, these guidelines classify coarse RCA into three categories namely **type I** (originated from demolished masonry rubble), **type II** (originated from concrete rubble), and **type III** (combination of recycled aggregates and natural aggregates). The provisions for the use of recycled aggregates in concrete are presented in Table 2.9.

Table 2.9 Provisions for the use of recycled aggregates in concrete (RILEM, 1994)

Recycled aggregates	Coarse RCA Type I	Coarse RCA Type II	Coarse RCA Type III
Max. allowable strength class	C16/20[a]	C50/60	No limit
Additional testing required when using in exposure class 1[b]	None	None	None
Additional testing required when used in exposure classes 2a, 4a	ASR expansion test [c] Use in class 4a not allowed	ASR expansion test	ASR expansion test
Additional testing required when used in exposure classes 2b, 4b	Use in classes 2b, 4b not allowed	ASR expansion test Bulk freeze-thaw test	ASR expansion test Bulk freeze-thaw test
Additional testing required when used in exposure class 3	Use in class 3 not allowed	ASR expansion test Bulk freeze-thaw test Deicing salt test	ASR expansion test Bulk freeze-thaw test Deicing salt test

[a] *However, the strength class may be increased to C30/37 subject to the condition that the saturated surface-dry (SSD) density of the recycled aggregates exceeds 2000 kg/m^3.*
[b] *Confirming with ENV 206.*
[c] *Expansion test to evaluate alkali-silica reactivity.*

2.6.10.5 German institute for standardisation

The German standard, DIN 4226-100 (2002), allows the use of RCA in concrete. All the aggregates should satisfy the requirements mentioned in Table 2.10. Four separate classes of RCA are recognised in this standard.

Table 2. 10 DIN 4226-100 requirements for use of RCA in concrete (DIN, 2002)

Constituents (% by mass)	Type 1	Type 2	Type 3	Type 4
Concrete and natural aggregates according to DIN 4226-1	≥ 90	≥ 70	≤ 20	≤ 80
Clinker, no porous clay bricks	≤ 10	≤ 30	≥ 80	
Calcium silicate bricks	-	-	≤ 5	
Other mineral materials (e.g., porous brick, lightweight concrete, plaster, mortar, porous slag)	≤ 2	≤ 3	≤ 5	≤ 20
Asphalt	≤ 10	≤ 30	≤ 1	
Foreign substances (e.g., glass, plastic, metal, wood, paper, other)	≤ 0.2	≤ 0.5	≤ 0.5	≤ 1
Oven-dry density (kg/m^3)	≥ 2000	≥ 2000	≥ 1800	≥ 1500
Maximum water absorption after 10 min (%)	10	15	20	No limit

2.6.10.6 Japanese industrial standard

According to the Japanese Standards Association, recycled aggregates are classified into three categories namely low quality, Class L, medium quality, Class M, and high quality, Class H. Class L aggregate concrete includes backfilling, filling and levelling concrete application. For members subjected to drying or freezing and thawing action, Class M can be used and for normal concrete applications Class H can be used. JIS A 5023 (2012), JIS A 5022 (2012) and JIS A 5021 (2011) give specifications for Class L, Class M and Class H recycled aggregates respectively. Physical property requirements for Class H recycled aggregates are presented in Table 2.11.

Table 2.11 JIS A 5021 requirements for use of high-quality RCA in concrete (JIS, 2011)

Items	Coarse aggregate	Fine aggregate
Oven-dry density, kg/m^3	≥ 2500	≥ 2500
Water absorption, %	≤ 3.0	≤ 3.0
Abrasion, %	≤ 35	NA
Solid volume percentage for shape determination, %	≥ 55	≥ 53
Amount of material passing test sieve 75 µm, %	≤ 1.0	≤ 7.0
Chloride ion content	≤ 0.04	-

2.6.10.7 Korean standard

The Korean standard KS F 2573:2011 (2011) allows the use of RCA in new concrete. The requirements specified in KS F 2573:2011 (2011) are compiled in Table 2.12.

Table 2.12 Korean standard requirements on use RCA in concrete (KSA, 2011)

Items	Coarse aggregate	Fine aggregate
Oven-dry density, kg/m^3	≥ 2440 – 2500	≥ 2200
Water absorption, %	≤ 3.0 – 10	-
Soundness, %	≤ 12	≤ 10
Clay lumps, %	≤ 0.2	-
Maximum aggregate size, mm	≤ 20 – 25	-
Fineness content (< 0.063 mm), %	≤ 1 – 10	-

2.7 PROPERTIES OF CONCRETE MADE WITH RECYCLED AGGREGATES

2.7.1 Mixture proportioning

Three RCA concrete mixture design methods namely Direct weight replacement (DWR) method, Equivalent mortar replacement (EMR) method, and Direct volume replacement (DVR) method are reported in the literature.

2.7.1.1 Direct weight replacement (DWR) method

Due to its simplicity, the direct weight replacement (DWR) method has been adopted by most researchers (Buck, 1977; Nishibayashi *et al*., 1984; Yamato, 1998; Dhir *et al*., 1999; Abbas *et al*., 2008; Xiao and Falkner, 2007; Knaack and Kurama, 2013). In this method, for any selected replacement level, the weight of the total coarse aggregate (i.e., coarse NCA and coarse RCA) is kept constant. The water content (mixing water beyond saturated surface-dry condition of the aggregates) and the cement content are also kept constant. Since the specific gravity of RCA is less than natural aggregate, the equal weight of RCA typically occupies a greater volume than natural aggregate. To maintain the same volumetric yield, a small reduction in the amount of fine aggregate may be made in the mixture. Dhir *et al*. (1999) reported that the increased volume of coarse aggregate in the mixture causes a gradual reduction in workability (Knaack and Kurama, 2013).

2.7.1.2 Equivalent mortar replacement (EMR) method

The equivalent mortar replacement (EMR) method was proposed and used by Abbas *et al*. (2008). Fathifazl *et al*. (2009) and Knaack and Kurama (2013) have also adopted this method. In this method the RCA is treated as a two-phase material made of the coarse recycled natural aggregate (RNA) (i.e., coarse natural aggregate in the RCA) and residual mortar (i.e., mortar attached to the RNA) rather than as a single material. Since the volume of the residual mortar (RM) is assumed to become a part of the total mortar volume in the concrete, the volume of total mortar (i.e., residual plus fresh mortar) and the total coarse natural aggregate (i.e, recycled plus new coarse natural aggregate) is taken to be the same as in the target NCA concrete (NAC) mixture. This requirement can be stated as (Equation 2.34)

$$V_{RM}^{EMR} + V_{FM}^{EMR} = V_{FM}^{NAC} \quad and \quad V_{RNA}^{EMR} + V_{NA}^{EMR} = V_{NA}^{NAC} \tag{2.34}$$

where V_{RM}^{EMR} is the volume of residual mortar (RM) in the EMR mixture, V_{FM}^{EMR} is the volume of fresh mortar (FM) in the EMR mixture, V_{FM}^{NAC} is the volume of FM in the NAC mixture, V_{RNA}^{EMR} is the volume of coarse recycled natural aggregate (RNA) in the EMR mixture, V_{NA}^{EMR} is the volume of new coarse natural aggregate (NA) in the EMR mixture, and V_{NA}^{NAC} is the volume of coarse natural aggregate in the NAC mixture. The reduction in fresh mortar in the EMR mixture significantly reduces the workability of concrete thus giving a limitation to the maximum aggregate replacement. As a result in EMR mixtures, Abbas *et al*. (2008) used significant amounts of water-reducing admixtures and relatively low levels of aggregate replacement in his EMR mixtures (Knaack and Kurama, 2013).

2.7.1.3 Direct volume replacement (DVR) method

Based on the volume of each ingredient, ACI 211.1-91 (1991) and ACI 211.4R-08 (2008) provide a method for proportioning NCA concrete for normal and for high-strengths respectively. The so-called direct volume replacement (DVR) method has also been used for designing RCA concrete mixtures (Topcu and Sengal, 2004; Etxeberria et al., 2007; Obla et al., 2007; Corinaldesi, 2010; Knaack and Kurama, 2013). The DVR method treats RCA as a single-phase coarse aggregate and a given volume of NCA in the target mixture is replaced by the same volume of RCA. Because the resulting volumetric proportions of total coarse aggregate (RCA plus NCA), fine aggregate, cement, and water remain unchanged between the NCA and the RCA concrete there will not be a significant loss in workability in DVR concrete other than that due to differences in the surface texture and angularity of the aggregates, as long as the greater absorption of RCA (as compared with NCA) is incorporated into the design (Knaack and Kurama, 2013).

2.7.2 Characteristic of fresh recycled aggregate concrete

2.7.2.1 Workability

It has been reported in the literature that as the amount of RCA in the concrete mixture increases the slump value decreases. This is attributed to the higher water absorption of the RCA particles. In RCA concretes produced with coarse RCA, Mukai *et al*. (1978) found that 5 % more free water was required to achieve the same slump as the control NCA concrete and when using both fine and coarse RCAs, 15 % more free water was required. Similar results were found by Buck (1977), Frondistou-Yannas (1977), Malhotra (1978), Hansen and Narud (1983), and by Ravindrarajah and Tam (1985). Poon *et al*., 2004 reported a slump loss was noticed when using RCA in SSD moisture condition. Researchers like Oliverira *et al*. (1996) and Poon *et al*. (2002, 2004) have

suggested that the change in moisture condition of the RCA particles will improve workability.

2.7.2.2 Wet unit weight and air content

Mix design and efficiency of compaction affects the air content and the density. Hansen (1986) concluded that in RCA concrete, air content may be slightly higher than that of control concrete made with natural aggregates. The density of RCA concretes is always lower than that of control mixtures. Reduction in density may vary from less than 5 % to more than 15 %. In the case of 100 % replacement with RCA, Katz (2003) found air content to be 4 to 5.5 % more than that in the control NCA concrete. It has been reported that whereas the bulk density of fresh concrete made with natural aggregate is about 2400 kg/m^3, the value for concrete made with RCA was about 2150 kg/m^3 (Topcu and Guncan, 1995; Katz, 2003).

2.7.3 Characteristic of hardened recycled aggregate concrete

2.7.3.1 Compressive strength

Based on the review of the literature, Nixon (1978) concluded that compressive strength of RCA concrete is up to 20 % lower than that of NCA concrete. On the basis of experimental work, BCSJ (1978) showed that the compressive strength of RCA concrete is between 14 to 32 % lower than that of NCA concrete. Xiao and Falkner (2007) reported 20 % reduction of compressive strength for 100 % replacement of NCA with RCA. Hansen and Naurd (1983) concluded that the compressive strength of RCA concrete depends on the strength of the original concrete. When others factors are essentially identical, the strength is largely controlled by the w/c ratio of both original and RCA concretes. If the w/c ratio of the original concrete is the same as or lower than that of the RCA concrete, then the new strength can be as good as the strength of the original concrete. The influence of the w/c ratio on compressive strength of 100 % RCA concrete was studied by Deng (2008). It was found that the compressive strength of RCA heavily depend on the w/c ratio. For w/c ratio higher than 0.57, compressive strength of RCA concrete decreases with increase in w/c ratio. However, if w/c ratio is below 0.57, the compressive strength of RCA concrete increases with increase of w/c ratio. With the same w/c ratio (w/c = 0.5) and cement quantity (325 kg of cement /m^3), Etxeberria *et al*. (2007) observed between 20 to 25 % reduction in compressive strength of RCA concrete at 28 days. The effect of mixture design on compressive strength of normal-strength RCA concrete has been reported by Knaack and Kurama (2013). It was found that using varying amounts of direct volume

aggregate replacement, direct weight replacement and equivalent mortar replacement gave similar compressive strengths and elastic modulus of RCA concrete.

2.7.3.2 Tensile strength

In general, tensile strength of concrete falls between 8 and 15 % of the compressive strength. The type of test, the type of aggregate, the compressive strength, and the presence of a compressive stress transverse to the tensile stress strongly affect tensile test results (Wight and MacGregor, 2012). Typical configurations for measuring the tensile strength of concrete include the direct tension test, the splitting tensile test using cylindrical specimens, and the flexural-tensile test using prismatic beam specimens. According to Neville (1997), tensile strength of concrete may be influenced by coarse aggregate properties and therefore the tensile strength of RCA concrete can be expected to be different from the tensile strength of NCA concrete. According to Etxeberria *et al*. (2007), splitting tensile strength of RCA concrete is comparable to that of NCA concrete and in some cases it may even be higher. This has been attributed to the absorption capacity of the residual mortar present in the recycled aggregate and the effectiveness of the new interfacial transition zone in the RCA concrete. The literature indicates that compared to the RCA content, the splitting tensile strength of RCA concrete is more sensitive to its compressive strength. As with NCA concrete, in RCA concrete also, as the compressive strength increases, the tensile strength also increases, but not at the same ratio. Ajdukiewicz and Kliszczewicz (2002) have reported that high performance concrete mixtures made with natural aggregate always had higher tensile strengths than comparable RCA concrete mixtures, though the difference was never more than 10 %.

2.7.3.3 Flexural strength

BCSJ (1978) reported that as with NCA concrete, the flexural strength of RCA concrete is between 1/5 and 1/8 of the compressive strength. Abou-Zeid *et al*. (2005) reported that the flexural strength of RCA concrete was similar or slightly less than NCA concrete. However the flexural-compressive strength ratio has been observed to be slightly higher for the RCA concrete. This may be attributed to superior bond between RCA particles and the cement binder due to the rough surface and angularity of the aggregate. Abou-Zeid *et al*. (2005) also believed that the relatively better flexural behaviour of RCA concrete may be due to some form of reaction between the recycled concrete and the surrounding cement paste. Unlike the above observations, Malhotra (1976) found lower flexural strengths for RCA concrete than for NCA concrete.

2.7.3.4 Modulus of elasticity and Poisson's ratio

Since the residual mortar has comparatively lower modulus of elasticity, the modulus of elasticity of RCA concrete is always lower than that of NCA concrete (Hansen, 1986). Compared to NCA concrete, RCA concrete may have up to 40 % lower modulus of elasticity. For example, Frondistou-Yannas (1977) and Gerardu and Hendriks (1985) respectively found elastic modulus of RCA concrete to be up to 40 % and 15 % lower when compared to NCA concrete. Xiao *et al*. (2005) investigated the mechanical properties of RCA concrete with various replacement levels (0 %, 30 %, 50 %, 70 % and 100 %) and measured the complete stress-strain behaviour. They found that as the replacement level increases, the modulus of elasticity decreases and a reduction of 45 % was observed for 100 % replacement level. Knaack and Kurama (2013) found that in the case of normal-strength concrete with recycled concrete aggregates mixture design methods such that direct volume aggregate replacement, direct weight replacement and equivalent mortar replacement had no significant effect on elastic modulus of RCA concrete. They also observed that while the effect of increased amounts of RCA on the concrete compressive strength was generally small for all the three mixture design methods, the concrete elastic modulus is more significantly affected by the amount of RCA.

Poisson's ratio of concrete is mainly dependent on the properties of aggregate and ranges between 0.15 and 0.22 and is generally the same under compressive or tensile loading (Neville, 1997). The Poisson's ratio for RCA concrete is found to vary between 0.15 and 0.23 (Hu *et al*., 2009; Li, 2007) and the values are similar to that of NCA concrete. On the basis of their investigations with RCA derived from high-strength concrete, Ajdukiewicz and Kliszczewicz (2002) reported that there is no significant difference in Poisson's ratio between NCA and RCA concretes for a range of compressive strengths (38.7 to 89.2 MPa). They reported 28 day Poisson's ratio vales ranging between 0.17 and 0.22.

2.7.3.5 Fracture energy

Ong and Ravindrarajah (1987) compared fracture energy of low and high strength concrete produced using natural aggregates, RCAs, and a combination of natural aggregates and RCAs. To determine the fracture engergy, 50 mmx 50 mmx 650 mm prisms were casted and tested with 25 mm notches cut at their mid-spans. They concluded that the concrete produced using natural aggregates had higher fracture energies than the RCA concretes. They attributed this difference to the weaker bond between the cement paste and the RCAs which causes less complex micro-cracking and consumes less energy during crack propogation. Casuccio et al. (2008) have reported

similar trends with their RCA concrete having lower stiffness (13 – 18 %) and significantly lower fracture energies (27 – 45 %) compared to the control NCA concrete. They attributed this difference to a decrease in elastic compatibility between the mortar and the coarse RCAs. Recently, Arezoumandi et al. (2014) have reported that fracture energy decreases with the increasing RCA replacement level.

2.8 BOND OF STEEL REINFORCEMENT IN RECYCLED AGGREGATE CONCRETE

Limited research has been carried out on bond behaviour between RCA concrete and steel bars. Ajdukiewicz and Kliszewicz (2002) conducted pullout tests (as per the recommendations of RILEM (1983)) on high performance RCA concrete using cubical specimens embedded with 14 mm diameter plain and ribbed bars. They have reported that for 100 % coarse and fine RCA replacement, 20 % reduction in peak bond stress was observed. When using 100 % coarse aggregate and natural fine aggregate, the reduction was only 8 %.

Xiao and Falkner (2007) performed pullout tests in accordance with the Chinese standard GB 50152-92 (1992) with three RCA replacement levels (0 %, 50 %, and 100 %). Both plain and deformed bars having 10 mm diameters embedded in cubes of size 100 mm x 100 mm x 100 mm were used in this investigation. Figure 2.14 and Figure 2.15 show a pullout specimen and the pullout test setup respectively. The slip of the bar was measured by two high precision linear variable differential transducers (LVDTs). It has been reported that the bond development and deterioration in RCA concrete is similar to that in NCA concrete. The authors report that under the condition of equivalent mix proportions, bond strength between plain bars and RCA concrete decreased by 12 % and 6 % for 50 % and 100 % RCA replacement level respectively. In the case of the deformed bars, the bond strength of NCA and RCA concrete was similar irrespective of the RCA replacement level. It has been postulated that since the bond of deformed bars mainly depends on mechanical anchorage and frictional resistance therefore the influence of RCA replacement level on bond of deformed bars is not very significant. The authors have recommended that for deformed bars embedded in 100 % RCA concrete, the anchorage length could be the same as NCA concrete. Based on a regression analysis of test data, the authors have presented a model for representing the bond-slip relationship of plain and deformed bars embedded in RCA concrete.

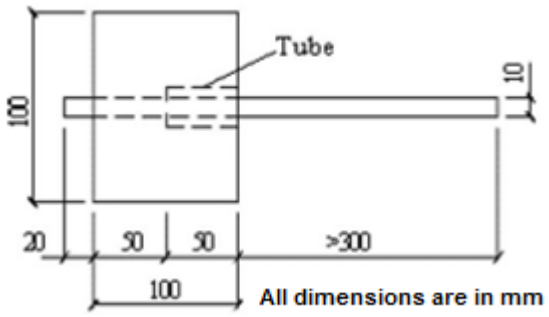

Figure 2.14 Pullout specimen configuration (Xiao and Falkner, 2007)

Figure 2.15 Pullout test setup (Xiao and Falkner, 2007)

Morohashi *et al*. (2007) tested RCA concrete splice specimens to evaluate splitting bond strength. The specimens were so designed that splitting bond failure would occur before flexural yielding of the main reinforcement. Figure 2.16 shows the dimensions and reinforcement details of the splice specimens. A lap splice length of 30 times the rebar diameter (570 mm) was adopted at the bottom of the specimens in the region of pure bending. It has been reported that bond splitting was independent of the substitution rate of high-quality coarse RCA and bond splitting in the RCA concrete was similar to that in NCA concrete. Similar flexural crack widths and bond strengths were obtained for the NCA and the 100 % RCA concretes. Based on their findings they have suggested that beams made with high-quality RCA concrete can be used for architectural structures.

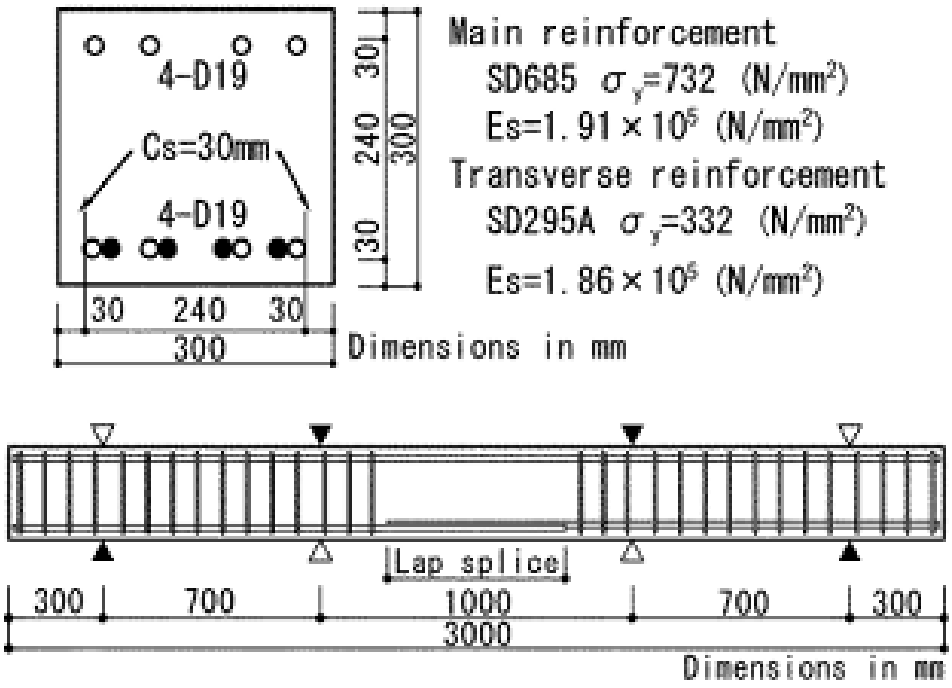

Figure 2.16 Dimensions and reinforcement details of the splice beam specimens (Morohashi *et al*., 2007)

Choi and Kang (2008) investigated bond behaviour of deformed bars in RCA concrete by using pullout test cube specimens of size 150 mm x 150 mm x 150 mm. The test parameters included three RCA grades namely (coarse RCA (RG) of grade I, coarse RCA (RG) of grade III, and fine RCA (RS) of grade II), two *w/c* ratios (40 % and 50 %), and four replacement levels (0 %, 30 %, 50 %, and 100 %). High-strength deformed bars of 16 mm diameter with yield strength of 800 MPa were used in the investigation. The pullout tests were carried out in accordance with ASTM A944-05 (2005). The loaded-end slip and the unloaded-end slip were measured by three electric dial gauges EDG) of accuracy 1/1000 mm. The test setup configuration is shown in Figure 2.17. The variation of mean pullout bond strength with RCA replacement levels and w/c ratio is presented in Figure 2.18. It was observed that the bond-slip relationship shows a similar trend for both RCA and NCA concretes having w/c ratio of 0.4 and up to 50 % replacement levels. But in the case of w/c ratio of 0.5 and up to 50 % replacement levels, the bond-slip relationship was seen to be more sensitive to the quality of the recycled aggregate and the replacement level. It was concluded that the ACI 408 model (ACI, 1966) over estimates bond strength of RCA concrete and therefore this model will lead to unconservative splice lengths.

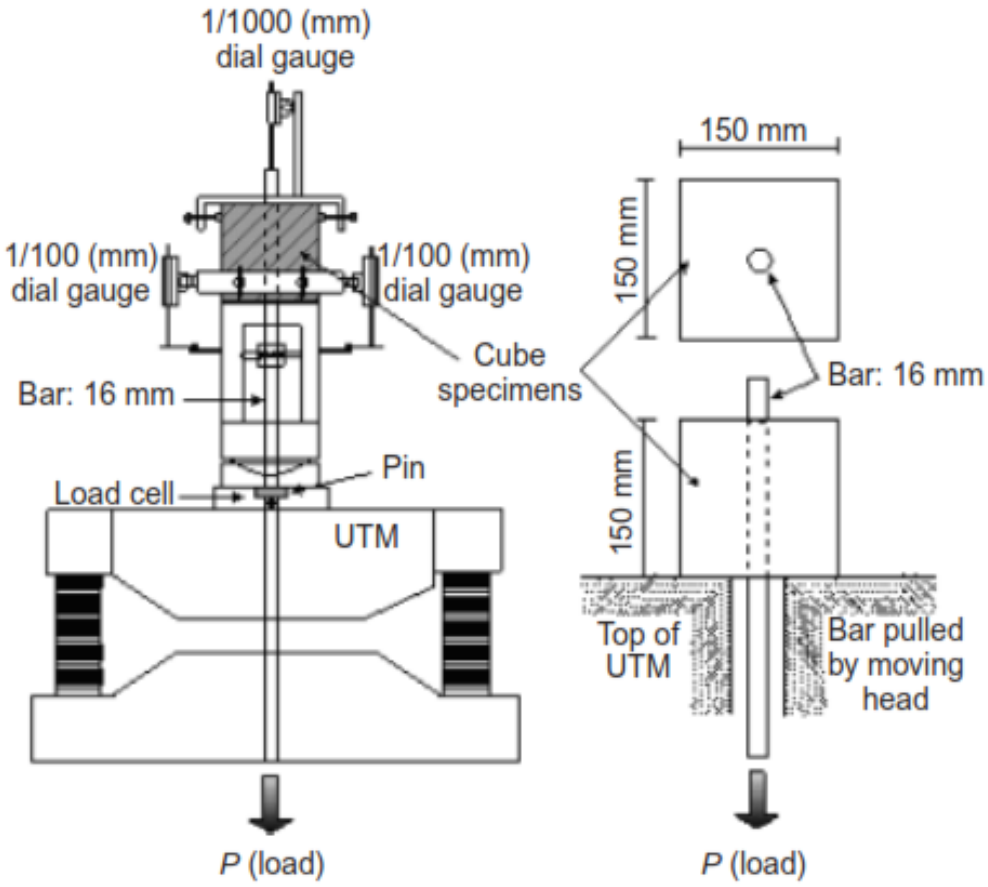

Figure 2.17 Test setup configuration of Choi and Kang (2008)

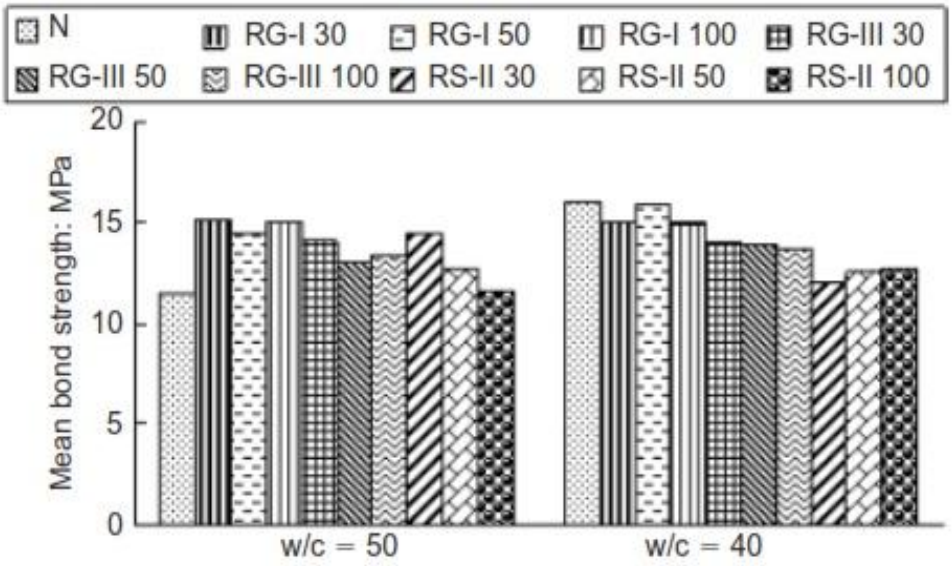

Figure 2.18 Variation of mean pullout bond strength with RCA replacement levels and w/c ratio (Choi and Kang, 2008)

Corinaldesi and Moriconi (2009) conducted pullout tests based on the recommendations of RILEM (1983) using 150 mm cubes embedded with 16 mm diameter plain and ribbed bars. The bonded length was 5 times the bar diameter. Three mixes, namely a reference mix (REF) made with NCA, RCA concrete without flyash (REC), and RCA concrete with flyash (REC+FA) were employed. It is worth nothing that both the natural coarse aggregate as well as the natural fine aggregate were completely replaced with recycled aggregates. A 6 % and 20 % increase in bond strength was observed for the REC and the REC+FA mix respectively. Typical load-slip curves for each category of concrete-bar coupling are shown in Figure 2.19.

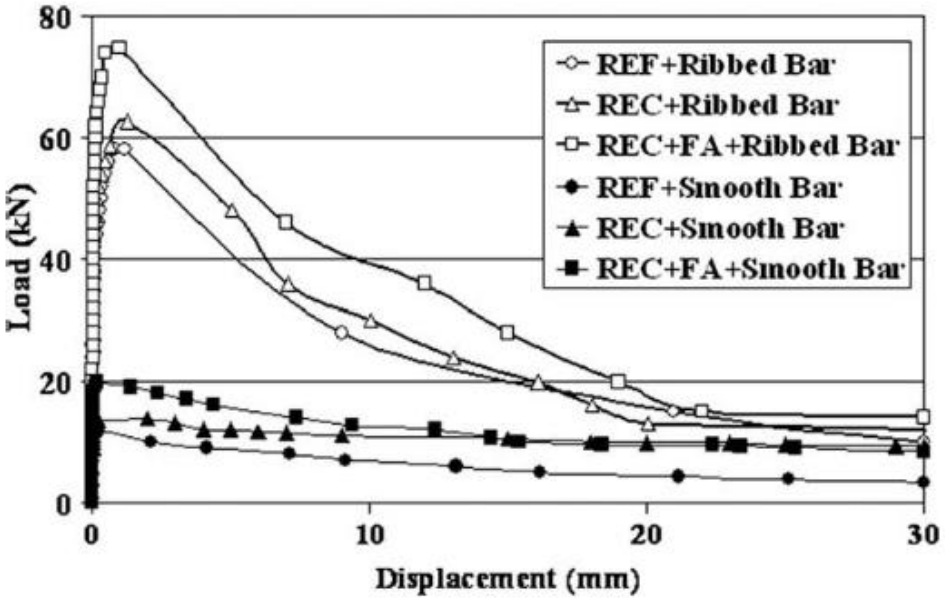

Figure 2.19 Typical load-slip curves for various concrete-rebar combinations (Corinaldesi and Moriconi, 2009)

In order to investigate the bond-slip behaviour between RCA concrete and steel bars, Bai *et al*. (2010) conducted 120 pullout tests in accordance with the Chinese standard GB 50152-92 (1992). The following were the parameters in this investigation: two w/c ratios (0.4 and 0.55), five RCA replacement levels (0 %, 30 %, 50 %, 70%, and 100 %), and four types of steel bars (12 mm plain bars, 25 mm, 18 mm and 12 mm deformed bars). Figure 2.20 shows the details of the pullout specimens. It was found that for the deformed bar specimens, as the cube strength increased, the bond strength also increased whereas cube strength had little effect on bond in the plain bar specimens. Further, when the RCA replacement level increased from 0 % to 100 %, the bond strength in the case of deformed bar decreased in the range of 5 % to 25 % but this effect was negligible in the case of the plain bars. It was observed that bond strength of the deformed bars embedded in RCA concrete was approximately 200% to 400 % higher than that for plain bars embedded in RCA concrete.

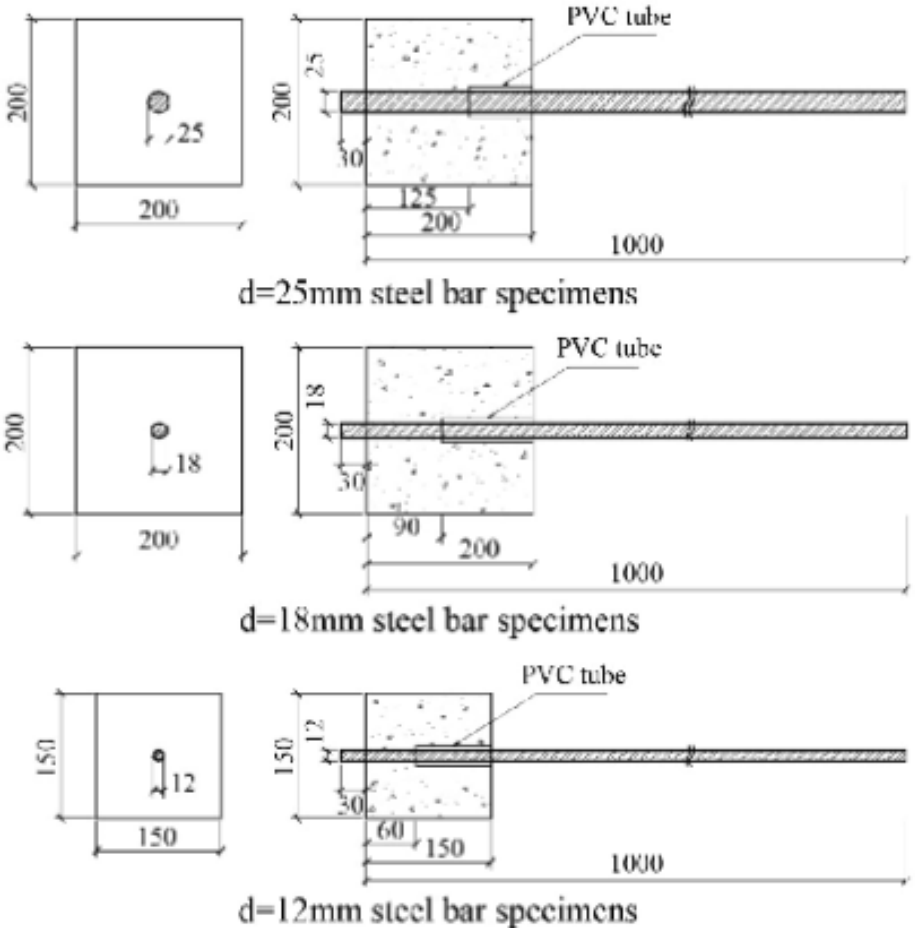

Figure 2.20 Details of the pullout specimens (Bai *et al*., 2010)

Butler *et al*. (2011) investigated bond strength between RCA concrete and steel reinforcement by testing beam-end specimens following the guidelines in ASTM A944-05 (2005). Three concrete mixtures were investigated namely, control (NAC), direct replacement (RAC1), and strength-based (RAC2). In order to achieve the target strengths of 30 and 50 MPa, two controls mixtures were proportioned with natural aggregate with slump values between 75 and 100 mm. Figure 2.21 shows the beam-end specimen dimensions and reinforcement details. The beam-end test setup configuration, the frame test setup and a typical beam-end specimen are depicted in Figure 2.22. It was concluded that for the natural aggregate concrete beam-end specimens the bond strengths were 10.4 % to 19 % higher than RCA1 and 9.4 % to 21.3 % higher than RCA2 concrete specimens. It has been reported that for a given grade of RCA concrete, the RCA replacement level had a significant impact on bond strength.

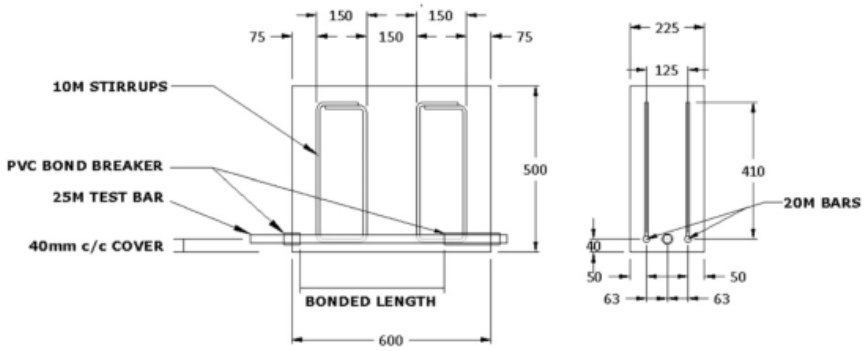

Figure 2.21 Beam-end specimen dimensions and reinforcement details (Butler *et al*., 2011)

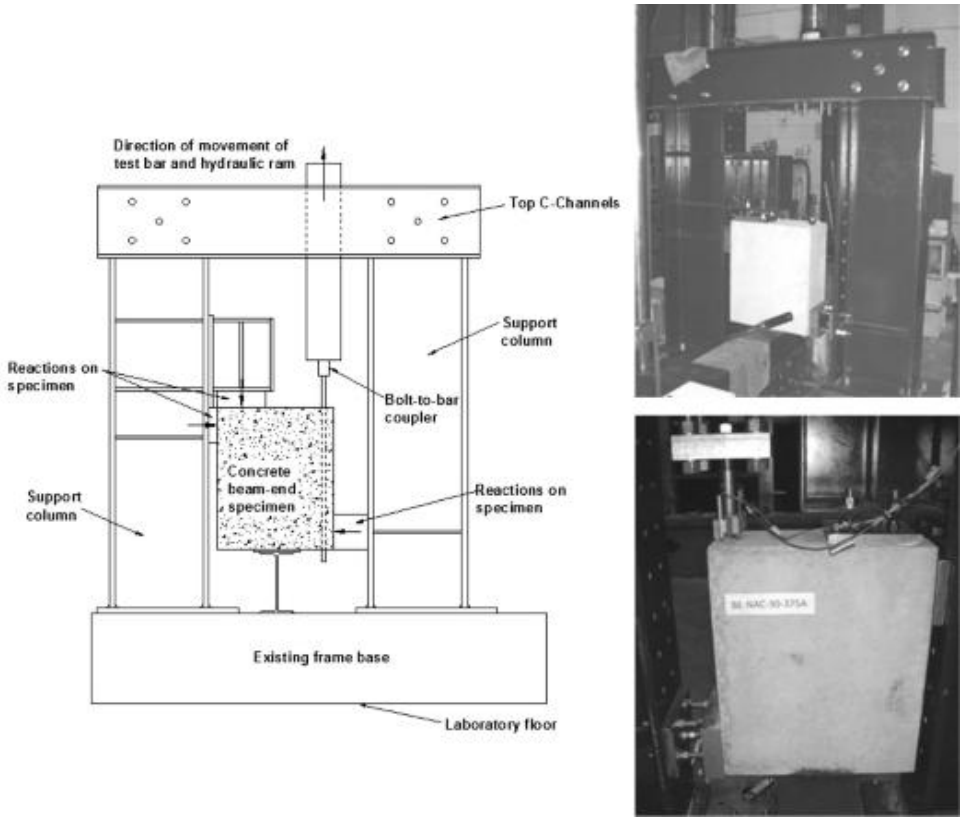

Figure 2.22 Beam-end test setup configuration, completed test frame and a typical beam-end specimen (Butler *et al*., 2011)

To investigate the bond strength of deformed steel bars in RCA concrete, Fathifazl *et al*. (2012) tested 12 beam-end specimens per the guidelines given in ASTM A944-05 (2005). The variables were: mix proportion method, bar size, and aggregate type. It has been reported that when proportioned using the equivalent mortar volume method, the bond strength of RCA concrete is comparable with NCA concrete whereas if the RCA concrete is proportioned using conventional methods, then 18 % to 33 % higher bond strengths were obtained in the NCA concrete compared to the RCA concrete.

To investigate the bond characteristics of RCA concrete, Kim *et al*. (2012) conducted pullout tests by modifying the specimen and the test setup configuration given in the Korean standard, KS F 2441 (2010). Deformed bars having a diameter of 19 mm were embedded in concrete prisms with five mixture proportions namely NN (100 % coarse NA + 100 % fine NA), RN (100 % coarse RCA + 100 % fine NA), RR30 (100 % coarse RCA + 30 % fine aggregate replaced with RCA), RR60 (100 % coarse RCA + 60 % fine aggregate replaced with RCA), and RR (100 % coarse RCA + 100 % fine aggregate replaced with RCA). The pullout load was applied at a stain- controlled rate of 0.5 mm/min and rebar slip was recorded by extensometers. It has been reported that bond strength decreased with increase in replacement of natural aggregates with recycled aggregates. It was observed that the bond strength predictive equations in CEB-FIP MC90 (1990), ACI 318-08 (2008), Orangun *et al*. (1977), MacGregor (1997), which were originally formulated for NCA concrete do not gave accurate predictions for bond strengths of RCA concrete. This has been attributed to the fact that the above equations do not effectively account for the various characteristics of RCA concrete. The authors proposed a new expression for evaluating bond strength of RCA concrete by introducing RCA replacement level as a parameter and this equation has been reported to give good prediction for their test results.

Kim and Yun (2013) conducted 144 pullout tests to investigate bond strength of deformed bars in RCA concrete. The variables were: aggregate size (20 mm and 25 mm), coarse RCA replacement level (0 %, 30 %, 60 %, and 100 %), bar direction (vertical and horizontal), and bar location (75 mm and 225 mm from the bottom). The RCA was classified into RCA-I (with 20 mm maximum size particles) and RCA-II (with 25 mm maximum size particles). The specimens were fabricated and tested in accordance with ASTM C234-91a (1994) and CSA S806-02 (2002) respectively. The load was applied at a rate of 1.2 mm/min in displacement control mode. It was observed that regardless of ageing, similar bond strength was obtained in the RCA-I specimens even though the compressive strength decreased with increase in RCA replacement level. It was also noted that settlement of coarse aggregates affects the uniformity of bond stress distribution in RCA-II.

Breccolotti and Materazzi (2013) evaluated bond strength between RCA concrete and steel rebars using pullout specimens fabricated and tested in accordance with RILEM (1983). The specimen size adopted was 200 x 200 mm cross section and 150 mm height with 14 mm diameter reinforcing steel casted in two groups of concrete mixtures having three mixtures in each group. It has been reported that in the case of concrete with 100 % coarse RCA a 19 % and 8 % reduction in bond strength in each group was noticed with respect to the control concrete.

Seara-Paz *et al*., (2014) evaluated bond strength of RCA concrete by conducting pullout tests on 100 mm x 100 mm x 100 mm cubic specimens with 10 mm deformed bars embedded in eight concrete mixtures. The parameters include the age of concrete (7, 28, 90, and 365 days), w/c ratio (0.5 and 0.65), and replacement level (0 %, 20 %, 50 %, and 100 %). The pullout specimens were tested at a constant rate of 0.6 mm/min in displacement control mode following the guidelines of RILEM (1983). It has been reported that at 28 days, for the RCA concretes H50-20, H50-50, and H50-100 the maximum bond stress was reduced by 9 %, 16 %, and 27 % respectively and for the RCA concretes H65-20, H65-50, and H65-100 the reductions were 4 %, 12 %, and 22 % respectively. Based on the experimental results, a bond strength equation based on *fib* MC 2010 (2013) has been proposed by introducing an additional term to account for the effect of RCA replacement level.

In extension of their previous work (Butler *et al*., 2011), Butler *et al*. (2014) carried out bond tests on RCA concrete in accordance with ASTM A944-05 (2005) using beam-end specimens. The test setup and the specimen configurations were similar to that used in their earlier investigation (Butler *et al*., 2011). One NCA and three RCA sources were evaluated and used in 14 different concrete mixtures with four compressive strength levels. A total of 48 beam-end specimens incorporating several bonded lengths were tested. They have reported that when comparing with the NCA concrete, up to 21 % reduction in bond strength was noticed in the RCA concrete. A regression model has been proposed to relate bond strength to coarse aggregate strength, concrete compressive strength, and the bonded length.

2.9 NEED FOR THIS INVESTIGATION

A review of the literature indicates that only a limited number of investigations have been carried on bond behaviour of deformed steel bars embedded in RCA concrete. In a majority of the aforesaid investigations, pullout tests have been conducted using cubical specimens, probably due to convenience of working with such specimens. It is recognised that c/d_b (cover/bar diameter) has a significant effect on bond behaviour and in a typical cubical pullout specimen, the c/d_b within the specimen will not be the same in plan. For example, at the vertical corners of the cubes the c/d_b will be larger compared to the value at the vertical side faces of the cube. This inconsistency can be eliminated using concentric rebar embedment in a cylindrical specimen. Towards this end, pullout tests using cylindrical specimens with concentric rebar embedment are proposed to be carried out in this investigation. To mitigate the effect of the inclined compressive struts, a majority of the investigators have used bond breakers only at the loaded end of the pullout specimens. For a more accurate assessment of bond-slip characteristics, it is reckoned

that bond breaker should be placed at the unloaded end of the pullout specimens also. This is proposed to be done in this investigation. Most of the past studies have focussed on only a selected number of bar diameters such that bond strength related recommendations have been made on the basis of a relatively small data base. In this investigation, rebar diameters in the range of 8 mm – 25 mm are proposed to be studied so as to cover nearly the entire range of practical bar sizes used in actual construction. Earlier investigations have used either pullout or splice beam or beam-end test specimens to study bond behaviour. In this investigation, selected number of splice beam tests are proposed to be carried out in addition to a larger number of pullout tests. The splice beam tests are meant to compliment the pullout tests and will serve the purpose of validating bond strengths predictive equations developed on the basis of the pullout tests.

2.10 CONCLUSION

The literature review presented in this chapter starts from the basics of bond strength in NCA concrete, discusses bond strength predictive models and reviews bond related recommendations of selected current design codes. A review of various properties of recycled aggregates and RCA concrete has also been presented. On the basis of literature review, the need for this investigation has been identified. The next chapter presents the experimental programme of this investigation.

Chapter 3

EXPERIMENTAL PROGRAMME

3.1 INTRODUCTION

To achieve the objectives of the present investigation, several series of experiments were carried out comprising a total of 270 pullout specimens and 24 scaled splice specimens. The experimental programme starts with material testing followed by concrete mixture design, test methods and bond testing. The bond testing was classified into pullout tests and splice beam specimens. The details of these tests are discussed in this chapter. Analysis of the measured data has been carried out in the next chapter.

3.2 MATERIALS

The test specimens were casted using locally available Ordinary Portland Cement (OPC), Fine Aggregate (FA), Natural Coarse Aggregate (NCA), Coarse Recycled Concrete Aggregate (RCA), potable water, High Range Water Reducing Admixture (HRWRA), Thermo-Mechanically Treated (TMT) steel rebars, all confirming to the relevant Indian Standards. The properties of the materials used in this investigation are presented in the following subsections.

3.2.1 Cement

Freshly packed 43-grade Ordinary Portland Cement (OPC) from a single source (Vikram Premium brand) confirming to the requirements of IS 8112:1989 (1989) was used throughout this investigation. The physical analysis of cement was carried out in accordance with the requirements of IS 4031(Part 2):1999 (1999a) and IS 4031(Parts 3 - 6):1988 (1988a, 1998b, 1998c, 1998d) while the chemical analysis was carried out in accordance with the requirements of IS 4032:1985 (1985a) and the measured values are presented in Table 3.1 and Table 3.2 respectively.

Table 3.1 Physical properties of the Ordinary Portland Cement

Property	Unit	Test result	Limiting values specified in IS 8112:1989 (1989)
Specific gravity	-	3.14	-
Fineness by Blaine's Air permeability test	m^2/kg	285	≥ 225
Soundness, Le-Chatelier	mm	1	≤ 10
Standard consistency	%	28	-
Initial setting time	minutes	74	≥ 30
Final setting time	minutes	168	≤ 600
72 ± 1 hours' compressive strength	MPa	25.2	≥ 23
168 ± 2 hours' compressive strength	MPa	37.5	≥ 33
672 ± 4 hours' compressive strength	MPa	45.8	≥ 43

Table 3.2 Chemical composition of the Ordinary Portland Cement

Chemical composition	Test result (%)	Limiting values specified in IS 8112:1989 (1989)
Silica (SiO_2)	22.3	-
Ferric oxide (Fe_2O_3)	3.7	-
Alumina (Al_2O_3)	5.7	-
Calcium oxide (CaO)	61.2	-
Magnesia (MgO)	3.5	≤ 6
Sulphur anhydride (SO_3)	1.74	≤ 3
Insoluble Residue (IR)	1.8	≤ 2
Loss of Ignition (LOI)	1.97	≤ 5
Total alkali in terms of sodium oxide and potassium oxide (Na_2O+K_2O)	0.46	≤ 0.6
Al_2O_3/Fe_2O_3	1.54	≥ 0.66
$\frac{CaO - 0.7SO_3}{2.8SiO_2 + 1.2Al_2O_3 + 0.65Fe_2O_3}$	0.84	≥ 0.66 and ≤ 1.02

3.2.2 Fine aggregates

Locally available coarse river sand confirming to Zone II of IS 383:1970 (1970) was used as fine aggregate (FA) (fineness modulus = 2.68) throughout this investigation. The fine aggregate was sieved through 4.75 mm sieve to remove the coarser particles and also sieved through a 150-micron sieve to remove silt and clay. A typical sample of this material is presented in Figure 3.1. This process makes the fine aggregate grading uniform and consistent.

Figure 3.1 A sample of the fine aggregates

3.2.3 Natural coarse aggregates

Locally available crushed stone aggregate of maximum size 12.5 mm procured from a single source was used as the natural coarse aggregates (NCA) (fineness modulus = 6.38) in the investigation. In order to maintain uniform grading confirming to IS 383:1970 (1970), the coarse aggregates were successively screened through 12.5 mm and 4.75 mm sieves. The coarse aggregates were washed with water by placing on 4.75 mm sieve, for removing the fine particles, clay lumps and all other impurities, and then stored in bags in sufficient quantities in the casting laboratory. Figure 3.2 shows a sample of the natural coarse aggregates.

Figure 3.2 A sample of the natural coarse aggregates

3.2.4 Coarse recycled concrete aggregates

The investigations with the recycled concrete aggregate were confirmed only to the coarser fraction since it is reported in the literature (Hansen, 1986) that fine recycled concrete aggregates are unsuitable for use in concrete, unless special precautions are taken. In the absence of sufficient and assured quantities of CDW in and around the vicinity of Roorkee (the town where that host institute of the author is located), the coarse recycled concrete aggregates (RCA) (fineness modulus = 6.4) for this investigation were produced by crushing with the help of a jaw crusher waste specimens obtained from the concrete laboratory of the author's host institute.

In the RILEM Report 6 (1992), 'Recycling of Demolished Concrete and Masonry' (edited by T.C. Hansen) it is stated under Section 6.2, pp. 16, that "jaw crushers provide the best grain-size distribution of recycled aggregate for concrete production". It is further mentioned in this report that "when it comes to other properties of recycled concrete aggregate than grain-size distribution, jaw crushers perform better than impact crushers because jaw crushers which are set at 1.2–1.5 times the maximum size of original aggregate will crush only a small proportion of the original aggregate particles in the old concrete. Impact crushers, on the other hand, will crush old mortar and original aggregate particles alike and thus produce a coarse aggregate of lower quality. Another disadvantage of impact crushers is high wear and tear and therefore relatively high maintenance costs". The aforementioned report also presents results of a comparison of

crusher efficiencies carried out by B.C.S.J. (1978) according to which "except for grain-size distribution the physical properties of recycled aggregates such as specific gravity, water absorption, sulfate soundness and Los Angeles abrasion loss percentage were not significantly affected by different types of crushers and crusher settings". In this investigation, the choice of a jaw crusher for processing waste concrete was made keeping the above mentioned facts in mind. The angular-shape of the RCA particles typically obtained from a jaw crusher is likely to have a conflicting effect on concrete properties. While on one hand, workability of fresh concrete is likely to be impaired, on the other hand the larger surface area of angular particles means that a larger adhesive force can be developed resulting in a better bond between the aggregate particle and cement mortar. Given the sheer volumes involved, it was practically impossible to confirm the grades of the various constituents of the waste concrete from which the RCA particles were sourced. The suitability of the waste concrete to be processed into RCA was decided on the premise that all the waste concrete (which was a conglomerate of various grades of concrete) which survived the crushing operation (i.e. it had not been reduced to a powder) in the jaw crushers was fit for use as coarse RCA. In this manner, the weaker grades of waste concrete were automatically filtered out during the crushing operations.

The nominal maximum size of the NCA and the RCA particles was kept equal to 12.5 mm and the size fractions of the RCA particles obtained from the jaw crusher were so blended that the grading curves of both the coarse aggregate types, presented in Figure 3.3, besides being similar to each other were also within the specified coarse aggregate grading limits of IS 383:1970 (1970). A sample of the coarse recycled concrete aggregates is showed in Figure 3.4. It may be noted that the output from the jaw crusher consisted of the following three types of materials: virgin aggregate particles covered partially or completely with the hardened cement paste, virgin aggregate particles with very little hardened cement paste on them and pieces of hardened cement paste in different shapes and sizes. None of these three constituents were discarded and as long as their size distribution fell within the grading requirements, they were used as coarse recycled concrete aggregates.

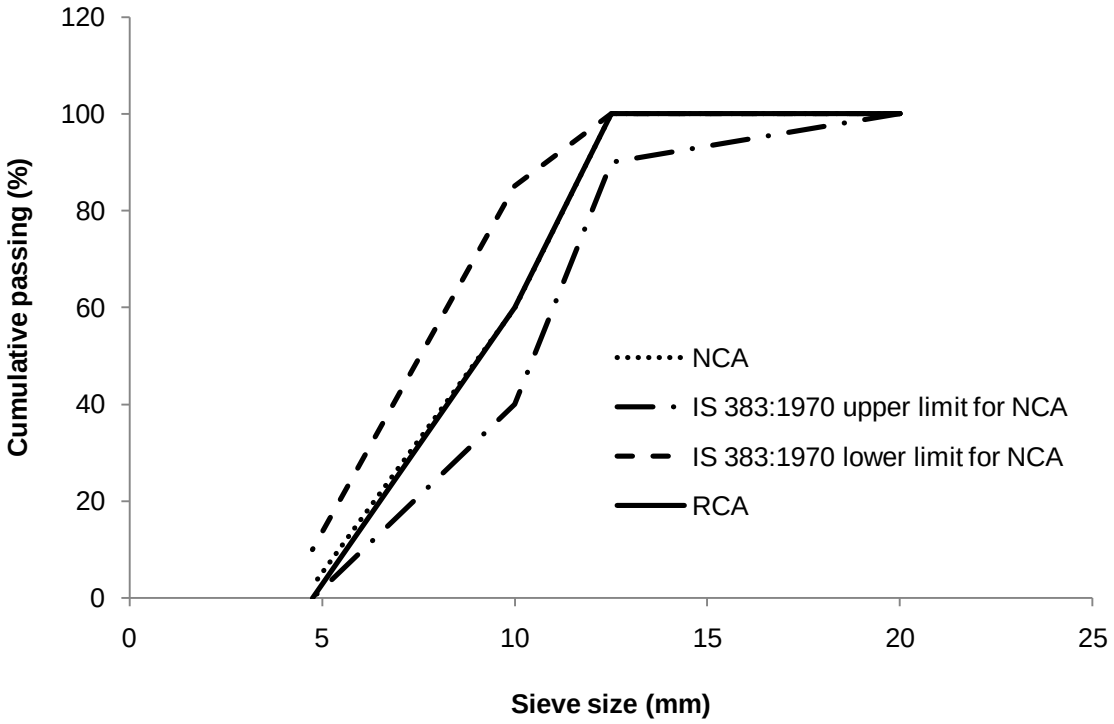

Figure 3.3 Grading curve of the NCA and RCA

Figure 3.4 A sample of the coarse recycled concrete aggregates

3.2.5 Water

Water used for mixing and curing shall be clean and free from injurious amounts of oils, acids, alkalis, salts, sugar, organic materials or other substances that may be deleterious to concrete or steel. IS 456:2000 (2000) considers potable water to be satisfactory for the purpose of mixing and curing of concrete. Accordingly, potable tap water confirms to IS 456:2000 (2000) has been used for mixing and curing of concrete in this investigation. Chemical tests on the water samples were conducted as per IS 3025 (Parts 1 - 36):1987 (1987) and the measured values are presented in Table 3.3.

Table 3.3 Chemical composition of the water

Chemical composition	Test result	Limiting values specified in IS 456:2000 (2000)
pH	7.4	≥ 6
Acidity (%)	4.9	-
Alkalinity (%)	92	-
Chloride (mg/l)	41	≤ 500
Sulphate (mg/l)	79.80	≤ 400
Organic solids (mg/l)	46	≤ 200
Inorganic solids (mg/l)	33	≤ 3000
Total suspended solids (mg/l)	1.86	≤ 2000

3.2.6 High-range water reducing admixture

A high-range water reducing admixture (HRWRA), Glenium 51, based on high molecular weight polymers and sulphonated melamine formaldehyde conforming to IS 9103:1999 (1999b) and ASTM C494/C494M -13 (2013) at a dosage of 0.4% by weight of the cement was used in the medium-strength and the high-strength concretes for achieving desired workability. Table 3.4 summarises the physical and chemical properties of the Glenium 51.

Table 3.4 Physical and chemical properties of the HRWRA

Chemical composition	Test result
pH	6.7
Relative density	1.10
Chloride ion (%)	0.001
Ash content (%)	0.20
Dry material content (%)	9.20

3.2.7 Steel reinforcement

Thermo-mechanically treated (TMT) type SD (Special Ductile) deformed steel reinforcement bars confirming to IS 1786:2008 (2008) having diameters 6 mm, 8 mm, 10 mm, 12 mm, 16 mm, 20 mm, and 25 mm were used in this investigation. Figure 3.5 shows the typical rib orientation in the bars used in this investigation. Surface characteristics of the steel bars were defined in terms of the parameters shown in Figure 3.6 (in accordance with the recommendations of RILEM (1983), ACI 408.3-01/408.3R-01 (2001a) and Lutz and Gergely (1967a)) and the measured values are reported in Table 3.5. To evaluate the mechanical properties, the steel bars were tested in tension as per IS 1608:2005/ISO 6892:1998 (2005) and IS 1599:1985 (1985b) using a 1000 kN capacity universal testing machine (UTM), Figure 3.7, and the measured values are compiled in Table 3.6. For the purpose of illustration, the measured stress-strain relationships of the 6 mm, 8 mm, 10 mm, and the 12 mm diameter bars are shown in Figures 3.8, 3.9, 3.10 and 3.11 respectively.

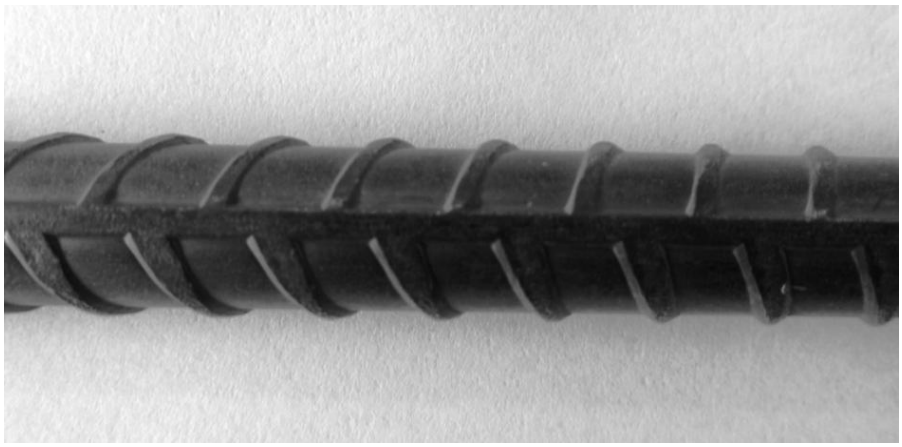

Figure 3.5 Typical rib orientation in the deformed steel bars

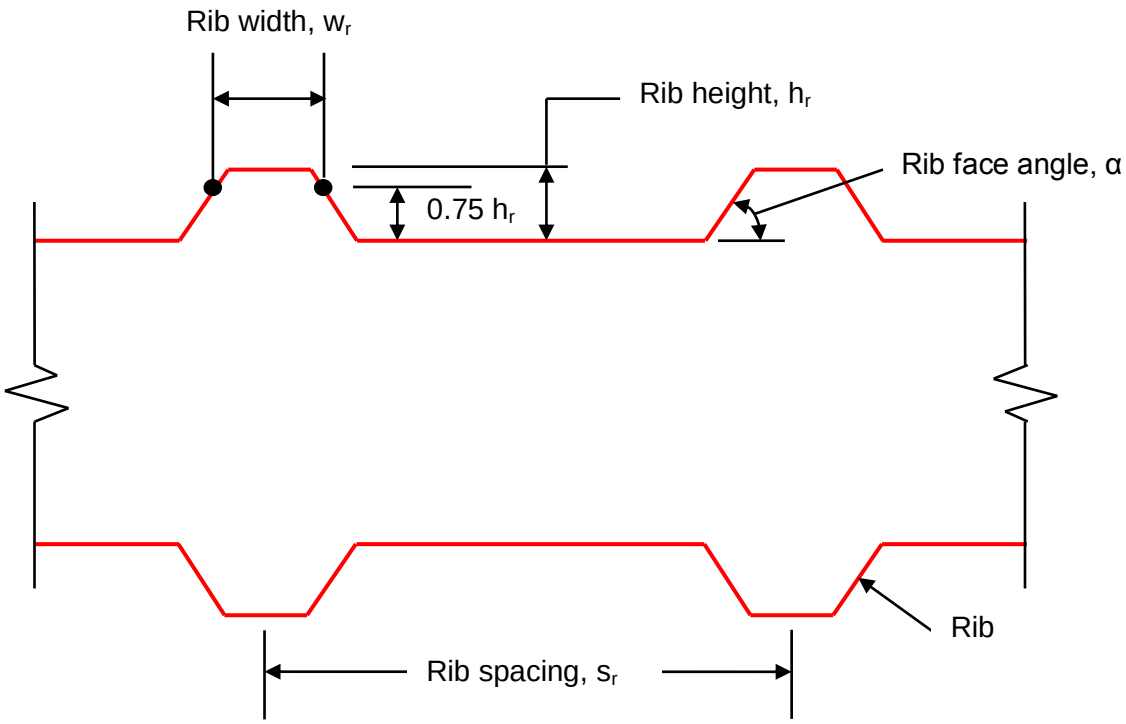

Figure 3.6 Definition of surface characteristics

Table 3.5 Surface characteristics of the steel reinforcing bars

Property	Rebar diameter						
	6 mm	**8 mm**	**10 mm**	**12 mm**	**16 mm**	**20 mm**	**25 mm**
Rib height, h_r (mm)	*	0.50	0.70	0.70	0.83	1.03	1.50
Rib width, w_r (mm)	*	1.19	1.21	1.43	1.52	2.10	2.00
Rib spacing, s_r (mm)	*	5.40	6.80	7.28	8.30	10.89	12.53
Relative rib area, (h_r/s_r)	*	0.093	0.103	0.096	0.100	0.095	0.120
Rib face angle, α (Degree)	*	48º	44º	45º	36º	41º	51º

** Accurate measurements were not possible*

Figure 3.7 Tension testing of a steel reinforcing bar

Table 3.6 Mechanical properties of the steel reinforcing bars

Sl. No.	Nominal size (mm)	Mass (kg/m)	Cross - sectional area (mm^2)	Yield stress, σ_p (MPa)	Ultimate tensile strength (MPa)	Elongation (%)	Bend test
1	6	0.207	26.38	633	775	20	Pass
2	8	0.394	50.18	600	720	25	Pass
3	10	0.596	75.90	576	660	26	Pass
4	12	0.879	111.98	532	616	23.33	Pass
5	16	1.560	198.74	574	694	23.75	Pass
6	20	2.398	305.43	588	691	25	Pass
7	25	3.810	485.31	601	706	24	Pass

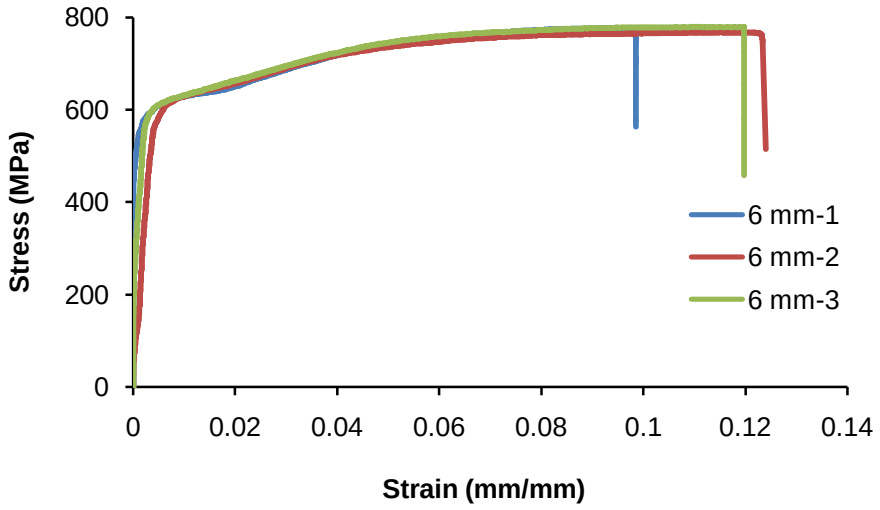

Figure 3.8 Measured stress-strain relationships of the 6 mm diameter bars

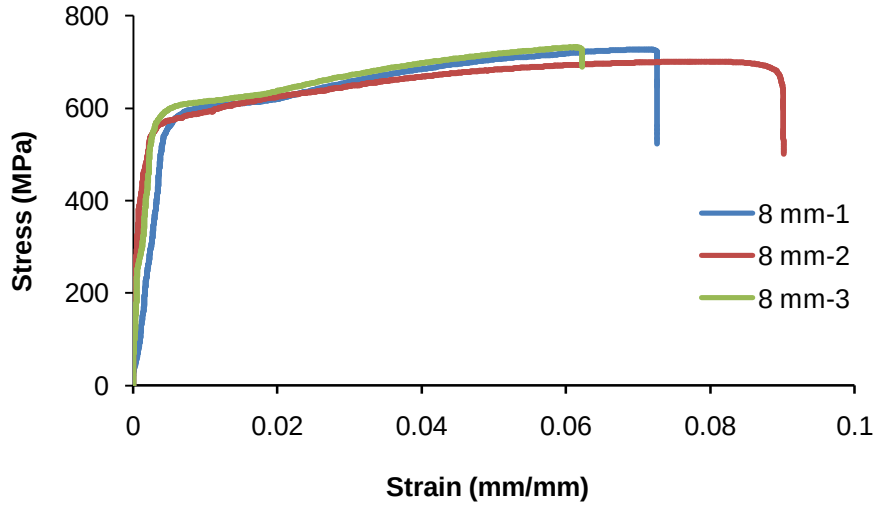

Figure 3. 9 Measured stress-strain relationships of the 8 mm diameter bars

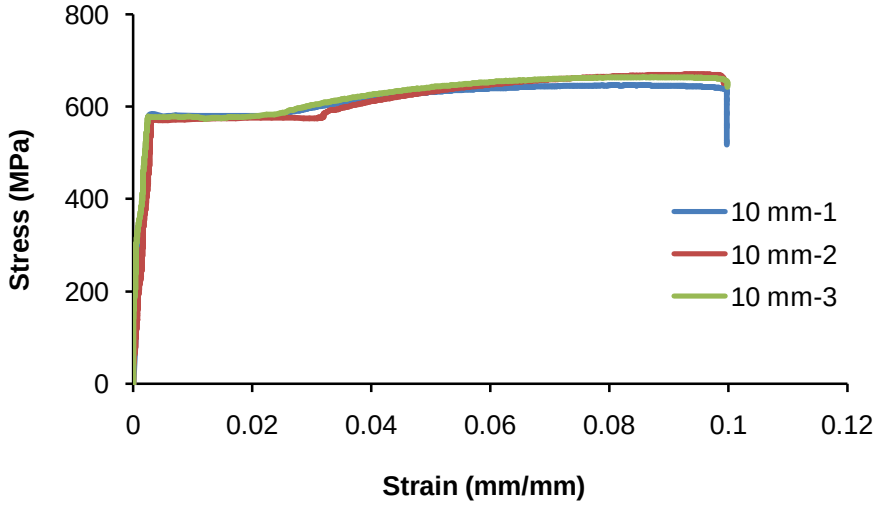

Figure 3.10 Measured stress-strain relationships of the 10 mm diameter bars

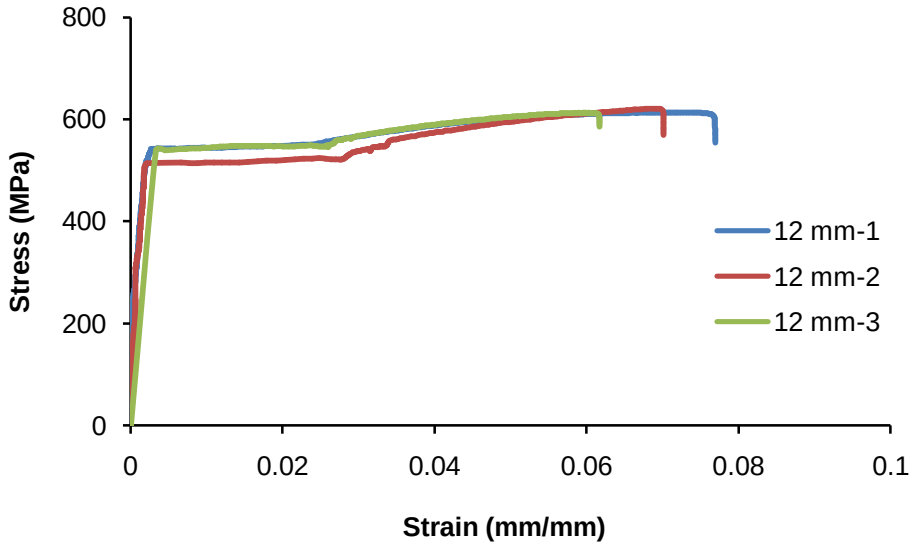

Figure 3.11 Measured stress-strain relationships of the 12 mm diameter bars

3.3 MATERIAL TESTING

Several tests were conducted to determine the physical properties of the fine and the coarse aggregates. These tests are briefly described and their results are discussed in the following sections.

3.3.1 Grading of the aggregates

Grading refers to the distribution of particle sizes present in an aggregate and it affects the workability of concrete. Well graded aggregates require minimum paste to fill voids which is conducive to producing high strength and durable concrete with low shrinkage. To determine grading, sieve analysis was conducted as per IS 2386 (Part I):1963 (1963b). The aggregates were dried in an oven at a temperature of 100ºC for 4 hours and then 1 kg of the FA was sieved in a set of sieves with sizes ranging from 10 mm to 0.15 mm and the weight of aggregate retained in each sieve was noted. Similarly, 10 kg of the coarse aggregate was sieved through a set of sieves with sizes ranging from 20 mm to 4.75 mm and the weight of aggregate retained in each sieves was noted. Table 3.7 and Figure 3.12 show a comparison of particle size distribution of the FA with the limits specified in IS 383:1970 (1970). Table 3.8 and Table 3.9 show a comparison of particle size distribution of the NCA and the RCA with the limits specified in IS 383:1970 (1970). A comparison of the particle size distribution of the NCA and the RCA with the grading limits in IS 383:1970 (1970) is also plotted in Figure 3.3. Figures 3.3 and 3.12 show that the size distribution of the fine and the coarse aggregates used in this investigation was within the grading limits specified in IS 383:1970 (1970).

Fineness modulus of the FA, NCA and the RCA was calculated using the following equations (Equations 3.1, 3.2 and 3.3) and the corresponding values were tabulated in Table 3.10.

$$\text{Fineness Modulus of FA} = \frac{\text{Total cumulative percentage retained}}{100} \quad (3.1)$$

$$\text{Fineness Modulus of NCA} = \frac{\text{Total cumulative percentage retained} + 500}{100} \quad (3.2)$$

$$\text{Fineness Modulus of RCA} = \frac{\text{Total cumulative percentage retained} + 500}{100} \quad (3.3)$$

Table 3.7 Sieve analysis of the fine aggregates

IS Sieve Size (mm)	Weight retained (g)	Percentage retained	Cumulative percentage retained	Percentage passing	Percentage passing for grading Zone II of IS 383:1970 (1970)
10	0	0	0	100.0	100
4.75	75	7.5	7.5	92.5	90-100
2.36	97	9.7	17.2	82.8	75-100
1.18	125	12.5	29.7	70.3	55-90
0.600	160	16.0	45.7	54.3	35-59
0.300	283	28.3	74.0	26.0	8-30
0.150	200	20.0	94.0	6.0	0-10
Residue	60	6	-	-	-

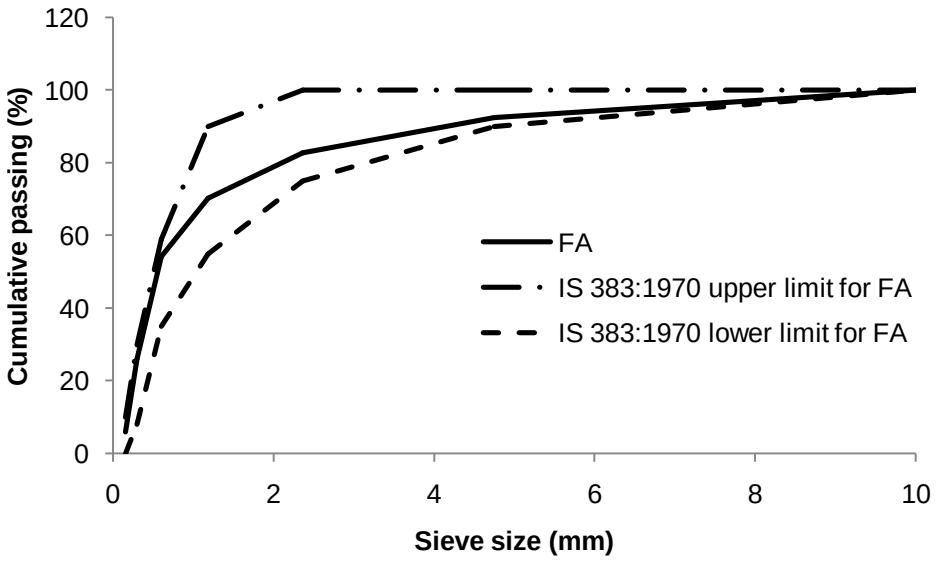

Figure 3.12 Grading curve of the fine aggregates

Table 3.8 Sieve analysis of the natural coarse aggregates

IS Sieve Size (mm)	Weight retained (g)	Percentage retained	Cumulative percentage retained	Percentage passing	Range specified for 12.5 mm maximum size graded coarse aggregates in IS 383:1970 (1970)
20	0	0	0	100.0	100
12.5	0	0	0	100.0	90-100
10	4020	40.2	40.2	59.8	40-85
4.75	5730	57.3	97.5	2.5	0-10
Residue	250	2.5	-	-	-

Table 3.9 Sieve analysis of the coarse recycled concrete aggregates

IS Sieve Size (mm)	Weight retained (g)	Percentage retained	Cumulative percentage retained	Percentage passing	Range specified for 12.5 mm maximum size graded coarse aggregates in IS 383:1970 (1970)
20	0	0	0	100.0	100
12.5	0	0	0	100.0	90-100
10	4000	40.0	40.0	60.0	40-85
4.75	6000	60.0	100.0	0	0-10
Residue	0	0	-	-	-

3.3.2 Residual mortar content of the RCA particles

The hardened cement mortar attached to the surface of the virgin aggregate in a coarse recycled concrete aggregate particle is called as the residual mortar. It may be noted that no attempts were made to separate the residual mortar from the virgin aggregates in this investigation. The residual mortar content was determined by using the hydrochloric acid dissolution method proposed by Nagataki *et al*. (1998). A 100 g oven dried (at a temperature of 100ºC for 24 hours) RCA sample was taken in a plastic container and 1:3 HCl solution was added such that the RCA sample was immersed by a

depth ranging between 12 mm to 15 mm below the surface of the HCl solution. The level of HCl in the container was maintained by adding more HCl as and when required. After 2 days of HCl immersion, the residual mortar in RCA begins to split up. Subsequently, the RCA particles, which still had some residual mortar attached to their surface, were transferred to a new container with fresh HCl solution. Again after 2 days, further degradation and removal of the residual mortar took place and this process was repeated until all the residual mortar stood removed. After all the residual mortar had been separated from the virgin aggregate particles, the latter were shifted to a 4.75 mm sieve and washed with hot water to remove all traces of the HCl and the aggregate particles were oven dried. The mass of the oven dried coarse aggregates were noted. The amount of residual mortar content was calculated based on Equation 3.4 and the results are presented in Table 3.10.

$$\textit{Residual mortar content (\%)} = \frac{\textit{Weight of RCA} - \textit{Weight of RCA after removal of mortar}}{\textit{Weight of RCA}} x100\% \tag{3.4}$$

3.3.3 Bulk specific gravity and water absorption of the aggregates

Bulk specific gravity and water absorption of both fine and coarse aggregates were determined by following the procedure of IS 2386 (Part III):1963 (1963c). The procedure for finding bulk specific gravity and water absorption of the fine aggregates is outlined here. A clean dry pycnometer, was weighed as W_1 gm, filled with distilled water and weighed as W_2 gm. A 500 g (W_3) sample of fine aggregate in SSD condition was placed in the pycnometer and filled with distilled water and weighed as W_4 gm. The contents of the pycnometer were emptied into a tray and the water was drained from the sample by decantation through a filter paper and any material retained returned to the sample. The sample was placed in an oven at a temperature 100ºC for 24 hours, cooled in air-tight container and weighed as W_5 gm. Bulk specific gravity and water absorption of the fine aggregates was evaluated using the Equations 3.5 and 3.6 respectively and the results are given in Table 3.10.

$$\textit{Bulk specific gravity of FA} = \frac{W_3}{W_3 - (W_4 - W_2)} \tag{3.5}$$

$$\textit{Water absorption of FA}\ (\%) = \frac{W_3 - W_5}{W_5} x100\% \tag{3.6}$$

The bulk specific gravity and water absorption of the coarse aggregates were determined by the following procedure. A wire basket was immersed in distilled water and weighed as W_1 gm. A 3000 g (W_2) sample of coarse aggregate in SSD condition was

placed in the wire basket and then immersed in distilled water such that the top of the basket was 50 mm below the water surface. The basket with aggregate in immersed condition was weighed as W_3 gm. Then, the sample was placed in an oven at a temperature 100ºC for 24 hours, cooled in air-tight container and weighed as W_4 gm. Bulk specific gravity and water absorption of the coarse aggregates was evaluated using the Equations 3.7 and 3.8 respectively and the results are presented in Table 3.10.

$$Bulk\ specific\ gravity\ of\ CA = \frac{W_2}{W_2 - (W_3 - W_1)} \tag{3.7}$$

$$Water\ absorption\ of\ CA\ (\%) = \frac{W_2 - W_4}{W_4} x100\% \tag{3.8}$$

3.3.4 Bulk density of the aggregates

Bulk density of both the fine and the coarse aggregates was determined by following the procedure given in IS 2386 (Part III):1963 (1963c). The aggregates were dried in an oven at a temperature of 100ºC for 4 hours. A clean and dry cylindrical metal measure of weight W_1 kg was filled with water and weighed as W_2 kg. The measure was filled with aggregate in three layers and each layer was tamped with 25 strokes using the rounded end of a tamping rod of 16 mm diameter and 600 mm long and weighed as W_3 kg. The measure was then emptied, refilled with the aggregate without compaction and levelled with a straightedge and weight as W_4 kg. Bulk density of fine and coarse aggregates, for both compacted and loose state was evaluated using the Equations 3.9 and 3.10 and the results are tabulated in Table 3.10.

$$Bulk\ density\ (compacted)\ (kg/m^3) = \frac{W_3 - W_1}{W_2 - W_1} \tag{3.9}$$

$$Bulk\ density\ (loose)\ (kg/m^3) = \frac{W_4 - W_1}{W_2 - W_1} \tag{3.10}$$

3.3.5 Crushing, impact and abrasion values of the coarse aggregates

The crushing, impact and abrasion values of the coarse aggregates were determined by following the procedure given in IS 2386 (Part IV):1963 (1963a). The procedure for finding the aggregate crushing value, which gives a relative measure of the resistance of an aggregate to crushing under a gradually applied load, is briefly presented here. Both NCA and RCA aggregates were tested in surface-dry condition. A 3000 g (W_1) sample which passed through a 12.5 mm IS sieve and was retained on a 10 mm IS sieve

was placed in an open ended 150 mm cylindrical cell with a base plate in three layers with each layer being tamped with 25 strokes using a tamping rod. The surface of the sample was levelled and the plunger inserted horizontally. The sample was placed in between the platens of the testing machine and loaded at a uniform rate such that the total load of 40 tonnes was reached in 10 minutes. Subsequently the load was released and the materials were removed from the cylinder, sieved on a 2.36 mm IS sieve and the fraction passing the sieve was weighed as W_2 gm. The aggregate crushing value was calculated using Equation 3.11 and the values are given in Table 3.10.

$$Aggregate\ crushing\ value\ (\%) = \frac{W_2}{W_1} x100\% \qquad (3.11)$$

The procedure for finding the aggregate impact value, which gives a measure of the resistance of an aggregate to sudden shock or impact, is outlined here. The NCA and RCA was oven dried at a temperature of 100ºC for 4 hours before testing. A sample passing through a 12.5 mm IS sieve and retained on a 10 mm IS sieve was placed in a cylindrical metal measure having a diameter of 75 mm and a depth 50 mm in three layers each layer being tamped with 25 strokes and the surplus aggregate was strucked off using the tamping rod as a straight-edge. The net weight of the aggregate was weighed as W_1 gm and this weight of aggregate was used for the replicate test on the same material. The aggregate sample was then placed in three layers (each layer was compacted using 25 strokes of the tamping rod) in a cylindrical steel cup having a diameter of 102 mm and a depth of 50 mm which was fixed firmly in position on the base of the impact testing machine. The impact hammer was raised until its lower face was 380 mm above the upper surface of the aggregate in the cup and allowed to fall freely on the test sample. The test sample was subjected to a total 15 such blows each being delivered at an interval of not less than one second and the crushed aggregate was then removed from the cup and sieved on a 2.36 mm IS sieve, the fraction passing being weighed as W_2 gm. The aggregate impact value was calculated using Equation 3.12 and the values are given in Table 3.10.

$$Aggregate\ impact\ value\ (\%) = \frac{W_2}{W_1} x100\% \qquad (3.12)$$

The aggregate abrasion value gives a measure of the resistance of an aggregate to being worn away by rubbing and friction or shattering upon impact. A brief outline of the test procedure is given here. The NCA and the RCA was oven dried at a temperature of 100ºC for 4 hours before testing. A 5000 g (W_1) sample, out of which 2500 g passed through a 20 mm IS sieve and was retained on 12.5 mm IS sieve and the other 2500 g

passed through a 12.5 mm IS sieve and was retained on a 10 mm IS sieve was placed together with the abrasive charge in a Los Angeles abrasion testing machine, and the machine was rotated for 500 revolutions at a speed of 30 revolutions/min. The tested aggregate were then removed from the machine, sieved through a 1.70 mm IS sieve and the retained material was then washed dried in an oven at 110ºC to a substantially constant weight and weighed as W_2 gm. The aggregate abrasion value was calculated using Equation 3.13 and the values are reported in Table 3.10.

$$Aggregate\ abrasion\ value\ (\%) = \frac{W_1 - W_2}{W_1} x100\% \qquad (3.13)$$

Table 3.10 Physical properties of the fine aggregate, the natural coarse aggregate and the recycled concrete aggregate

Characteristic	Test result		
	FA	NCA	RCA
Grading	Zone II	12.5 mm maximum size aggregate	12.5 mm maximum size aggregate
Fineness modulus	2.68	6.38	6.40
Bulk specific gravity	2.68	2.67	2.50
Density (Compacted) (kg/m^3)	1866	1630	1385
Density (Loose) (kg/m^3)	1675	1419	1230
Water absorption (%)	0.7	1	6
Crushing value (%)	-	21.2	21.7
Impact value (%)	-	17.3	22.2
Abrasion value (%)	-	18	20.2
Residual mortar content (%)	-	-	32.2

3.4 DESIGN OF THE CONCRETE MIXTURES

Two types of concrete mixtures were used in the investigation. In the control mixture, only natural aggregates were used and this mixture has been identified as NCA concrete in this investigation. In the other concrete mixture, designated as RCA concrete, coarse recycled concrete aggregate has been used as either partial or full replacement of

the coarse natural aggregates in the concrete. The fine aggregates in the RCA concrete were sourced naturally.

3.4.1 Control concrete mixtures

Since concrete grade was a parameter in the investigation, three grades of the control mixtures were designed following recommendations of the relevant ACI code. The normal-strength control concrete mixture (Mix A), having a 56-day cylinder compressive strength of 36 MPa was proportioned on the basis of the guidelines laid down in ACI 211.1-91 (1991), whereas for design of the medium-strength (Mix B) and the high-strength (Mix C) control concrete mixtures, ACI 211.4R-08 (2008) was followed. Although ACI 318-11 (2011), does not formally classify concrete being medium-strength, this designation has been conventionally used in this investigation to identify the concrete grade which is intermediate between the lowest (normal-strength, Mix A) and the highest concrete grade (high-strength, Mix C). The medium-strength concrete, Mix B, was designated for a 56-day cylinder strength of 51 MPa, whereas the high-strength concrete, Mix C, was designed for a 56-day cylinder compressive strength of 68 MPa. The mixture design was carried out using the absolute volume method and in order to order to achieve the desired workability, high range water reducing admixture (Glenium 51) at a dosage of 0.4% by weight of cement was used in the medium-strength and the high-strength concrete mixtures.

3.4.2 RCA concrete mixtures

Corresponding to the control concrete mixtures, three grades of RCA concrete mixtures were designed using equivalent mix proportions wherein the mixture proportions for the three grades of the RCA concrete were nominally kept the same as the three corresponding grades of NCA concrete except for weight-to-weight replacement of NCA with RCA, depending upon the desired RCA replacement level. Four RCA replacement levels viz. 25 %, 50 %, 75 % and 100 % were investigated. In the 25 % replacement level for example, 25 % of the weight of NCA in the control concrete mixture was replaced by an equal weight of the RCA particles in the SSD moisture condition and so on. Admittedly, the equal weight replacement strategy adopted in the investigation will affect the concrete yield and some other investigators (Topcu and Sengal, 2004; Etxeberria et al., 2007; Obla et al., 2007; Corinaldesi, 2010; Knaack and Kurama, 2013) have adopted equal volume rather than equal weight replacement of NCA with RCA. The equal weight replacement is reckoned to be conceptually more convenient and easier to implement in field practice and has been adopted by Buck (1977), Nishibayashi *et al*. (1984), Yamato (1998), Dhir *et al*. (1999), Abbas *et al*. (2008), Xiao and Falkner (2007) and Knaack and Kurama (2013)

in their experimental investigations on RCA concrete. The following five weight combinations of NCA and RCA were adopted: 100% NCA (control mixture), 75% NCA + 25% RCA, 50%NCA + 50% RCA, 25% NCA + 75% RCA, 100% RCA. The control and the RCA concrete mixture are identified together with their proportions (ratios by weight) in Table 3.11. It may be noted in Table 3.11 that in the control as well as the RCA concrete mixtures, the water-cement ratio, w/c, in the normal-strength, the medium-strength and in the high-strength concretes was kept nominally equal to 0.54, 0.42 and 0.37 respectively.

Table 3.11 Concrete mixture proportions

Mix ID*	RCA replacement level, *r* (%)	Cement	Fine aggregate	NCA	RCA	Mixing water including HRWRA#	HRWRA# (% by weight of cement)
AR0	0	1	2.31	2.47	0	0.54	-
AR25	25	1	2.31	1.85	0.62	0.54	-
AR50	50	1	2.31	1.24	1.24	0.54	-
AR75	75	1	2.31	0.62	1.85	0.54	-
AR100	100	1	2.31	0	2.47	0.54	-
BR0	0	1	2.08	2.9	0	0.42	0.4
BR25	25	1	2.08	2.18	0.73	0.42	0.4
BR50	50	1	2.08	1.45	1.45	0.42	0.4
BR75	75	1	2.08	0.73	2.18	0.42	0.4
BR100	100	1	2.08	0	2.9	0.42	0.4
CR0	0	1	1.73	2.56	0	0.37	0.4
CR25	25	1	1.73	1.92	0.64	0.37	0.4
CR50	50	1	1.73	1.28	1.28	0.37	0.4
CR75	75	1	1.73	0.64	1.92	0.37	0.4
CR100	100	1	1.73	0	2.56	0.37	0.4

* *Mix ID: The alphabet in the first place-holder represents concrete grade (A: normal-strength, B: medium-strength, C: high-strength), the alphabet R in the second place-holder stands for 'replacement level', the numerals in the remaining place holders represent RCA replacement levels (0: 0%, 25: 25%, 50: 50%, 75: 75% and 100: 100%).*

\# *High Range Water Reducing Admixture*

3.4.3 Aggregate preparation, batching and curing of concrete

The natural coarse aggregates consisted of locally available crushed rock and no processing was required before their use. As has been mentioned earlier, the (coarse) RCA was obtained from the waste concrete specimens, Figure 3.13, in the concrete laboratory of the author's host institute. The waste specimens were manually broken down into small pieces and then fed into the jaw crusher, Figure 3.14, locally fabricated in the institute. After crushing, the aggregates were sieved and separated into two size fractions. The nominal maximum size of the NCA and the RCA particles was kept at 12.5 mm and the size fractions of the RCA particles obtained from the jaw crusher were so blended that the grading curves of both the coarse aggregate types besides being similar to each other were also within the specified coarse aggregate grading limits of IS 383:1970 (1970).

Casting of both the concrete types was done in a tilting-drum type mixer. Since the RCA used in this investigation had water absorption values which were about 6 times higher than that of the NCA, the uniform w/c across all the concrete mixtures in each group was achieved by ensuring that the NCA and the RCA particles were in the saturated surface-dry (SSD) moisture condition at the time of batching. To achieve the SSD condition, the NCA and the RCA particles were immersed separately in water for 24 hours. At the end of the immersion period, the aggregates were taken out of the immersion tank and any water attached to the surface of the aggregate particles was removed with the help of a hessian cloth by spreading the aggregate particles on the laboratory floor. Immediately afterwards, the aggregates were batched in the concrete mixer. While mixing, first the coarse aggregates were added to the mixer along with one-third the total amount of total water so that all the aggregates become wet. Subsequently one-third the total amount of cement was added and the constituents were mixed for about one minute. Subsequently, fine aggregates were added followed by the remaining quantity of cement and water. It was ensured that the total mixing time was not less than 3 minutes. The inside surface of the moulds for casting of the test specimens were coated with shutter release oil and after compaction on a vibrating table, the specimens were stored in humidity conditions the laboratory for a period of 24 h after casting by covering them with a wet hessian cloth. After this period, the specimens were demoulded and moist cured by immersion in a curing tank for a period of 56-days after casting. The water of the curing tank was changed every week. For strength testing, the concrete specimens (100 mm x 200 mm cylinders for compressive strength and splitting tensile strength), after being taken out of the curing tank, were tested in the SSD moisture condition. For the bond tests, the pullout specimens were prepared for testing at the end of the curing period and the relevant details are explained in a subsequent section.

Figure 3.13 Waste concrete specimens used for producing the RCA

Figure 3.14 Jaw crusher used for crushing of the waste concrete

3.5 TESTING OF CONCRETE

3.5.1 Workability

Workability is the property of concrete which determines the amount of useful internal work necessary to produce complete compaction. Workability was measured using the slump test carried out as per the procedure mentioned in IS 1199:1959 (1959a). The mould for the slump test is in the form of the frustum of a cone, 300 mm high with 200 mm bottom diameter and 100 mm top diameter. The concrete was filled in the mould in four layers, each layer being compacted with 25 strokes of a 16 mm diameter tamping rod and the top surface was strucked off level with a trowel. The mortar which leaked out between the mould and the base plate was cleaned and the mould was slowly lifted, the initial slump was measured, and the recorded values are presented in Figure 3.15.

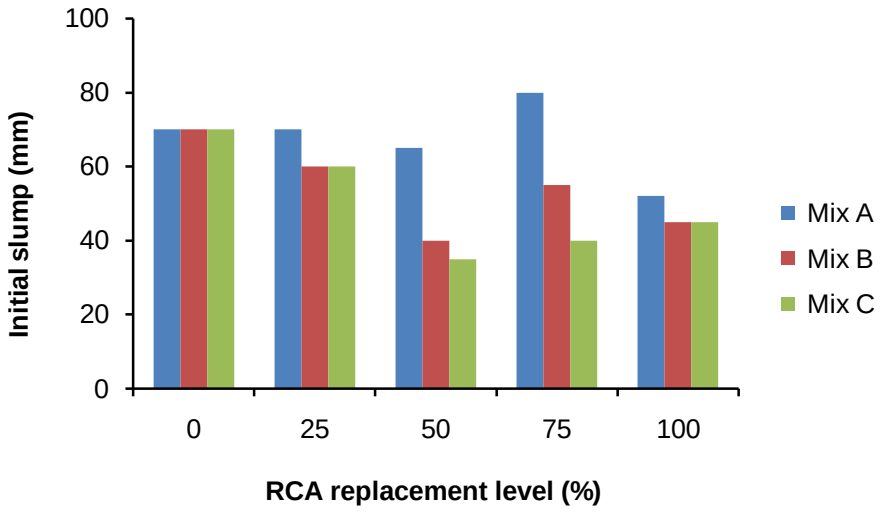

Figure 3.15 Variation of initial slump of concrete with RCA replacement level

3.5.2 Density

Three replicate control cylindrical specimens (100 mm diameter x 200 mm height) were used to determine the density of the hardened concrete. The mass (W) and average measurements of the cylinders (diameter, d and height, h) were noted and the density of hardened concrete in kg/m^3 (ρ_c) was evaluated by the mass of the cylinder divided by its volume, Equation 3.14. A minimum of three specimens were tested for each mix and average values are presented in Figure 3.16.

$$\rho_c = \frac{W}{\left(\frac{\pi\ d^2}{4}\right)h} \qquad (3.14)$$

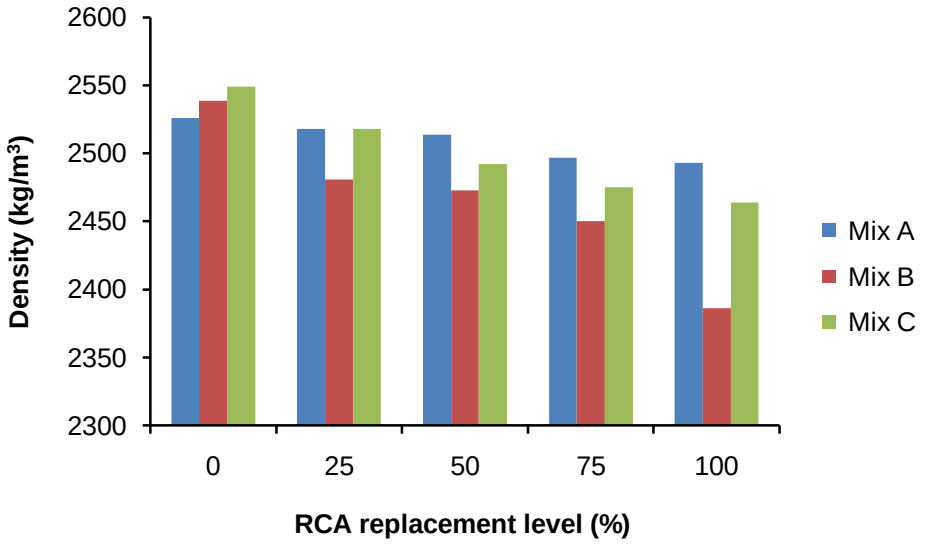

Figure 3.16 Variation of density of hardened concrete with RCA replacement level

3.5.3 Compressive strength

Since the pullout tests were carried out at an age of 56 days, the compressive strength measurements of the 100 mm diameter x 200 mm height control cylindrical specimens were carried out at an age of 56 days. Compressive strength measurements were done following the procedures recommended in IS 516:1959 (1959b) and ASTM C39/C39M -12a (2012). After 56-days curing, the specimens were taken out from the curing tank and the surface moisture was cleaned with the help of an absorbent cloth. The irregular end surfaces were made level and ground smooth with a hand-held grinder. Then the test cylinder was placed vertically between the platens of a 2500 kN capacity close-loop servo-controlled universal testing machine (UTM), Figure 3.17, and the load was applied at a displacement rate of 0.1 mm/min. The cylinder compressive strength in MPa (f'_c) was calculated by dividing the peak load by the cross-sectional area of the cylinder, Equation 3.15. A minimum of three specimens were tested in each sample and typical failure modes in the cylinders is shown in Figure 3.18. The average compressive strength values were presented in Figure 3.19. A discussion of the compressive strength trends in Figure 3.19 is presented in the next chapter, Results and Discussion.

$$f_c^{'} = \frac{P}{\left(\frac{\pi \ D^2}{4}\right)} \qquad (3.15)$$

where f'_c = cylinder compressive strength in MPa, P = maximum applied load in N, and D = diameter of the cylinder in mm.

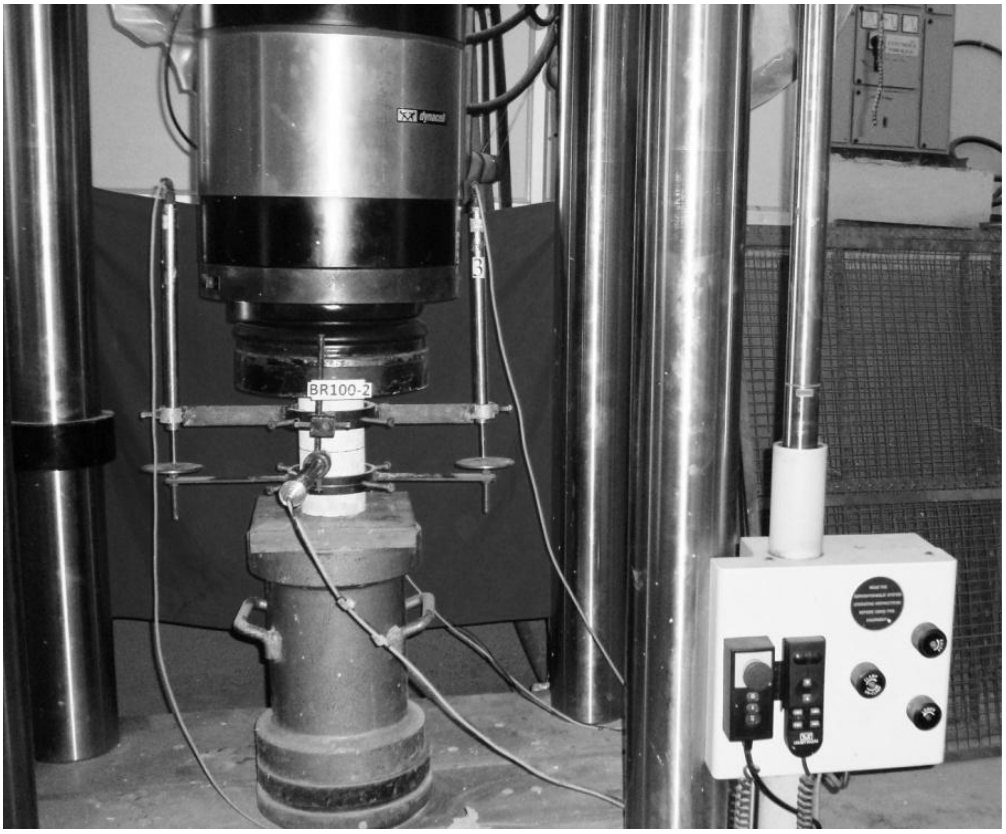

Figure 3.17 Compression testing of a cylindrical specimen

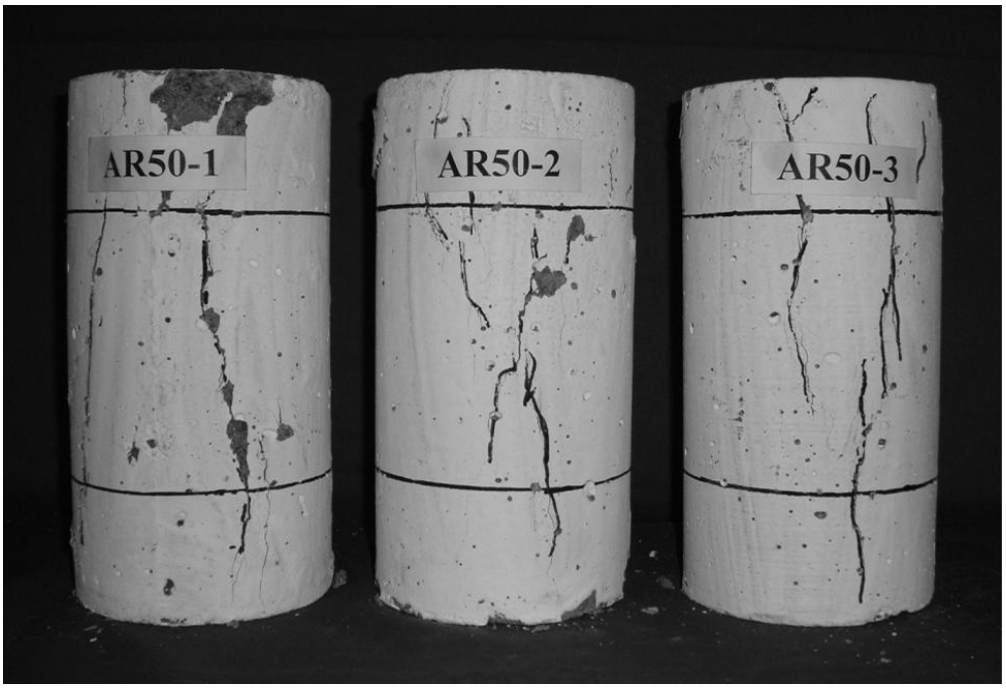

Figure 3.18 Typical failure after compression testing of cylinders

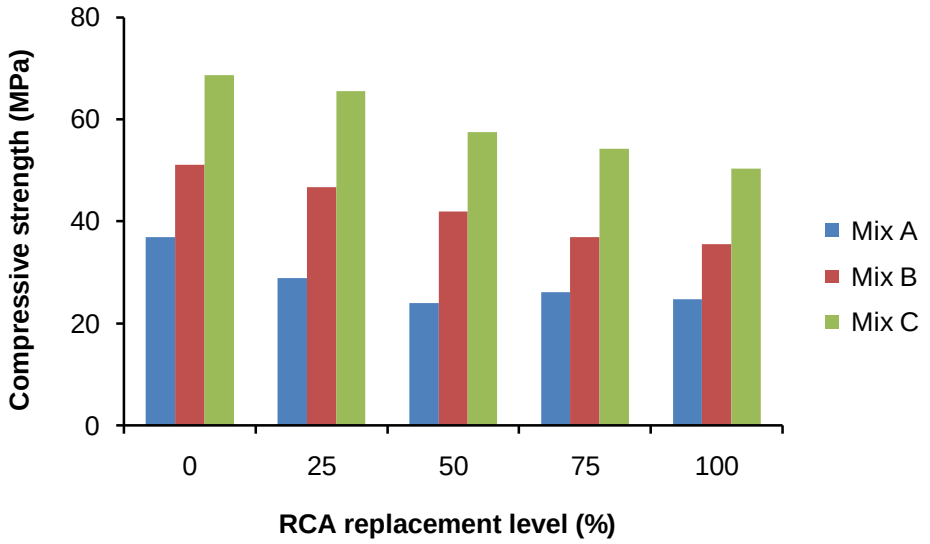

Figure 3.19 Variation of compressive strength with RCA replacement level

3.5.4 Splitting tensile strength

Like the compressive strength, the splitting tensile strength was also evaluated at an age of 56 days by testing cylindrical specimens (100 mm diameter x 200 mm height) following the procedures given in IS 5816:1999 (1999c) and ASTM C496/C496M-11 (2011). After 56-days curing, the specimens were taken out from the curing tank and the surface moisture was cleaned with the help of an absorbent cloth. The test the cylinder was placed horizontally along with two hardboard packing strips, Figure 3.20, in between the platens of the 2500 kN capacity close-loop servo-controlled universal testing machine (UTM) and the load was applied at a displacement loading rate of 0.1 mm/min. The cylinder splitting tensile strength in MPa (f_{ct}) was calculated using the Equation 3.16. A minimum of three specimens were tested in each group and the average values were presented in Figure 3.21. Trends in the splitting tensile strengths shown in Figure 3.21 are discussed in the next chapter.

$$f_{ct} = \frac{2P}{(\pi L D)} \qquad (3.16)$$

where f_{ct} = cylinder splitting tensile strength in MPa, P = maximum applied load in N, L = length of the cylinder in mm, and D = diameter of the cylinder in mm.

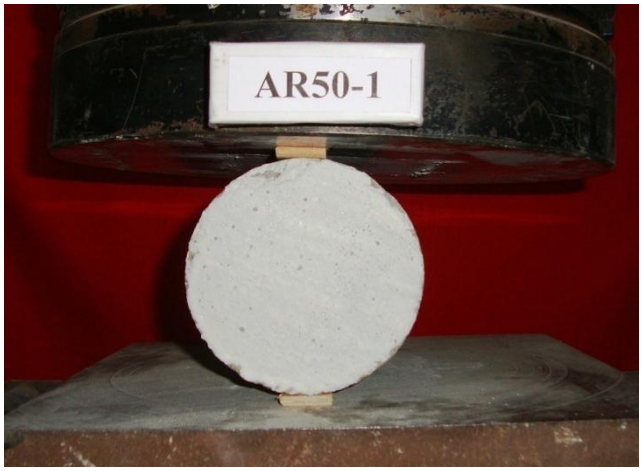

Figure 3.20 Splitting tensile strength testing of a cylinder

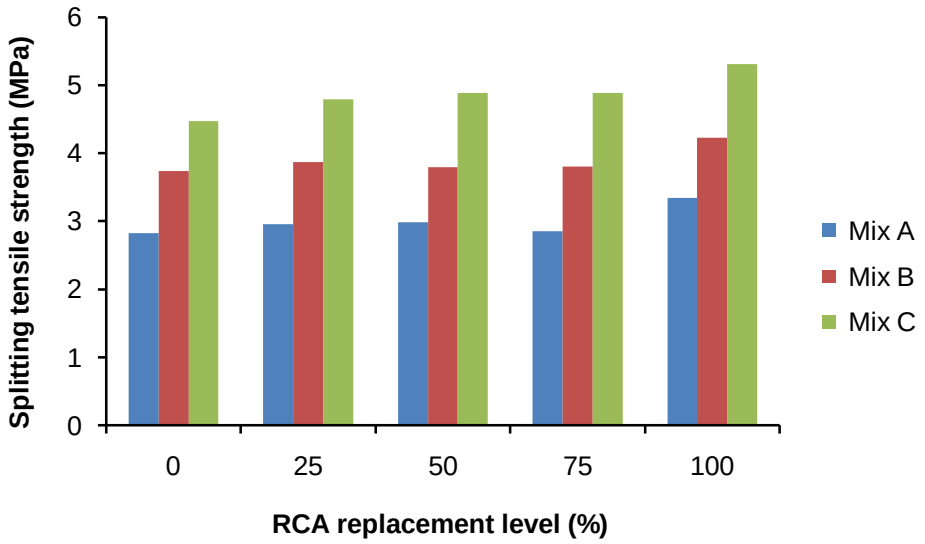

Figure 3.21 Variation of splitting tensile strength with RCA replacement level

3.6 BOND TESTING

Bond between the reinforcement bars and concrete was investigated through pullout and through splice beam tests. A total of 270 pullout specimens and 24 scaled splice beams were cast and tested. The specimen details and the test procedures are described in the following sections.

3.6.1 Pullout tests

A major part of the investigation of bond behaviour was carried out with the help of pullout tests. According to ACI 408R-03 (2003), a variety of test specimen configurations have been used to study bond between reinforcing bars and concrete and a schematic of the four most common configurations are shown in Figure 3.22.

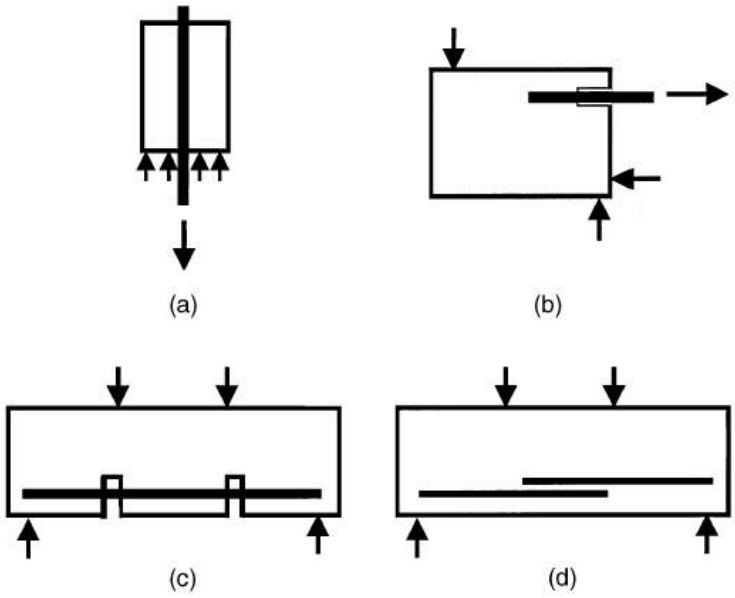

Figure 3.22 Schematic of commonly used test specimen configurations in bond studies (ACI 408R-03)

Among the four test specimen configurations shown in Figure 3.22, the pullout specimen, Figure 3.22 (a), is considered to be the least realistic because it has little resemblance to bond conditions in actual construction. Unlike the stress condition in a pullout specimen wherein the bar is placed in tension and the concrete in compression, in most of the reinforced concrete members in practice, both the steel bar and the surrounding concrete are in tension. Further in such members, the bearing surface of the bar ribs are subjected to a compressive force only when there is relative movement between the bar and the surrounding concrete. On the other hand, in a pullout test, the bearing action of the ribs is mobilised due to the pullout load applied on the ribs is mobilised due to the pullout load applied on the embedded steel bar in the test specimen. Therefore, bond strengths obtained from pullout tests may have little application is structural design. According to the ACI 408R-03 (2003), the configurations shown in Figure 3.22 (b) though (d) provide bond strength measurements which are more relevant to actual construction. In the beam-end specimen in Figure 3.22 (b), the steel bar as well as the surrounding concrete are simultaneously placed in tension whereas the beam anchorage specimen (Figure 3.22 (c)) and the splice beam specimen (Figure 3.22 (d)) represent large-scale specimens ideally suited for direct measurement of development and splice strengths in prototype members.

In spite of their above mentioned drawbacks, pullout specimens have been widely used for investigation of bond behaviour because of their ease of fabrication and the simplicity of the test. Pullout tests also provide a simple and a convenient means for relative comparison of bond behaviour. One of the drawbacks of the pullout test

configuration is that the compressive struts formed between the test bearing surface and the surface of the embedded rebar place the rebar surface in compression. This however can be mitigated by suitable modifications in the setup of the test specimen which is described in more detail in a following section. According to ACI Committee 408 (1966), pullout tests remain useful for bond studies because:

(a) They give a reasonable estimate of the required anchorage length for a bar embedded in a pier or an inactive mass of concrete.

(b) It emphasises the idea of anchorage based on the requirement of a certain length of bar embedment beyond the section of maximum steel stress to prevent the bar from pulling out.

(c) It approximately simulates conditions adjacent to a concrete crack where the bar carries more tension than exists in nearby sections.

(d) The bar slip at the loaded face of the pullout specimen can be approximately correlated with crack width in a beam having comparable levels of steel stress as in the pullout specimens.

(e) The pullout test configuration can be very conveniently adopted to simulate the effect of cover on bond behaviour.

3.6.1.1 Pullout specimen parameters

The pullout tests were carried out using cylindrical specimens 100 mm in diameter and 200 mm long. Steel bar of the selected diameters (8 mm, 10 mm, 12 mm, 16 mm, 20 mm and 25 mm) were concentrically embedded in the cylindrical specimens. Although guidelines given in IS 2770(Part-I):1967 (1967b) and RILEM (1983) were generally followed with respect to the pullout specimen configuration, a significant deviation was also made with respect to the type of the pullout specimen. Both the above mentioned codes recommend cube specimens for pullout tests whereas in this investigation cylindrical specimens were used in order to ensure a uniform cover for a given rebar diameter. It may however be noted that since the size of the cylindrical specimens was kept the same for all the rebar sizes under investigation the ratio of the cover, c, and the rebar diameter, d_b, was not constant across the investigation. Hence, the c/d_b varied from 5.75 for the 8 mm bars to 1.5 for the 25 mm bars. The whole length of the embedded rebar was not bonded to the surrounding concrete. The bonded length of the rebar was kept equal to five times the rebar diameter (5 d_b) as per RILEM (1983) so as to avoid potential yielding of the bar during pullout. In order to eliminate the effect of compressive struts in pullout specimens, RILEM (1983) recommends the use of bond-breaker at the loaded end of the specimen. In this investigation however, the bond breaker was placed both at the loaded as well as the unloaded end of the pullout specimens with the 5 d_b

bonded length being located symmetrically in between. Typical arrangement of bond-breakers in the steel rebars is presented in Figure 3.23. Schematic details of a pullout specimen are shown in Figure 3.24.

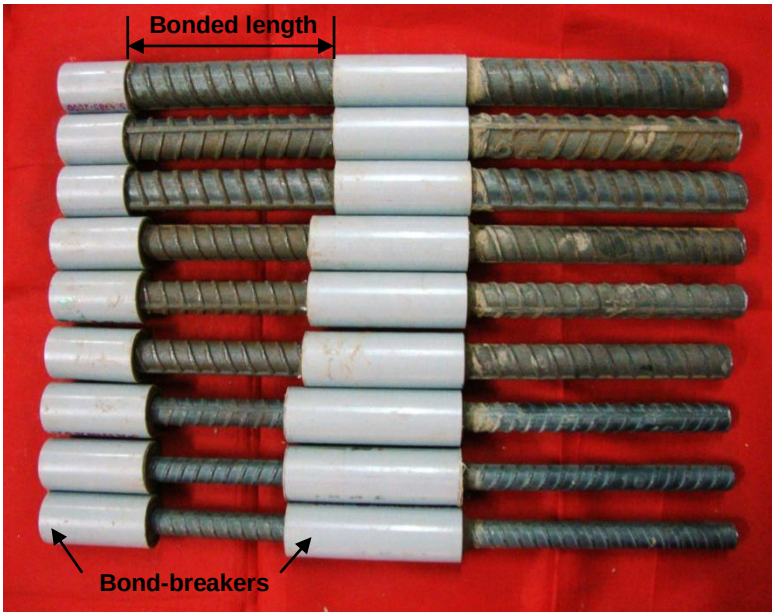

Figure 3.23 Typical rebars fixed with plastic tubes as bond-breaker

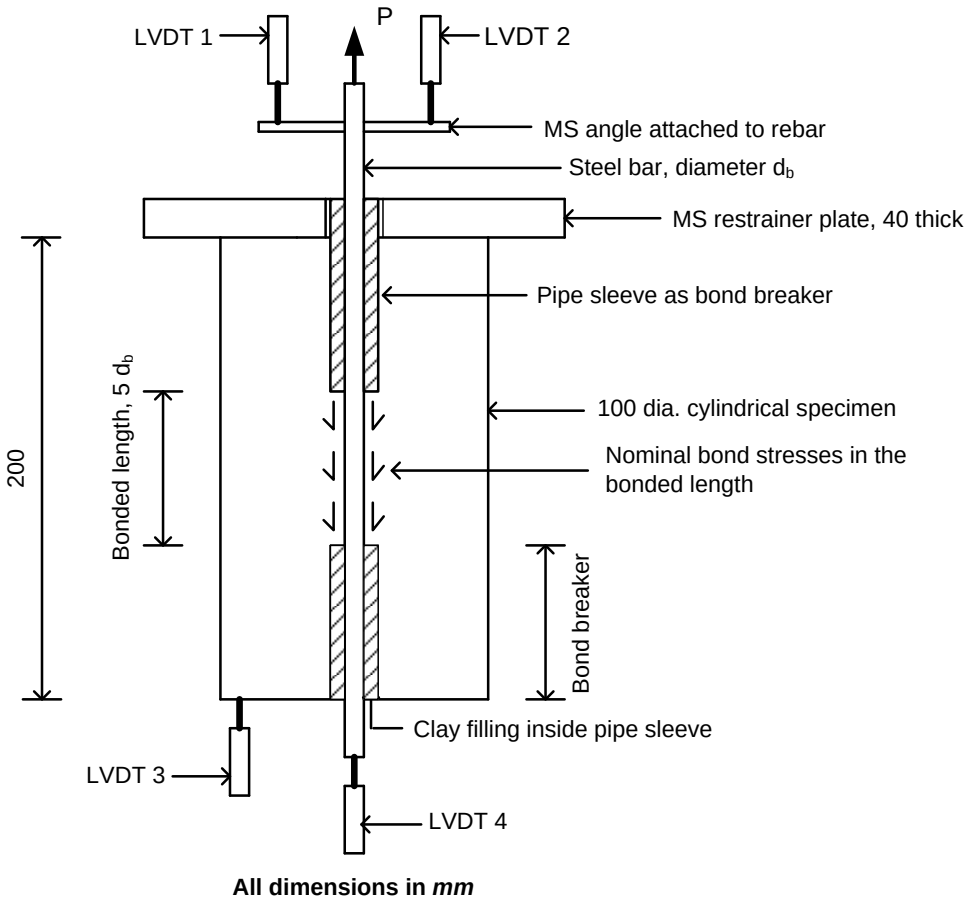

Figure 3.24 Pullout test setup configuration in elevation

3.6.1.2 Pullout specimen fabrication

The pullout specimens were cast in a vertical position in the laboratory using steel moulds and during casting and subsequent compaction, the concentrically placed steel bars were held in position using a specially designed steel fixture, Figure 3.25. Contact between the concrete and the rebar along the debonded length of the embedded rebar was broken using a soft plastic tube placed coaxially with the rebar and the annular space between the rebar and the plastic tube was filled with clay, which was subsequently removed after curing. Concrete was mixed in the laboratory using a tilting drum-type concrete mixer, poured into the moulds and compacted using a vibrating table. For preventing excessive evaporation from the fresh concrete, the pullout specimens were covered with a plastic sheet soon after casting. To ensure repeatability of results, a sample consisting of three nominally identical companion specimens were cast for each parameter under investigation. Six cylinders (100 mm diameter x 200 mm height) were also cast as control specimens with each batch of pullout specimens for finding the 56-day compressive strengths and the splitting tensile strengths. All the specimens were demoulded 24 h after casting following which they were moist cured in the laboratory for a nominal period of 56 days by immersion in a curing tank whose water was changed every week.

Figure 3.25 Pullout moulds with steel fixture

3.6.1.3 Pullout test setup

The pullout tests were performed in a stiff electro-hydraulic test frame using a specially fabricated mild steel rig rigidly connected to the testing machine. A schematic illustration of a test specimen and the instrumentation used in the pullout tests is shown in

Figure 3.24 and the test setup is presented in Figure 3.26. The RILEM (1983) recommended loading rate of 0.5 d_b^2 N/s (where d_b is the rebar diameter) was adopted in the pullout tests. During loading, the top cross-section the cylindrical pullout specimen was pressed against a stiff 40 mm thick mild steel restrainer plate, Figure 3.26, with a thin sheet of softwood and a layer of grease being placed between the soffit of the restrainer plate and the pullout specimen to ensure uniform contact and to minimise platen friction respectively. The test was performed by pulling the embedded rebar upward from the specimen and the applied load was measured with the help of a pressure sensor whose output was fed to an automatic data acquisition system. With reference to Figure 3.24, the average loaded end slip was measured with the help of the LVDT's (Linear Variable Differential Transformer) 1 and 2 and the net slip at the unloaded end was measured with the help of LVDT's 3 and 4, the output the LVDT's being recorded with the help of the data acquisition system. After reaching peak loads, in order to record the descending branch of the load-slip relationship, the pulling of the embedded rebar was continued such that the increase in slip was accompanied by a decrease in the load resisted by the specimen. The pullout tests were terminated when either of the following conditions occurred: (i) pull-through or rupture of the rebar (ii) splitting of concrete enclosing the rebar (iii) unloaded end slip in the range of 9 - 20 mm.

Figure 3.26 Pullout test setup

3.6.1.4 Variables in the pullout tests

Three concrete grades viz. normal-strength, medium-strength and high-strength, six rebar diameters and four RCA replacement levels were used in the pullout tests of this investigation. These variables are summarised in Table 3.12.

Table 3.12 Variables in the pullout test specimens

Concrete mix	RCA replacement level, *r* (%)	Rebar diameter (mm)	Number of replicate specimens in each variable	Total number of specimens
Mix A Mix B Mix C	0 25 50 75 100	8 10 12 16 20 25	3	270

3.6.1.5 Summary of the pullout test specimens

A total of 270 specimens were cast and tested and the summary of the pullout test specimens in normal-strength, medium-strength and high-strength concrete are presented in Tables 3.13, 3.14 and 3.15 respectively.

Note to Tables 3.13, 3.14 and 3.15:

[#] *Specimen ID: The alphabet in the first place-holder represents concrete grade (A: normal-strength, B: medium-strength, C: high-strength), the numerals in the second/third place-holders represent the nominal rebar diameters (8 mm, 10 mm, 12 mm, 16 mm, 20 mm, 25 mm) and the alpha-numeric characters in the remaining place holders represent RCA replacement levels (0: 0%, 25: 25%, 50: 50%, 75: 75% and 100: 100%).*

***** *Cover: The cover presented here is the side cover measured from the sides of the rebar to the extreme concrete face*

Table 3.13 Summary of the pullout test specimens – normal-strength concrete

Specimen ID[#]	Rebar diameter (mm)	RCA replacement level, *r* (%)	Cover[*] (mm)	c/d_b
A8R0	8	0	46	5.75
A8R25		25		
A8R50		50		
A8R75		75		
A8R100		100		
A10R0	10	0	45	4.50
A10R25		25		
A10R50		50		
A10R75		75		
A10R100		100		
A12R0	12	0	44	3.67
A12R25		25		
A12R50		50		
A12R75		75		
A12R100		100		
A16R0	16	0	42	2.63
A16R25		25		
A16R50		50		
A16R75		75		
A16R100		100		
A20R0	20	0	40	2.00
A20R25		25		
A20R50		50		
A20R75		75		
A20R100		100		
A25R0	25	0	37.5	1.50
A25R25		25		
A25R50		50		
A25R75		75		
A25R100		100		

Table 3.14 Summary of the pullout test specimens – medium-strength concrete

Specimen ID[#]	Rebar diameter (mm)	RCA replacement level, *r* (%)	Cover[*] (mm)	c/d_b
B8R0	8	0	46	5.75
B8R25		25		
B8R50		50		
B8R75		75		
B8R100		100		
B10R0	10	0	45	4.50
B10R25		25		
B10R50		50		
B10R75		75		
B10R100		100		
B12R0	12	0	44	3.67
B12R25		25		
B12R50		50		
B12R75		75		
B12R100		100		
B16R0	16	0	42	2.63
B16R25		25		
B16R50		50		
B16R75		75		
B16R100		100		
B20R0	20	0	40	2.00
B20R25		25		
B20R50		50		
B20R75		75		
B20R100		100		
B25R0	25	0	37.5	1.50
B25R25		25		
B25R50		50		
B25R75		75		
B25R100		100		

Table 3.15 Summary of the pullout test specimens – high-strength concrete

Specimen ID[#]	Rebar diameter (mm)	RCA replacement level, *r* (%)	Cover[*] (mm)	c/d_b
C8R0	8	0	46	5.75
C8R25		25		
C8R50		50		
C8R75		75		
C8R100		100		
C10R0	10	0	45	4.50
C10R25		25		
C10R50		50		
C10R75		75		
C10R100		100		
C12R0	12	0	44	3.67
C12R25		25		
C12R50		50		
C12R75		75		
C12R100		100		
C16R0	16	0	42	2.63
C16R25		25		
C16R50		50		
C16R75		75		
C16R100		100		
C20R0	20	0	40	2.00
C20R25		25		
C20R50		50		
C20R75		75		
C20R100		100		
C25R0	25	0	37.5	1.50
C25R25		25		
C25R50		50		
C25R75		75		
C25R100		100		

3.6.2 Splice beam specimens

In addition to the pullout tests, a selected number of splice beam specimens were also tested for better simulation of bond conditions in actual construction. The splice beam specimens were so designed that the splice was located in the constant moment region of the beam so that the compressive struts do not affect bond behaviour.

3.6.2.1 Splice beam specimen design

The splice beam specimens were designed keeping the recommendations of ACI 408R-03 (2003) in mind. Singly reinforced beams 1700 mm long and simply supported on an effective span of 1500 mm were tested. The beams had a rectangular section 225 mm deep with the width being 110 mm for the 12 mm diameter longitudinally steel bars and 180 mm for the 20 mm diameter longitudinal bars. The tension steel ratio, $\rho = \frac{A_b}{b\,d}$, was nominally kept constant at 0.01 and 0.018 respectively so that the beam sections were under-reinforced. With respect to the size of the longitudinal rebars, the scope of the splice beam investigations was limited to only two bar sizes viz. 12 mm and 20 mm and one splice length each was investigated for both the bars. For both these bar sizes, the c/d_b was nominally kept constant at 1.25. Typical detailing of the splice beam specimens reinforced with the 12 mm and the 20 mm bars is presented in Figure 3.27 and Figure 3.28 respectively. For the 12 mm and the 20 mm bars, the splice lengths were kept equal to 25 d_b and 20 d_b respectively with each of these lengths being significantly smaller than the ACI 318-11 (2011) required development length in tension. This was done in order to ensure that flexural failure did not pre-empt bond failure in the splice beam specimens. The other parameters in the splice beam tests were concrete grade (normal-strength, Mix A, and high-strength, Mix C) and the RCA replacement level (50 % and 100 %). A summary of the splice beam specimens is presented in Table 3.16. To ensure repeatability of results, a pair of two nominally identical specimens were cast for each parameter under investigation. An estimation of the maximum tensile force induced in the spliced longitudinal reinforcement bars is a vital input for calculating the average local bond stress in the beam specimens. Electrical-resistance type strain gauges having a gauge length of 5 mm were mounted on the spliced reinforcement at the locations shown in Figure 3.27 and Figure 3.28 for measuring strains. It may be noted that these figures that the strain gauges were intentionally mounted at the ends of the splice just outside that splice lead ends in order to minimise any disturbance to the distribution of bond forces in the spliced lengths.

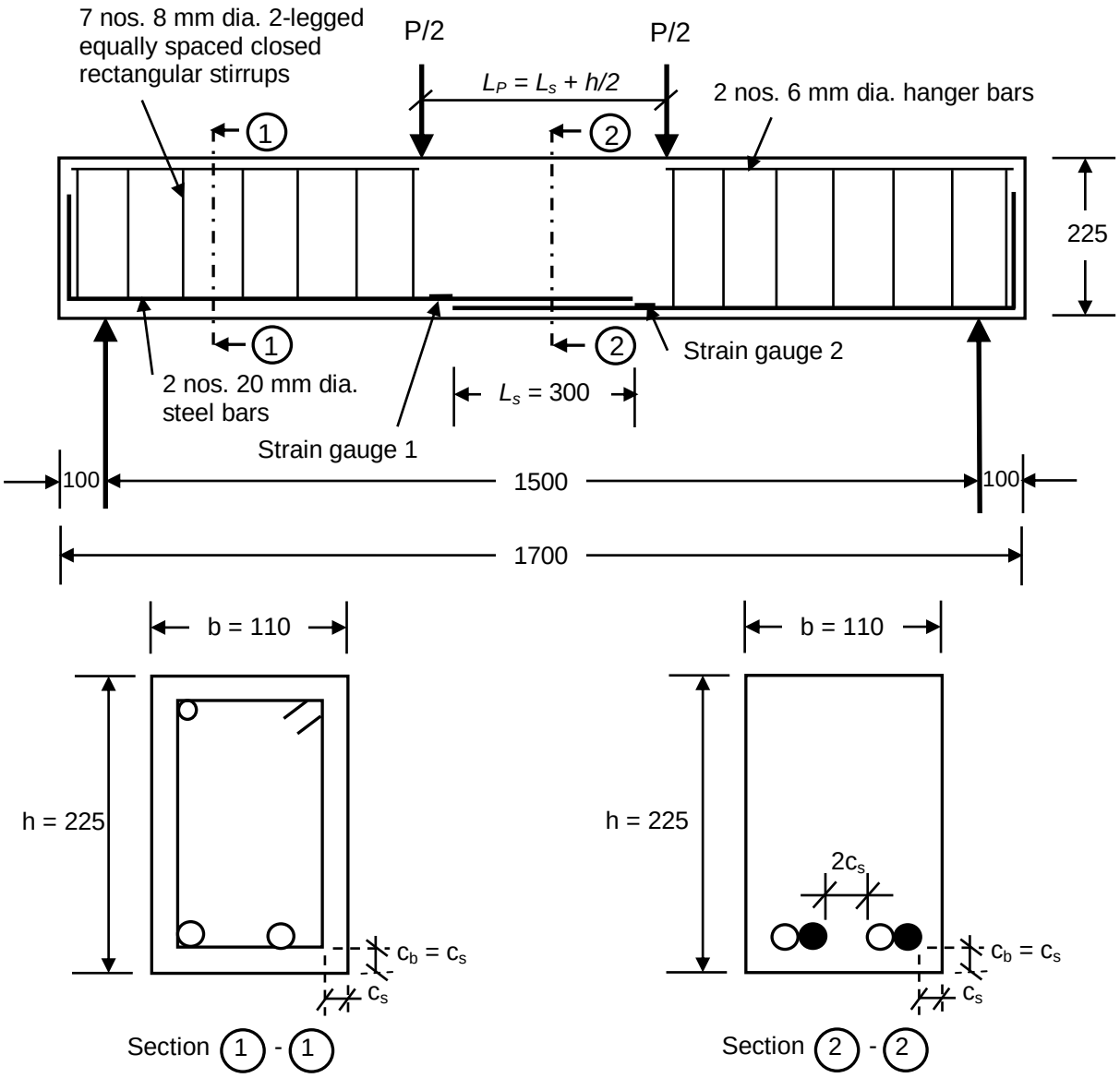

Note: All dimensions are in mm

Figure 3.27 Dimensions and reinforcement details of the splice beam specimens with 12 mm dia. main bars

The tensile force in the spliced rebars was calculated from the stress induced in the rebars due to the measured strain. The average local bond stress was calculated as follows:

$$\tau_{max} = \frac{A_b f_s}{\pi d_b L_s} \qquad (3.17)$$

where $\tau_{max,}$ the peak bond stress (MPa) between concrete and steel rebar, is also termed as the bond strength; A_b is the area of the reinforcing bar (mm^2); f_s is the stress in steel at failure (MPa); d_b is the nominal rebar diameter (mm) and L_s is the splice length (mm).

The stress was obtained from a moment-curvature analysis of the beam section. The details of this analysis are presented in Appendix A. The experimentally obtained bond strengths from the splice beam specimens were compared with predictions from the literature and from the bond stress model presented in this investigation and relevant conclusions drawn.

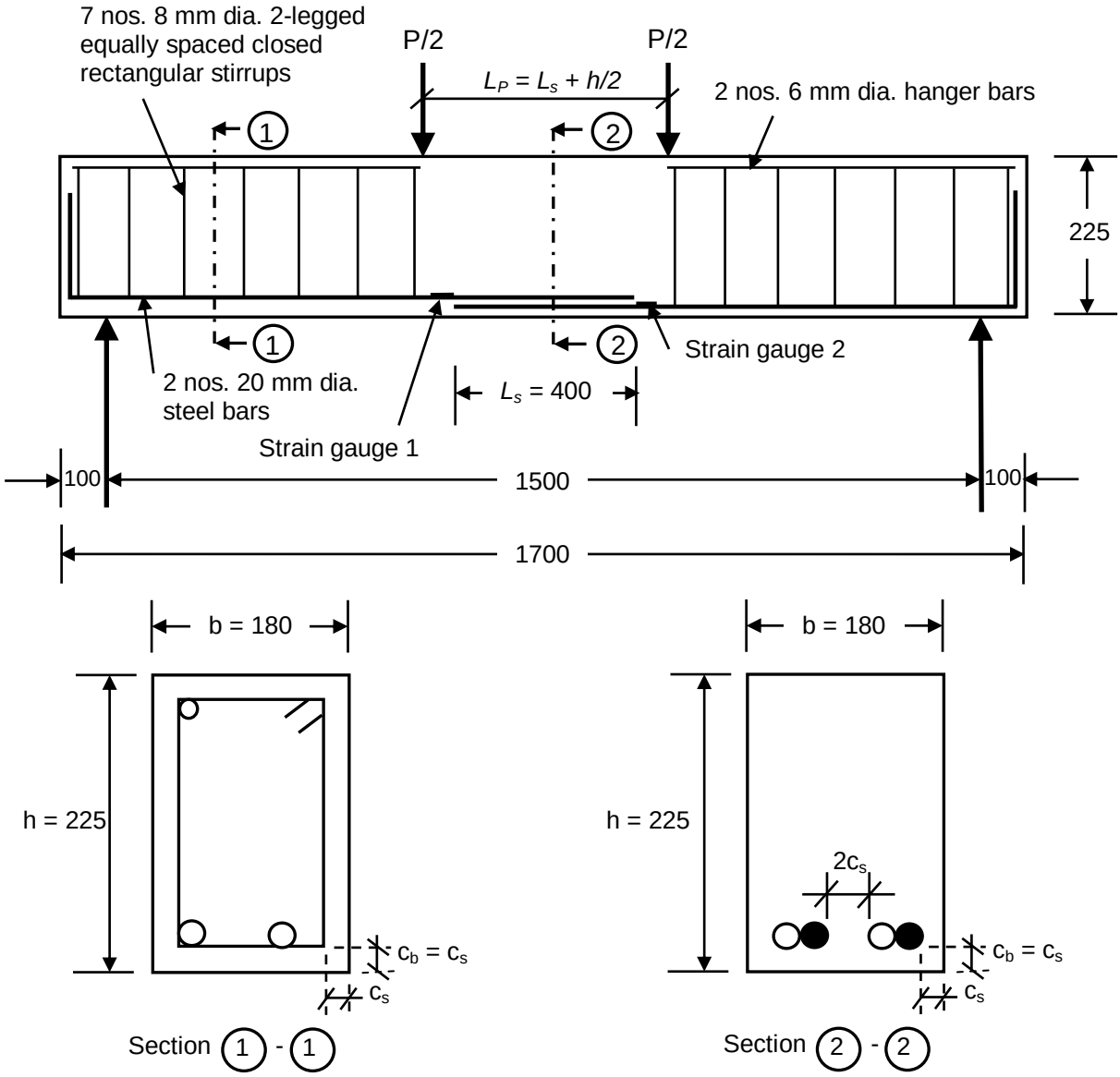

Note: All dimensions are in mm

Figure 3.28 Dimensions and reinforcement details of the splice beam specimens with 20 mm dia. main bars

Table 3.16 Summary of the splice specimens

Specimen ID[#]	Rebar dia. d_b (mm)	RCA replacement level, r (%)	b (mm)	h (mm)	c (mm)	L_s (mm)	c/d_b	L_s/d_b	L_p
1	2	3	4	5	6	7	8	9	10
AS12R0-1	12	0	110	225	15	300	1.25	25	420
AS12R0-2	12	0	110	225	15	300	1.25	25	420
AS12R50-1	12	50	110	225	15	300	1.25	25	420
AS12R50-2	12	50	110	225	15	300	1.25	25	420
AS12R100-1	12	100	110	225	15	300	1.25	25	420
AS12R100-2	12	100	110	225	15	300	1.25	25	420
AS20R0-1	20	0	180	225	25	400	1.25	20	520
AS20R0-2	20	0	180	225	25	400	1.25	20	520
AS20R50-1	20	50	180	225	25	400	1.25	20	520
AS20R50-2	20	50	180	225	25	400	1.25	20	520
AS20R100-1	20	100	180	225	25	400	1.25	20	520
AS20R100-2	20	100	180	225	25	400	1.25	20	520
CS12R0-1	12	0	110	225	15	300	1.25	25	420
CS12R0-2	12	0	110	225	15	300	1.25	25	420
CS12R50-1	12	50	110	225	15	300	1.25	25	420
CS12R50-2	12	50	110	225	15	300	1.25	25	420
CS12R100-1	12	100	110	225	15	300	1.25	25	420
CS12R100-2	12	100	110	225	15	300	1.25	25	420
CS20R0-1	20	0	180	225	25	400	1.25	20	520
CS20R0-2	20	0	180	225	25	400	1.25	20	520
CS20R50-1	20	50	180	225	25	400	1.25	20	520
CS20R50-2	20	50	180	225	25	400	1.25	20	520
CS20R100-1	20	100	180	225	25	400	1.25	20	520
CS20R100-2	20	100	180	225	25	400	1.25	20	520

Note to Table 3.16:

Column 1 = Specimen ID: The alphabet in the first place-holder represents concrete grade (A: normal-strength, C: high-strength), the alphabet in the second place-holder represents splice specimen, the numerals in the third/forth place-holders represent the nominal rebar diameters (12 mm, 20 mm) and the alpha-numeric characters in the remaining place holders represent RCA replacement levels (0: 0%, 50: 50%, and 100: 100%). Column 4 = b: breadth of the beam. Column 5 = h: height of the beam. Column 6 = c: concrete cover (minimum of bottom cover, c_b and side cover, c_s). Column 7 = L_s: splice length. Column 10 = L_p: distance between two load points.

3.6.2.2 Splice beam specimen fabrication

All the splice beam specimens were fabricated in the laboratory with the pre-assembled steel reinforcement cages being lowered into the steel formwork followed by casting of concrete. Before assembly, strain gauge locations were marked on the longitudinal rebars and at these locations the rebar surface was ground smooth with a hand grinder and cleaned with emery paper and acetone. After reinforcement caging, the strain gauges were pasted on to the bar surface with a thin film of adhesive and allowed to dry. Wires were soldered to the strain gauges and a flexible tube was inserted to safeguard the wires during casting. The strain gauges were covered with a thick film of water resistant paste to arrest the entry of water during casting. A set of assembled reinforcement cages together with strain gauges mounted on the spliced bars is shown in Figure 3.29. Prior to casting, a thin layer of shutter-release oil was applied on the inner surface of the steel forms. Then the reinforcement cages are placed inside the forms before which the precast concrete cover blocks were inserted to maintain the required side and bottom covers. Figure 3.30 shows two splice specimens ready for casting. Concrete was mixed in the laboratory using a tilting drum-type mixer, poured into the forms and compacted layer-by-layer using a needle-type vibrator and the top surface was levelled. To prevent excessive evaporation from the fresh concrete, the splice specimens were covered with a plastic sheet soon after casting. Six cylinders (100 mm diameter x 200 mm height) were also cast together with every set of the splice beams to serve as control specimens for finding the 56-day compressive strengths and splitting tensile strengths. All the specimens were demoulded 24 h after casting following which they were moist cured in the laboratory for a nominal period of 56 days by immersion in a curing tank whose water was changed every week.

Figure 3.29 A set of reinforcement cages for the splice beam specimens

Figure 3.30 A pair of splice beam specimens ready for casting

3.6.2.3 Test setup

Bending tests under displacement-controlled loading were performed on the splice beam specimens in a close-loop servo-controlled 2500 kN capacity universal testing machine using a specially fabricated mild steel loading frame. The specimens were simply supported at both their ends with one support simulating a hinge and the other a roller. Test setup configuration is shown in Figure 3.31 and a splice beam test in progress is presented in Figure 3.32. The splice beams were tested in four-point bending with the loads being applied using a stiff spreader beam on top of the test specimen. The applied load was measured using the internal load cell in the actuator and the deflections under the load points as well as at the beam mid-span were measured using Linear Variable Differential Transformers (LVDTs). The outputs of the LVDTs, the steel strain gauges as well as that of the load cell mounted in the UTM actuator was recorded with the help of a data acquisition system at a sampling frequency of 1 s.

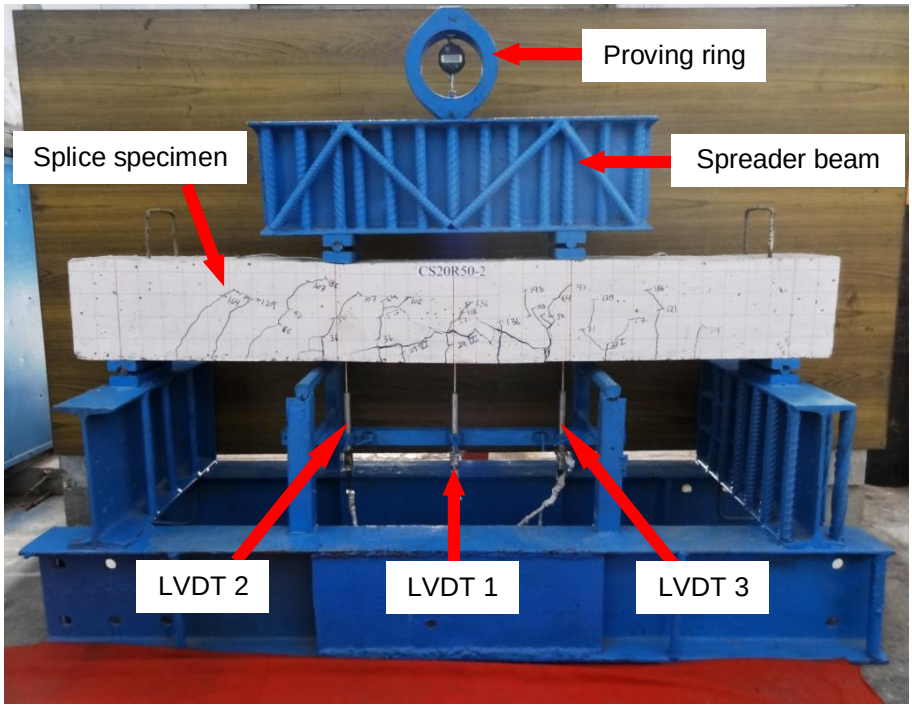

Figure 3.31 Splice beam test setup

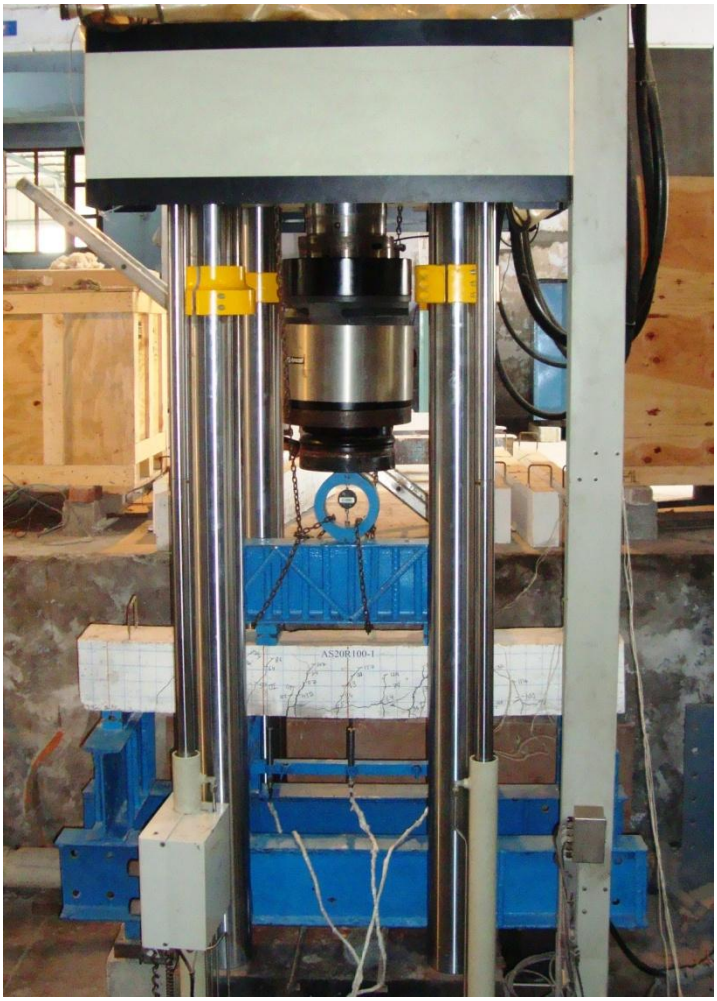

Figure 3.32 Splice beam test in progress

The splice beams were white-washes and allowed to surface dry before testing. A rectangular grid with a line spacing of 50 mm in the vertical direction and a line spacing of 50 mm in the horizontal direction was marked on the side faces. The soffit of the 110 mm width beams are marked at a spacing of 27.5 mm in width direction and 50 mm in longitudinal direction while the soffit of the 180 mm width beams are marked at a spacing of 30 mm in width direction and 50 mm in longitudinal direction. The beams were tested under a displacement-controlled loading rate of 0.3 mm/min till failure. It may be noted that since flexural cracks tend to develop close to the load points which in turn may effect bond force in the bars within the splice zone, the two-point loads were spaced at a distance $L_p=L_s+h/2$ from each other as per the recommendations of Harajli and Abouniaj (2010). This arrangement is meant to ensure that flexural cracking has minimal effect on distribution of bond forces in the spliced rebars. Because the displacement-controlled loading was applied in a continuous manner it was not possible to physical monitor crack widths in the beams with a hand-held crack comparator. Hence, no cracks widths have been reported for the splice beam specimens. The average time taken for testing each splice beam specimen was 20 min. The control cylinders were tested for compressive strength and splitting tensile strength on the same day as the companion beam specimen. A summary of all the splice beam specimens is presented in Table 3.16.

3.6.2.4 Variables in the splice beam tests

A summary of the variables investigated in the splice beam test programme is presented in Table 3.17.

Table 3. 17 Variables in the splice beam test specimens

Concrete mix	RCA replacement level, *r* (%)	Rebar diameter (mm)	Number of replicate specimens in each variable	Total number of specimens
Mix A Mix C	0 50 100	12 20	2	24

3.7 CONCLUSION

This experimental programme described in this chapter includes the relevant material properties and specifications of the ingredients of concrete, reinforcement steel etc., the testing procedures and the associated instrumentation. The properties of the fresh and hardened concrete have been presented graphically under the relevant subsections. The details of the pullout and splice beam specimens have been presented. The test results, their analysis and subsequent discussions follow in the next chapter, Results and Discussion.

Chapter 4

RESULTS AND DISCUSSION

4.1 INTRODUCTION

The results of the experimental investigation are presented and discussed in this chapter. The results of Phase I of the experimental investigation which focused on bond behaviour of RCA concrete investigated with the help of pullout specimens are presented first followed by results of Phase II wherein bond of steel reinforcement in RCA concrete was studied with the help of splice beam specimens. Conclusions of this investigation are presented in the next chapter.

4.2 PHASE I: INVESTIGATION OF BOND BEHAVIOUR WITH PULLOUT SPECIMENS

4.2.1 Experimental results

4.2.1.1 Compressive strength

The measured 56-day cylinder compressive strengths of the three grades of recycled aggregate concrete are presented in Tables 4.1, 4.2 and 4.3. The variation of compressive strength as a function of the RCA replacement level is presented in Figure 4.1. The trends in this figure show that for the normal-strength concrete, compressive strength decreased by 33 % as the RCA replacement level increased from 0 % to 100 % and the corresponding figure for the medium-strength concrete was about 30 %. Unlike the aforesaid concrete grades, a uniform decrease in compressive strength with increasing RCA replacement levels was not observed in the case of the high-strength concrete, though between the lower-bound and upper-bound replacement levels of 0 % and 100 % respectively, the measured compressive strength decreased by about 27 % for this concrete grade. The above observations are in agreement with results reported in the literature to the effect that compressive strength decreases (to varying degrees) with increase in the amount of RCA particles in concrete.

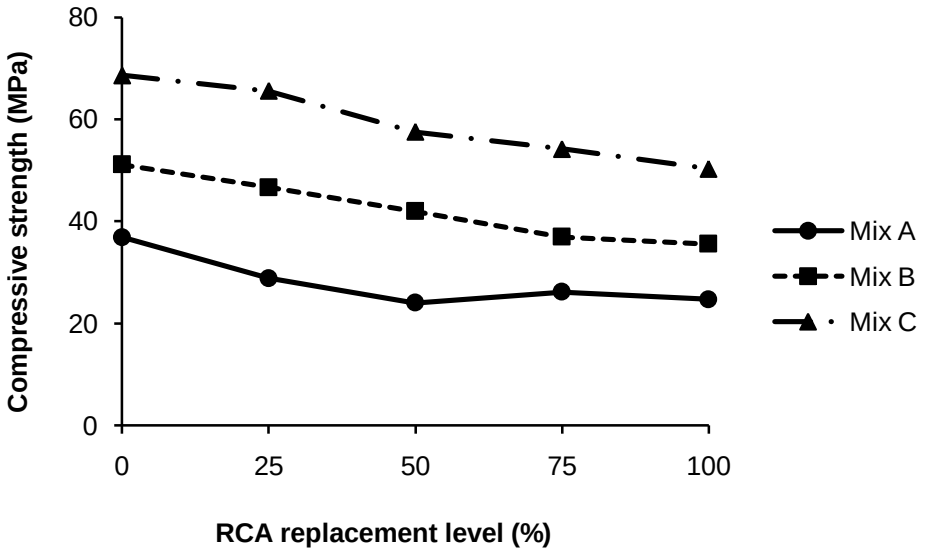

Figure 4. 1 Variation of compressive strength with RCA replacement level

4.2.1.2 Splitting tensile strength

The trends in the measured splitting tensile strengths of the three concrete grades are presented in Figure 4.2. The trends in Figure 4.2 show that the splitting tensile strength increased by 18 %, 13 % and 19 % for the normal-, medium- and the high-strength concrete respectively, as the RCA replacement level increased from 0 % to 100 %. It may be noted that for all the three concrete grades, this gain in splitting tensile strength was not uniform across the four replacement levels of 25 %, 50 %, 75 % and 100 % considered in this investigation. In the literature, no significant difference is reported between indirect tensile strength of recycled aggregate concrete (made with coarse recycled aggregate) and that of conventional concrete (BCSJ, 1978; Mukai *et al*., 1978; Ravindrarajah and Tam, 1985). According to Gerardu and Hendriks (1985), at the most, the indirect tensile strength of recycled aggregate concrete made with coarse recycled aggregate and natural sand may be 10 % lower compared to that of conventional concrete. On the other hand, the results of this investigation indicate a significant increase in the indirect tensile strength, irrespective of the concrete grade, when all the natural coarse aggregate was replaced with recycled aggregate. Although in the absence of any widely accepted test, the quality of bond between the aggregate particles and the hardened cement paste could not be measured, the observed higher splitting tensile strength of the recycled aggregate concretes is attributed to the relatively better aggregate-cement paste bond in recycled aggregate concrete due to higher surface roughness of the recycled concrete aggregate particles. It may be of relevance to note that according to Regan *et al.* (2005), in a heterogeneous material like concrete, beyond a very early age, the main parameters affecting the crack path under the action of a tensile

force are the strength of the parent rock (which makes up the coarse aggregate) and the shape and surface texture of the aggregate particles. Hence, if the recycled aggregate has been derived from quality parent concrete, a more tortuous crack path can be expected in recycled aggregate concrete with the result that behaviour under a tensile stress can be significantly different from that of conventional concrete.

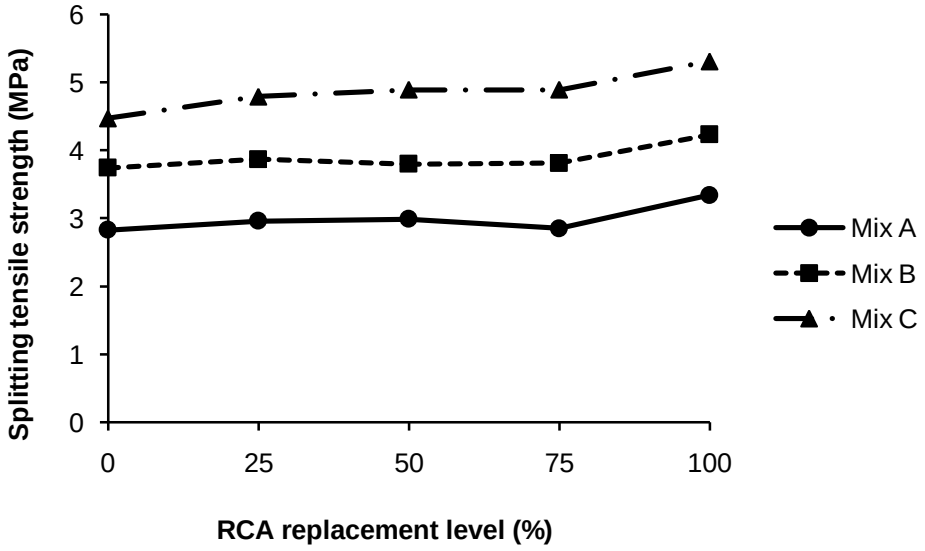

Figure 4. 2 Variation of splitting tensile strength with RCA replacement level

4.2.1.3 Bond strength

Assuming a uniform bond stress distribution over the short embedded length of a steel rebar in concrete, the bond strength is given by the following relationship

$$\tau_{\max} = \frac{P_{\max}}{\pi d_b L_d} \tag{4.1}$$

where $\tau_{\max}$, the peak bond stress (MPa) between concrete and steel rebar, is also termed as the bond strength; P_{max} is the peak load (N), d_b is the nominal rebar diameter (mm) and L_d is the bonded length (mm) taken equal to 5 d_b in this investigation. The experimental results of all the 270 pullout specimens made of the normal-, medium- and the high-strength concrete are presented in Tables 4.1, 4.2 and 4.3 respectively. For each parameter under investigation, three nominally identical pullout specimens were tested. The average value of the peak bond stress as well as the corresponding slip for each of the specimens is also given in the above mentioned tables.

Note to Tables 4.1, 4.2 and 4.3:

Column 1 = Specimen ID: The alphabet in the first place-holder represents concrete grade (A: normal-strength, B: medium-strength, C: high-strength), the numerals in the second/third place-holders represent the nominal rebar diameters (8 mm, 10 mm, 12 mm, 16 mm, 20 mm, 25 mm) and the alpha-numeric characters in the remaining place holders represent RCA replacement levels (0: 0%, 50: 50%, and 100: 100%). Column 2 = $f_c^{'}$ *: cylinder compressive strength. Column 3 =* P_{max} *: peak load. Column 4 = Average* P_{max} *: average peak load of companion specimens. Column 5 =* τ_{max} *: peak bond stress. Column 6 = Mean* τ_{max} *: mean peak bond stress of companion specimens. Column 7 = s: slip at unloaded end. Column 8 = average s: average slip at unloaded end. Column 9 =* $\tau_{r,max}$ *: normalised bond strength. Column 10 = failure mode.*

Table 4.1 Experimental results of the normal-strength concrete pullout specimens

Specimen ID	f_c'	P_{max}	Average, P_{max}	Bond stress τ_{max}	Mean τ_{max}	Slip at unloaded end s	Average slip at unloaded end s	Normalised bond strength $\tau_{r,max}$	Failure Mode
	MPa	kN	kN	MPa	MPa	mm	mm	MPa^(1/2)	
1	2	3	4	5	6	7	8	9	10
A8R0-1		25.20		25.06		0.662			
A8R0-2	36.91	22.87	23.46	22.74	23.34	0.863	0.713	3.84	PO
A8R0-3		22.32		22.20		0.613			
A8R25-1		15.31		15.22		0.354			
A8R25-2	28.88	13.73	14.01	13.66	13.94	0.421	0.508	2.59	PO
A8R25-3		13.00		12.93		0.747			
A8R50-1		21.02		20.91		0.393			
A8R50-2	24.04	20.06	21.25	19.95	21.14	0.615	0.560	4.31	PO
A8R50-3		22.69		22.57		0.671			
A8R75-1		16.81		16.73		0.361			
A8R75-2	26.16	17.66	17.03	17.57	16.94	0.322	0.348	3.31	PO
A8R75-3		16.61		16.52		0.360			
A8R100-1		21.78		21.66		0.432			
A8R100-2	24.71	24.08	22.83	23.96	22.71	0.619	0.517	4.57	PO
A8R100-3		22.64		22.52		0.500			
A10R0-1		28.37		18.06		0.598			
A10R0-2	36.91	27.67	28.24	17.61	17.98	0.595	0.576	2.96	PO
A10R0-3		28.67		18.25		0.536			
A10R25-1		29.12		18.54		0.535			
A10R25-2	28.88	31.34	30.25	19.95	19.26	0.619	0.708	3.58	PO
A10R25-3		30.29		19.28		0.968			
A10R50-1		24.48		15.58		0.476			
A10R50-2	24.04	29.15	27.12	18.56	17.27	1.046	0.590	3.52	PO
A10R50-3		27.74		17.66		0.249			
A10R75-1		24.72		15.74		0.467			
A10R75-2	26.16	28.83	27.64	18.36	17.59	0.505	0.486	3.44	PO
A10R75-3		29.35		18.69		0.485			
A10R100-1		28.92		18.41		0.666			
A10R100-2	24.71	30.15	28.77	19.20	18.32	0.556	0.595	3.68	PO
A10R100-3		27.24		17.34		0.562			
A12R0-1		43.58		19.27		0.555			
A12R0-2	36.91	43.03	42.25	19.02	18.68	0.585	0.561	3.07	PS
A12R0-3		40.13		17.74		0.542			
A12R25-1		44.03		19.47		0.946			
A12R25-2	28.88	45.04	44.19	19.91	19.54	0.286	0.651	3.64	PS
A12R25-3		43.50		19.23		0.720			
A12R50-1		43.23		19.11		0.831			
A12R50-2	24.04	40.85	42.69	18.06	18.87	0.447	0.657	3.85	PS
A12R50-3		43.99		19.45		0.694			
A12R75-1		35.60		15.74		0.752			
A12R75-2	26.16	45.52	43.01	20.12	19.01	0.674	0.710	3.72	PS
A12R75-3		47.90		21.18		0.705			
A12R100-1		43.47		19.22		0.627			
A12R100-2	24.71	44.39	43.23	19.63	19.11	0.617	0.636	3.84	PS
A12R100-3		41.82		18.49		0.665			

PO : Pullout *PS : Pullout failure induced by through splitting*

Table 4.1 (*Continued*)

Specimen ID	f_c'	P_{max}	Average P_{max}	Bond stress τ_{max}	Mean τ_{max}	Slip at unloaded end *s*	Average slip at unloaded end *s*	Normalised bond strength $\tau_{r,max}$	Failure Mode
	MPa	kN	kN	MPa	MPa	mm	mm	MPa^(1/2)	
1	2	3	4	5	6	7	8	9	10
A16R0-1		61.22		15.23		0.539			
A16R0-2	36.91	58.31	59.92	14.50	14.90	0.512	0.512	2.45	PS
A16R0-3		60.22		14.98		0.486			
A16R25-1		56.83		14.13		0.481			
A16R25-2	28.88	60.18	58.50	14.97	14.55	0.492	0.498	2.71	PS
A16R25-3		58.50		14.55		0.521			
A16R50-1		47.87		11.90		0.469			
A16R50-2	24.04	50.40	50.38	12.53	12.53	0.499	0.479	2.56	PS
A16R50-3		52.88		13.15		0.468			
A16R75-1		56.11		13.95		0.465			
A16R75-2	26.16	52.10	54.10	12.96	13.45	0.440	0.445	2.63	PS
A16R75-3		54.08		13.45		0.430			
A16R100-1		53.14		13.21		0.392			
A16R100-2	24.71	56.28	55.03	14.00	13.68	0.427	0.417	2.75	PS
A16R100-3		55.66		13.84		0.433			
A20R0-1		83.02		13.21		0.502			
A20R0-2	36.91	86.73	84.63	13.80	13.47	0.517	0.495	2.22	PS
A20R0-3		84.13		13.39		0.466			
A20R25-1		76.11		12.11		0.486			
A20R25-2	28.88	75.62	77.12	12.04	12.27	0.456	0.463	2.28	PS
A20R25-3		79.64		12.67		0.447			
A20R50-1		78.44		12.48		0.452			
A20R50-2	24.04	75.61	75.71	12.03	12.05	0.467	0.447	2.46	PS
A20R50-3		73.08		11.63		0.422			
A20R75-1		79.23		12.61		0.410			
A20R75-2	26.16	82.82	82.61	13.18	13.15	0.409	0.420	2.57	PS
A20R75-3		85.79		13.65		0.442			
A20R100-1		83.16		13.24		0.376			
A20R100-2	24.71	81.22	83.13	12.93	13.23	0.392	0.395	2.66	PS
A20R100-3		85.02		13.53		0.416			
A25R0-1		95.82		9.76		0.459			
A25R0-2	36.91	97.35	95.55	9.92	9.73	0.496	0.480	1.60	PS
A25R0-3		93.47		9.52		0.485			
A25R25-1		92.59		9.43		0.461			
A25R25-2	28.88	90.45	89.89	9.21	9.16	0.446	0.444	1.70	PS
A25R25-3		86.63		8.82		0.425			
A25R50-1		77.11		7.85		0.398			
A25R50-2	24.04	78.63	79.45	8.01	8.09	0.426	0.405	1.65	PS
A25R50-3		82.60		8.41		0.392			
A25R75-1		77.46		7.89		0.371			
A25R75-2	26.16	82.67	80.51	8.42	8.20	0.380	0.381	1.60	PS
A25R75-3		81.40		8.29		0.392			
A25R100-1		84.15		8.57		0.395			
A25R100-2	24.71	80.16	82.14	8.16	8.37	0.370	0.374	1.68	PS
A25R100-3		82.12		8.36		0.356			

PO : Pullout *PS : Pullout failure induced by through splitting*

Table 4.2 Experimental results of the medium-strength concrete pullout specimens

Specimen ID	f_c'	P_{max}	Average P_{max}	Bond stress τ_{max}	Mean τ_{max}	Slip at unloaded end s	Average slip at unloaded end s	Normalised bond strength $\tau_{r,max}$	Failure Mode
	MPa	kN	kN	MPa	MPa	mm	mm	MPa^^(1/2)	
1	2	3	4	5	6	7	8	9	10
B8R0-1	51.14	28.77	28.17	28.62	28.02	0.516	0.539	3.92	PO
B8R0-2		27.42		27.27		0.549			
B8R0-3		28.33		28.18		0.552			
B8R25-1	46.70	29.36	28.81	29.21	28.65	0.608	0.560	4.19	PO
B8R25-2		27.44		27.29		0.550			
B8R25-3		29.62		29.46		0.521			
B8R50-1	41.96	29.42	30.42	29.27	30.26	0.542	0.583	4.67	PO
B8R50-2		30.58		30.42		0.628			
B8R50-3		31.26		31.09		0.580			
B8R75-1	36.97	33.46	32.49	33.28	32.32	0.568	0.619	5.32	PO
B8R75-2		33.04		32.86		0.675			
B8R75-3		30.99		30.83		0.613			
B8R100-1	35.58	28.83	29.49	28.68	29.33	0.652	0.598	4.92	PO
B8R100-2		29.15		28.99		0.568			
B8R100-3		30.49		30.33		0.574			
B10R0-1	51.14	39.03	39.29	24.85	25.01	0.497	0.486	3.50	PO
B10R0-2		39.06		24.86		0.431			
B10R0-3		39.78		25.33		0.529			
B10R25-1	46.70	37.29	37.91	23.74	24.13	0.475	0.518	3.53	PO
B10R25-2		39.93		25.42		0.567			
B10R25-3		36.52		23.25		0.512			
B10R50-1	41.96	41.93	40.92	26.70	26.05	0.618	0.567	4.02	PS
B10R50-2		40.57		25.83		0.572			
B10R50-3		40.25		25.62		0.511			
B10R75-1	36.97	41.30	40.40	26.29	25.72	0.562	0.585	4.23	PS
B10R75-2		40.34		25.68		0.549			
B10R75-3		39.58		25.19		0.643			
B10R100-1	35.58	36.25	35.45	23.08	22.57	0.515	0.537	3.78	PS
B10R100-2		36.58		23.29		0.492			
B10R100-3		33.53		21.35		0.603			
B12R0-1	51.14	48.13	44.75	21.28	19.78	0.489	0.456	2.77	PS
B12R0-2		44.24		19.56		0.457			
B12R0-3		41.89		18.52		0.423			
B12R25-1	46.70	46.05	46.09	20.36	20.38	0.523	0.475	2.98	PS
B12R25-2		45.49		20.11		0.456			
B12R25-3		46.73		20.66		0.447			
B12R50-1	41.96	37.56	38.24	16.61	16.90	0.401	0.432	2.61	PS
B12R50-2		38.29		16.93		0.482			
B12R50-3		38.86		17.18		0.412			
B12R75-1	36.97	46.34	47.92	20.49	21.19	0.609	0.543	3.48	PS
B12R75-2		48.82		21.58		0.514			
B12R75-3		48.61		21.49		0.506			
B12R100-1	35.58	45.44	44.24	20.09	19.56	0.467	0.497	3.28	PS
B12R100-2		43.21		19.10		0.534			
B12R100-3		44.08		19.49		0.489			

PO : Pullout *PS : Pullout failure induced by through splitting*

Table 4.2 (*Continued*)

Specimen ID	f_c'	P_{max}	Average P_{max}	Bond stress τ_{max}	Mean τ_{max}	Slip at unloaded end *s*	Average slip at unloaded end *s*	Normalised bond strength $\tau_{r,max}$	Failure Mode
	MPa	kN	kN	MPa	MPa	mm	mm	MPa^(1/2)	
1	2	3	4	5	6	7	8	9	10
B16R0-1		57.14		14.21		0.421			
B16R0-2	51.14	61.56	59.53	15.31	14.80	0.456	0.426	2.07	PS
B16R0-3		59.90		14.90		0.401			
B16R25-1		57.64		14.33		0.491			
B16R25-2	46.70	57.73	57.68	14.36	14.34	0.421	0.442	2.10	PS
B16R25-3		57.68		14.34		0.414			
B16R50-1		50.53		12.57		0.432			
B16R50-2	41.96	50.74	53.12	12.62	13.21	0.385	0.392	2.04	PS
B16R50-3		58.09		14.45		0.360			
B16R75-1		60.44		15.03		0.449			
B16R75-2	36.97	67.71	63.55	16.84	15.80	0.487	0.492	2.60	PS
B16R75-3		62.51		15.54		0.541			
B16R100-1		50.75		12.62		0.452			
B16R100-2	35.58	56.54	54.45	14.06	13.54	0.431	0.461	2.27	PS
B16R100-3		56.07		13.94		0.501			
B20R0-1		70.30		11.19		0.434			
B20R0-2	51.14	74.76	74.26	11.90	11.82	0.402	0.395	1.65	PS
B20R0-3		77.71		12.37		0.350			
B20R25-1		74.27		11.82		0.374			
B20R25-2	46.70	86.09	77.93	13.70	12.40	0.453	0.410	1.81	PS
B20R25-3		73.42		11.69		0.402			
B20R50-1		64.16		10.21		0.321			
B20R50-2	41.96	62.87	62.41	10.01	9.93	0.374	0.363	1.53	PS
B20R50-3		60.22		9.58		0.395			
B20R75-1		70.36		11.20		0.438			
B20R75-2	36.97	68.86	69.49	10.96	11.06	0.475	0.441	1.82	PS
B20R75-3		69.24		11.02		0.410			
B20R100-1		68.54		10.91		0.423			
B20R100-2	35.58	71.44	70.30	11.37	11.19	0.459	0.456	1.88	PS
B20R100-3		70.93		11.29		0.486			
B25R0-1		87.77		8.94		0.421			
B25R0-2	51.14	89.72	86.78	9.14	8.84	0.443	0.412	1.24	PS
B25R0-3		82.85		8.44		0.372			
B25R25-1		72.44		7.38		0.334			
B25R25-2	46.70	86.20	78.10	8.78	7.96	0.360	0.335	1.16	PS
B25R25-3		75.68		7.71		0.312			
B25R50-1		70.30		7.16		0.335			
B25R50-2	41.96	80.70	74.61	8.22	7.60	0.371	0.364	1.17	PS
B25R50-3		72.84		7.42		0.387			
B25R75-1		71.13		7.25		0.412			
B25R75-2	36.97	73.73	73.04	7.51	7.44	0.391	0.381	1.22	PS
B25R75-3		74.28		7.57		0.340			
B25R100-1		75.55		7.70		0.394			
B25R100-2	35.58	71.83	73.65	7.32	7.50	0.418	0.420	1.26	PS
B25R100-3		73.57		7.49		0.447			

PO : Pullout *PS : Pullout failure induced by through splitting*

Table 4.3 Experimental results of the high-strength concrete pullout specimens

Specimen ID	f_c'	P_{max}	Average P_{max}	Bond stress τ_{max}	Mean τ_{max}	Slip at unloaded end s	Average slip at unloaded end s	Normalised bond strength $\tau_{r,max}$	Failure Mode
	MPa	kN	kN	MPa	MPa	mm	mm	MPa^^(1/2)	
1	2	3	4	5	6	7	8	9	10
C8R0-1	68.65	34.18	33.48	34.00	33.31	0.521	0.481	4.02	PO
C8R0-2		32.65		32.47		0.481			
C8R0-3		33.62		33.44		0.441			
C8R25-1	65.60	33.65	32.28	33.47	32.11	0.482	0.450	3.96	PO
C8R25-2		33.83		33.65		0.418			
C8R25-3		29.36		29.21		0.450			
C8R50-1	57.54	28.94	32.38	28.79	32.21	0.462	0.497	4.25	PO
C8R50-2		34.26		34.07		0.538			
C8R50-3		33.95		33.77		0.492			
C8R75-1	54.20	33.73	33.13	33.55	32.96	0.531	0.516	4.48	PO
C8R75-2		33.30		33.12		0.562			
C8R75-3		32.38		32.21		0.454			
C8R100-1	50.30	34.86	32.85	34.68	32.67	0.594	0.534	4.61	PO
C8R100-2		30.45		30.29		0.483			
C8R100-3		33.23		33.06		0.525			
C10R0-1	68.65	46.48	46.52	29.59	29.61	0.401	0.436	3.57	PO
C10R0-2		47.77		30.41		0.455			
C10R0-3		45.30		28.84		0.453			
C10R25-1	65.60	47.54	46.28	30.27	29.46	0.504	0.454	3.64	PS
C10R25-2		44.08		28.06		0.432			
C10R25-3		47.21		30.05		0.425			
C10R50-1	57.54	43.63	45.22	27.77	28.79	0.512	0.509	3.79	PS
C10R50-2		47.38		30.16		0.544			
C10R50-3		44.65		28.42		0.471			
C10R75-1	54.20	46.25	43.16	29.44	27.48	0.538	0.494	3.73	PS
C10R75-2		43.69		27.81		0.442			
C10R75-3		39.56		25.19		0.503			
C10R100-1	50.30	39.71	41.50	25.28	26.42	0.432	0.476	3.72	PS
C10R100-2		43.88		27.94		0.507			
C10R100-3		40.90		26.04		0.488			
C12R0-1	68.65	59.71	59.00	26.40	26.08	0.431	0.464	3.15	PS
C12R0-2		58.42		25.83		0.463			
C12R0-3		58.86		26.02		0.497			
C12R25-1	65.60	55.97	59.25	24.74	26.20	0.525	0.481	3.23	PS
C12R25-2		59.92		26.49		0.434			
C12R25-3		61.87		27.35		0.483			
C12R50-1	57.54	55.19	53.12	24.40	23.49	0.458	0.418	3.10	PS
C12R50-2		52.30		23.12		0.426			
C12R50-3		51.88		22.94		0.371			
C12R75-1	54.20	55.91	51.16	24.72	22.62	0.352	0.394	3.07	PS
C12R75-2		49.42		21.85		0.392			
C12R75-3		48.13		21.28		0.439			
C12R100-1	50.30	46.31	50.04	20.48	22.12	0.487	0.443	3.12	PS
C12R100-2		48.38		21.39		0.437			
C12R100-3		55.43		24.50		0.404			

PO : Pullout *PS : Pullout failure induced by through splitting*

Table 4.3 (*Continued*)

Specimen ID	f_c'	P_{max}	Average P_{max}	Bond stress τ_{max}	Mean τ_{max}	Slip at unloaded end *s*	Average slip at unloaded end *s*	Normalised bond strength $\tau_{r,max}$	Failure Mode
	MPa	kN	kN	MPa	MPa	mm	mm	MPa^(1/2)	
1	2	3	4	5	6	7	8	9	10
C16R0-1		92.26		22.94		0.423			
C16R0-2	68.65	94.40	94.95	23.47	23.61	0.463	0.469	2.85	PS
C16R0-3		98.19		24.42		0.521			
C16R25-1		79.30		19.72		0.421			
C16R25-2	65.60	74.66	75.05	18.57	18.66	0.332	0.376	2.30	PS
C16R25-3		71.18		17.70		0.374			
C16R50-1		82.73		20.57		0.384			
C16R50-2	57.54	84.25	83.76	20.95	20.83	0.407	0.414	2.75	PS
C16R50-3		84.30		20.96		0.452			
C16R75-1		83.77		20.83		0.468			
C16R75-2	54.20	85.04	82.87	21.15	20.61	0.452	0.442	2.80	PS
C16R75-3		79.82		19.85		0.407			
C16R100-1		82.09		20.41		0.402			
C16R100-2	50.30	71.39	77.97	17.75	19.39	0.432	0.394	2.73	PS
C16R100-3		80.44		20.00		0.347			
C20R0-1		124.14		19.76		0.488			
C20R0-2	68.65	118.93	115.45	18.93	18.37	0.428	0.435	2.22	PS
C20R0-3		103.28		16.44		0.389			
C20R25-1		97.91		15.58		0.321			
C20R25-2	65.60	87.45	92.63	13.92	14.74	0.366	0.331	1.82	PS
C20R25-3		92.53		14.73		0.305			
C20R50-1		92.65		14.75		0.395			
C20R50-2	57.54	90.31	89.22	14.37	14.20	0.354	0.355	1.87	PS
C20R50-3		84.70		13.48		0.317			
C20R75-1		105.90		16.85		0.428			
C20R75-2	54.20	92.94	95.78	14.79	15.24	0.371	0.403	2.07	PS
C20R75-3		88.50		14.09		0.409			
C20R100-1		94.41		15.03		0.415			
C20R100-2	50.30	95.43	91.72	15.19	14.60	0.398	0.387	2.06	PS
C20R100-3		85.31		13.58		0.347			
C25R0-1		133.29		13.58		0.350			
C25R0-2	68.65	119.28	127.01	12.15	12.94	0.342	0.362	1.56	PS
C25R0-3		128.45		13.08		0.395			
C25R25-1		103.00		10.49		0.298			
C25R25-2	65.60	101.57	105.65	10.35	10.76	0.342	0.315	1.33	PS
C25R25-3		112.39		11.45		0.305			
C25R50-1		108.72		11.07		0.342			
C25R50-2	57.54	107.98	111.98	11.00	11.41	0.305	0.340	1.50	PS
C25R50-3		119.26		12.15		0.374			
C25R75-1		118.15		12.03		0.437			
C25R75-2	54.20	112.42	117.20	11.45	11.94	0.365	0.393	1.62	PS
C25R75-3		121.04		12.33		0.378			
C25R100-1		107.09		10.91		0.409			
C25R100-2	50.30	123.90	114.44	12.62	11.66	0.368	0.411	1.64	PS
C25R100-3		112.34		11.44		0.455			

PO : Pullout *PS : Pullout failure induced by through splitting*

4.2.2 Analysis of pullout test results

Towards development of a predictive model for bond strength, linear regression analysis of the 270 pullout test results was carried out using the following non-dimensional parameters which are known to influence bond strength of deformed steel bars in conventional concrete: $f_c^{'}$, $\frac{c}{d_b}$, $\frac{d_b}{L_d}$, $\frac{h_r}{s_r}$. It may be noted that although the parameter $\frac{d_b}{L_d}$ was held constant in the pullout specimens of this investigation, it has still been included in the regression analysis in order to maintain uniformity with bond strength predictive equations in the literature. In order that the proposed predictive model is applicable to RCA concrete also, the RCA replacement level, *r*, was also included in the regression analysis. It may be noted that for conventional concrete with compressive strength of up to 55 MPa, the effect of concrete properties on bond strength is usually represented using the square root of the compressive strength, $\sqrt{f_c^{'}}$. One of the objectives of the regression analysis was to examine whether $\sqrt{f_c^{'}}$ accurately represents the effect of concrete strength on bond in RCA concrete or not. The following 4 regression equations in which the effect of concrete strength on bond has been modelled in terms of $\left(f_c^{'}\right)^{1/4}$, $\left(f_c^{'}\right)^{1/2}$, $\left(f_c^{'}\right)^{3/4}$ and $\left(f_c^{'}\right)^{1.0}$ were obtained after analysis of the test data.

$$\tau_{\max} = \left(f_c^{'}\right)^{1/4}\left[4.98 + 1.50\left(\frac{c}{d_b}\right) + 1.00\left(\frac{d_b}{L_d}\right) - 30.63\left(\frac{h_r}{s_r}\right) + 0.0028\,r\right] \qquad (4.2)$$

$$\tau_{\max} = \left(f_c^{'}\right)^{1/2}\left[1.92 + 0.58\left(\frac{c}{d_b}\right) + 0.38\left(\frac{d_b}{L_d}\right) - 12.69\left(\frac{h_r}{s_r}\right) + 0.0037\,r\right] \qquad (4.3)$$

$$\tau_{\max} = \left(f_c^{'}\right)^{3/4}\left[0.75 + 0.23\left(\frac{c}{d_b}\right) + 0.15\left(\frac{d_b}{L_d}\right) - 5.33\left(\frac{h_r}{s_r}\right) + 0.0025\,r\right] \qquad (4.4)$$

$$\tau_{\max} = \left(f_c^{'}\right)^{1.0}\left[0.29 + 0.09\left(\frac{c}{d_b}\right) + 0.06\left(\frac{d_b}{L_d}\right) - 2.21\left(\frac{h_r}{s_r}\right) + 0.0014\,r\right] \qquad (4.5)$$

where $\tau_{\max}$ = peak bond stress (MPa), $f_c^{'}$ = cylinder compressive strength (MPa), *c* = minimum cover (mm), d_b = bar diameter (mm), L_d = bonded length (mm), h_r = rib height (mm), s_r = rib spacing (mm), *r* = replacement level (%).

A comparison of the bond strength predictions of Equations 4.2 – 4.5 with the experimental results of the 270 pullout specimens of this investigation is presented in Figure 4.3 which also includes four best-fit lines corresponding to the four descriptive

equations above. Figure 4.3 shows that the best-fit lines corresponding to $\left(f_c^{'}\right)^{3/4}$ and $\left(f_c^{'}\right)^{1.0}$ have a negative slope while that corresponding to $\left(f_c^{'}\right)^{1/4}$ has a positive slope. However, the best-fit line based on $\left(f_c^{'}\right)^{1/2}$ has approximately a horizontal slope which indicates that the ½ power provides an unbiased representation of the effect of concrete strength on bond strength. It may also be noted that in Figure 4.3, the best-fit line based on $\left(f_c^{'}\right)^{1/2}$ has when compared to all the other best-fit lines, the highest R^2 value at 0.853. this lends further support to the descriptive equation containing $\left(f_c^{'}\right)^{1/2}$ for bond strength prediction of RCA concrete. The results of this investigation therefore show that as with conventional concrete, $\left(f_c^{'}\right)^{1/2}$ gives an accurate representation of the effect of concrete properties on bond strength of RCA concrete. The following bond strength predictive equation for short embedded lengths is therefore proposed for RCA concrete. This equation may be used for conventional concrete also by setting the parameter '*r* ' to zero.

$$\tau_{\max} = \sqrt{f_c^{'}}\left[1.92 + 0.58\left(\frac{c}{d_b}\right) + 0.38\left(\frac{d_b}{L_d}\right) - 12.69\left(\frac{h_r}{s_r}\right) + 0.0037\,r\right] \qquad (4.6)$$

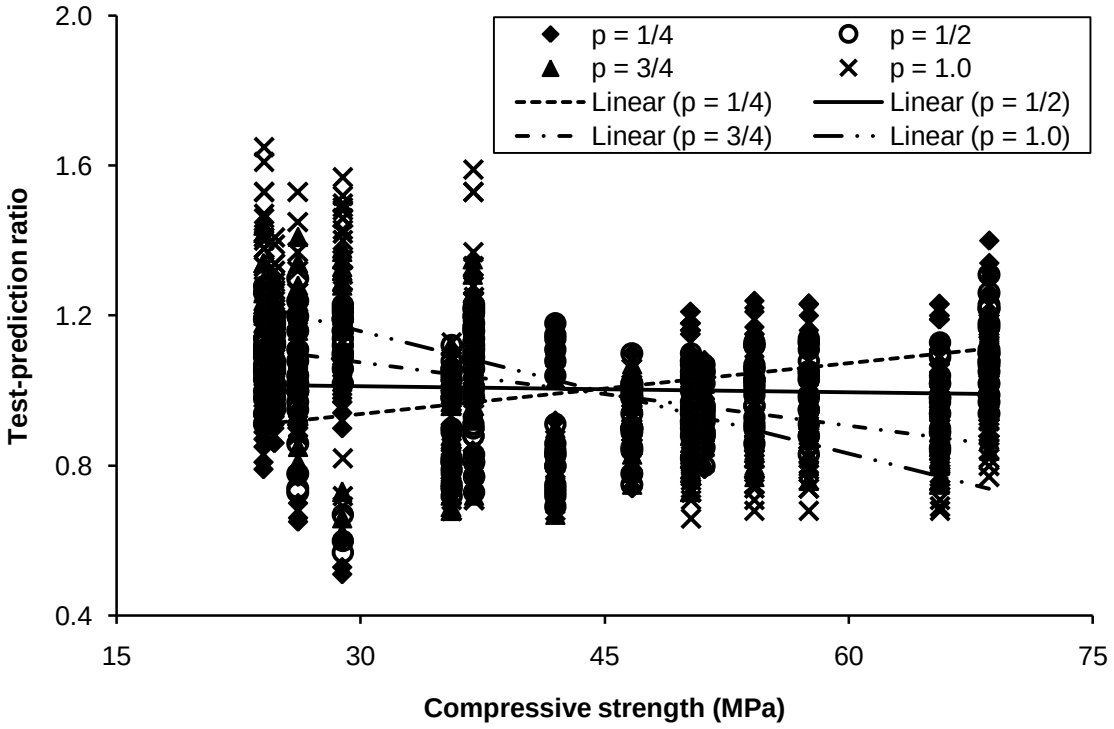

Figure 4.3 Variation of test-prediction ratio versus compressive strength

4.2.3 Normalised bond strength

On the basis of the aforesaid analysis, the measured bond strengths have been normalised with respect to $\sqrt{f_c'}$ and the normalised bond strengths, $\tau_{r,\max}$, so obtained are presented in column number 9 of the Tables 4.1, 4.2 and 4.3. The effect coarse aggregate type (RCA/NCA) and RCA replacement level on bond behaviour of the 8 mm, 10 mm, 12 mm, 16 mm, 20 mm and 25 mm diameter bars has been studied in terms of the variation of the normalised bond strength with these parameters. For direct comparison, the normalised bond strengths of the normal- (Mix A), medium- (Mix B) and the high-strength (Mix C) RCA concretes are plotted with respect to the RCA replacement level in Figures 4.4, 4.5 and 4.6 respectively together with the results of Xiao and Falkner (2007) and the results of Kim and Yun (2013). The best-fit lines in Figures 4.4, 4.5 and 4.6 are indicative of the following trends:

(i) For each of the three concrete grades, the normalised bond strengths were inversely proportional to the bar diameter. Hence, for all the three grades and across all the RCA replacement levels the descending order of the rebar bond strengths were: 8 mm, 10 mm, 12 mm, 16 mm, 20 mm and 25 mm. This trend is particularly evident in the case of the medium-strength (Mix B) and the high-strength (Mix C) concrete in Figures 4.5 and 4.6 respectively. This behaviour has to be seen in the context that pullout failure was observed in the 8 mm, the 10 mm and to some extent the 12 mm bars, whereas pullout-induced-through splitting was observed in the case of the larger bar sizes. Since the $\frac{c}{d_b}$ was not held constant in this investigation, the relatively larger sized bars (16 mm, 20 mm and 25 mm) would be increasing vulnerable to splitting failure since the size of the pullout test specimens was kept the same across all the rebar sizes.

(ii) Across all the three grades of concrete, for the relatively smaller sized bars (8 mm, 10 mm and 12 mm) and more so for the 8 mm and the 10 mm bars, the normalised bond strength increased with an increase in the RCA replacement level with the highest bond strength being obtained for the 100 % RCA replacement level. However, this trend was not as pronounced for the relatively larger sized bars (16 mm, 20 mm, 25 mm). These trends in the normalised bond strengths of the smaller sized bars are in agreement with the trends for the 10 mm bars of Xiao and Falkner (2007) and the 16 mm bars of Kim and Yun (2013), also plotted in Figures 4.4, 4.5 and 4.6. According to Xiao and Falkner (2007), the superior bond strength of the RCA concrete when compared to that of NCA concrete is due to the similar elastic moduli of coarse RCA and the cement paste of the recycled

aggregate concrete. They state that this characteristic of RCA concrete should improve composite action between these two phases and reduce deformation incompatibilities under applied loads. In this investigation it is reckoned that water entrainment due to the use of coarse RCA particles in the SSD moisture state improves curing, reduces shrinkage and associated cracking and improves hydration. All these effects together produce a higher quality paste and enhanced mechanical properties of the concrete conglomerate which can be expected to improve bond strength as well.

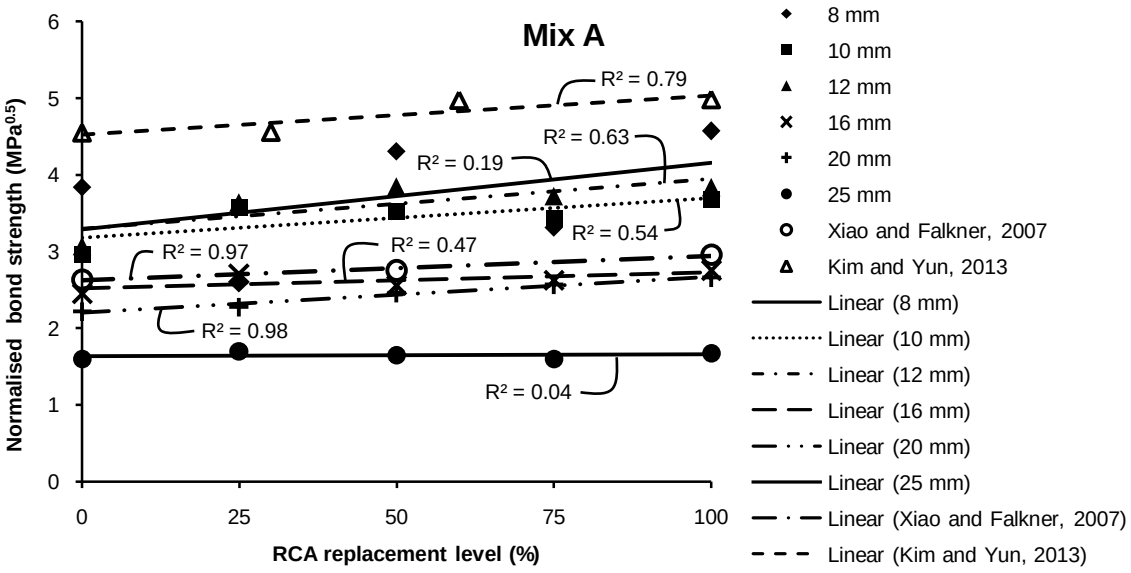

Figure 4.4 Normalised bond strengths for various RCA replacement levels of normal-strength concrete

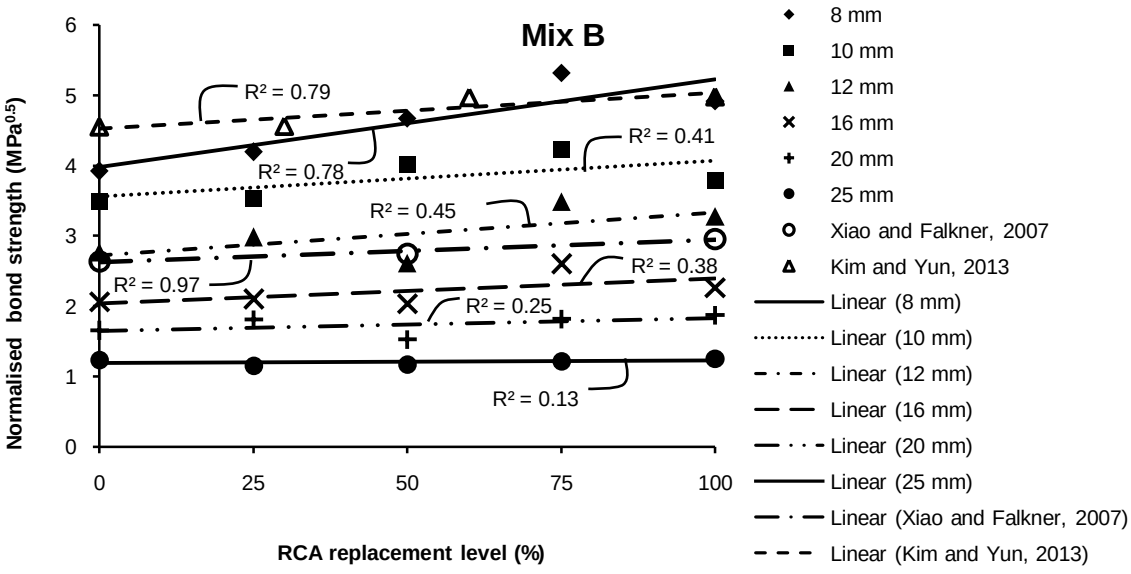

Figure 4.5 Normalised bond strengths for various RCA replacement levels of medium-strength concrete

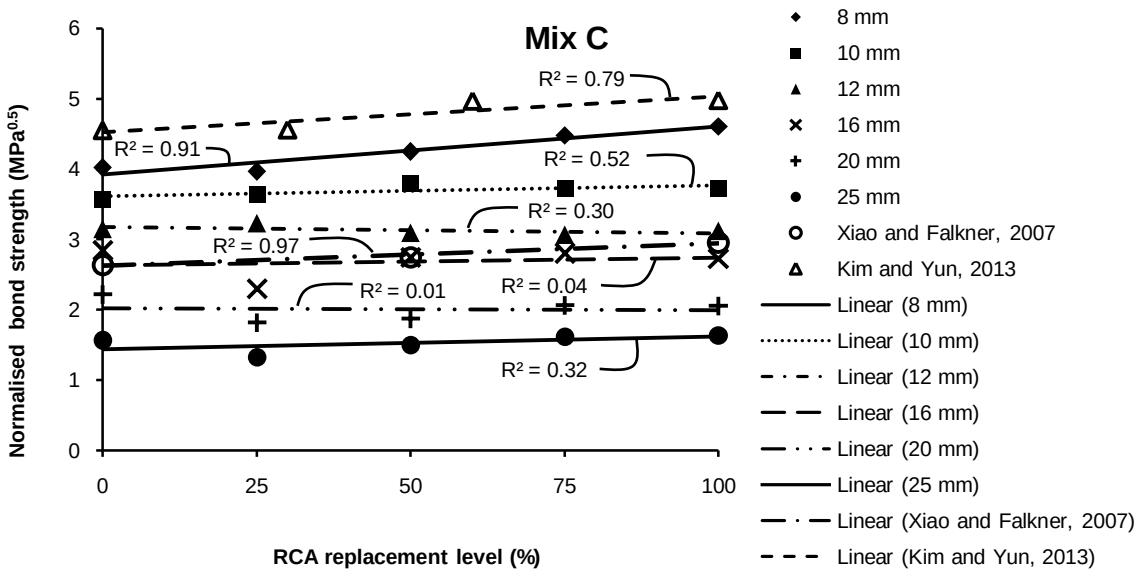

Figure 4.6 Normalised bond strengths for various RCA replacement levels of high-strength concrete

4.2.4 Comparison of measured and predicted bond strengths

Table 4.4 presents a comparison of the measured bond strengths and predictions from the bond strength model proposed in this investigation Equation 4.6 as well as the predictions from selected models for short embedded lengths in the literature (*fib*, 2013; Kim *et al*., 2012; Esfahani and Rangan, 1998a). The graphical representation of this comparison is presented in Figures 4.7 – 4.9 for normal-, medium- and high-strength concretes respectively. These figures show that the most accurate predictions were obtained from the proposed model whereas the predictions of the model of Kim *et al*. (2012) were overly conservative. It may be mentioned that the model in *fib* (2013) and the model of Esfahani and Rangan (1998a) are applicable to conventional concrete whereas the model of Kim *et al*. (2012) has been developed for recycled aggregate concrete. Table 4.4 shows that relatively, the most accurate predictions were obtained from the proposed model with the mean, the standard deviation (SD) and the coefficient of variation (COV) associated with this model being 1.01, 0.13 and 12.87 % respectively. Next in the order of accuracy were the predictions from the *fib* bond strength model (*fib*, 2013) for which the aforesaid values were 1.46, 0.27 and 18.49 % respectively. The robustness of the *fib* bond strength model is noteworthy considering the fact that it has been derived for NCA concrete and its application to RCA concrete is not strictly valid.

Table 4.4 Comparison of measured and predicted bond strengths

Specimen ID	Peak bond stress, τ_{max} (MPa)					Measured bond strength / Predicted bond strength			
	Test	*fib* MC2010	Kim *et al.*, 2012	Esfahani and Rangan, 1998a	Proposed Model				
	A	*B*	*C*	*D*	*E*	*A/B*	*A/C*	*A/D*	*A/E*
A8R0	23.34	15.19	20.84	10.94	25.22	1.54	1.12	2.13	0.93
A8R25	13.94	13.44	18.21	9.68	22.80	1.04	0.77	1.44	0.61
A8R50	21.14	12.26	16.39	8.83	21.26	1.72	1.29	2.39	0.99
A8R75	16.94	12.79	16.96	9.21	22.65	1.32	1.00	1.84	0.75
A8R100	22.71	12.43	16.28	8.95	22.47	1.83	1.40	2.54	1.01
A10R0	17.98	15.19	16.18	10.11	20.04	1.18	1.11	1.78	0.90
A10R25	19.26	13.44	14.09	8.94	18.23	1.43	1.37	2.15	1.06
A10R50	17.27	12.26	12.63	8.16	17.08	1.41	1.37	2.12	1.01
A10R75	17.59	12.79	13.03	8.51	18.29	1.38	1.35	2.07	0.96
A10R100	18.32	12.43	12.46	8.27	18.24	1.47	1.47	2.22	1.00
A12R0	18.68	12.74	13.07	9.39	17.65	1.47	1.43	1.99	1.06
A12R25	19.54	11.98	11.34	8.30	16.11	1.63	1.72	2.35	1.21
A12R50	18.87	11.45	10.12	7.58	15.15	1.65	1.87	2.49	1.25
A12R75	19.01	11.69	10.41	7.90	16.27	1.63	1.83	2.41	1.17
A12R100	19.11	11.52	9.92	7.68	16.28	1.66	1.93	2.49	1.17
A16R0	14.90	10.77	9.19	8.22	13.67	1.38	1.62	1.81	1.09
A16R25	14.55	10.13	7.90	7.27	12.59	1.44	1.84	2.00	1.16
A16R50	12.53	9.68	6.98	6.63	11.94	1.29	1.79	1.89	1.05
A16R75	13.45	9.88	7.14	6.92	12.92	1.36	1.88	1.94	1.04
A16R100	13.68	9.74	6.74	6.73	13.02	1.40	2.03	2.03	1.05
A20R0	13.47	9.42	6.85	7.31	11.85	1.43	1.97	1.84	1.14
A20R25	12.27	8.86	5.84	6.47	10.98	1.39	2.10	1.90	1.12
A20R50	12.05	8.46	5.10	5.90	10.47	1.42	2.36	2.04	1.15
A20R75	13.15	8.64	5.18	6.15	11.40	1.52	2.54	2.14	1.15
A20R100	13.23	8.52	4.83	5.98	11.53	1.55	2.74	2.21	1.15
A25R0	9.73	8.19	4.99	6.42	8.16	1.19	1.95	1.52	1.19
A25R25	9.16	7.70	4.19	5.68	7.72	1.19	2.19	1.61	1.19
A25R50	8.09	7.36	3.59	5.18	7.49	1.10	2.25	1.56	1.08
A25R75	8.20	7.52	3.61	5.41	8.29	1.09	2.27	1.52	0.99
A25R100	8.37	7.41	3.31	5.25	8.52	1.13	2.53	1.59	0.98

Table 4.4 (*Continued*)

Specimen ID	Peak bond stress, τ_{max} (MPa)					Measured bond strength / Predicted bond strength			
	Test	*fib* MC2010	Kim *et al*., 2012	Esfahani and Rangan, 1998a	Proposed Model				
	A	*B*	*C*	*D*	*E*	*A/B*	*A/C*	*A/D*	*A/E*
B8R0	28.02	17.88	24.61	18.79	29.68	1.57	1.14	1.49	0.94
B8R25	28.66	17.08	23.32	12.31	29.00	1.68	1.23	2.33	0.99
B8R50	30.26	16.19	21.90	11.67	28.09	1.87	1.38	2.59	1.08
B8R75	32.32	15.20	20.33	10.95	26.93	2.13	1.59	2.95	1.20
B8R100	29.33	14.91	19.76	10.75	26.97	1.97	1.48	2.73	1.09
B10R0	25.01	17.88	19.12	16.91	23.59	1.40	1.31	1.48	1.06
B10R25	24.13	17.08	18.08	11.37	23.18	1.41	1.34	2.12	1.04
B10R50	26.05	14.60	16.93	10.78	22.57	1.78	1.54	2.42	1.15
B10R75	25.72	14.14	15.67	10.12	21.75	1.82	1.64	2.54	1.18
B10R100	22.57	14.01	15.18	9.92	21.88	1.61	1.49	2.27	1.03
B12R0	19.78	13.82	15.46	15.38	20.77	1.43	1.28	1.29	0.95
B12R25	20.38	13.51	14.58	10.56	20.48	1.51	1.40	1.93	0.99
B12R50	16.90	13.16	13.61	10.01	20.01	1.28	1.24	1.69	0.84
B12R75	21.19	12.75	12.56	9.40	19.35	1.66	1.69	2.25	1.09
B12R100	19.56	12.62	12.13	9.22	19.53	1.55	1.61	2.12	1.00
B16R0	14.80	11.69	10.89	13.01	16.09	1.27	1.36	1.14	0.92
B16R25	14.34	11.42	10.21	9.25	16.00	1.26	1.41	1.55	0.90
B16R50	13.21	11.12	9.47	8.76	15.77	1.19	1.39	1.51	0.84
B16R75	15.80	10.78	8.67	8.23	15.36	1.47	1.82	1.92	1.03
B16R100	13.54	10.67	8.31	8.07	15.63	1.27	1.63	1.68	0.87
B20R0	11.82	10.22	8.14	11.28	13.95	1.16	1.45	1.05	0.85
B20R25	12.40	9.99	7.59	8.22	13.96	1.24	1.63	1.51	0.89
B20R50	9.93	9.72	6.99	7.79	13.83	1.02	1.42	1.27	0.72
B20R75	11.06	9.42	6.33	7.32	13.55	1.17	1.75	1.51	0.82
B20R100	11.19	9.33	6.02	7.18	13.84	1.20	1.86	1.56	0.81
B25R0	8.84	8.89	5.95	9.66	9.61	0.99	1.49	0.91	0.92
B25R25	7.96	8.69	5.49	7.22	9.81	0.92	1.45	1.10	0.81
B25R50	7.60	8.46	5.00	6.85	9.90	0.90	1.52	1.11	0.77
B25R75	7.44	8.19	4.47	6.43	9.85	0.91	1.67	1.16	0.76
B25R100	7.50	8.12	4.19	6.30	10.22	0.92	1.79	1.19	0.73

Table 4.4 (*Continued*)

Specimen ID	Peak bond stress, τ_{max} (MPa)					Measured bond strength / Predicted bond strength			
	Test	*fib* MC2010	Kim *et al*., 2012	Esfahani and Rangan, 1998a	Proposed Model				
	A	*B*	*C*	*D*	*E*	*A/B*	*A/C*	*A/D*	*A/E*
C8R0	33.31	20.71	28.58	21.77	34.39	1.61	1.17	1.53	0.97
C8R25	32.11	20.25	27.75	21.28	34.37	1.59	1.16	1.51	0.93
C8R50	32.21	18.96	25.78	19.93	32.89	1.70	1.25	1.62	0.98
C8R75	32.96	18.41	24.82	19.35	32.60	1.79	1.33	1.70	1.01
C8R100	32.67	17.73	23.70	18.64	32.06	1.84	1.38	1.75	1.02
C10R0	29.61	20.71	22.22	19.60	27.33	1.43	1.33	1.51	1.08
C10R25	29.46	16.32	21.53	19.16	27.47	1.80	1.37	1.54	1.07
C10R50	28.79	15.80	19.96	17.94	26.43	1.82	1.44	1.60	1.09
C10R75	27.48	15.56	19.17	17.41	26.33	1.77	1.43	1.58	1.04
C10R100	26.42	15.27	18.26	16.77	26.02	1.73	1.45	1.57	1.02
C12R0	26.08	14.88	17.98	17.81	24.06	1.75	1.45	1.46	1.08
C12R25	26.20	14.71	17.39	17.41	24.27	1.78	1.51	1.50	1.08
C12R50	23.49	14.24	16.07	16.31	23.43	1.65	1.46	1.44	1.00
C12R75	22.62	14.02	15.40	15.83	23.43	1.61	1.47	1.43	0.97
C12R100	22.12	13.77	14.63	15.25	23.22	1.61	1.51	1.45	0.95
C16R0	23.61	12.58	12.68	15.07	18.64	1.88	1.86	1.57	1.27
C16R25	18.66	12.44	12.21	14.73	18.97	1.50	1.53	1.27	0.98
C16R50	20.83	12.04	11.22	13.80	18.47	1.73	1.86	1.51	1.13
C16R75	20.61	11.86	10.69	13.39	18.60	1.74	1.93	1.54	1.11
C16R100	19.39	11.64	10.09	12.90	18.58	1.67	1.92	1.50	1.04
C20R0	18.37	11.00	9.50	13.06	16.16	1.67	1.93	1.41	1.14
C20R25	14.74	10.87	9.10	12.77	16.55	1.36	1.62	1.15	0.89
C20R50	14.20	10.52	8.31	11.96	16.20	1.35	1.71	1.19	0.88
C20R75	15.24	10.37	7.87	11.61	16.40	1.47	1.94	1.31	0.93
C20R100	14.60	10.18	7.37	11.18	16.46	1.43	1.98	1.31	0.89
C25R0	12.94	9.57	6.96	11.20	11.13	1.35	1.86	1.16	1.16
C25R25	10.76	9.46	6.62	10.95	11.63	1.14	1.63	0.98	0.93
C25R50	11.41	9.15	5.98	10.25	11.59	1.25	1.91	1.11	0.98
C25R75	11.94	9.02	5.61	9.95	11.93	1.32	2.13	1.20	1.00
C25R100	11.66	8.85	5.19	9.58	12.15	1.32	2.24	1.22	0.96
					Mean	1.46	1.63	1.72	1.01
					SD	0.27	0.36	0.45	0.13
					COV (%)	18.49	22.09	26.16	12.87

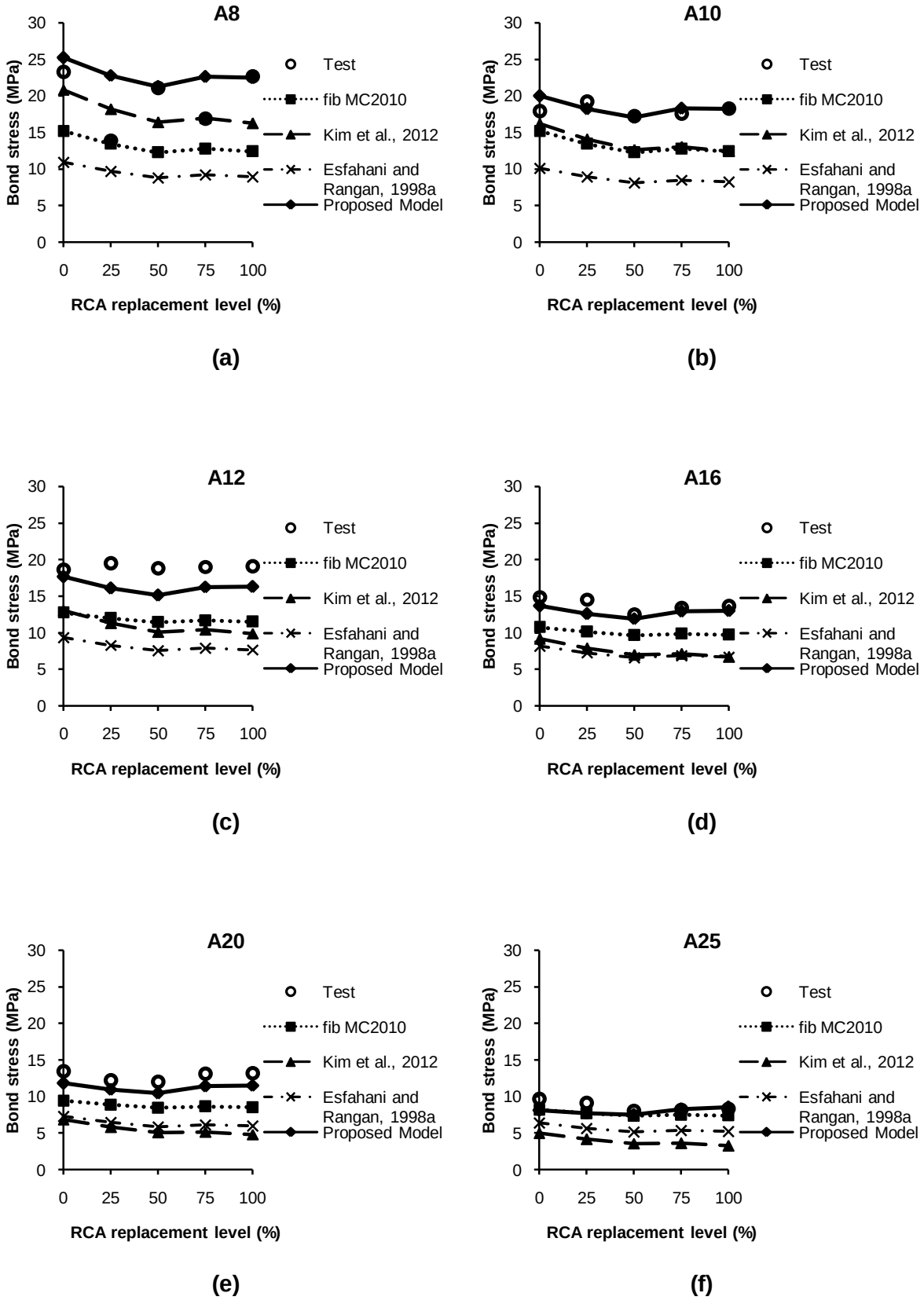

Figure 4.7 Comparison of measured and predicted bond strengths for the normal-strength concrete

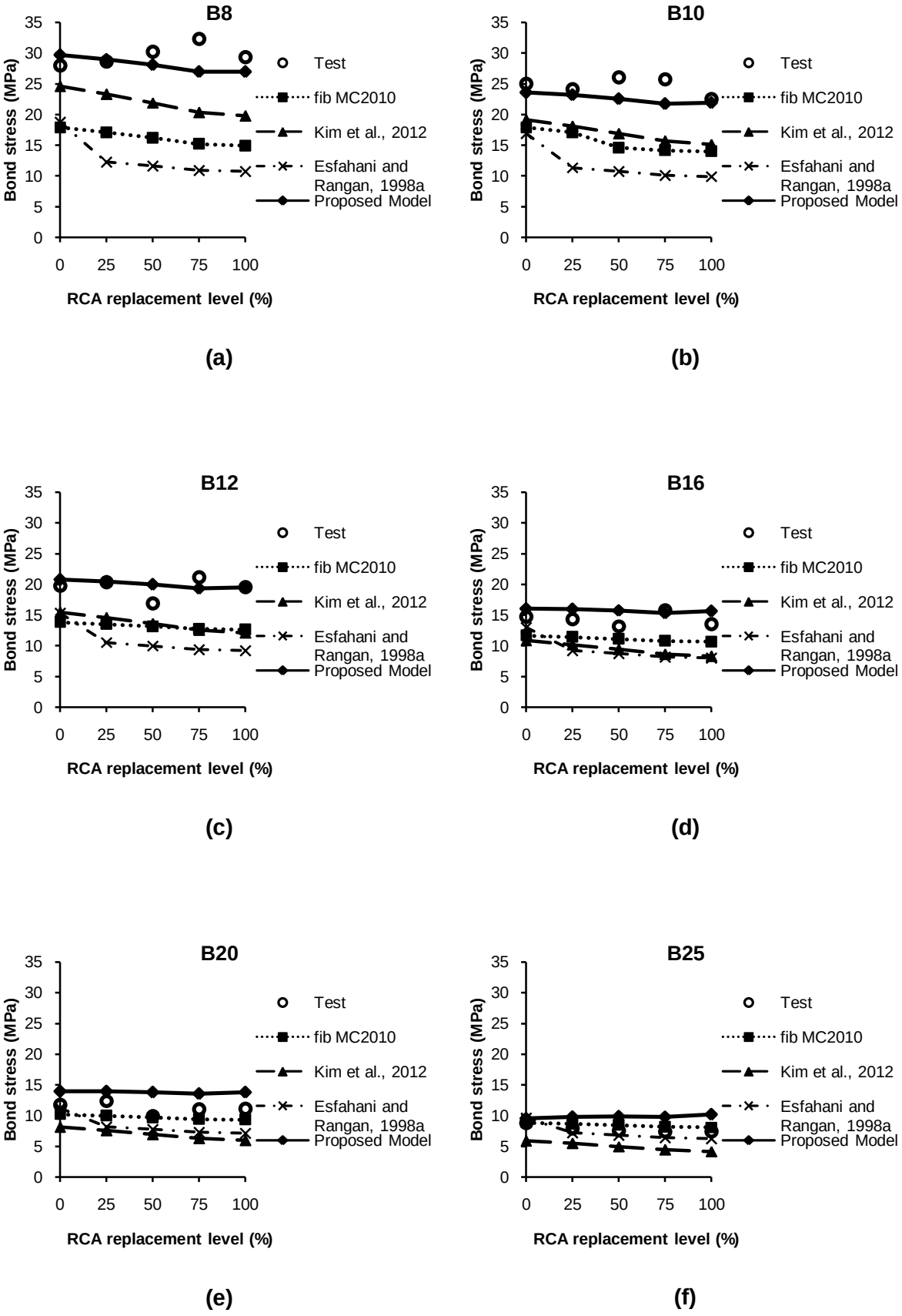

Figure 4.8 Comparison of measured and predicted bond strengths for the medium-strength concrete

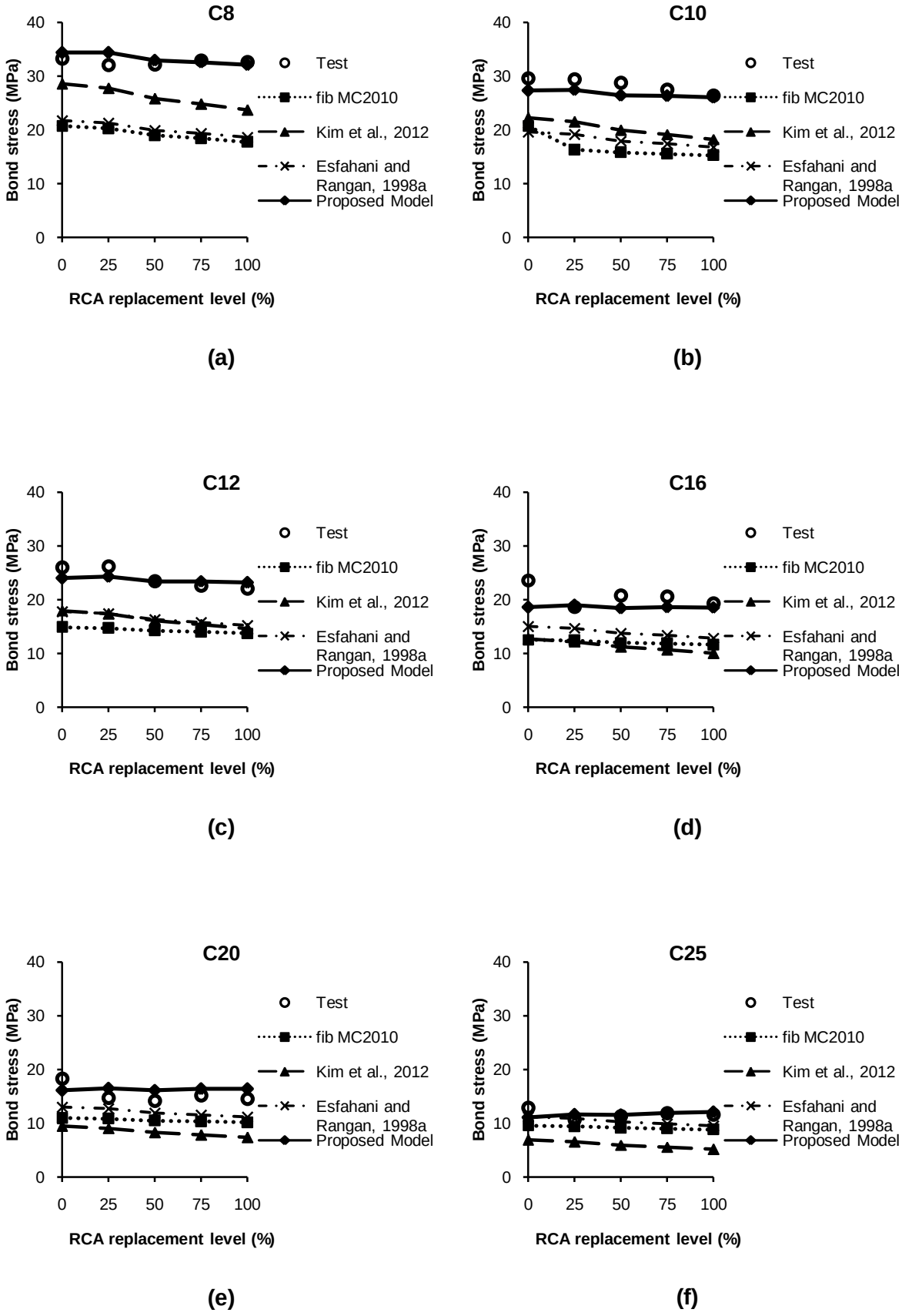

Figure 4.9 Comparison of measured and predicted bond strengths for the high-strength concrete

Due to scarcity of data related to bond strength of RCA concrete for short embedded lengths in the literature, the validation of the proposed bond strength model could be carried only with reported data of Xiao and Falkner (2007) for their RCA concrete specimens. The results of this validation exercise are presented in Table 4.5 wherein the predictive efficacy of the proposed model is compared with that of the following models: *fib* MC2010 (2013) ; Kim *et al*. (2012) and Esfahani and Rangan (1998a). Table 4.5 shows that relatively the most accurate predictions were obtained from the model proposed in this investigation followed by the model in *fib* MC2010. It is hoped that as more information on bond behaviour of RCA concrete becomes available in the literature, the proposed model can be made more robust by calibrating it against a larger data base.

Table 4.5 Validation of the proposed model with the data of Xiao and Falkner (2007)

Specimen ID	Peak bond stress, τ_{max} (MPa)					Measured bond strength / Predicted bond strength			
	Test	*fib* MC2010	Kim *et al*., 2012	Esfahani and Rangan, 1998a	Proposed Model				
	A	***B***	***C***	***D***	***E***	***A/B***	***A/C***	***A/D***	***A/E***
RAC-II-0	17.39	14.75	16.08	9.82	15.66	1.18	1.08	1.77	1.11
RAC-II-50	17.24	14.01	14.92	9.32	15.91	1.23	1.16	1.85	1.08
RAC-II-100	17.39	13.16	13.64	8.76	15.92	1.32	1.27	1.99	1.09
					Mean	1.24	1.17	1.87	1.09
					SD	0.07	0.10	0.11	0.02
					COV (%)	5.65	8.55	5.88	1.83

4.2.5 Brittleness index

A more objective explanation for the superior bond strength of the RCA concretes relative to the NCA concrete has been sought here in the mechanical properties of concrete. It is well established that besides the rebar characteristics, bond behaviour is also a function of the tensile strength and fracture toughness of concrete (Opera *et al.*, 1994). Brittleness is an important attribute of concrete related to its fracture toughness (Kahraman and Altindag, 2004), and drawing upon an analogy with rock mechanics, the brittleness of the NCA and the RCA concretes has been calculated here in terms of the brittleness index, *BI*, (Gong and Zhao, 2007) which is a widely used parameter for quantifying rock brittleness (Perera and Mutsuyoshi, 2013) and is calculated as follows.

$$BI = \frac{f_c^{'}}{f_{ct}} \tag{4.7}$$

where $f_c^{'}$ and f_{ct} are the compressive and the splitting tensile strengths of the material respectively.

The higher the brittleness index, the more brittle the material can be expected to be and therefore the lower is its fracture toughness. It is reckoned in rock mechanics that as brittleness index increases, the size of the crushed zone as well as the number and length of main cracks outside the crushed zone also increases (Perera and Mutsuyoshi, 2013). Assuming that this phenomenon holds true for concrete also it can be expected that the bond strength of concrete should be inversely proportional to its brittleness index. The *BI* values for the concretes of this investigation have been calculated from Equation 4.7 using the measured data presented in Figures 4.1 and 4.2 and the brittleness index trend lines for the three concrete grades are plotted in Figure 4.10, which also includes the BI values calculated from Kim and Yun (2013). This figure shows a consistent decrease in brittleness index with increase in the RCA replacement level, which on the basis of the fracture toughness hypothesis postulated above is indicative of an increase in bond strength with increase in RCA replacement level. This observation therefore lends support to the trends in Figures 4.4, 4.5 and 4.6 and suggests that brittleness index may be a valid indicator of concrete bond strength.

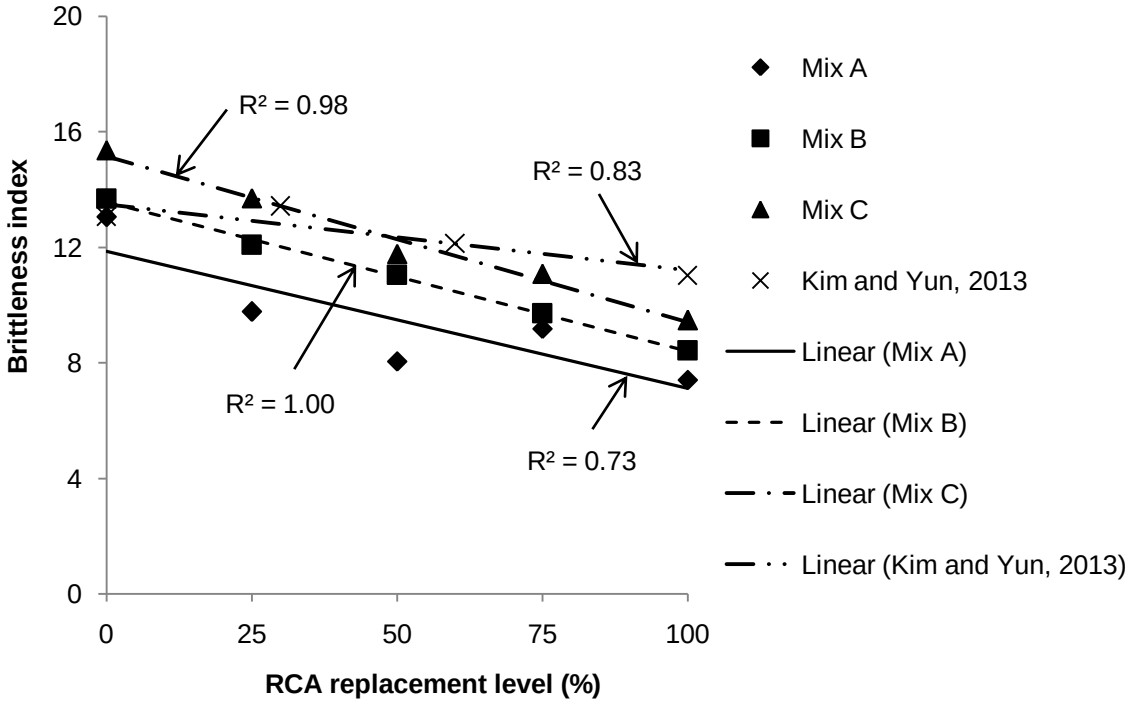

Figure 4.10 Variation of brittleness index with RCA replacement level

4.2.6 Failure modes and interface in NCA and RCA concrete

Two types of bond failure were observed in the pullout specimens and these have been classified as pullout (PO) and pullout-induced by through splitting (PS) in the Tables 4.1, 4.2 and 4.3. Traditionally, in conventional concrete, two types of bond failure have been acknowledged viz pullout and splitting. In the former case, bond failure is due to mostly to the shearing-off of the concrete keys between successive ribs and is more of an interface collapse in a so called 'local mechanism'. In the extreme, pullout failure may take the form of complete separation of the rebar from the concrete. Pullout failures may be accompanied by no or partial concrete splitting cracks and are associated with high confinement of the rebar and/or large concrete cover. In the normal-strength concrete specimens, pullout failure was observed in all the specimens with the 8 mm and the 10 mm diameter bars whereas in the medium-strength specimens, pullout failure was seen in all the specimens with the 8 mm bars and in the specimens with the 10 mm bars embedded in RCA concrete with replacement levels of up to 25 %. In the case of the high-strength concretes, besides the specimens with the 8 mm bars, pullout failure for the specimens with the 10 mm bars was noted only in NCA concrete. None of the pullout failures were accompanied by any visible splitting cracks in concrete. The pullout failure in the NCA and the RCA concrete specimens embedded with the 8 mm bars is consistent with the fact that all these specimens were well confined (concrete cover > 5 d_b) and hence were susceptible to pullout failure as per the fib code for conventional concrete, Model Code 2010 (*fib*, 2013). The aforesaid observations indicate that the limiting values of concrete cover for a pullout failure seem to be the same for the NCA as well as the RCA concrete of this investigation.

It may be noted that unlike the case of Xiao and Falkner (2007), the pullout failures reported in this investigation were not characterised by complete separation of the embedded rebar from the test specimens. Instead, this failure mode was identified on the basis of the large slip values measured in the range of 4 mm – 6 mm at the culmination of the descending branch the load-slip relationships. Hence, physical separation of the rebar need not be the sole criterion for identification of a pullout failure. Confirmation of pullout failure in the specimens with the 8 mm and the 10 mm bars was obtained from examination of interface between the rebars and surrounding concrete. A discussion of this interface follows. The failure mode in some of the specimens embedded with 10 mm diameter deformed bars and in all the specimens with the 12 mm, 16 mm, 20 mm and the 25 mm deformed bars has been classified as pullout-induced by through splitting which is different from the traditional acknowledged splitting failure associated with no confinement and/or very limited cover.

Pullout-induced by through splitting is in essence a pullout failure induced by partial or through splitting and is identified by the presence of visible splitting cracks in the test specimens, which are absent in the case of a classical pullout failure. According to *fib* (2000), the failure mode is associated with moderate confinement and/or limited concrete cover. In this context, note may be made of the fact cover/bar diameter was in the range of 3.7 – 1.5 as the rebar size increased in the pullout specimens from 12 mm to 25 mm. The above range of cover/diameter is taken to correspond to the category of moderate to low confinement and hence pullout-induced by through splitting failure can be expected in the specimens embedded with bar sizes ≥ 12 mm. The pullout-induced through splitting failure was independent of the concrete type (NCA concrete or RCA concrete) and hence the criteria for this failure in terms of cover/bar diameter seem to be applicable to both the NCA as well as the RCA concretes of this investigation. According to *fib* (2000), pullout failure induced by through splitting is characterised by shearing-off the concrete keys accompanied by concrete slip on rib faces. It is reckoned that the residual tail in the measured bond-slip relationship of the specimens which failed by pullout induced by through splitting is indicative of frictional resistance due to concrete slip on rib faces during rebar pullout. Examples of pullout failure by through splitting are presented in Figure 4.11.

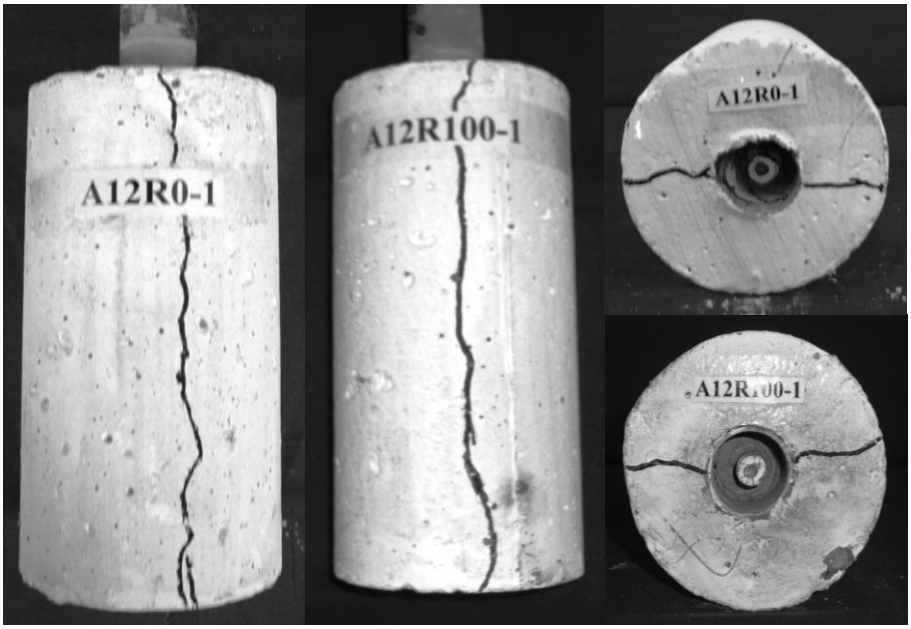

Figure 4. 11 Typical pullout failure induced by through-splitting

All the tested specimens were dissected to examine the interface between the steel bars and concrete. The specimens were cut using a water-cooled diamond-tipped saw and then pried open to reveal the interface. For the purpose of illustration, Figures 4.12 – 4.17 present interfaces in selected NCA and RCA concrete specimens. It may be noted that these figures include interfaces of specimens failing in both the observed bond

failure modes viz: Pullout and pullout failure induced by through splitting. In order to clearly distinguish characteristics of the interface in the two types of concrete (NCA and RCA concrete) used in this investigation, for each rebar diameter, interfaces in the NCA concrete and in the RCA concrete with 100 % RCA replacement level are presented next to each other for ease of comparison in Figures 4.12 – 4.17. The following observations are made with respect to these figures:

(i) Across all the three concrete grades, for the 8 mm and the 10 mm bars, the interface was predominantly made up of sheared concrete keys between successive ribs, which is indicative of a pullout failure. No significant difference could be observed between NCA and the RCA concrete specimens.

(ii) It is observed that for both the concrete types and across all the concrete grades as the rebar diameter increased beyond 10 mm up to 25 mm, the degree of shearing of concrete keys decreased and the interface was increasingly characterised by crushing of concrete in front of the ribs over almost the interface embedded length of the rebars. Crushing of concrete in front of ribs is associated with development of splitting cracks in the pullout specimens. It may be noted in particular in Figures 4.12 – 4.17, that the interface in the 25 mm diameter bars consisted predominantly of crushed concrete in front of the ribs, with very little shearing of concrete keys.

(iii) In the case of the 12 mm diameter bars in Figures 4.12 – 4.17, it may be noted that for both the NCA as well as the RCA concrete specimens, crushing of concrete in front of the ribs was relatively the least in the high-strength concrete followed by the medium-strength concrete and maximum crushing may be seen in the normal-strength concrete pullout specimens. This behaviour is also seen to some extent in the case of the 16 mm bars though it was not very evident for the 20 mm and the 25 mm bars. The decrease in the degree of crushing with increase in concrete strength observed in some of the bars is similar to the observations of Esfahani and Rangan (1996) for their pullout specimens made of NCA concrete with cylinder crushing strengths of 26 MPa, 50 MPa and 75 MPa, which are approximately analogous to the normal-, the medium- and the high-strength concretes of this investigation. Azizinamini *et al*. (1993) have also reported a relatively larger degree of concrete crushing in front of the ribs in normal-strength concrete compared to that in high-strength concrete.

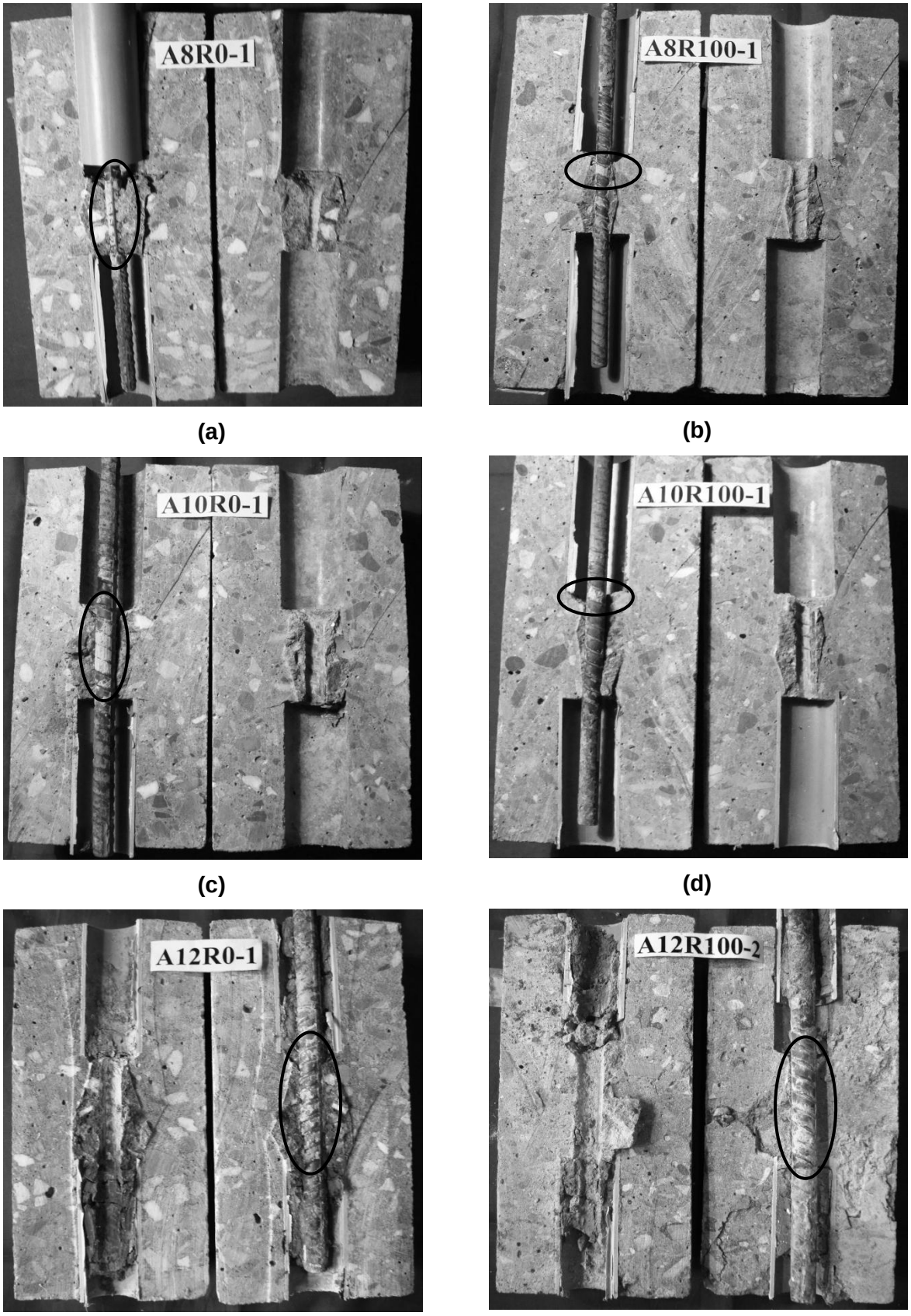

Figure 4.12 Interface of normal-strength NCA and RCA concrete: (a) A8R0-1 (b) A8R100-1 (c) A10R0-1 (d) A10R100-1 (e) A12R0-1 (f) A12R100-2

(a)

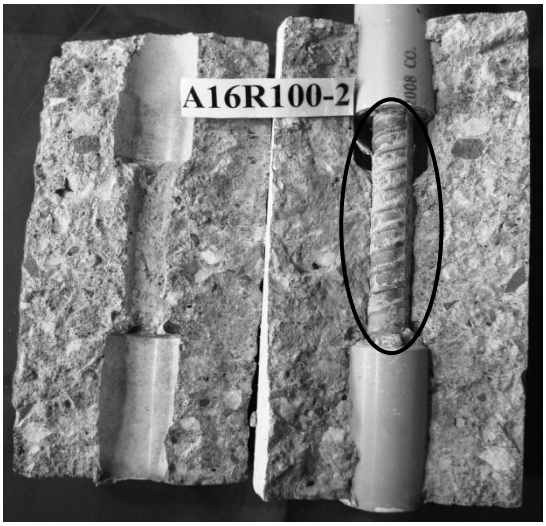

(b)

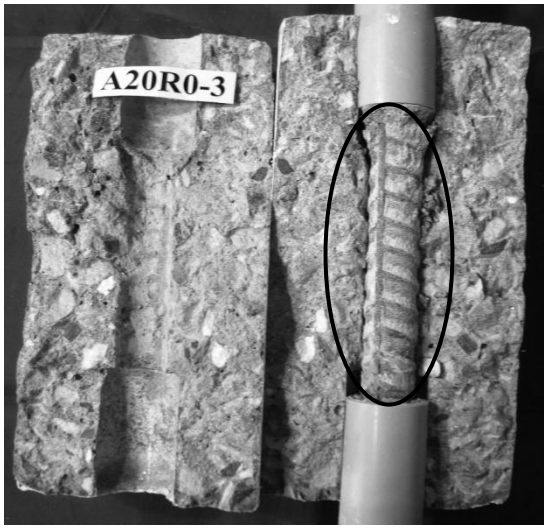

(c)

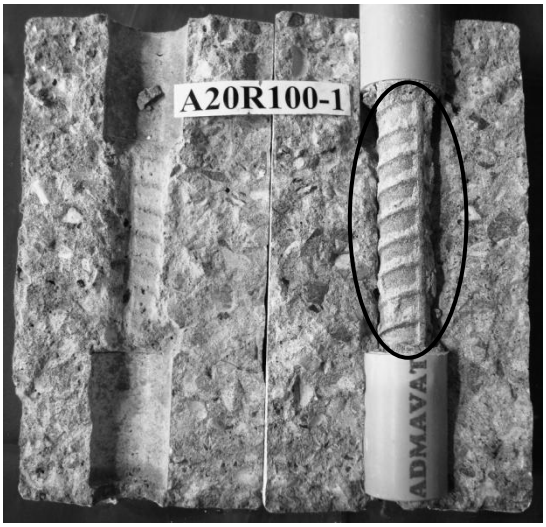

(d)

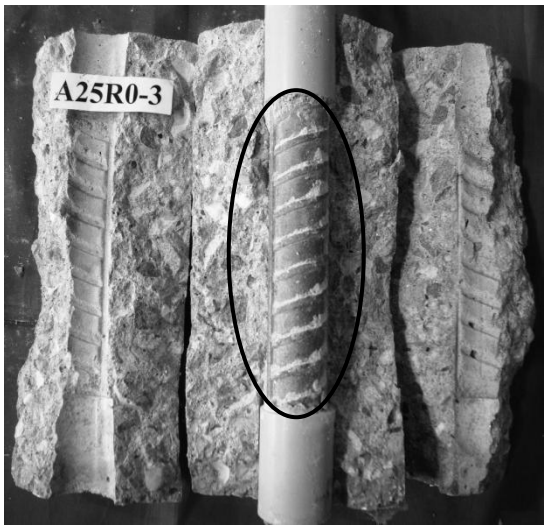

(e)

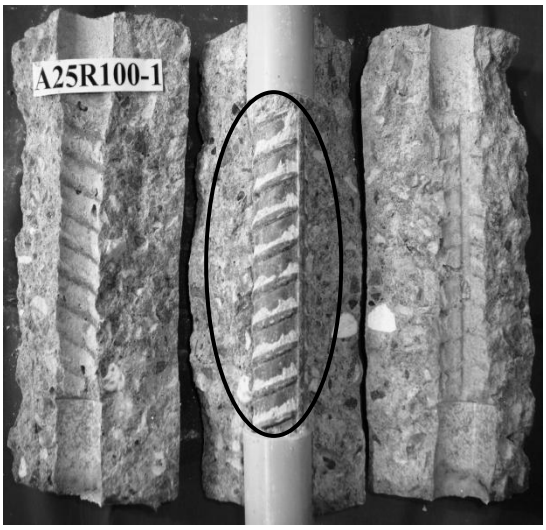

(f)

Figure 4.13 Interface of normal-strength NCA and RCA concrete: (a) A16R0-1 (b) A16R100-2 (c) A20R0-3 (d) A20R100-1 (e) A25R0-3 (f) A25R100-1

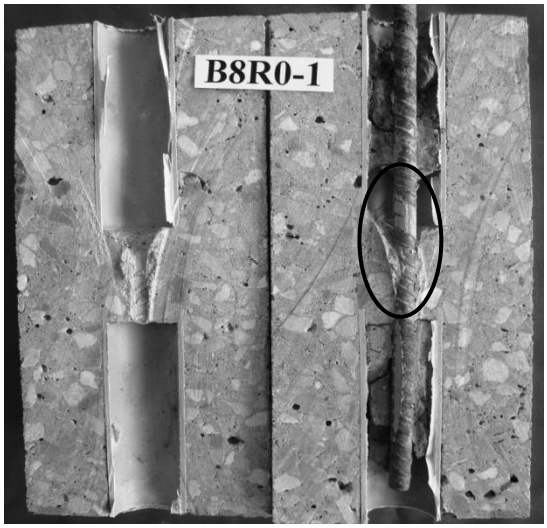

(a)

(b)

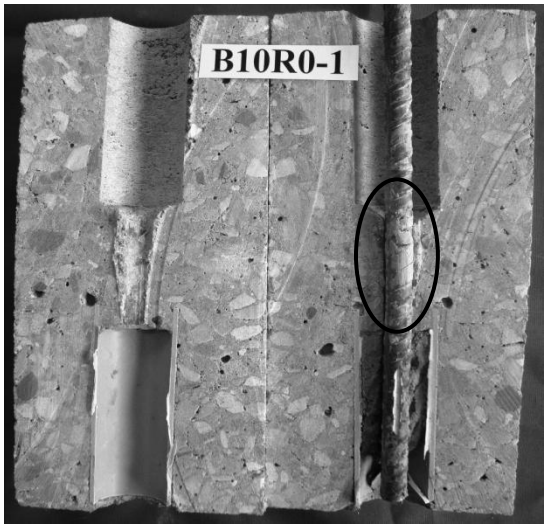

(c)

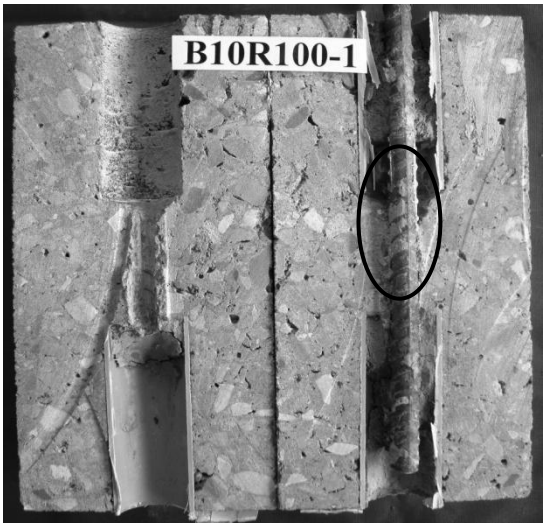

(d)

(e)

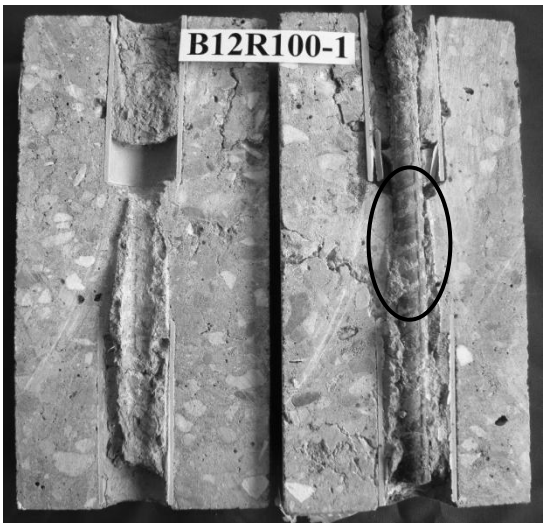

(f)

Figure 4.14 Interface of medium-strength NCA and RCA concrete: (a) B8R0-1 (b) B8R100-1 (c) B10R0-1 (d) B10R100-1 (e) B12R0-1 (f) B12R100-1

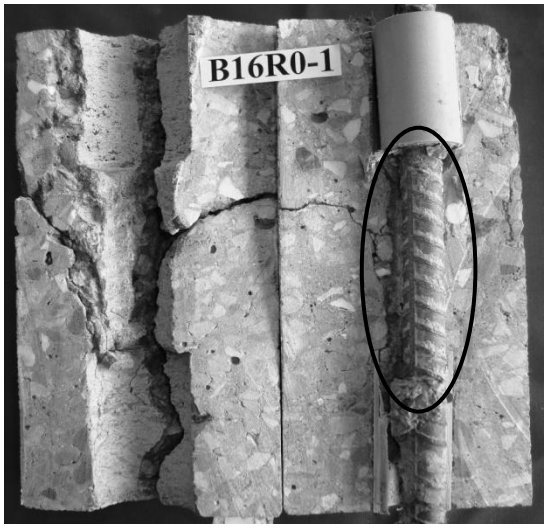

(a)

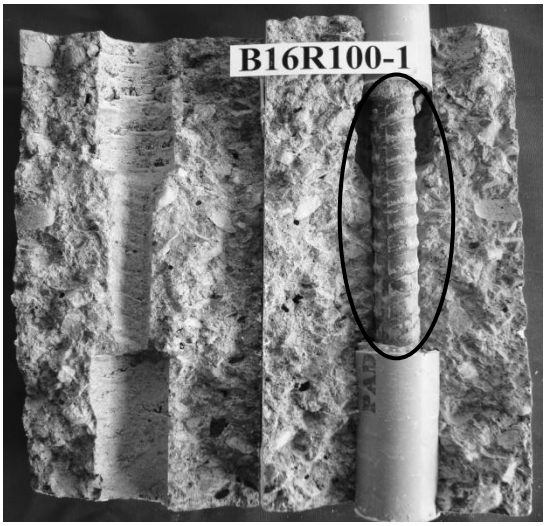

(b)

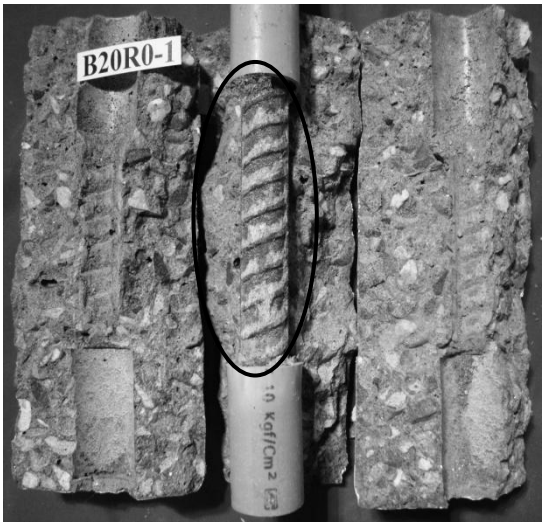

(c)

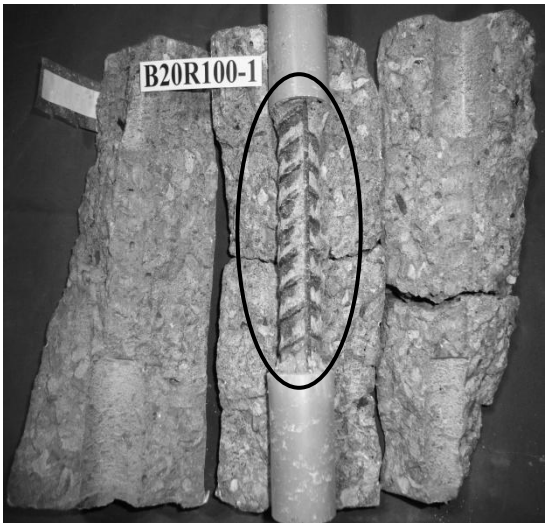

(d)

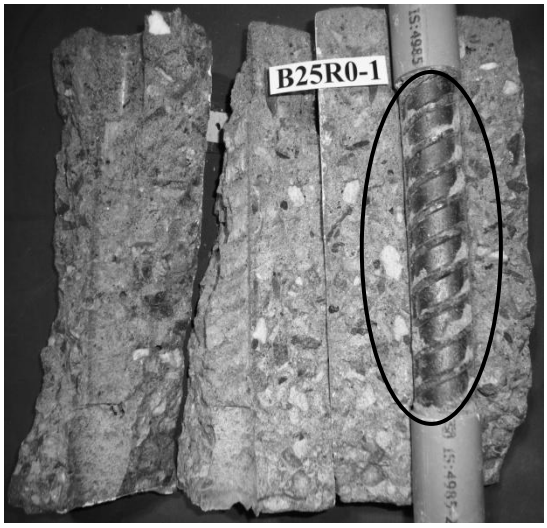

(e)

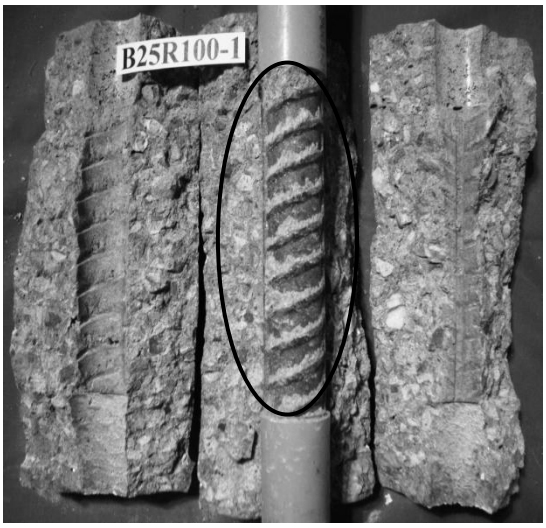

(f)

Figure 4.15 Interface of medium-strength NCA and RCA concrete: (a) B16R0-1 (b) B16R100-1 (c) B20R0-1 (d) B20R100-1 (e) B25R0-1 (f) B25R100-1

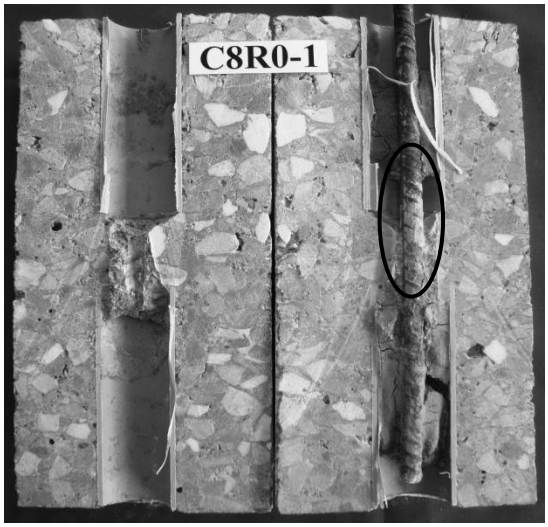

(a)

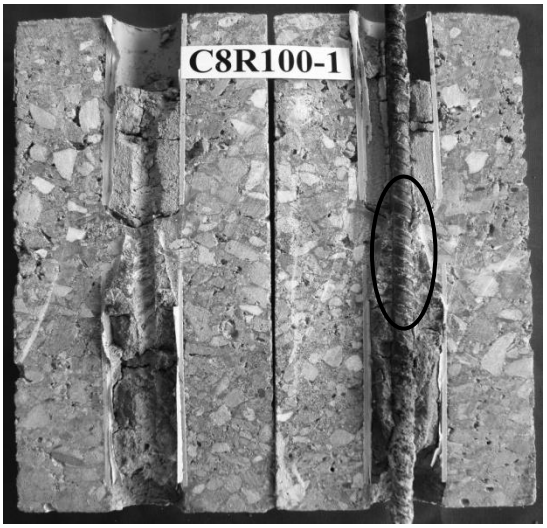

(b)

(c)

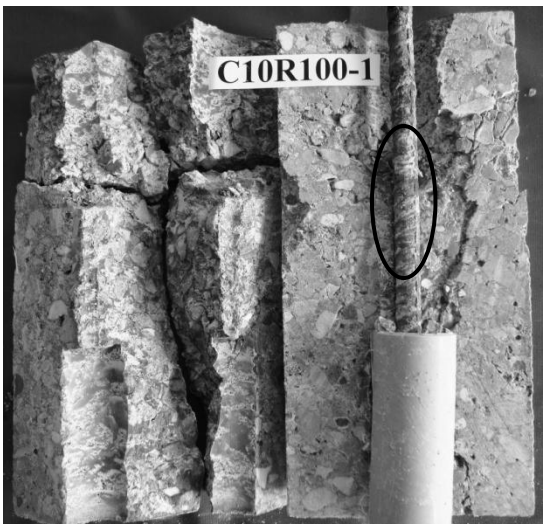

(d)

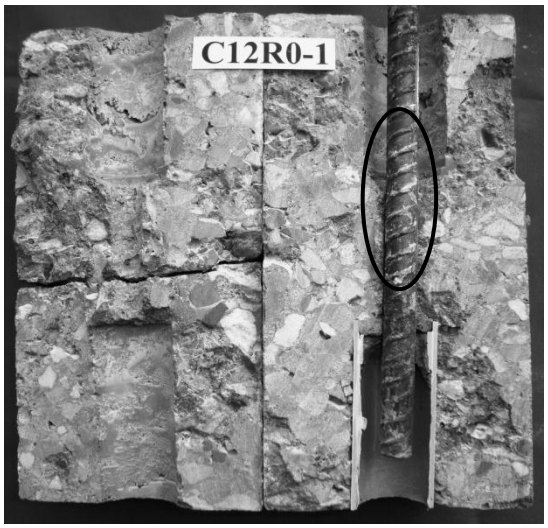

(e)

(f)

Figure 4.16 Interface of high-strength NCA and RCA concrete: (a) C8R0-1 (b) C8R100-1 (c) C10R0-1 (d) C10R100-1 (e) C12R0-1 (f) C12R100-1

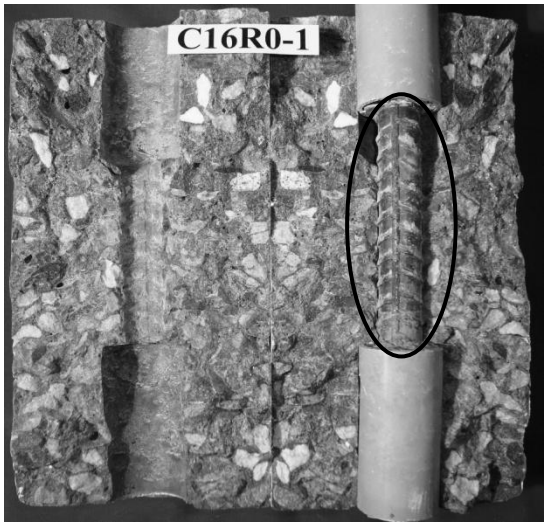

(a)

(b)

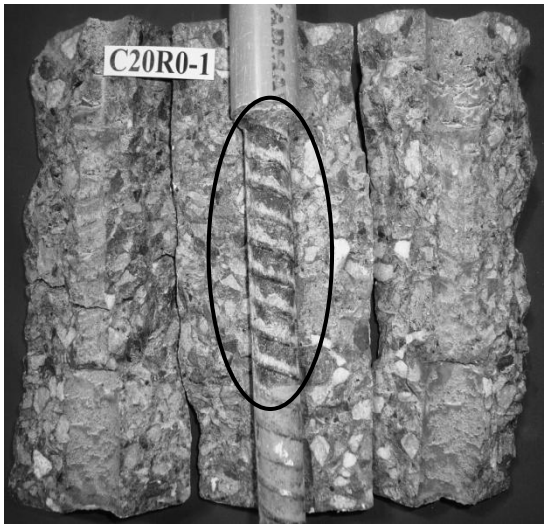

(c)

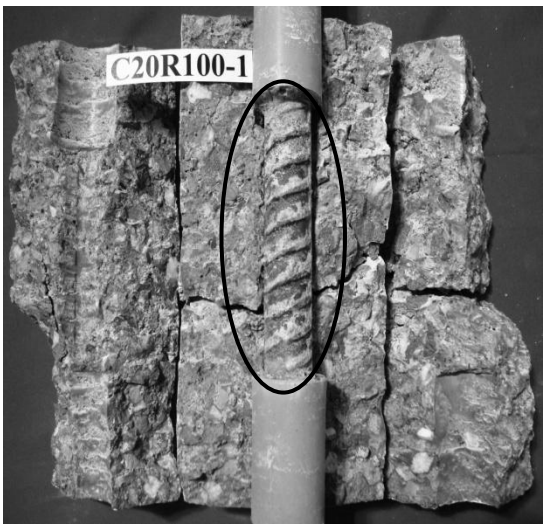

(d)

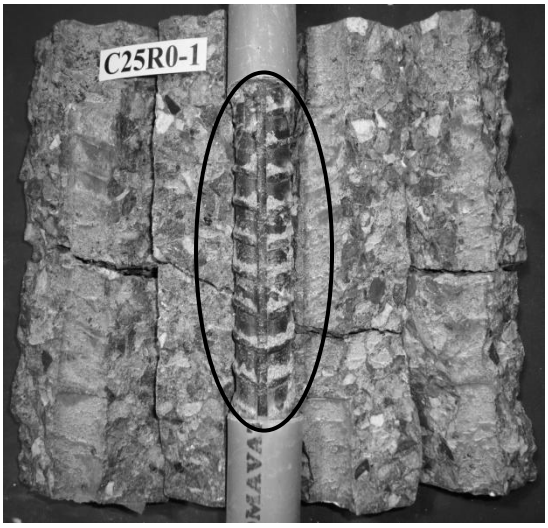

(e)

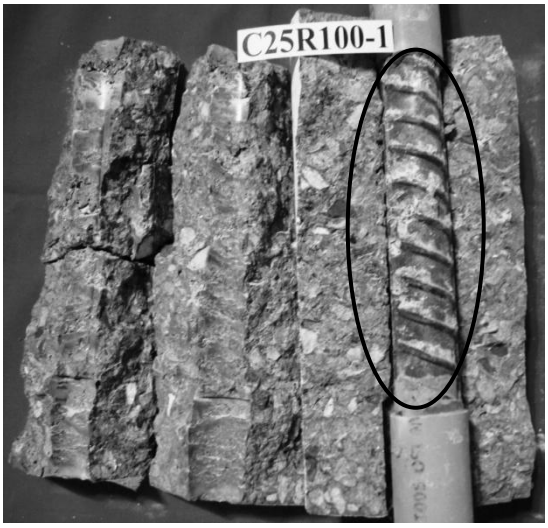

(f)

Figure 4.17 Interface of high-strength NCA and RCA concrete: (a) C16R0-1 (b) C16R100-1 (c) C20R0-1 (d) C20R100-1 (e) C25R0-1 (f) C25R100-1

4.2.7 Measured bond stress-slip relationship

The measured bond stress versus unloaded-end slip curves of the pullout specimens for all the three concrete grades (normal-, medium- and high-strength) after elimination of outliers, are presented in Figures 4.18 – 4.35. The outliers were eliminated in order to remove extreme values relative to other observations in the data set. The extreme values could have been caused either due to an experimental or a measurement error or a combination of both. For example, in a typical pullout test, 300 to 400 load and corresponding slip values were recorded and while plotting the load-slip relationship through this data, the measured values which were extreme relative to other observations in the data set were eliminated so as to get a reasonable curve, such extreme values did not exceed 10 in a total of 300 to 400 data points. Each curve is the average of the measured relationship of three companion specimens. It may be noted in the above figures that for all the three concrete grades, the measured bond stress-slip relationships of the RCA and the NCA concrete are similar to each other. The trends in Figures 4.18 – 4.35 support the observation of Xiao and Falkner (2007) that bond development and deterioration between RCA concrete and deformed steel bars is fundamentally similar to that observed in NCA concrete. A perusal of the relationships presented in the Figures 4.18 – 4.35 indicates two types of failure modes in bond in the context of post-peak behaviour. In the case of the 8 mm and the 10 mm diameter bars, irrespective of the concrete grade and type (NAC and RAC), there is a gradual loss of bond strength with increasing slip and the descending of the bond-stress relationship is distinctly non-linear and concave upwards. In the experiments, pullout mode of bond failure was observed in all the specimens with the 8 mm and the 10 mm diameter bars. In the pullout specimens with the 12 mm, 16 mm, 20 mm and 25 mm diameter bars, the observed failure mode was pullout-induced by through splitting. It may be seen in the Figures 4.18 – 4.35 that for the 12 mm, 16 mm, 20 mm and 25 mm diameter bars, the post-peak branch of the curves in a majority of the cases consists of a sharply descending linear portion, indicative of unstable crack propagation, culminating into a tail approximately parallel to the X-axis. In the specimens with the 12 mm, 16 mm, 20 mm and the 25 mm bars, pullout failure was accompanied by the formation of through splitting cracks. The formation of these splitting cracks correlates well with the unstable crack propagation indicated by the linear descending branch of the bond stress-slip relationships of the pullout specimens embedded with the aforementioned bars.

The following five stages of bond behaviour (ACI, 1966; Bazant and Sener, 1988; Tepfers, 1979; Gambarova *et al.*, 1989a, 1989b; Gambarova and Rosati, 1996) can be identified in the measured bond stress-slip relationships for specimens with the pullout failure: (i) micro-slip (ii) internal cracking (iii) pullout (iv) descending and (v) residual. Stage

I of the bond stress-slip behaviour consists of that part of the relationship which is sharply ascending (because of adhesion) and nearly linear up to about 60% to 70% of the ultimate load and this stage encompasses micro-slip (load is small and no obvious slip occurs at the free end) in the initial part followed by internal cracking in the later part which results in slip of the free end of the rebar, i.e., the adhesion mechanism of bond resistance has been exhausted.

After stage I, the rate of slip begins to increase in stage II in which the ascending branch of the curve becomes distinctly nonlinear with a relatively small increase in bond resistance such that significantly pullout of the bar occurs and the load resisted reaches a peak value, P_{max}. Significant rebar pullout characteristics stage III of the relationship. The dominant mechanism of bond resistance in stage II is attributed to mechanical interlock accompanied by some contribution from frictional resistance due to wedging of displaced mortar particles between the rebar and surrounding concrete. On increasing the applied load further, the bond stress-slip relationships were seen to undergo a gradual change in slope signifying a breakdown of bond strength and development of significant non-recoverable slip. The descending branch of the bond stress-slip relationships represents stage IV wherein a continuous decrease in bond resistance with rapid increase in slip was observed until the residual stage set in wherein the tail of the relationship became approximately parallel to the X-axis. It may be noted that the pullout tests were terminated at an unloaded end slip in the range of 9 mm – 10 mm. In contrast to the pullout specimens with the relatively smaller bars (8 mm, 10 mm), which failed in the pullout mode, the following four stages of bond behaviour have been identified in the measured bond stress-slip relationships of the specimens embedded with the relatively larger bars (12 mm, 16 mm, 20 mm and 25 mm) in which the failure mode has been classified as pullout failure induced by through splitting: (i) micro-slip (ii) internal cracking (iii) descending (iv) residual. In this failure mode, bond behaviour in stage (i) and (ii) is similar to that observed in pullout failure with the significant difference being the sharp change in slope at peak load followed by the descending stage characterised by an almost linear response indicative of unstable crack propagation (associated with the formation of splitting cracks in the specimens). The descending stage culminated in a residual tail which was almost parallel to the X-axis. The length of the tail varied across the rebar diameters but noteworthy is the fact that for specimens in which bond failure was due to pullout induced by through splitting, the residual bond strength was about 10 % to 20 % or less of the peak strength whereas in the specimens with pullout failure this figure was in the range of 20 % to 25 % or in some cases even more.

With reference to the Tables 4.1, 4.2 and 4.3, it may be noted that the slips corresponding to peak loads measured in the range of 0.348 mm – 0.713 mm, 0.335 mm

– 0.619 mm, 0.315 mm – 0.534 mm for the normal-, the medium- and the high-strength concretes. It is pertinent to mention here that these values are significantly higher than the slip values of 0.025 mm and 0.25 mm recommended for example in the IS 2770(Part-I):1967 (1967b) for the calculation of nominal bond stresses used in structural design. The aforesaid slip values recommended in the IS code are valid for plain bars in which the load at first visible slip is small and the maximum pullout load is not significantly different from the load at first visible slip. Moreover, the slip values at peak loads in the case of plain bars are themselves small when compared to those in deformed bars, which in this investigation where measured to be large as 0.713 mm in some cases. Hence, the IS code limiting slip values of 0.025 mm and 0.25 mm will not be valid for deformed bars also. At the same time it may be noted that in actual construction, other failure modes such as shear, flexure etc. may occur before slip values correspond to peak bond stresses are attained in a structural element reinforced with deformed bars. However, if bond strengths of plain and deformed bars are sought to be compared, then such a comparison can be made at the IS code recommended slip values of 0.025 mm and 0.25 mm which are reckoned to be arbitrarily selected values equal to $1/1000^{th}$ and $1/100^{th}$ of an inch respectively.

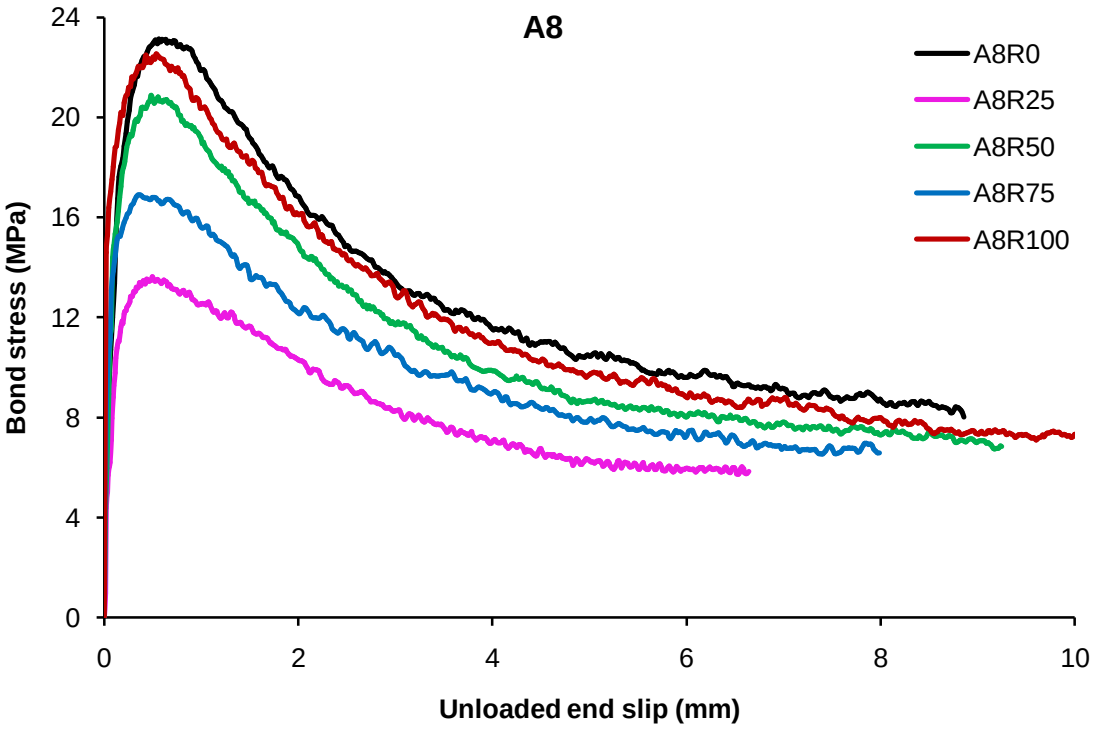

Figure 4.18 Bond-slip curves for the 8 mm diameter deformed bars embedded in normal-strength concrete

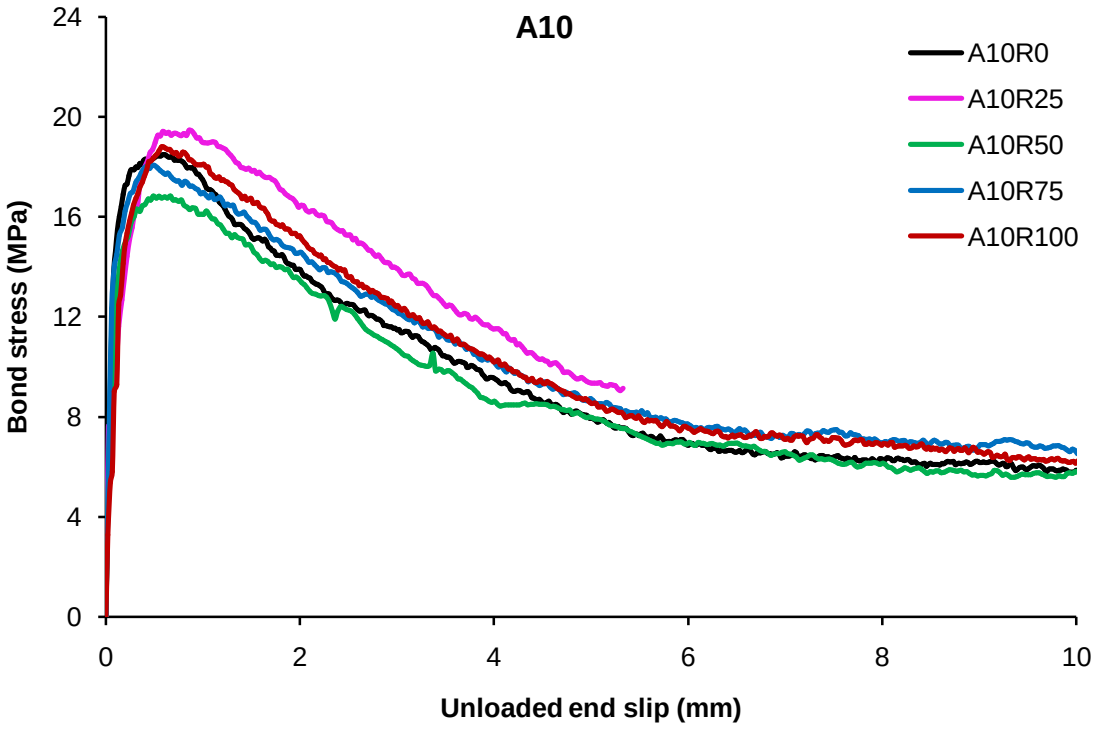

Figure 4.19 Bond-slip curves for the 10 mm diameter deformed bars embedded in normal-strength concrete

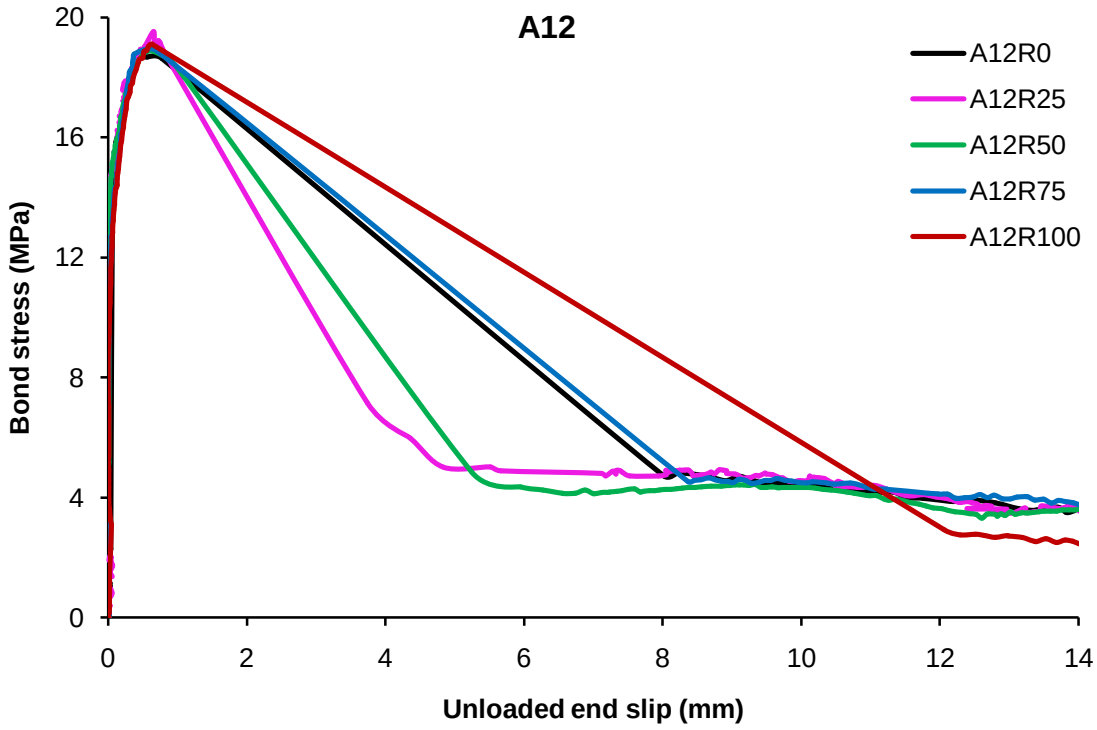

Figure 4.20 Bond-slip curves for the 12 mm diameter deformed bars embedded in normal-strength concrete

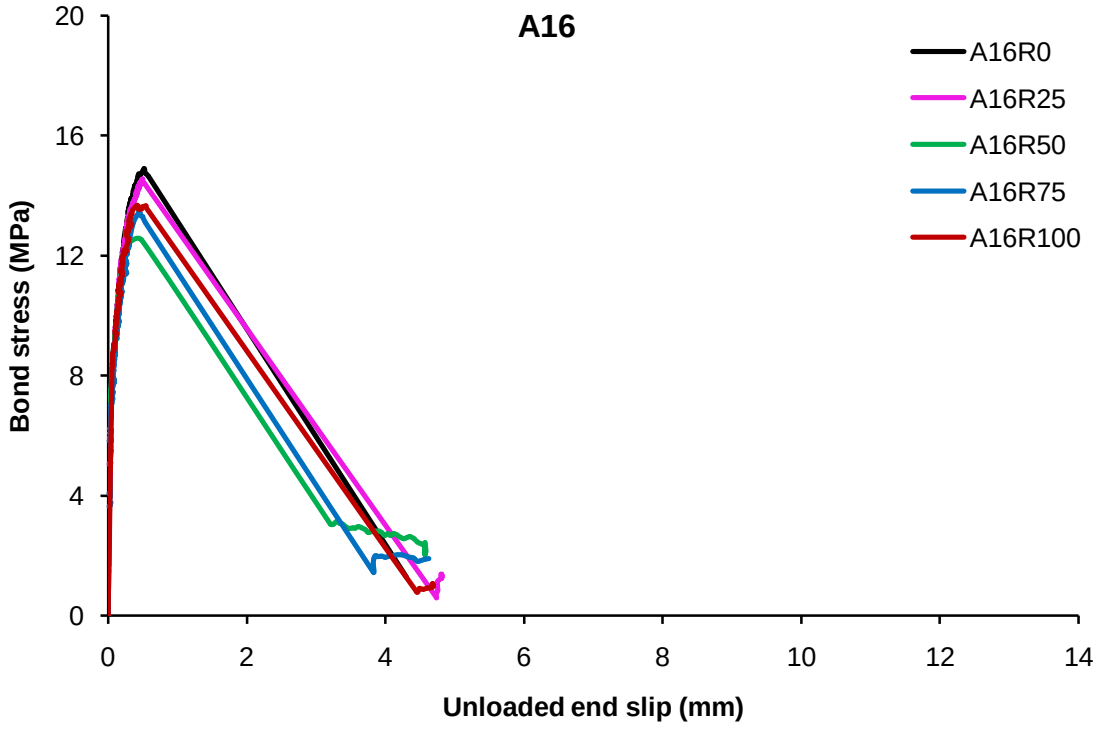

Figure 4.21 Bond-slip curves for the 16 mm diameter deformed bars embedded in normal-strength concrete

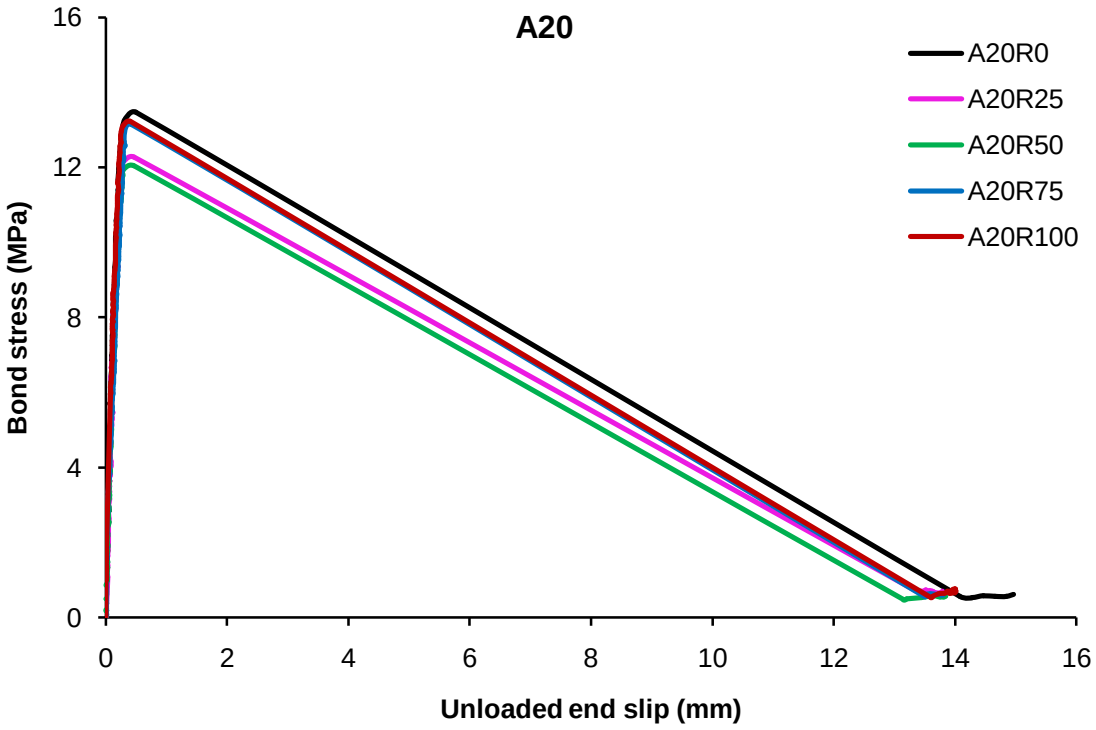

Figure 4.22 Bond-slip curves for the 20 mm diameter deformed bars embedded in normal-strength concrete

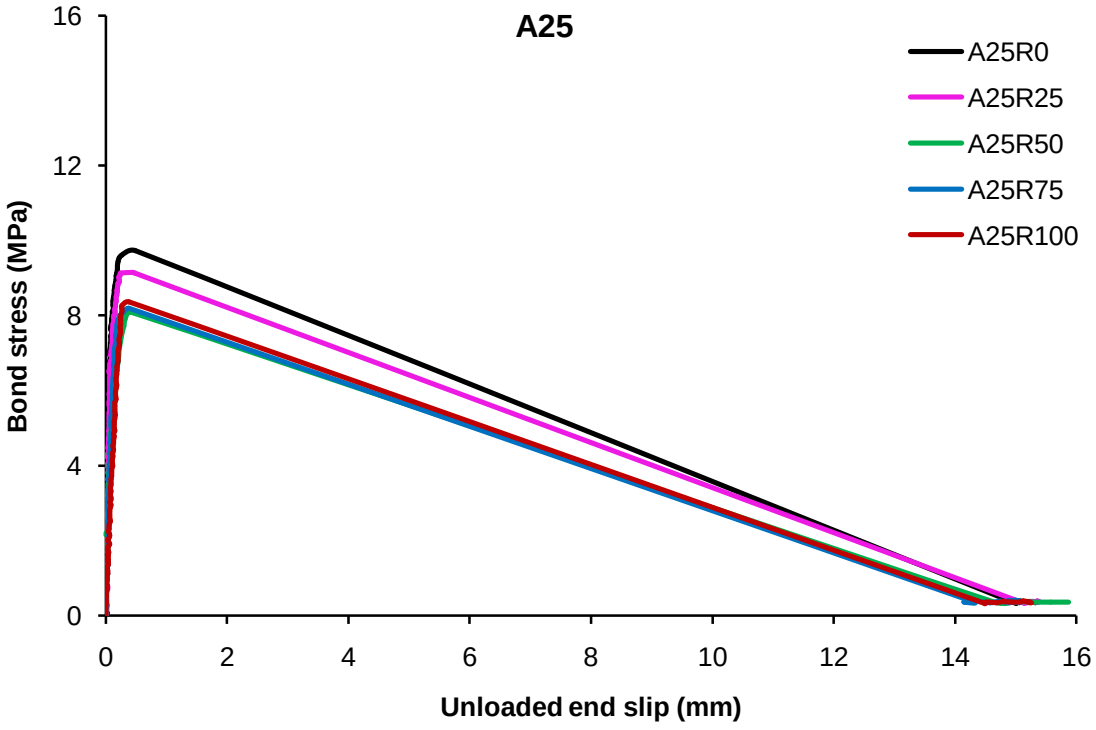

Figure 4.23 Bond-slip curves for the 25 mm diameter deformed bars embedded in normal-strength concrete

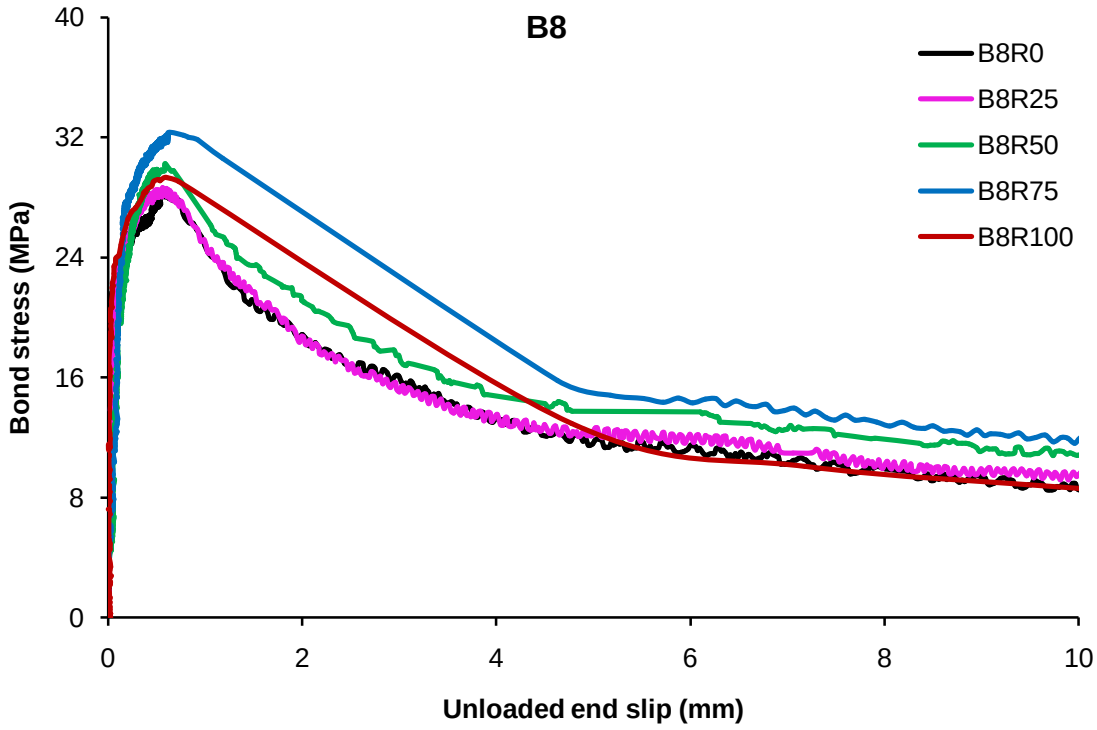

Figure 4.24 Bond-slip curves for the 8 mm diameter deformed bars embedded in medium-strength concrete

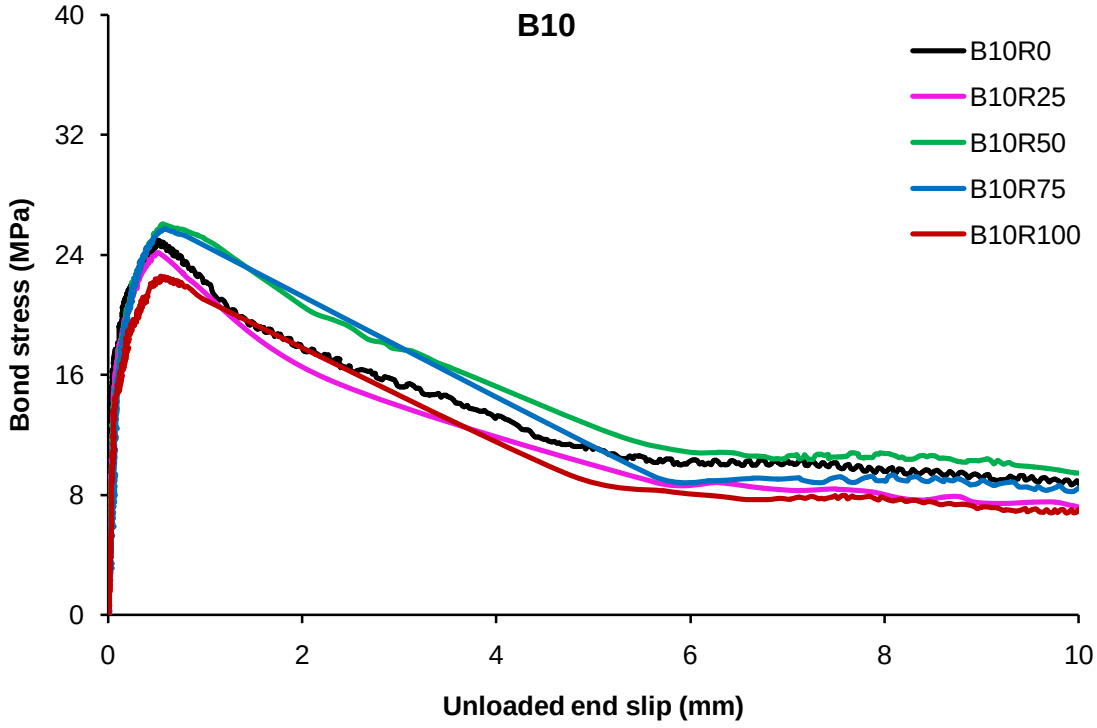

Figure 4.25 Bond-slip curves for the 10 mm diameter deformed bars embedded in medium-strength concrete

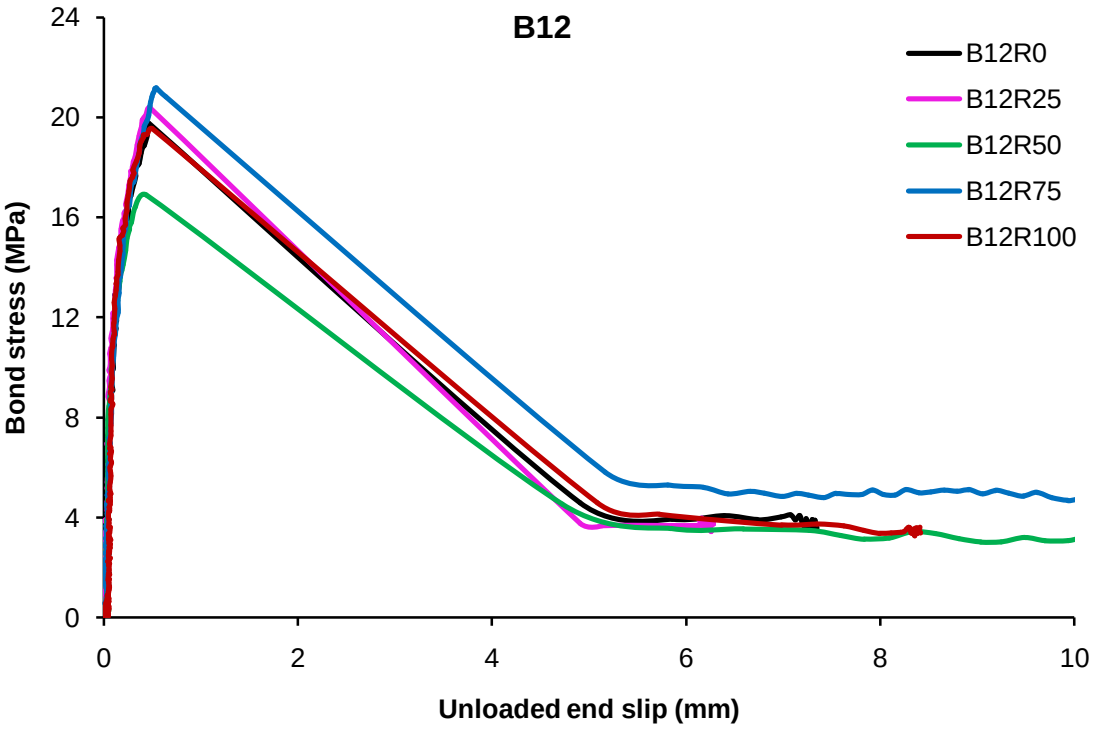

Figure 4.26 Bond-slip curves for the 12 mm diameter deformed bars embedded in medium-strength concrete

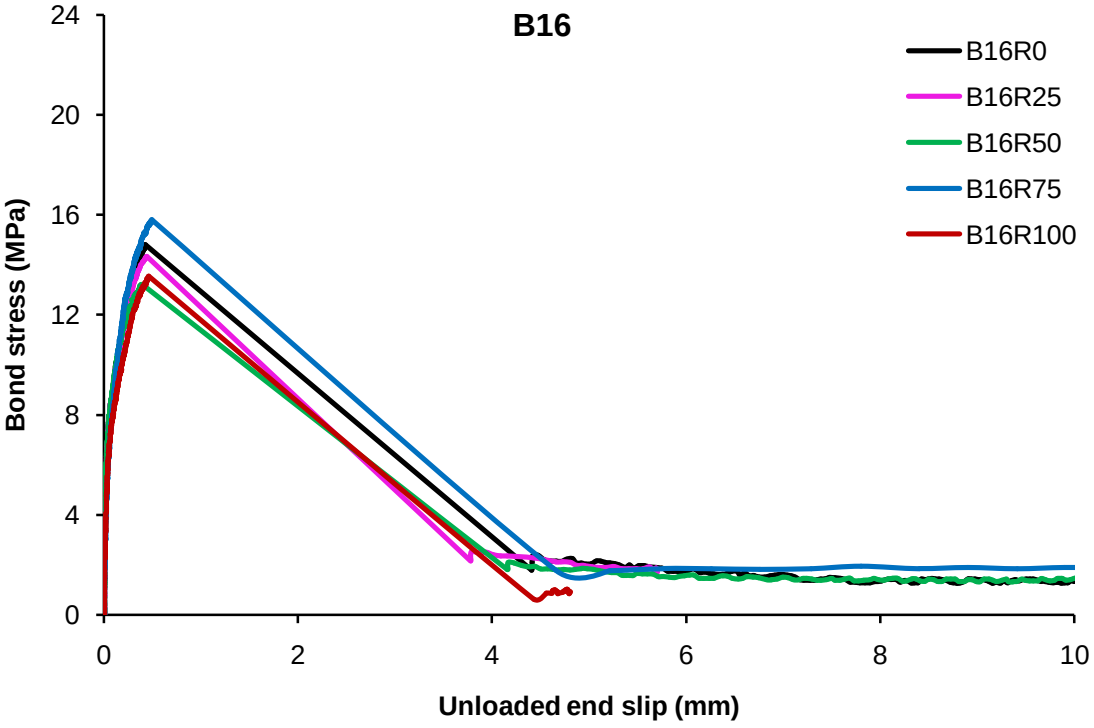

Figure 4.27 Bond-slip curves for the 16 mm diameter deformed bars embedded in medium-strength concrete

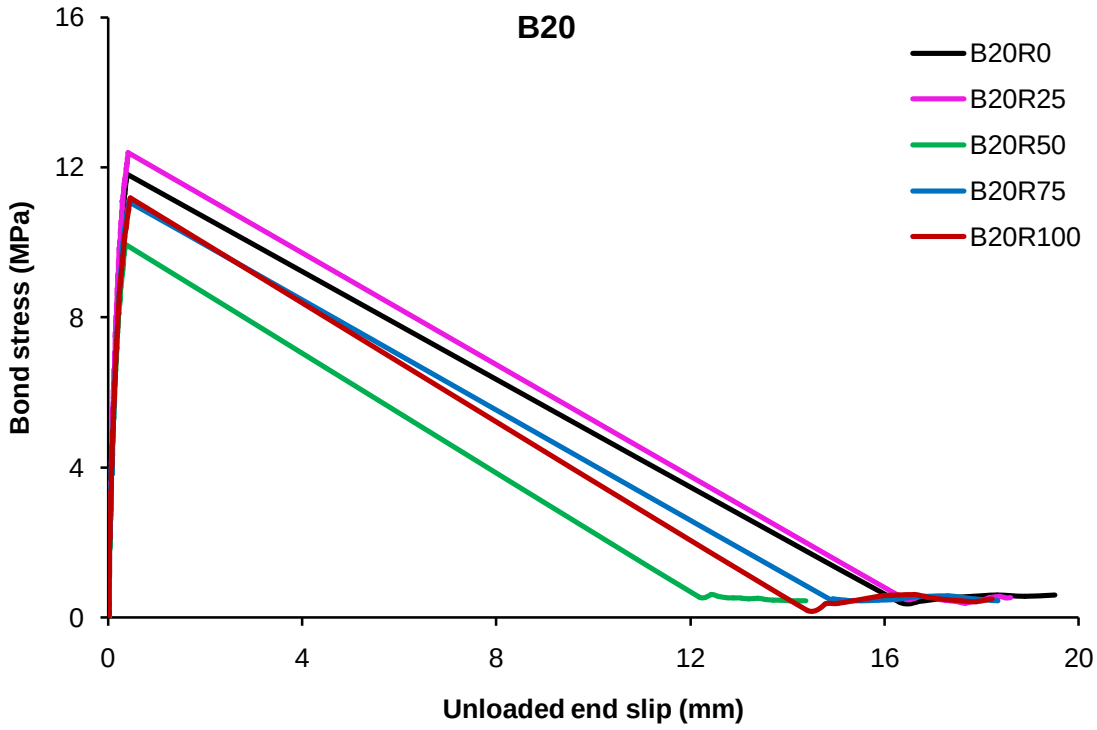

Figure 4.28 Bond-slip curves for the 20 mm diameter deformed bars embedded in medium-strength concrete

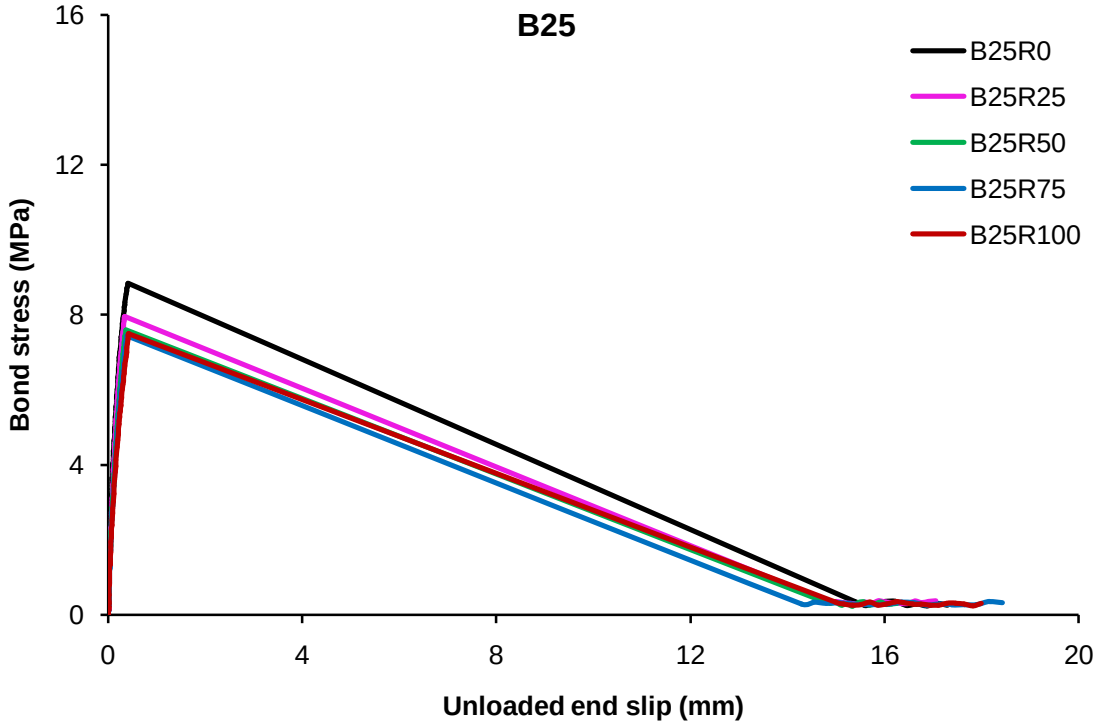

Figure 4.29 Bond-slip curves for the 25 mm diameter deformed bars embedded in medium-strength concrete

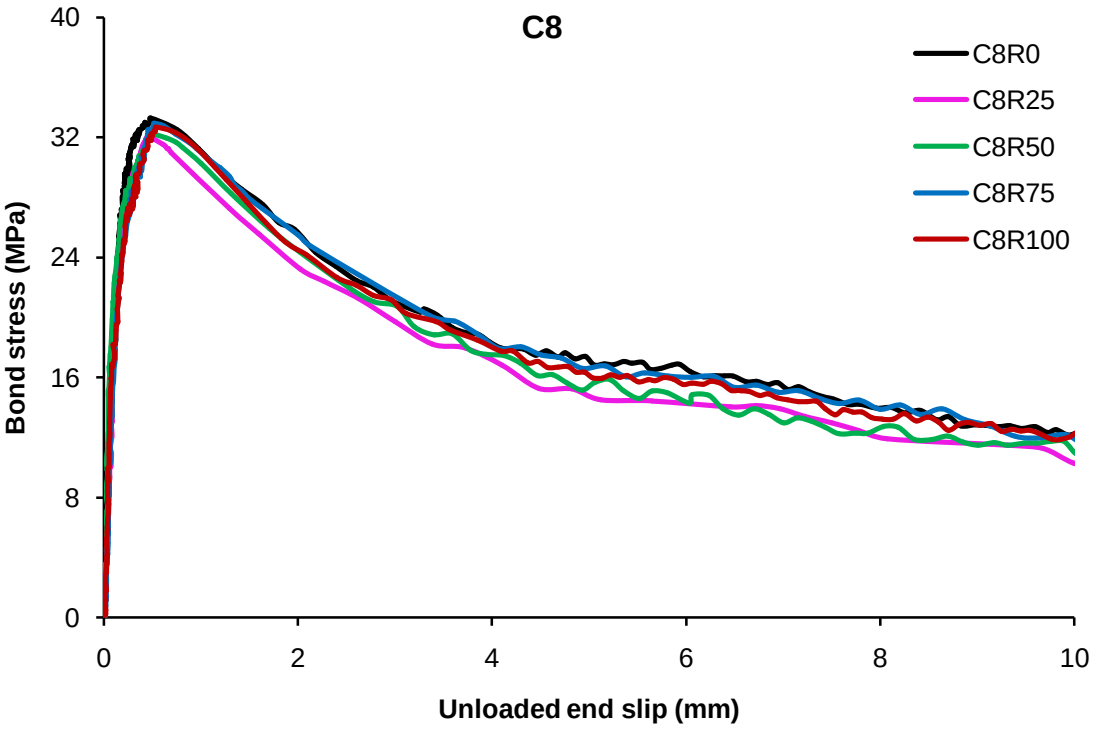

Figure 4.30 Bond-slip curves for the 8 mm diameter deformed bars embedded in high-strength concrete

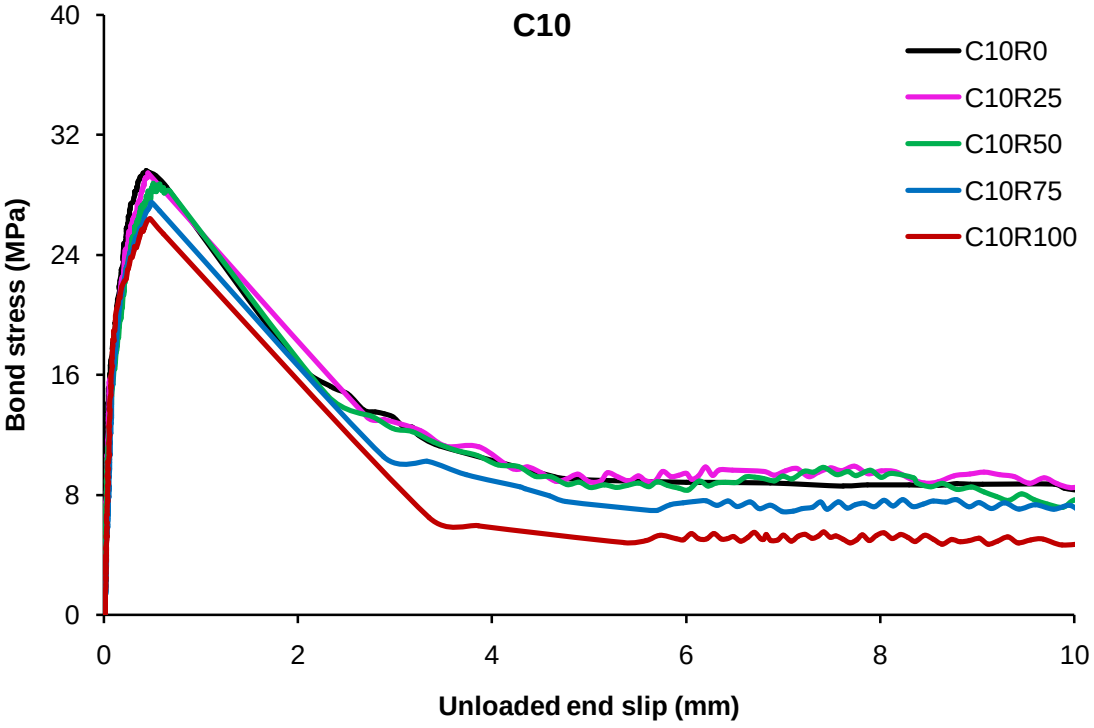

Figure 4.31 Bond-slip curves for the 10 mm diameter deformed bars embedded in high-strength concrete

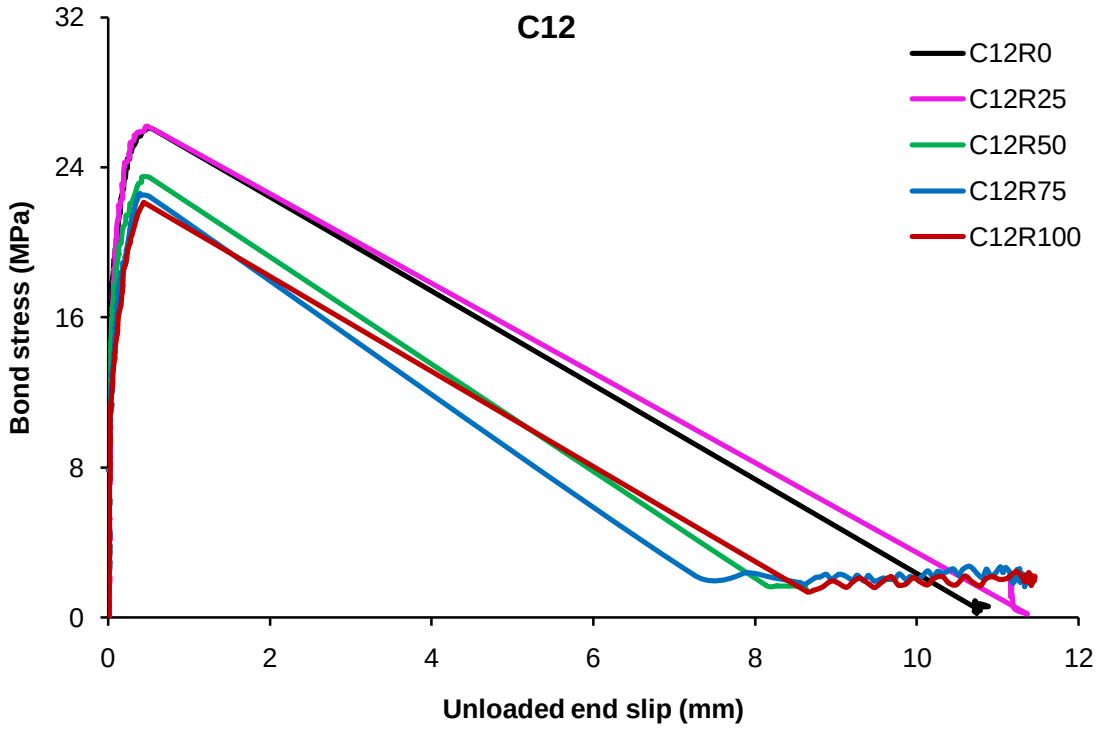

Figure 4.32 Bond-slip curves for the 12 mm diameter deformed bars embedded in high-strength concrete

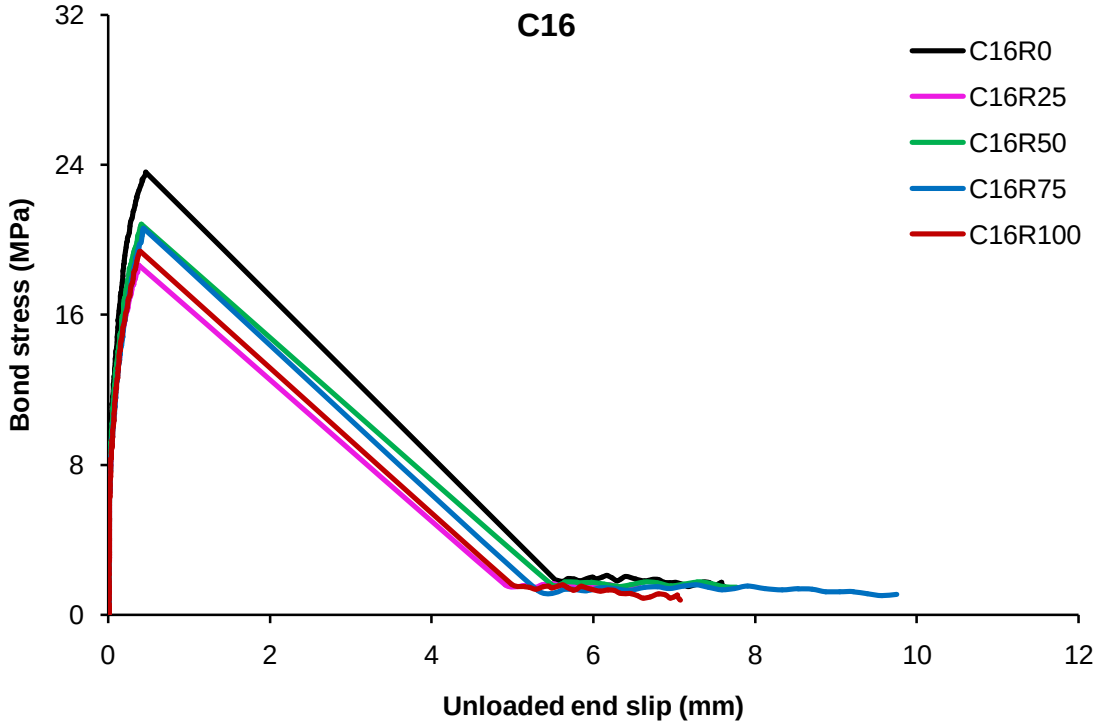

Figure 4.33 Bond-slip curves for the 16 mm diameter deformed bars embedded in high-strength concrete

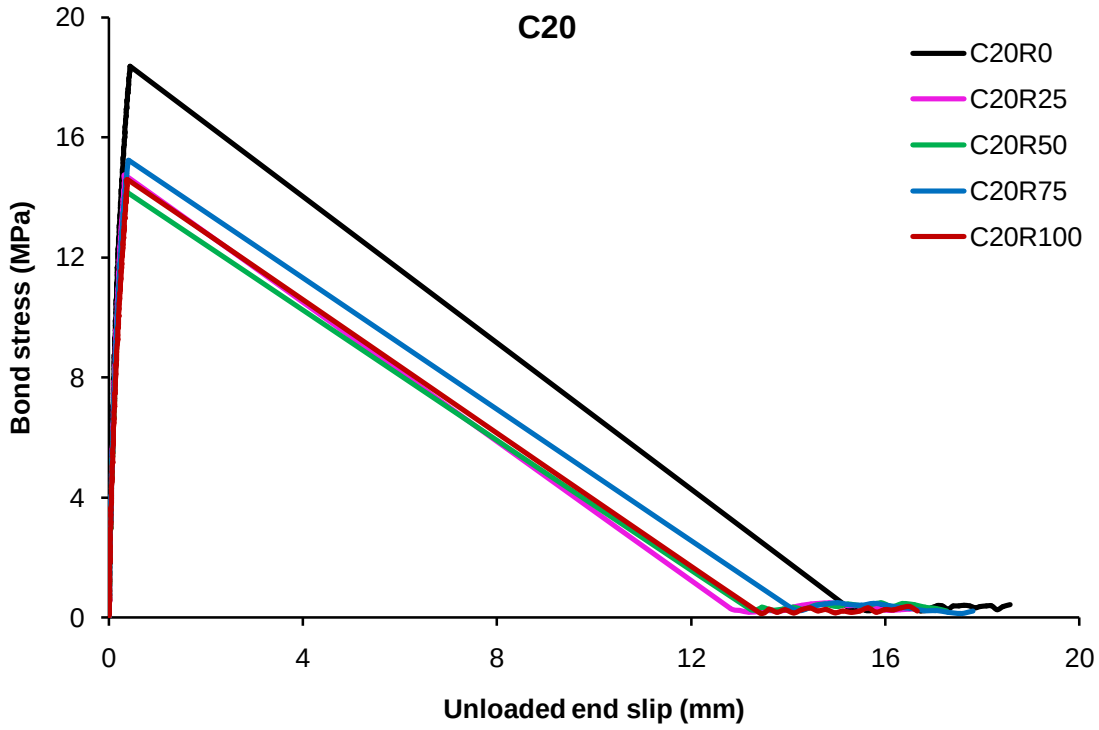

Figure 4.34 Bond-slip curves for the 20 mm diameter deformed bars embedded in high-strength concrete

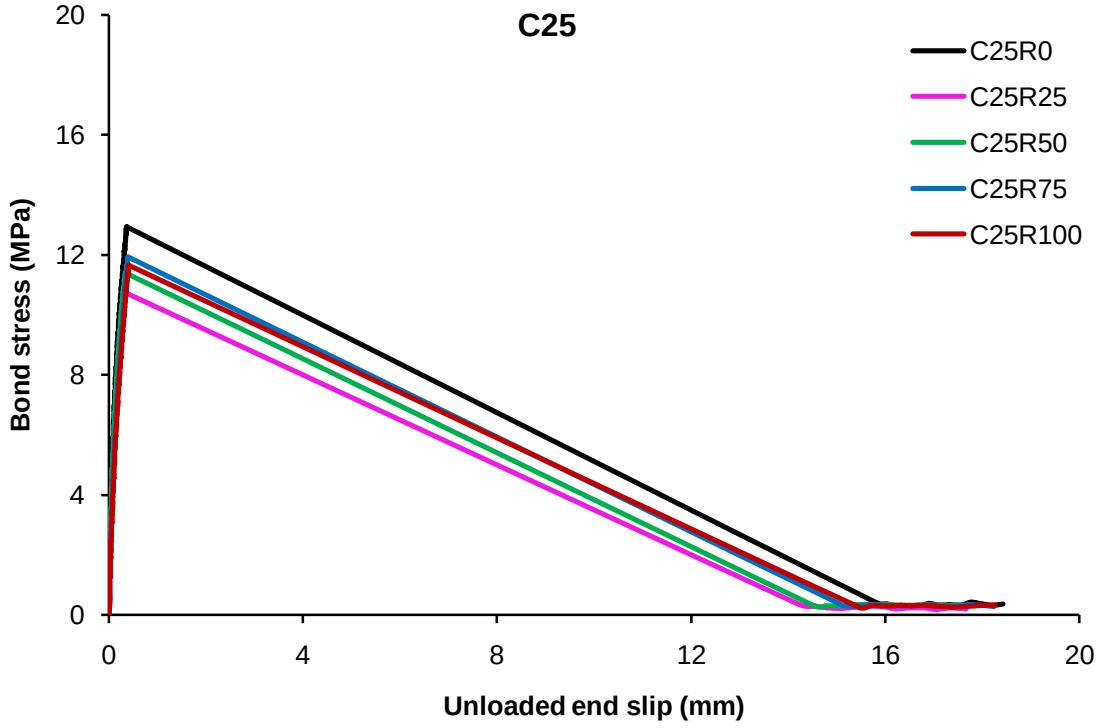

Figure 4.35 Bond-slip curves for the 25 mm diameter deformed bars embedded in high-strength concrete

4.2.8 Modelling of bond-slip relationship

For numerical analysis of reinforced RCA concrete members, modelling of bond behaviour at the steel-concrete interface is necessary and towards this end, a normalised bond-slip relationship is proposed in terms of the following dimensionless parameters of Xiao and Falkner (2007)

$$\bar{\tau} = \frac{\tau}{\tau_{max}}, \qquad \bar{s} = \frac{s}{s_{max}}, \tag{4.8}$$

where s_{max} is the slip corresponding to peak bond stress τ_{max}.

Two separate numerical models, one for pullout failure (Equation 4.13) and the other for pullout failure induced by through splitting (Equation 4.14) are presented for representing the bond stress-slip behaviour of the recycled aggregate concretes. In both the models, the ascending branch has been modelled by estimating on the basis of a regression analysis of test data the constant *a* in the following constitutive equation for normal-strength concrete proposed by Harajli (1994).

$$\bar{\tau} = \left(\bar{s}\right)^a \qquad \bar{s} \le 1 \tag{4.9}$$

where $\bar{\tau} = \frac{\tau}{\tau_{max}}$ and $\bar{s} = \frac{s}{s_{max}}$ and the constant *a* has to be determined from test results.

The above equation has been recast as follows to model the ascending branch for both the pullout failure as well as the pullout failure induced by through splitting.

$$\bar{\tau} = \left(\bar{s}\right)^a \qquad \bar{s} \le 1 \tag{4.10}$$

where *a* is a function of the slope of the ascending branch of the measured bond stress-slip relationship.

The descending branch associated with the pullout failure has been modelled using the following equation of Guo (1997) where *b* is related to the area under the descending branch of bond stress-slip curve.

$$\bar{\tau} = \frac{\bar{s}}{b\left(\bar{s} - 1\right)^2 + \bar{s}} \qquad \bar{s} > 1 \tag{4.11}$$

Hence, in summary, the following model is proposed for pullout failure.

$$\bar{\tau} = \begin{cases} \left(\bar{s}\right)^a & \bar{s} \le 1, \\ \dfrac{\bar{s}}{b\left(\bar{s} - 1\right)^2 + \bar{s}} & \bar{s} > 1 \end{cases} \tag{4.12}$$

The following model is proposed for the ascending branch of pullout failure induced by through splitting.

$$\bar{\tau} = (\bar{s})^a \qquad \bar{s} \leq 1 \tag{4.13}$$

The constants '*a*' and '*b*' in the above models obtained by regression analysis of the test data are presented in Table 4.6. It may be noted in Table 4.6 that the constants *a* and *b* vary only with concrete grade and rebar diameter and they are taken to be independent of the RCA replacement level. For the purpose of illustration, typical plots of the average of the measured normalised bond stress-slip relationships of the companion pullout specimens are presented together with the predictions from the proposed models in Figures 4.36 – 4.39. These figures show a good correlation between the measured and the predicted relationships for the NCA as well as the RCA concretes. Xiao and Falkner (2007) have also reported accurate predictions of the measured bond stress-slip relationships of their RCA concretes with the help of Equation 4.12 which therefore lends support to the validity of this equation for predictive assessment of the bond-slip behaviour of RCA concrete.

Table 4.6 Regression parameters *a* and *b*

Specimen	*a*	*b*	Specimen	*a*	*b*	Specimen	*a*	*b*
A8R0	0.30	0.18	B8R0	0.18	0.20	C8R0	0.28	0.14
A8R25			B8R25			C8R25		
A8R50			B8R50			C8R50		
A8R75			B8R75			C8R75		
A8R100			B8R100			C8R100		
A10R0	0.30	0.15	B10R0	0.20	0.15	C10R0	0.25	0.28
A10R25			B10R25			C10R25		-
A10R50			B10R50		-	C10R50		
A10R75			B10R75			C10R75		
A10R100			B10R100			C10R100		
A12R0	0.20	-	B12R0	0.30	-	C12R0	0.20	-
A12R25			B12R25			C12R25		
A12R50			B12R50			C12R50		
A12R75			B12R75			C12R75		
A12R100			B12R100			C12R100		
A16R0	0.25	-	B16R0	0.30	-	C16R0	0.30	-
A16R25			B16R25			C16R25		
A16R50			B16R50			C16R50		
A16R75			B16R75			C16R75		
A16R100			B16R100			C16R100		
A20R0	0.35	-	B20R0	0.55	-	C20R0	0.55	-
A20R25			B20R25			C20R25		
A20R50			B20R50			C20R50		
A20R75			B20R75			C20R75		
A20R100			B20R100			C20R100		
A25R0	0.25	-	B25R0	0.55	-	C25R0	0.55	-
A25R25			B25R25			C25R25		
A25R50			B25R50			C25R50		
A25R75			B25R75			C25R75		
A25R100			B25R100			C25R100		

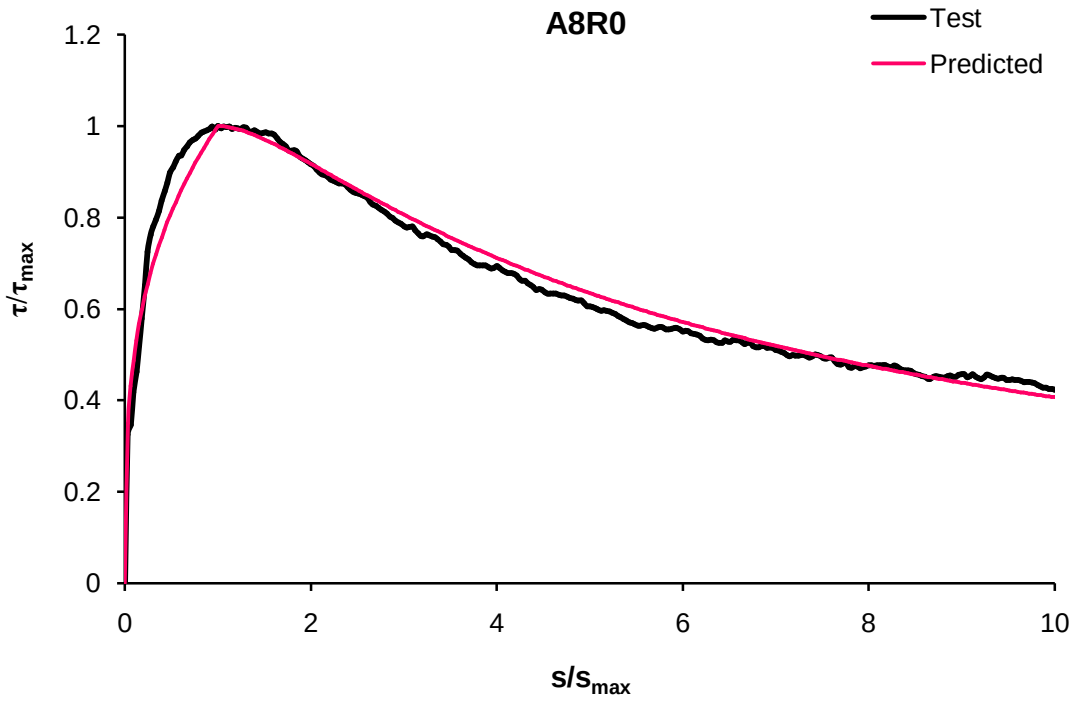

Figure 4.36 Typical measured versus predicted bond stress-slip relationships for the 8 mm diameter deformed bars embedded in normal-strength concrete

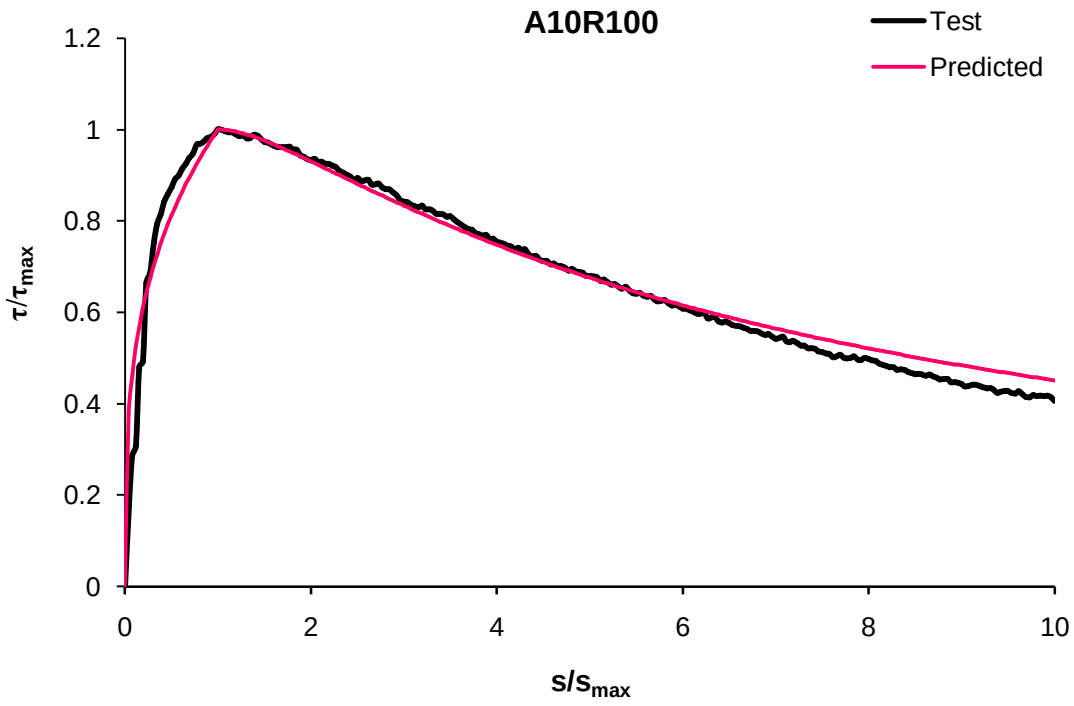

Figure 4.37 Typical measured versus predicted bond stress-slip relationships for the 10 mm diameter deformed bars embedded in normal-strength concrete

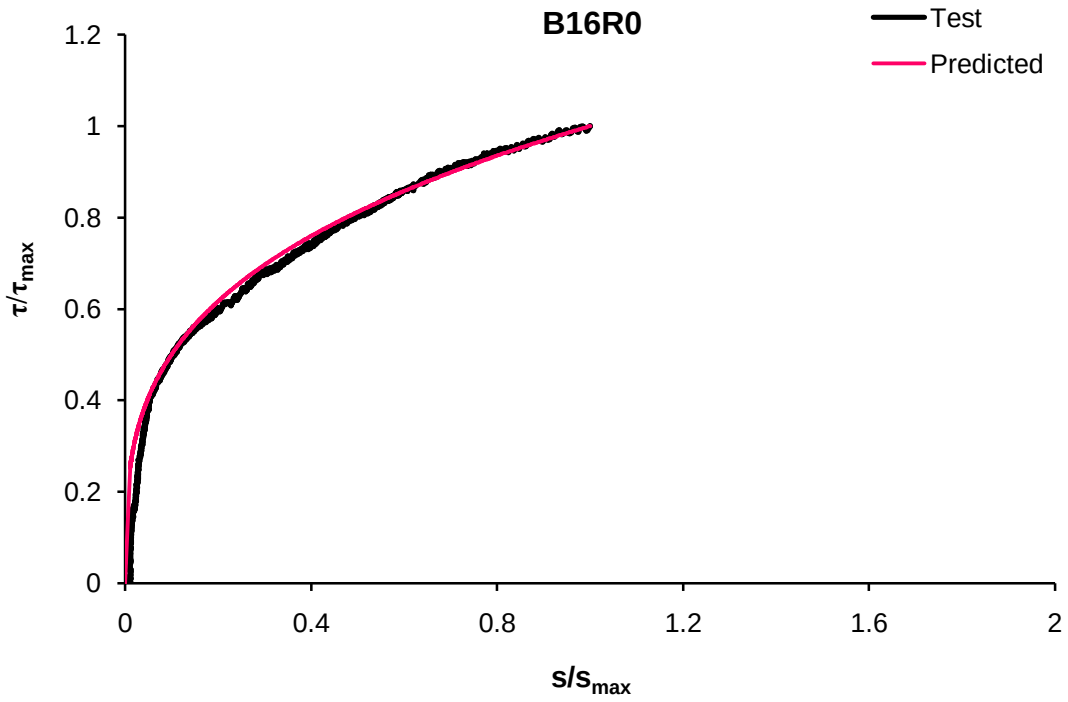

Figure 4.38 Typical measured versus predicted bond stress-slip relationships for the 16 mm diameter deformed bars embedded in medium-strength concrete

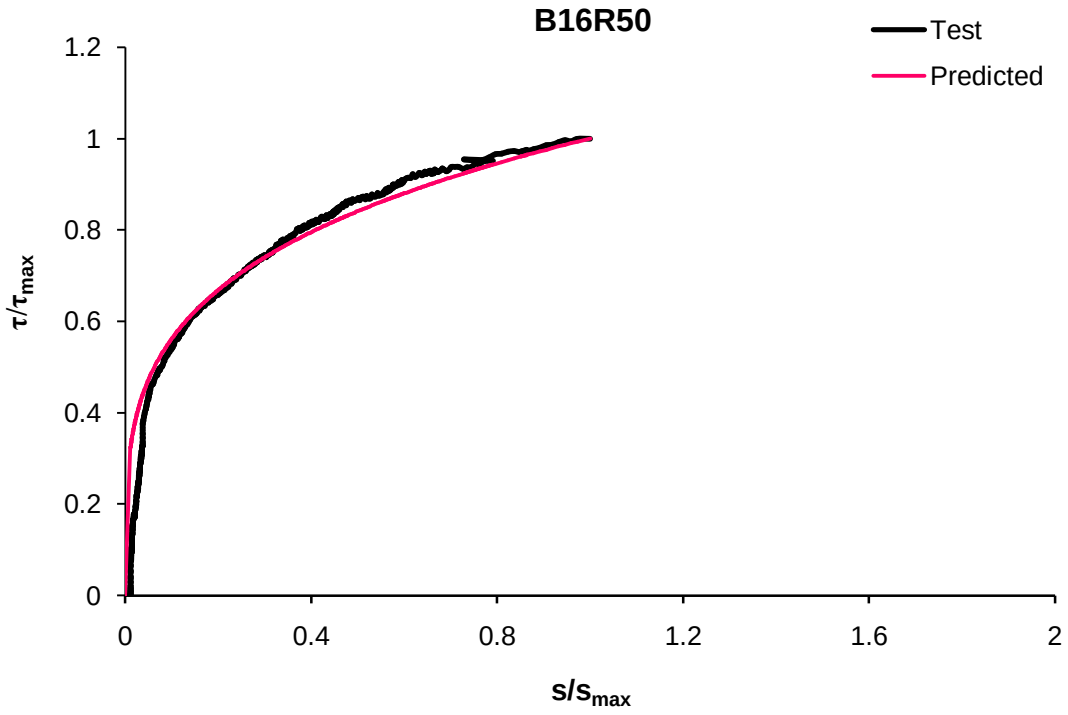

Figure 4.39 Typical measured versus predicted bond stress-slip relationships for the 16 mm diameter deformed bars embedded in medium-strength concrete

4.2.9 Anchorage lengths in RCA concrete based on results of the pullout tests

Rebar anchorage in RCA concrete is of practical interest and in general anchorage length is influenced by a number of parameters, amongst which the material parameters of interest are compressive strength of concrete and yield strength of rebars. Although the anchorage characteristics have not been considered explicitly in this investigation, some relevant suggestions implied by the observed behaviour of the RCA concretes are made here. Since the RCA concrete mixtures were designed on the basis of equivalent mix proportions, a perusal of Tables 4.1, 4.2 and 4.3 shows that compressive strengths of the RCA concretes were lower than those of the control NCA concrete and further, the compressive strength of the RCA concretes decreased with increase in the RCA replacement level. However, when the peak bond stress values were normalised with the respective compressive strengths and plotted in Figures 4.4, 4.5 and 4.6, then the normalised bond strengths of the RCA concretes across all RCA replacement levels for the 8 mm, 10 mm, 12 mm, 16 mm, 20 mm and 25 mm bars were higher than that of the NCA concrete. Further, the trends in brittleness index in Figure 4.10 indicate that fracture toughness of the concretes increased with an increase in the RCA replacement level which supports the trends in the normalised bond strength. The aforesaid observations suggest that anchorage lengths of steel bars in RCA concrete can be smaller than those in NCA concrete. However, as a conservative measure, it is suggested that for the 8 mm, 10 mm, 12 mm, 16 mm, 20 mm and 25 mm diameter deformed rebars used in this investigation, similar anchorage lengths can be adopted in comparable NCA and RCA concretes.

4.3 PHASE II: INVESTIGATION OF BOND BEHAVIOUR WITH SPLICE BEAM SPECIMENS

Splice beam specimens were tested to get more realistic assessments of development and splice strengths. This section presents discussion of the experimental results obtained from the splice beam tests.

4.3.1 Experimental results

4.3.1.1 Bond strength

Assuming a uniform bond stress distribution over the splice length in concrete, the bond strength is given by the following relationship

$$\tau_{max} = \frac{A_b f_s}{\pi d_b L_s} \qquad (4.14)$$

where $\tau_{max,}$ the peak bond stress (MPa) between concrete and steel rebar, is also termed as the bond strength; A_b is the area of the reinforcing bar (mm^2); f_s is the stress in steel at failure (MPa); d_b is the nominal rebar diameter (mm) and L_s is the splice length (mm). The experimental results in terms of the peak load, P_{max}, the measured strains in the spliced rebars and the failure mode of all the 24 splice beam specimens were presented in Table 4.7. The average value of the peak bond stress τ_{max} and the corresponding slip s also presented.

Table 4. 7 Experimental results of the splice beam specimens

Specimen ID	f_c'	P_{max}	M_{max}	ε_s (M - φ)	ε_s (SG)	f_s (M - φ)	τ_{max}	Mean τ_{max}	$\tau_{r,max}$	Failure Mode
	MPa	kN	kNm	x 10^{-3}	x 10^{-3}	MPa	MPa	MPa	MPa^^(1/4)	
1	2	3	4	5	6	7	8	9	10	11
AS12R0-1	36.91	71.78	19.38	2.350	2.510	470.0	4.70	5.01	2.03	SP
AS12R0-2		85.49	23.09	*	**	532.0	5.32			SP+Y
AS12R50-1	24.04	75.51	20.39	2.560	2.646	512.0	5.12	5.09	2.30	SP
AS12R50-2		74.48	20.11	2.524	2.640	504.8	5.05			
AS12R100-1	24.71	77.28	20.87	2.614	2.079	522.8	5.23	4.87	2.18	SP
AS12R100-2		66.93	18.07	2.255	2.281	451.0	4.51			
AS20R0-1	36.91	192.72	47.22	2.185	2.227	437.0	5.46	5.16	2.09	SP
AS20R0-2		170.81	41.85	1.939	1.979	387.8	4.85			
AS20R50-1	24.04	164.93	40.41	1.926	1.730	385.2	4.82	4.67	2.11	SP
AS20R50-2		154.73	37.91	1.807	1.812	361.4	4.52			
AS20R100-1	24.71	180.30	44.17	2.120	2.541	424.0	5.30	5.22	2.34	SP
AS20R100-2		176.32	43.20	2.057	2.481	411.4	5.14			
CS12R0-1	68.65	114.45	30.90	*	**	532.0•	5.32	5.32	1.85	SP+Y
CS12R0-2		102.94	27.79	*	**	532.0•	5.32			
CS12R50-1	57.54	102.83	27.76	*	**	532.0•	5.32	5.32	1.93	SP+Y
CS12R50-2		109.92	29.68	*	**	532.0•	5.32			
CS12R100-1	50.30	94.23	25.44	*	**	532.0•	5.32	5.32	2.00	SP+Y
CS12R100-2		86.84	23.45	*	**	532.0•	5.32			
CS20R0-1	68.65	216.09	52.94	2.484	2.021	496.8	6.21	6.27	2.18	SP
CS20R0-2		220.33	53.98	2.533	2.828	506.6	6.33			
CS20R50-1	57.54	204.87	50.19	2.383	2.372	476.6	5.96	5.91	2.14	SP
CS20R50-2		201.21	49.29	2.339	2.259	467.8	5.85			
CS20R100-1	50.30	200.36	49.09	2.355	2.163	471.0	5.89	5.63	2.11	SP
CS20R100-2		182.65	44.75	2.142	2.015	428.4	5.36			

** Rebar has yielded*

*** Due to yielding, a unique strain reading at failure cannot be reported*

• *Measured yield stress of the rebar*

Note to Table 4.7:

Column 1 = Specimen ID: The alphabet in the first place-holder represents concrete grade (A: normal-strength, C: high-strength), the alphabet in the second place-holder represents splice beam specimen, the numerals in the third/forth place-holders represent the nominal rebar diameters (12 mm, 20 mm) and the alpha-numeric characters in the remaining place holders represent RCA replacement levels (0: 0%, 50: 50%, and 100: 100%). Column 2 = f_c' *: cylinder compressive strength. Column 3 =* P_{max}*: Peak load. Column 4 =* M_{max}*: Maximum bending moment. Column 5 =* ε_s *: strain in steel based on moment-curvature analysis. Column 6 =* ε_s *: strain in steel based on strain gauge reading. Column 7 =* f_s *: stress in steel derived from its constitutive model. Column 8 =* $\tau_{\max}$ *: peak bond stress. Column 9 =* $\tau_{\max}$ *: mean peak bond stress. Column 10 =* $\tau_{r,\max}$ *: normalised bond stress. Column 11 = Failure mode (SP: Splitting, SP+Y: Splitting+Yielding of the spliced rebars).*

4.3.2 Strains and stresses in the spliced bars

Plots of the loads and the corresponding strains in the spliced bars measured using electrical resistance type strain gauges are presented in Figures 4.40 – 4.43. It may be noted that Figure 4.42 shows yielding of the spliced bars of 12 mm diameter in the high-strength concrete specimens. Strains in the spliced bars were also estimated from moment-curvature analysis of the beam sections. The details of a typical moment-curvature analysis are presented in Appendix A. Corresponding to the experimentally obtained peak load and the associated moment, the strains were read off from the moment-strain plot obtained in the moment-curvature analysis. The measured as well as the strains estimated from the moment-curvature analysis are presented in Table 4.7. For the cases where the spliced bars yielded prior to failure a unique value of the steel strain at failure could not be identified from the measured strains. In such cases, the steel strain was taken corresponding to the yield moment in the moment-curvature analysis of the relevant beam section. It may be noted in Table 4.7 that the steel strains obtained from the instrumentation and those obtained from the moment-curvature analysis are comparable to each other. For calculation of stresses in the spliced bars at failure the strains obtained from the moment-curvature analysis were multiplied by the elastic modulus of steel except for those cases where the splice beam tests indicated yielding of the steel bars. For all such cases, the stress in the spliced reinforcement was taken equal to the yield stress of this reinforcement measured during the course of the axial tensile tests. Once the stresses in the spliced bars at failure were known, the bond strengths in the splice beam specimens were calculated using Equation 4.14 and the results are presented in column 9 of the Table 4.7.

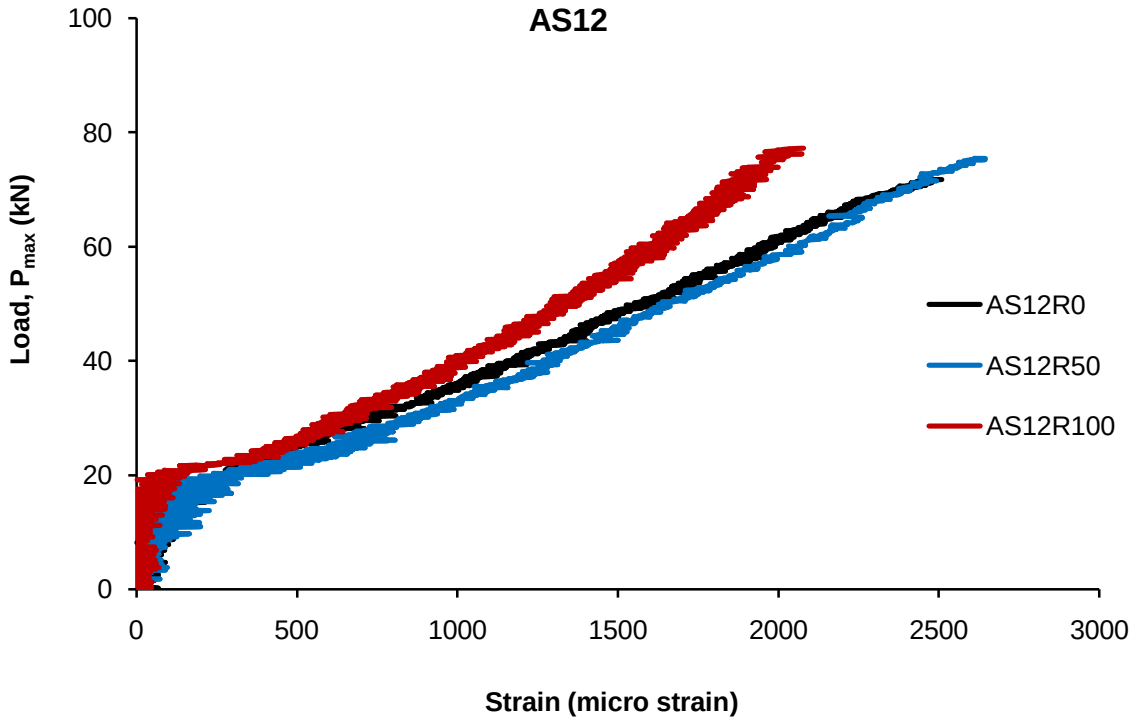

Figure 4.40 Typical load versus strain for the normal-strength splice beam specimens with the 12 mm bars

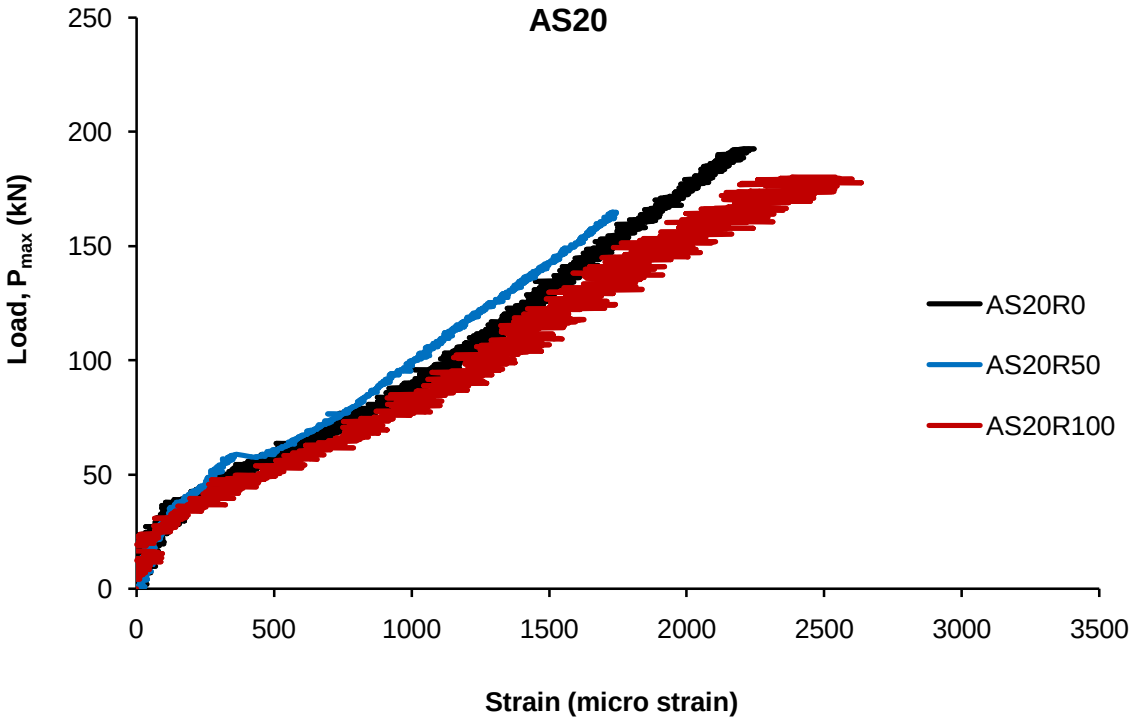

Figure 4.41 Typical load versus strain for the normal-strength splice beam specimens with the 20 mm bars

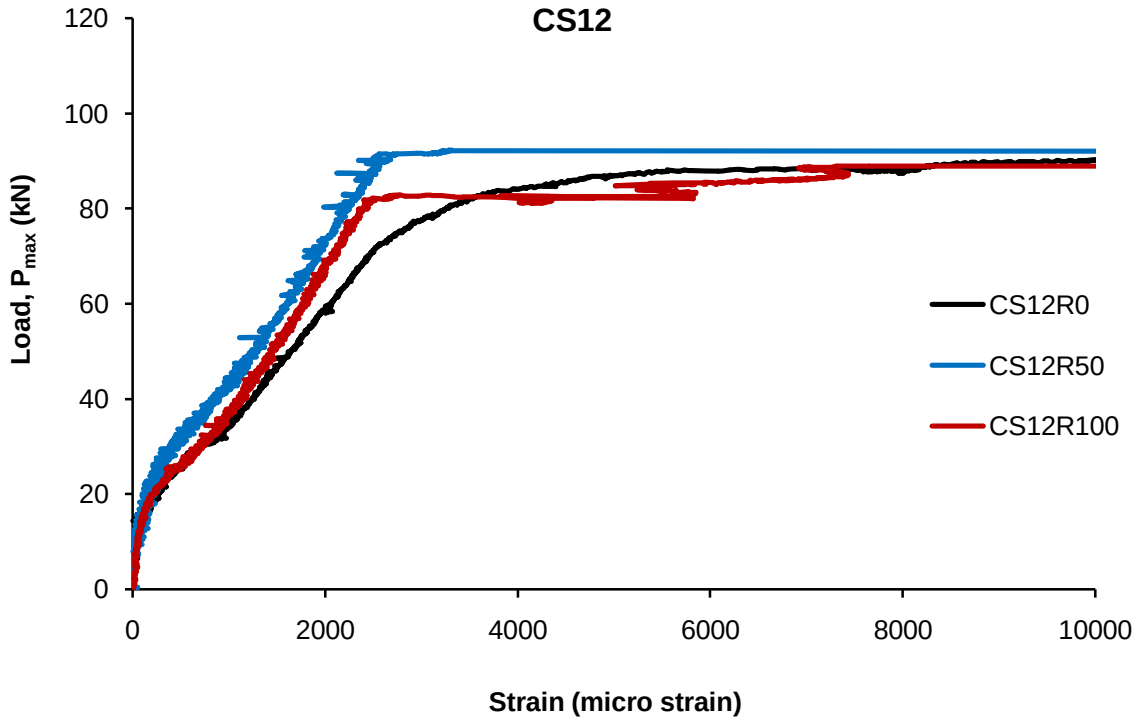

Figure 4.42 Typical load versus strain for the high-strength splice beam specimens with the 12 mm bars

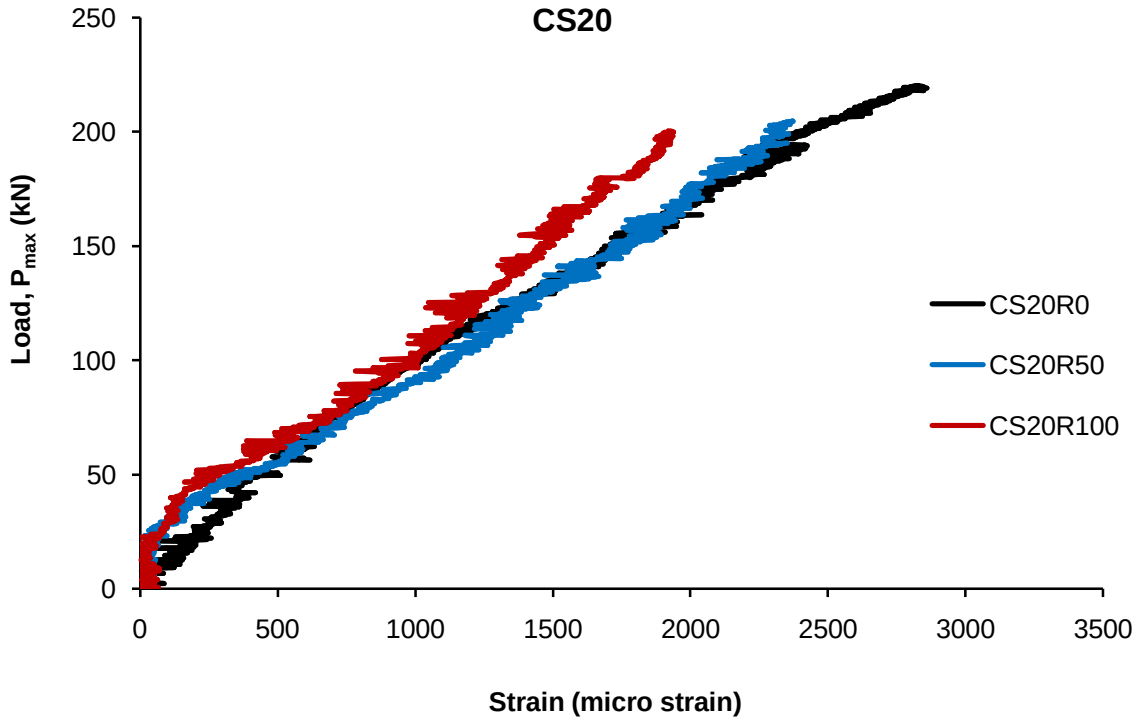

Figure 4.43 Typical load versus strain for the high-strength splice beam specimens with the 20 mm bars

4.3.3 Analysis of splice beam results

In order to develop a predictive equation for bond strength in the splice beam specimens, regression analysis of the results from the 24 splice beams was carried out considering the following parameters which are known to affect bond behaviour: f_c', $\frac{c}{d_b}$, $\frac{d_b}{L_d}$, $\frac{h_r}{s_r}$. Since the proposed model is to be applicable to recycled aggregate concrete, the RCA replacement level, *r*, was also taken as a parameter in the regression analysis. One of the objectives of the regression analysis was to examine whether $\sqrt{f_c'}$ accurately represents the effect of concrete strength on bond in RCA concrete or not. The following 4 regression equations in which the effect of concrete strength on bond has been modelled in terms of $(f_c')^{1/4}$, $(f_c')^{1/2}$, $(f_c')^{3/4}$ and $(f_c')^{1.0}$ were obtained after analysis of the test data.

$$\tau_{max} = (f_c')^{1/4}\left[0.64 + 0.8\left(\frac{c}{d_b}\right) + 11.31\left(\frac{d_b}{L_d}\right) - 1.07\left(\frac{h_r}{s_r}\right) + 0.0012\,r\right] \qquad (4.15)$$

$$\tau_{max} = (f_c')^{1/2}\left[0.25 + 0.31\left(\frac{c}{d_b}\right) + 4.13\left(\frac{d_b}{L_d}\right) + 0.39\left(\frac{h_r}{s_r}\right) + 0.00126\,r\right] \qquad (4.16)$$

$$\tau_{max} = (f_c')^{3/4}\left[0.1 + 0.12\left(\frac{c}{d_b}\right) + 1.49\left(\frac{d_b}{L_d}\right) - 0.14\left(\frac{h_r}{s_r}\right) + 0.0008\,r\right] \qquad (4.17)$$

$$\tau_{max} = (f_c')^{1.0}\left[0.04 + 0.05\left(\frac{c}{d_b}\right) + 0.5\left(\frac{d_b}{L_d}\right) - 0.05\left(\frac{h_r}{s_r}\right) + 0.00046\,r\right] \qquad (4.18)$$

where τ_{max} = peak bond stress (MPa), f_c' = cylinder compressive strength (MPa), *c* = minimum cover (mm), d_b = bar diameter (mm), L_d = bonded length (mm), h_r = rib height (mm), s_r = rib spacing (mm), *r* = replacement level (%).

A comparison of the bond strength predictions of Equations 4.15 – 4.18 with the experimental results of the 24 splice beam specimens is presented in Figure 4.44. This figure also includes the four best-fit lines corresponding to the four descriptive equations above. Figure 4.44 shows that the best-fit lines corresponding to $(f_c')^{1/2}$, $(f_c')^{3/4}$ and $(f_c')^{1.0}$ have a negative slope while the best-fit line based on $(f_c')^{1/4}$ has approximately a horizontal slope. This observation indicates that the ¼ power provides an unbiased representation of the effect of concrete strength on bond strength. It may be noted that on

the basis of pullout tests the ½ power provided an unbiased representation of the effect of concrete strength on bond strength. The results of the splice beam tests therefore discount the effect of concrete strength on bond strength when compared to the pullout tests. Hence, for long embedded lengths which are typical in full size members and practical construction, the following bond strength model applicable to both RCA concrete and NCA concrete (r = 0) is proposed.

$$\tau_{\max} = \left(f_c^{'}\right)^{1/4}\left[0.64 + 0.8\left(\frac{c}{d_b}\right) + 11.31\left(\frac{d_b}{L_d}\right) - 1.07\left(\frac{h_r}{s_r}\right) + 0.0012\,r\right] \qquad (4.19)$$

It is pertinent to point out although $\frac{c}{d_b}$ was kept constant in the splice beam tests; it still was considered as a parameter in the regression analysis in order to ensure uniformity of the bond strength model with other similar models in the literature.

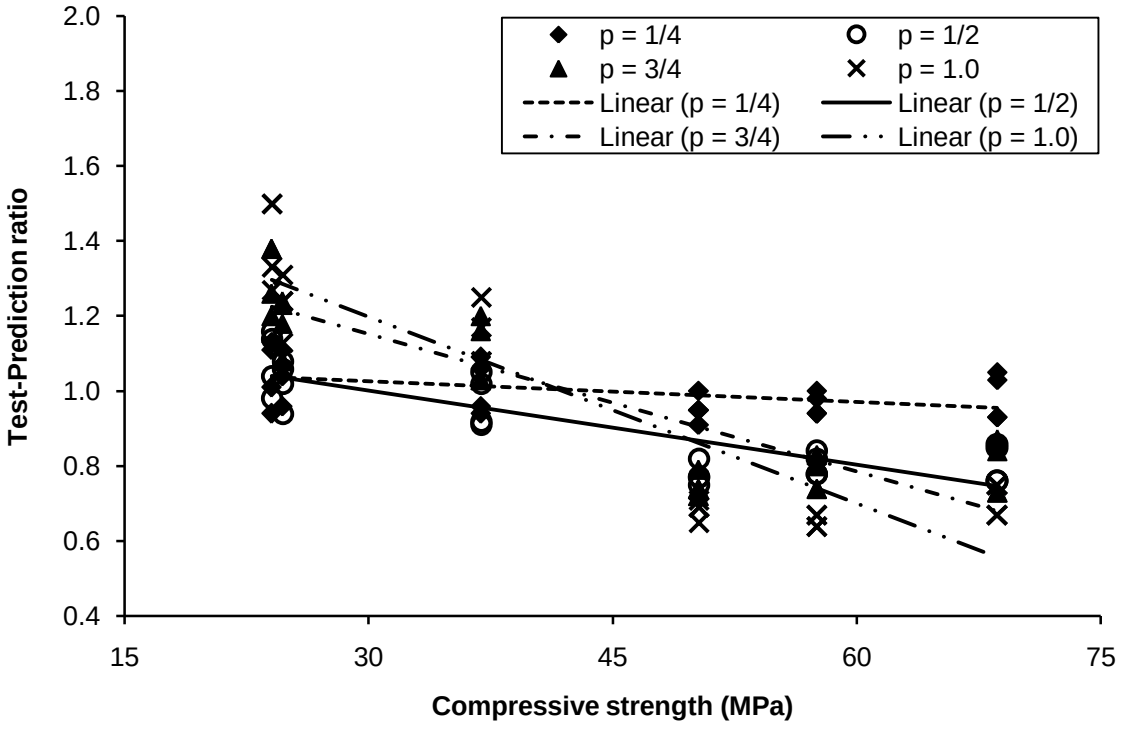

Figure 4. 44 Variation of test-prediction ratio versus compressive strength

4.3.4 Comparison of measured and predicted bond strengths

In the absence of data on RCA concrete splice beams in the literature, validation of the bond strength model proposed above with data from independent sources could not be carried out. However, the predictive efficacy of the proposed model has been evaluated by comparing its predictions of the measured bond strengths with those obtained from selected bond strength models in the literature (Orangun *et al.*, 1975, 1977; Darwin *et al.*, 1996; Zuo and Darwin, 1998, 2000; MacGregor, 1997; ACI 408R-03; CSA A 23.3-04; AS 3600-2009; ACI 318-11). The results of this comparison are presented in Table 4.8 where it may be noted that the models selected from the literature are all valid for long embedded lengths. The results of this comparison show that relatively the most accurate predictions were obtained from the proposed model and next in the order of accuracy were the predictions from the ACI 408R-03 (2003) although the ACI model has been developed for NCA concrete. It is hoped that as more experimental data on RCA concrete splice beams become available, the proposed model can be refined and made more robust. A graphical representation of the comparison in Table 4.8 is presented in Figures 4.45 and 4.46.

Table 4. 8 Comparison of measured and predicted bond stress values

Specimen ID	Peak bond stress, τ_{max} (MPa)										Measured bond strength / Predicted bond strength								
	Test	Orangun *et al.*, 1975, 1977	Darwin *et al.*, 1996	Zuo and Darwin, 1998, 2000	ACI 408R-03	MacGregor, 1997	ACI 318-11	CSA A 23.3-04	AS 3600-2009	Proposed Model									
	A	*B*	*C*	*D*	*E*	*F*	*G*	*H*	*I*	*J*	*A/B*	*A/C*	*A/D*	*A/E*	*A/F*	*A/G*	*A/H*	*A/I*	*A/J*
AS12R0	5.01	3.51	2.29	2.37	2.4	3.78	3.65	3.68	3.78	4.9	1.43	2.19	2.11	2.09	1.33	1.37	1.36	1.33	1.02
AS12R50	5.09	2.83	2.05	2.13	2.15	3.05	2.95	2.97	3.05	4.54	1.8	2.48	2.39	2.37	1.67	1.73	1.71	1.67	1.12
AS12R100	4.87	2.87	2.07	2.14	2.17	3.09	2.99	3.01	3.09	4.7	1.7	2.35	2.28	2.24	1.58	1.63	1.62	1.58	1.04
AS20R0	5.16	3.76	2.6	2.71	2.75	3.78	3.65	3.68	3.78	5.19	1.37	1.98	1.9	1.88	1.37	1.41	1.4	1.37	0.99
AS20R50	4.67	3.03	2.34	2.44	2.47	3.05	2.95	2.97	3.05	4.79	1.54	2	1.91	1.89	1.53	1.58	1.57	1.53	0.97
AS20R100	5.22	3.08	2.35	2.45	2.49	3.09	2.99	3.01	3.09	4.96	1.69	2.22	2.13	2.1	1.69	1.75	1.73	1.69	1.05
CS12R0	5.32	4.78	2.67	2.76	2.8	5.16	4.98	5.02	5.16	5.73	1.11	1.99	1.93	1.9	1.03	1.07	1.06	1.03	0.93
CS12R50	5.32	4.38	2.56	2.64	2.68	4.72	4.56	4.59	4.72	5.65	1.21	2.08	2.02	1.99	1.13	1.17	1.16	1.13	0.94
CS12R100	5.32	4.09	2.47	2.56	2.59	4.41	4.27	4.29	4.41	5.62	1.3	2.15	2.08	2.05	1.21	1.25	1.24	1.21	0.95
CS20R0	6.27	5.13	3.04	3.17	3.21	5.16	4.98	5.02	5.16	6.06	1.22	2.06	1.98	1.95	1.22	1.26	1.25	1.22	1.03
CS20R50	5.91	4.69	2.91	3.03	3.07	4.72	4.56	4.59	4.72	5.96	1.26	2.03	1.95	1.93	1.25	1.3	1.29	1.25	0.99
CS20R100	5.63	4.39	2.81	2.93	2.97	4.41	4.27	4.29	4.41	5.92	1.28	2	1.92	1.9	1.28	1.32	1.31	1.28	0.95
									Mean		1.41	2.13	2.05	2.02	1.36	1.4	1.39	1.36	1
									SD		0.22	0.16	0.16	0.15	0.21	0.22	0.22	0.21	0.06
									COV (%)		15.6	7.51	7.8	7.43	15.44	15.71	15.83	15.44	6

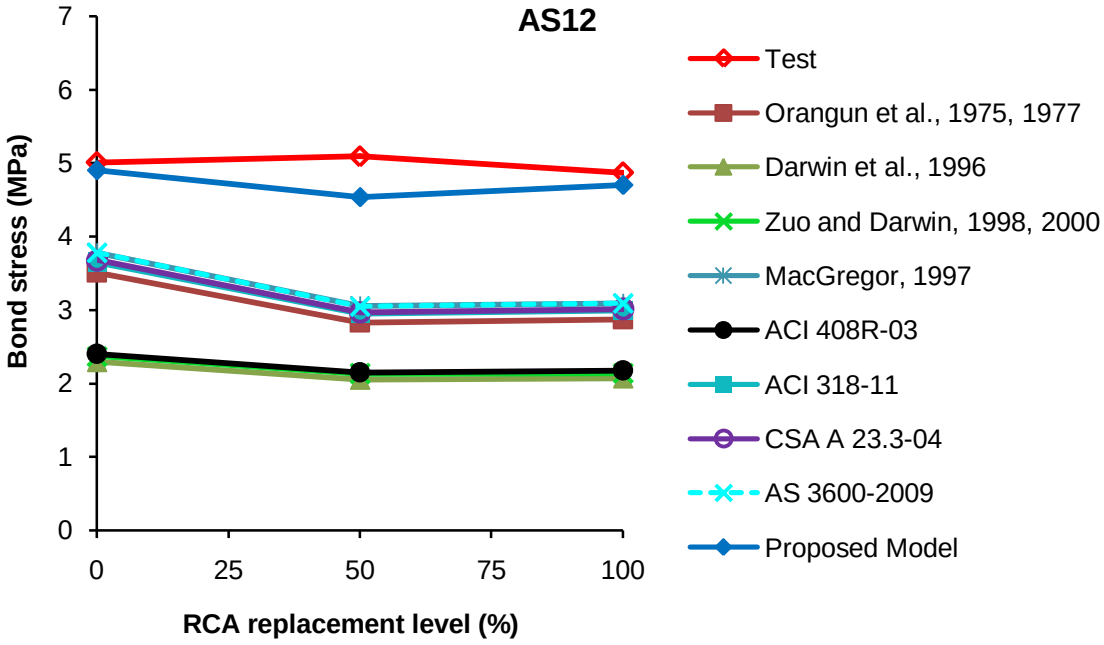

(a)

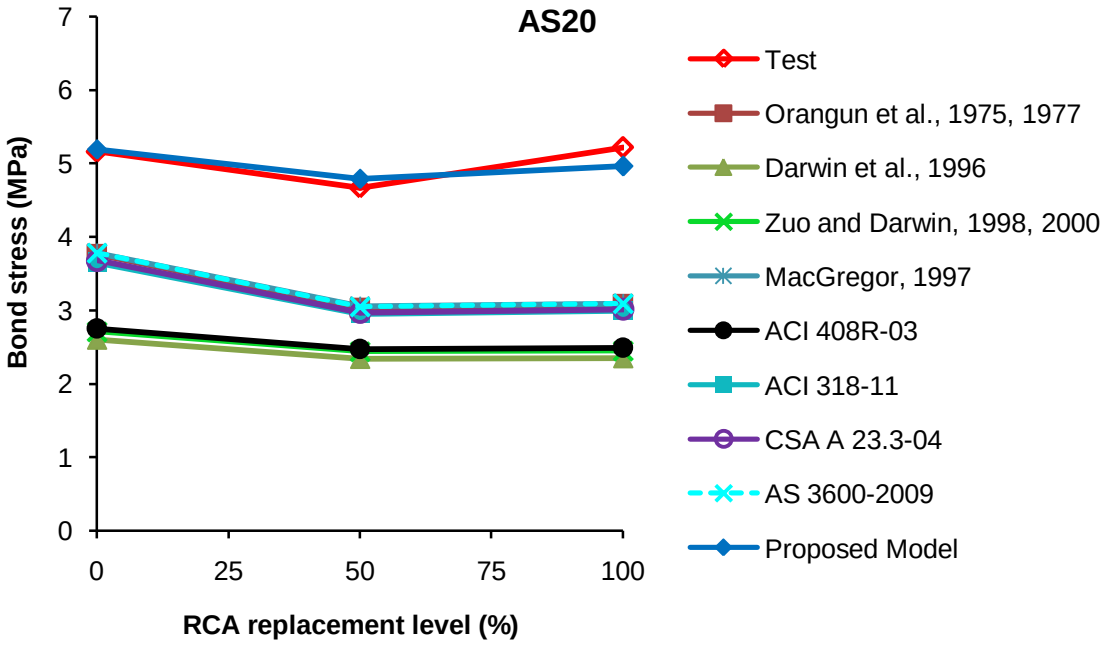

(b)

Figure 4.45 Comparison of measured and predicted bond stress values for the normal-strength concrete splice beam specimens: (a) AS12 (b) AS20

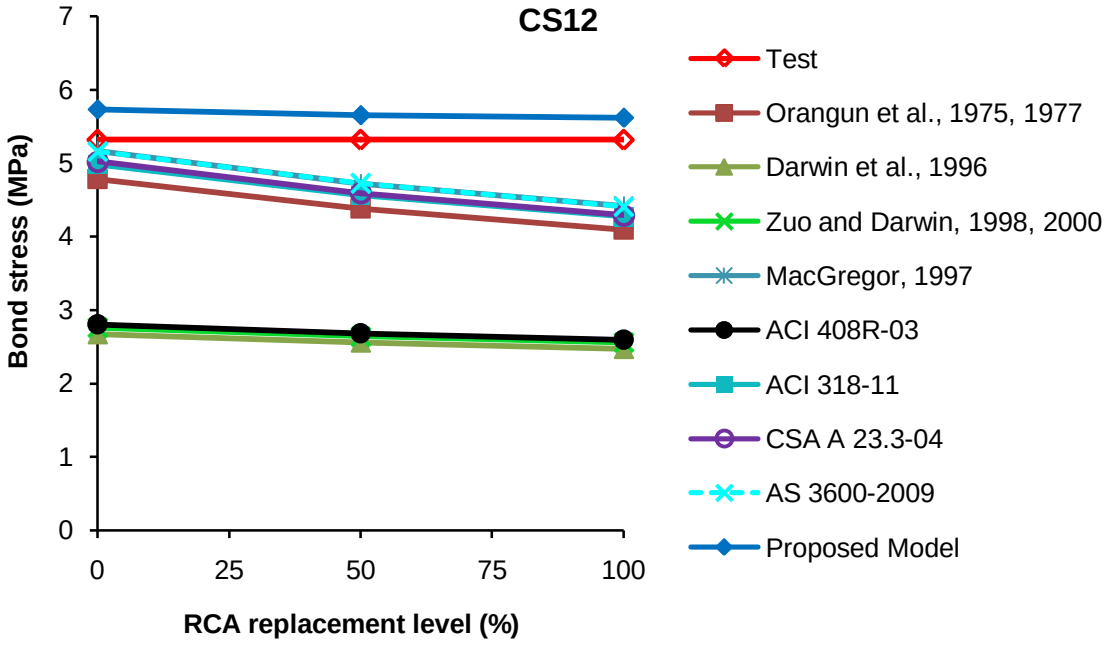

(a)

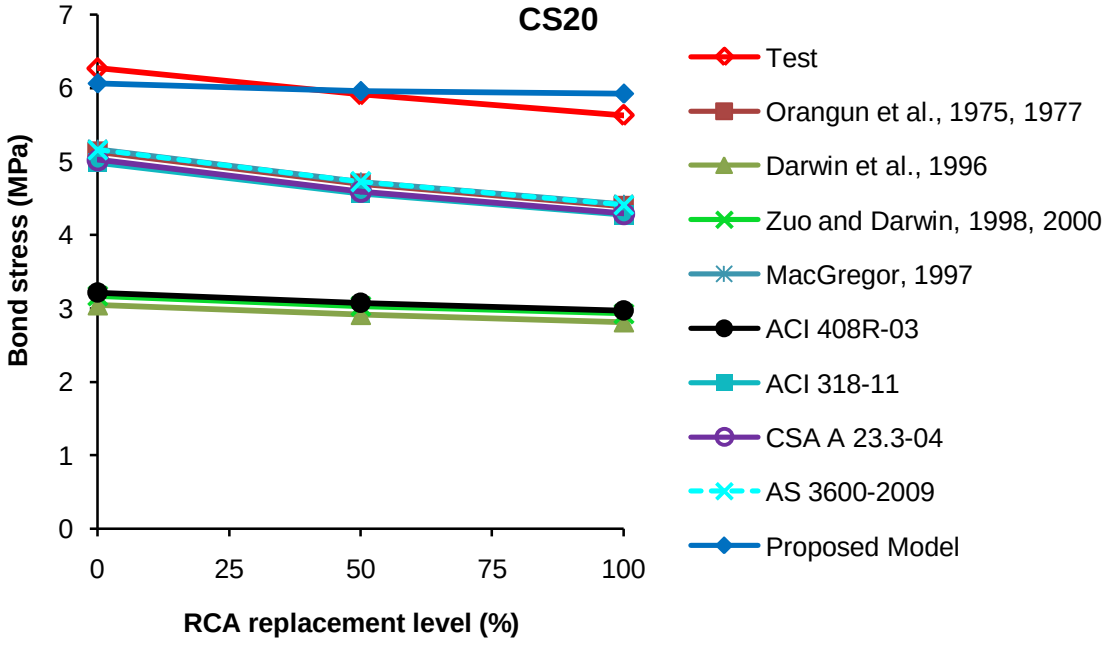

(b)

Figure 4.46 Comparison of measured and predicted bond stress values for the high-strength concrete splice beam specimens: (a) CS12 (b) CS20

4.3.5 General behaviour and failure mode

All the splice beam specimens exhibited similar crack patterns during testing. During early stages of loading, flexural cracks were formed in the constant moment zone just outside the splice region and as the load increased, theses cracks propagated along the length of the splice zone and were also formed in the shear spans. At approximately 60 % of the ultimate load, splitting cracks formed simultaneously in the vertical faces of the beams at both ends of the splice and propagated towards the mid-span. In addition to the aforementioned side splitting cracks, splitting cracks were also noted to have initiated on the beam soffit, originating from the existing transverse flexural cracks. At failure which was sudden and violent, there was a rapid propagation of the splitting cracks over almost the entire splice length accompanied by loss of concrete cover. Typical failure crack patterns in selected NCA concrete and RCA concrete beams are presented in Figures 4.47 – 4.50. No significant difference was noted in the failure crack patterns of the NCA and the RCA concrete specimens.

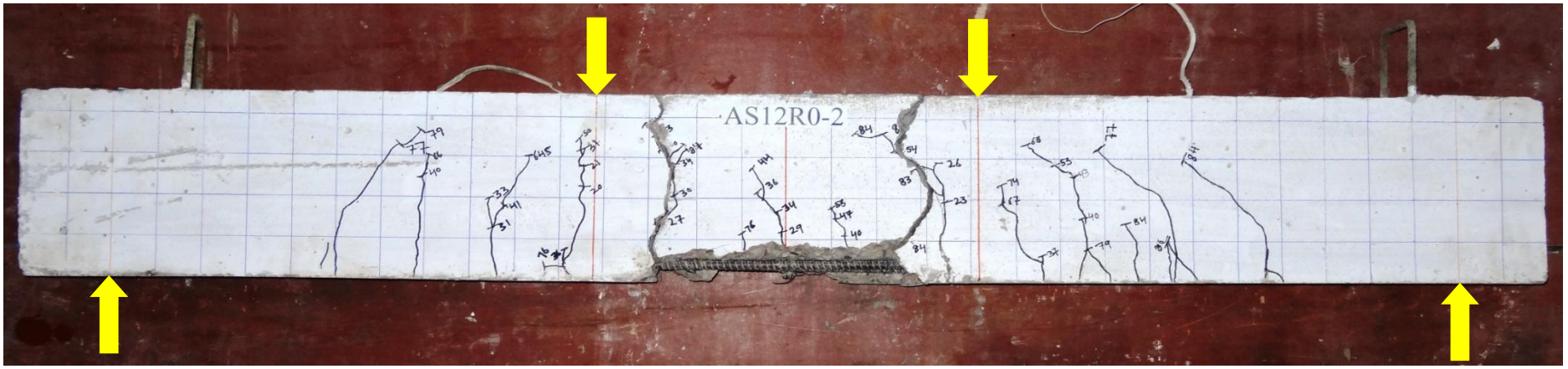

(a)

(b)

Figure 4.47 Typical failure crack patterns for the normal-strength splice beam specimen AS12R0-2: (a) elevation (b) soffit

(a)

(b)

Figure 4.48 Typical failure crack patterns for the normal-strength splice beam specimen AS20R100-1: (a) elevation (b) soffit

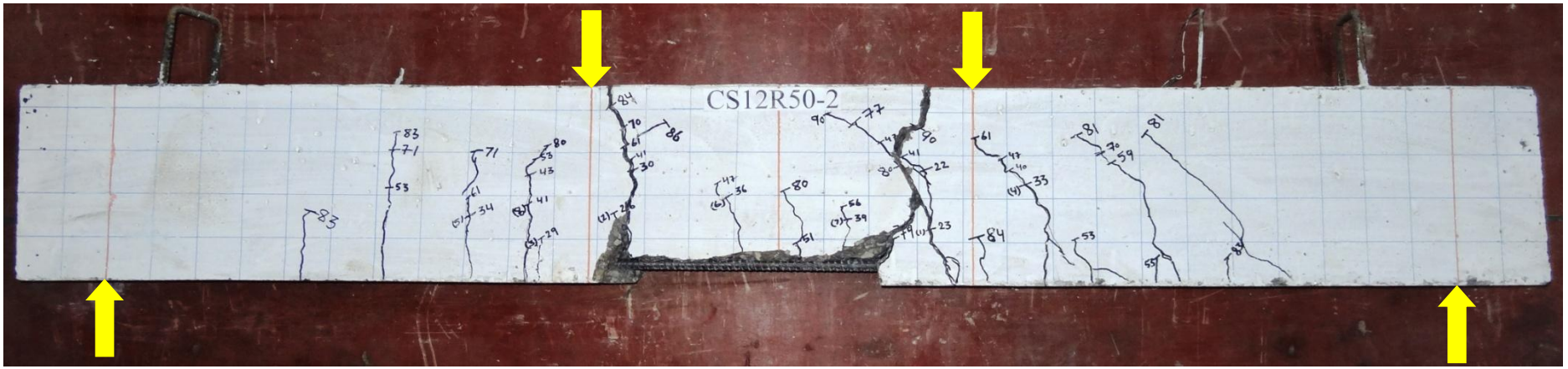

(a)

(b)

Figure 4.49 Typical failure crack patterns for the high-strength splice beam specimen CS12R50-2: (a) elevation (b) soffit

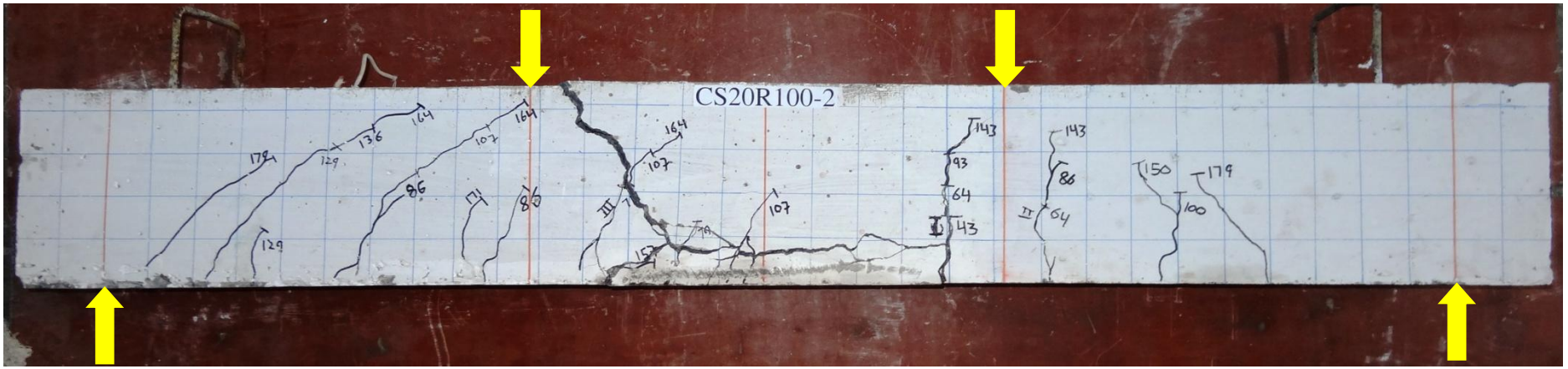

(a)

(b)

Figure 4.50 Typical failure crack patterns for the high-strength splice beam specimen CS20R100-2: (a) elevation (b) soffit

4.3.6 Measured load-deflection behaviour

The measured load mid-span deflection relationships of the splice beam specimens presented in Figures 4.51 – 4.54 show similarities for the NCA and the RCA concretes. For a given bar diameter, the ascending branch of the relationship of the RCA concrete specimens, irrespective of the RCA replacement level, is similar to that of the NCA concrete. In almost all the cases, the ascending branch is linear up to about 25 % of the peak load beyond which there is a change in slope with the ascending branches gradually curving up to peak loads. Beyond peak loads, the failure of all specimens was catastrophic with a sudden and complete loss of load carrying capacity.

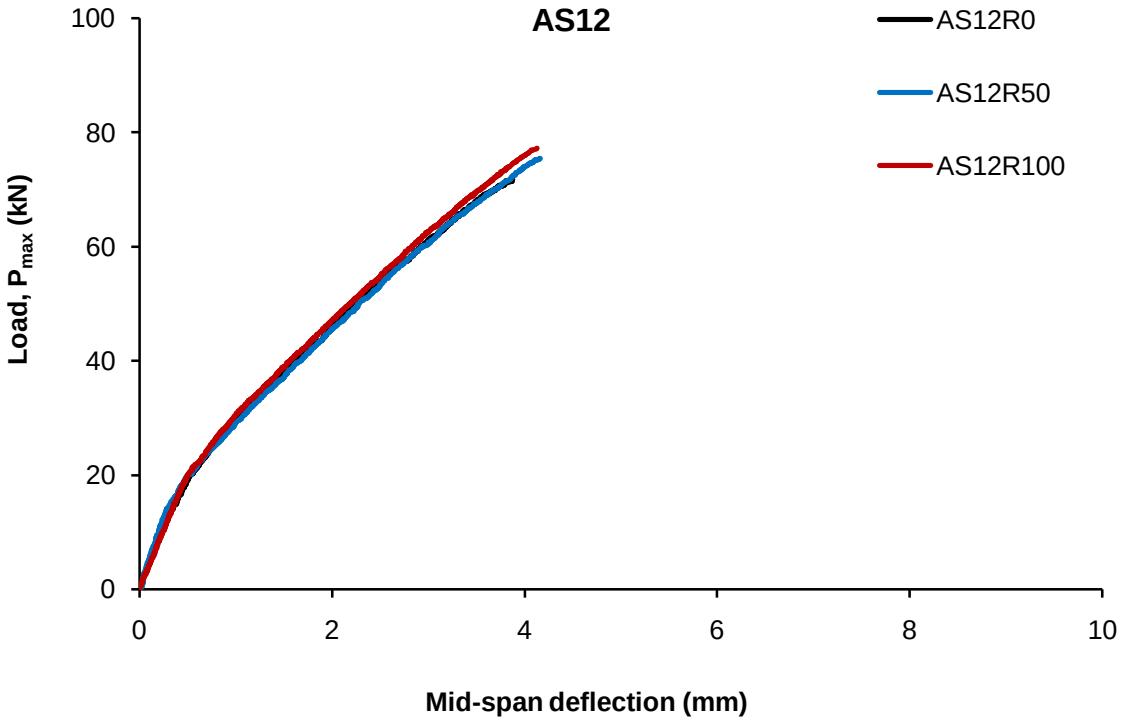

Figure 4.51 Typical load versus mid-span deflection for the normal-strength splice beam specimens with the 12 mm bars

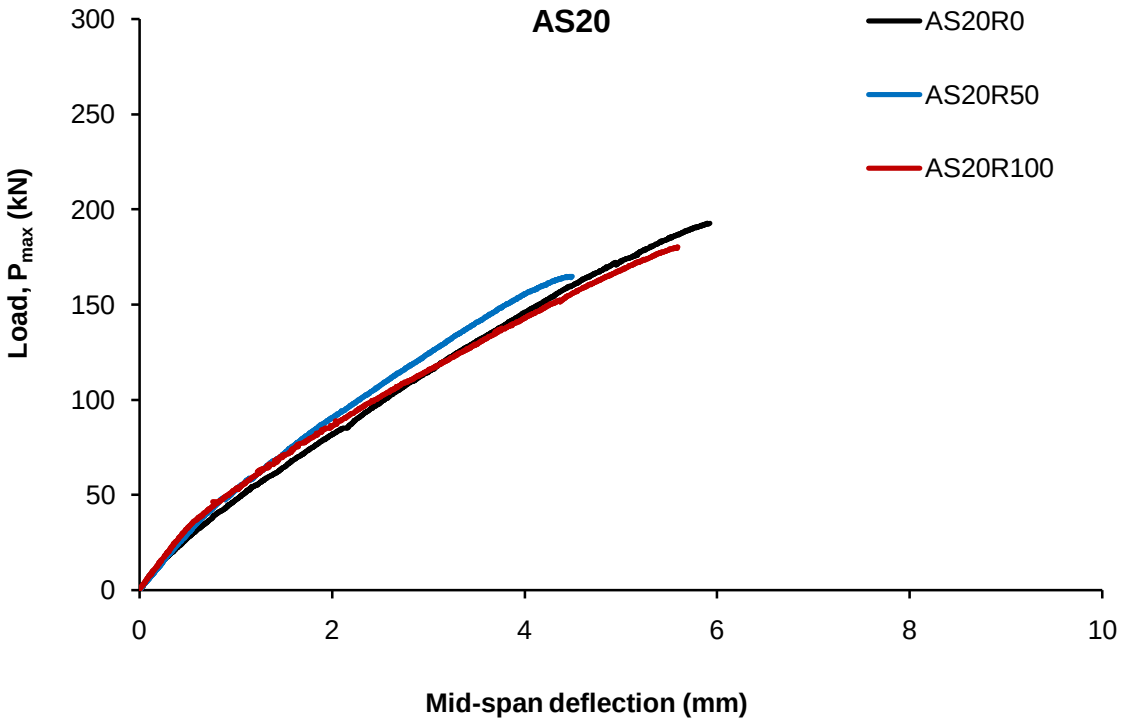

Figure 4.52 Typical load versus mid-span deflection for the normal-strength splice beam specimens with the 20 mm bars

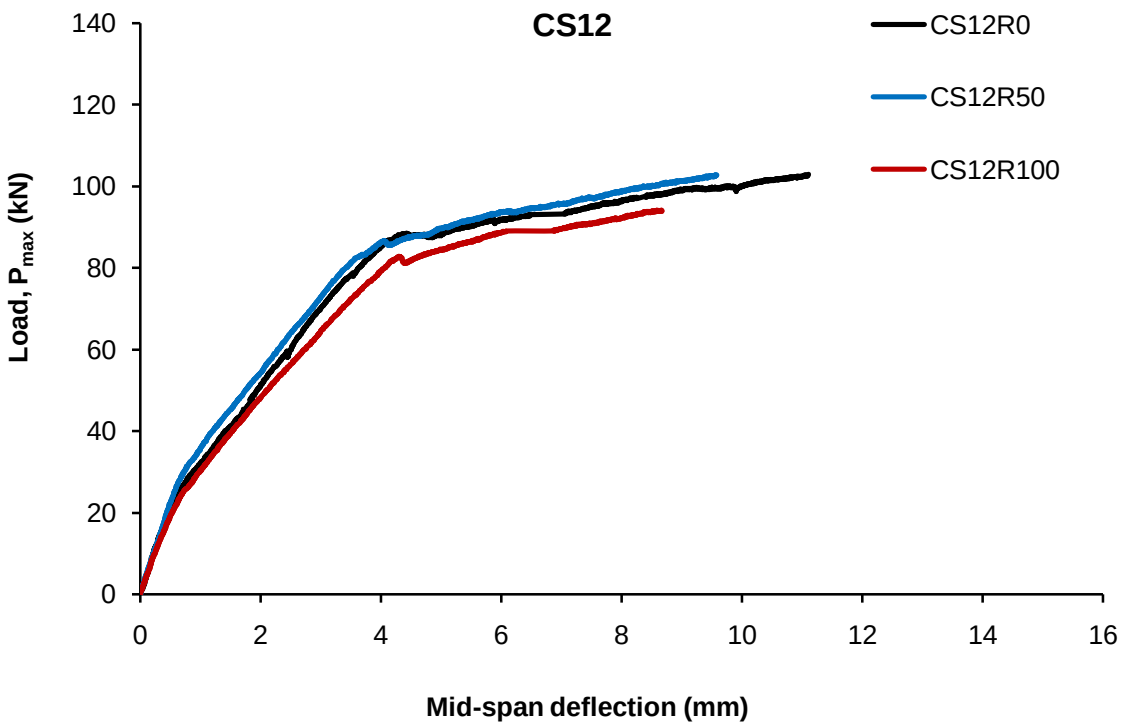

Figure 4.53 Typical load versus mid-span deflection for the high-strength splice beam specimens with the 12 mm bars

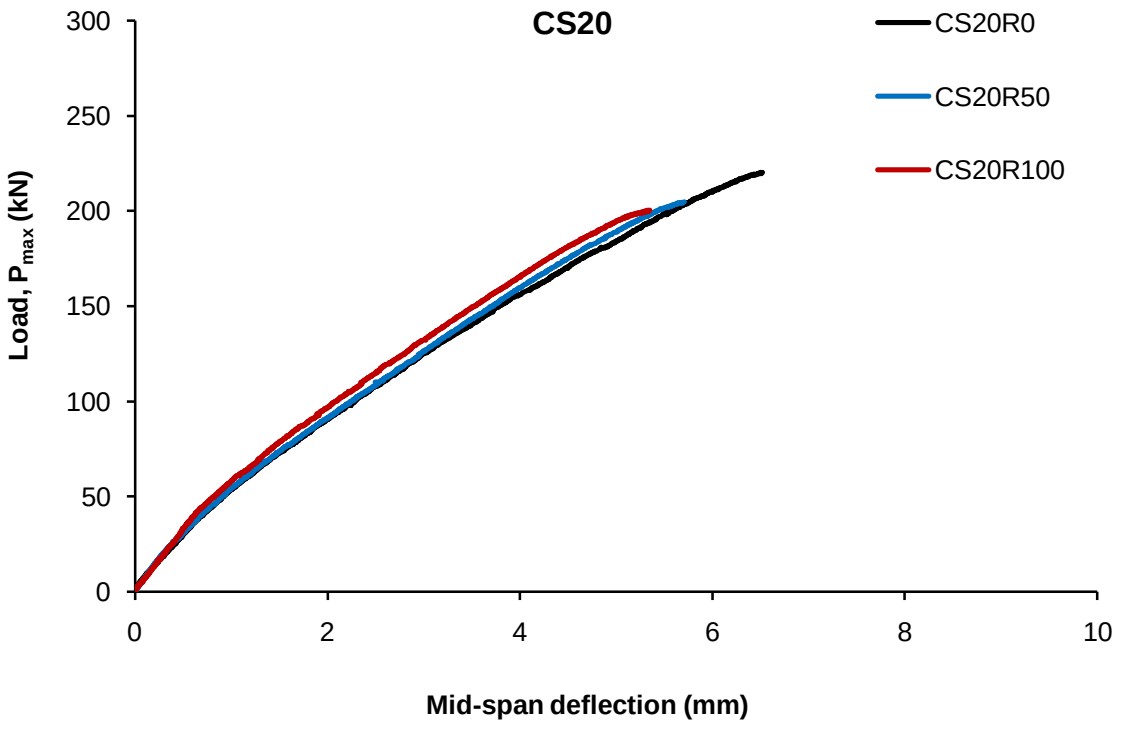

Figure 4.54 Typical load versus mid-span deflection for the high-strength splice beam specimens with the 20 mm bars

Chapter 5

CONCLUSIONS

5.1 INTRODUCTION

The objectives and the scope of this investigation have been outlined in sections 1.4 and 1.5 of Chapter 1. Towards achieving the proposed objectives, a comprehensive experimental programme has been planned and executed within the constraints imposed by available resources. The data generated by the experimentation has been sifted, critically analysed and relevant conclusions drawn. The conclusions from this investigation are presented next.

5.2 CONCLUSIONS

The following conclusions are drawn from this investigation:

1. The 56-day compressive strengths of the three concrete grades taken to be representative of normal-, medium- and high-strength concrete, decreased by approximately 33%, 30% and 27% respectively when the natural coarse aggregates were completely replaced with coarse recycled concrete aggregates in the saturated surface-dry moisture condition.

2. The 56-day splitting tensile strength of the three concrete grades taken to be representative of normal-, medium- and high-strength concrete, increased by approximately 18%, 13% and 19% respectively when the natural coarse aggregates were completely replaced with coarse recycled concrete aggregates (in the saturated surface-dry moisture condition). This is attributed to the relatively better aggregate-cement paste bond in recycled aggregate concrete due to the higher surface roughness of the recycled concrete aggregate particles.

3. A bond strength predictive model for short embedded lengths valid for NCA as well as RCA concrete and which takes into account the parameters f_c', $\frac{c}{d_b}$, $\frac{d_b}{L_d}$, $\frac{h_r}{s_r}$ and r has been proposed. In this model, the effect of concrete properties on bond strength has been represented using the square root of compressive strength, $\sqrt{f_c'}$. This model is valid for cylinder compressive strengths up to 70 MPa. The

proposed model can be used for predicting bond strengths of conventional concrete also by setting the RCA replacement level, *r*, to zero.

4. Across all the three concrete grades, for the relatively smaller sized bars (8 mm, 10 mm and 12 mm) and more so for the 8 mm and the 10 mm bars, the normalised bond strength increased with an increase in the RCA replacement level, with the highest bond strength being obtained for the 100% RCA replacement level. This trend was not as pronounced for the relatively larger sized bars (16 mm, 20 mm and 25 mm). Hence, for the 8 mm, the 10 mm and to some extent for the 12 mm bars, there was no penalty in terms of the normalised bond strength when the natural coarse aggregate particles were replaced with the coarse RCA particles of this investigation. This behaviour is attributed to water entrainment by the saturated RCA particles. The aforesaid trends in bond strength of the RCA concretes have been explained in terms of fracture toughness of concrete estimated using the brittleness index, an analogous parameter from rock mechanics. It has been shown in terms of this parameter that fracture toughness of all the grades of RCA concretes increased with an increase in the RCA replacement level which correlates well with the observed trends in bond strength. Therefore, brittleness index, calculated as the ratio of the concrete compressive and the splitting tensile strength may be a valid indicator of concrete bond strength.

5. For each of the three concrete grades, bond failure modes were similar in the NCA and the RCA concrete specimens across all the rebar sizes under investigation. Pullout failure was observed in the specimens embedded with the 8 mm and the 10 mm diameter bars (these specimens having high confinement) whereas pullout failures induced by through splitting was noted in the specimens embedded with the 12 mm, 16 mm, 20 mm and the 25 mm bars, these specimens being moderately confined. The aforesaid observations indicate that limiting values of concrete cover for a pullout failure are the same for the NCA and the RCA concretes of this investigation. For all specimens, no significant difference in the interfaces of the NCA and the RCA concrete specimens could be observed though the degree of concrete crushing in front of ribs in the case of the 12 mm and the 16 mm diameter bars was noted to be inversely proportional to the concrete grades of this investigation.

6. Compared to the bond strength models for short embedded lengths in the *fib* Model Code 2010 and those proposed by Kim et al. (2012) and Esfahani and

Rangan (1998a), the predictive efficacy of the bond strength model proposed in this investigation was the highest. Next in the order of accuracy was the model in the *fib* Model Code 2010, though this model has been derived for natural aggregate concrete only. This bears testimony to the robustness of the fib bond strength model. It is hoped that as more information on bond behaviour of RCA concrete becomes available in the literature, the robustness of the proposed model can be increased by calibrating it against a larger data base.

7. In all the three concrete grades, the measured bond stress-slip relationships of the deformed steel bars embedded in the RCA concretes were similar to those for the deformed bars embedded in NCA concrete. This indicates that the mechanisms of bond resistance are similar in RCA and in NCA concrete. The following five stages of bond behaviour were identified in the NCA and RCA specimens failing in pullout: (i) micro-slip (ii) internal cracking (iii) pullout (iv) descending and (v) residual. For the case of pullout failure induced by through splitting, the following four stages of bond behaviour were identified in the measured bond stress-slip relationships of the NCA concrete as well as the RCA concrete: (i) micro-slip (ii) internal cracking (iii) descending and (iv) residual.

8. The proposed empirical model for the bond stress-slip relationship associated with pullout failure and with pullout failure induced by through splitting gave predictions which were in good agreement with the measured data. The regression parameters in the proposed models, which have been adapted from a model available in the literature are a function of the slope of the ascending branch of the measured bond stress-slip relationship and the area under the descending branch of this relationship.

9. Failures modes of the NCA and the RCA concrete specimens in the splice beam tests, carried out to investigate bond in long embedded lengths, were similar. By regression analysis of the splice beam test results, a bond strength predictive model for long embedded lengths valid for the NCA as well as the RCA concrete and which takes into account the parameters $f_c^{'}$, $\frac{c}{d_b}$, $\frac{d_b}{L_d}$, $\frac{h_r}{s_r}$ and r has been proposed. In this model, the effect of concrete properties on bond strength has been represented using $\left(f_c^1\right)^{1/4}$ and is valid for cylinder compressive strengths of up to 70 MPa. The use of $\left(f_c^1\right)^{1/4}$ in the bond strength model for long embedded lengths therefore discounts the effect of compressive strength on bond strength

when seen in context of the use of $\left(f_c^1\right)^{1/2}$ in the bond strength model for short embedded lengths. The bond strength model in the ACI 408R-03 (2003), originally developed for NCA concrete, gave reasonably accurate predictions for the bond strengths measured in the splice beam tests.

5.3 SUGGESTIONS FOR FUTURE WORK

1. This investigation is limited to only one-grade of deformed steel bars. Other grades of reinforcement bars should also be investigated.

2. The bond strength database for RCA concrete can be extended by increasing the range of the following parameters: grade of concrete; clear cover; rebar diameter; bonded length/splice length; rib height; rib spacing and replacement level of RCA concrete.

3. For development of recommendations directly applicable to design, more splice beam tests with RCA concrete should be carried out.

4. Bond behaviour of RCA concrete under cyclic loading should also be investigated.

REFERENCES

1. Abbas A, Fathifazl G, Isgor OB, Razaqpur AG, Fournier B and Foo S (2008) Proposed method for determining the residual mortar content of recycled concrete aggregates. *Journal of ASTM International* **5(1)**: Paper ID JAI101087.

2. Abrams DA (1913) *Tests of Bond between Concrete and Steel*. Engineering Experiment Station, University of Illinois, Urbana, Bulletin No. **71.**

3. Abou-Zeid MN, Shenouda MN, McCabe SL, and El-Tawil FA (2005) Reincarnation of concrete. *Concrete International* **27(2)**: 53-59.

4. ACI (American Concrete Institute) (1966) Bond stress - The state of the art. *ACI Journal* **63(11)**: 1161-1190.

5. ACI (American Concrete Institute) (1973) ACI 439-73: Uses and limitations of high strength steel reinforcement $f_y \geq 60$ ksi (413.8 MPa). American Concrete Institute, Farmington Hills, MI, USA.

6. ACI (American Concrete Institute) (1991) ACI 211.1-91(Reapproved 2002): Standard practice for selecting proportions for normal, heavyweight and mass concrete. American Concrete Institute, Farmington Hills, MI, USA.

7. ACI (American Concrete Institute) (1995) ACI 318-95: Building code requirements for structural concrete (ACI 318-95) and commentary (ACI 318R-95). American Concrete Institute, Farmington Hills, MI, USA.

8. ACI (American Concrete Institute) (1999) ACI 544.1R-96: Fiber reinforced concrete (ACI 544.1R-96). American Concrete Institute, Farmington Hills, MI, USA.

9. ACI (American Concrete Institute) (2001a) ACI 408.3-01/408.3R-01: Splice and development length of high relative rib reinforcing bars in tension (408.3-01) and commentary (408.3R-01). American Concrete Institute, Farmington Hills, MI, USA.

10. ACI (American Concrete Institute) (2001b) ACI 555R-01: Removal and reuse of hardened concrete. American Concrete Institute, Farmington Hills, MI, USA.

11. ACI (American Concrete Institute) (2003) ACI 408R-03: Bond and development of straight reinforcing bars in tension. American Concrete Institute, Farmington Hills, MI, USA.

12. ACI (American Concrete Institute) (2008) ACI 211.4R-08: Guide for selecting proportions for high-strength concrete using Portland cement and other cementitious materials. American Concrete Institute, Farmington Hills, MI, USA.

13. ACI (American Concrete Institute) (2008) ACI 318-08: Building code requirements for structural concrete (ACI 318-08) and commentary. American Concrete Institute, Farmington Hills, MI, USA.

14. ACI (American Concrete Institute) (2011) ACI 318-11: Building code requirements for structural concrete (ACI 318-11) and commentary. American Concrete Institute, Farmington Hills, MI, USA.

15. Ahmad SH and Shah SP (1985) Standard properties of high strength concrete and its implications for precast prestressed concrete. *PCI* Journal **30(6)**: 92-119.

16. Ajdukiewicz A and Kliszczewicz A (2002) Influence of recycled aggregates on mechanical properties of HS/HPC. *Cement and Concrete Composites* **24**: 269-279.

17. Arezoumandi M, Drury J and Volz JS (2014) Effect of recycled concrete aggregate replacement level on the fracture behaviour of concrete. *Journal of Frontiers in Construction Engineering* **3(1)**: 1-8.

18. AS (Australian Standard) (2009) AS 3600-2009: Concrete structures. Standards Australia, Sydney, NSW, Australia.

19. ASTM (1991) C234-91: Standard test method for concretes on the basis of the bond developed with reinforcing steel. ASTM International, West Conshohocken, PA, USA. (Withdrawn 2000).

20. ASTM (2005) A944-05: Standard test method for comparing bond strength of steel reinforcing bars to concrete using beam-end specimens. ASTM International, West Conshohocken, PA, USA.

21. ASTM (2011) C496/C496M-11: Standard test method for splitting tensile strength of cylindrical concrete specimens. ASTM International, West Conshohocken, PA, USA.

22. ASTM (2012) C39/C39M-12a: Standard test method for compressive strength of cylindrical concrete specimens. ASTM International, West Conshohocken, PA, USA.

23. ASTM (2013) C494/C494M-13: Standard specification for chemical admixture for concrete. ASTM International, West Conshohocken, PA, USA.

24. Azizinamini A, Stark M, Roller, JJ and Ghosh SK (1993) Bond performance of reinforcing bars embedded in high-strength concrete. *ACI Structural Journal* **90(5)**: 554-561.

25. Bai G, Wu S, and Li X (2010) Investigation of bond-slip behaviour between recycled concrete and steel bars under pullout test. In *Proceedings of the 2nd International conference on waste engineering and management ICWEM 2010,13-15 October 2010,* Shanghai, China (Xiao JZ, Zhang Y, Cheung MS and Reuben PKC (eds.)). RILEM Publications SARL, France, pp. 628-637.

26. Banthia N and Trottier JF (1994) Concrete reinforcement with deformed steel fibers, part I: Bond-slip mechanics *ACI Materials Journal* **91(5)**: 435-446.

27. Banthia N, Yan C and Bindiganavile V (2000) Development and application of high performance hybrid fiber reinforced concrete. In *Proceedings of the RILEM, BEFIB Conference-15,* Sep. 12-15, 2000, Lyon, France.

28. Bindiganavile V and Banthia N (2002) Some studies on the impact response of fiber reinforced concrete. *Journal of the Indian Concrete* Institute **3(3)**:: 23-27.

29. Bindiganavile V and Banthia N (2005) Impact response of fiber-matrix bond in concrete. *Canadian Journal of Civil Engineering* **32(5)**: 924-933.

30. Baruah P and Talukdar S (2007a) A comparative study of compressive, flexural, tensile and shear strength of concrete with fibres of different origins. *The Indian Concrete Journal* **81(7)**: 17-24.

31. Bazant ZP and Sener S (1988) Size effect in pullout tests. *ACI Materials Journal* 85(4): 347-351.

32. Belén GF, Fernando MA, Diego CL and Sindy SP (2011) Stress-strain relationship in axial compression for concrete using recycled saturated coarse aggregate. *Construction and Building Materials* **25**: 2335-2342.

33. BCSJ (1977) Proposed standard for the use of recycled aggregate and recycled aggregate concrete. Building Contractors Society of Japan. Committee on disposal and reuse of construction waste. (English version published in June 1981).

34. BCSJ (1978) Study on recycled aggregate and recycled aggregate concrete, Building Contractors Society of Japan. Committee on disposal and reuse of

concrete construction waste. *Summary in Concrete Journal, Japan*, 16(7): 18-31 (in Japanese).

35. Bhaskar S, Gettu R, Bharatkumar BH and Neelamegam M (2008) Bond behaviour of rebars in flyash based high performance concrete. In *Proceedings of the sixth structural engineering convention, 2008,* Chennai, India (Iyer NR, Prasad AM, Knight GMS and Ramanjaneyulu K (eds.)). CBA Publications, Chennai, India, pp. 1189-1196.

36. Bhaskar S, Gettu R, Bharatkumar BH and Neelamegam M (2012) Strength, bond and durability related properties of concretes with mineral admixtures. *The Indian Concrete Journal* **86(2)**: 9-16.

37. Bindra S, Sana BK and Talukdar S (2003) Behaviour of concrete made using recycled cement mortar as fine aggregate. In *Proceedings of the national Conference on Modern Trends on Cement Concrete and Bituminous Road*, Dec. 18-20, 2003, Visakapattanam, India.

38. Bindra S, Sana BK and Talukdar S (2007b) Investigation of the quality of concrete made using recycled cement mortar as fine aggregate. *Indian Concrete Institute Journal* **8(3)**: 19-23.

39. BIS (Bureau of Indian Standards) (1959a) IS 1199:1959 (Reaffirmed 2004). Methods of sampling and analysis of concrete. Bureau of Indian Standards, New Delhi, India.

40. BIS (Bureau of Indian Standards) (1959b) IS 516:1959 (Reaffirmed 2004). Methods of tests for strength of concrete. Bureau of Indian Standards, New Delhi, India.

41. BIS (Bureau of Indian Standards) (1963a) IS 2386(Part IV):1963 (Reaffirmed 2007). Methods of test for aggregates for concrete – Part IV Mechanical properties. Bureau of Indian Standards, New Delhi, India.

42. BIS (Bureau of Indian Standards) (1963b) IS 2386(Part I):1963 (Reaffirmed 2007). Methods of test for aggregates for concrete – Part I Particle size and shape. Bureau of Indian Standards, New Delhi, India.

43. BIS (Bureau of Indian Standards) (1963c) IS 2386(Part III):1963 (Reaffirmed 2002). Methods of test for aggregates for concrete – Part III Specific gravity, density, voids, absorption and bulking. Bureau of Indian Standards, New Delhi, India.

44. BIS (Bureau of Indian Standards) (1967b) IS 2770(Part I):1967 (Reaffirmed 2002). Methods of testing bond in reinforced concrete – Part I Pullout test. Bureau of Indian Standards, New Delhi, India.

45. BIS (Bureau of Indian Standards) (1970) IS 383:1970 (Reaffirmed 2002). Specification for coarse and fine aggregates from natural sources for concrete. Bureau of Indian Standards, New Delhi, India.

46. BIS (Bureau of Indian Standards) (1985a) IS 4032:1985 (Reaffirmed 2005). Methods of chemical analysis of hydraulic cement. Bureau of Indian Standards, New Delhi, India.

47. BIS (Bureau of Indian Standards) (1985b) IS 1599:1985 (Reaffirmed 2006). Method for bend test. Bureau of Indian Standards, New Delhi, India.

48. BIS (Bureau of Indian Standards) (1987) IS 3025(Parts 1 - 36):1987. Methods of sampling and test (physical and chemical) for water and wastewater. Bureau of Indian Standards, New Delhi, India.

49. BIS (Bureau of Indian Standards) (1988a) IS 4031(Part 3):1988 (Reaffirmed 2005). Methods of physical tests for hydraulic cement – Part 3 Determination of soundness. Bureau of Indian Standards, New Delhi, India.

50. BIS (Bureau of Indian Standards) (1988b) IS 4031(Part 4):1988 (Reaffirmed 2005). Methods of physical tests for hydraulic cement – Part 4 Determination of consistence of standard cement paste. Bureau of Indian Standards, New Delhi, India.

51. BIS (Bureau of Indian Standards) (1988c) IS 4031(Part 5):1988 (Reaffirmed 2005). Methods of physical tests for hydraulic cement – Part 5 Determination of initial and final setting times. Bureau of Indian Standards, New Delhi, India.

52. BIS (Bureau of Indian Standards) (1988d) IS 4031(Part 6):1988 (Reaffirmed 2005). Methods of physical tests for hydraulic cement – Part 6 Determination of compressive strength of hydraulic cement other than masonry cement. Bureau of Indian Standards, New Delhi, India.

53. BIS (Bureau of Indian Standards) (1989) IS 8112:1989 (Reaffirmed 2005). 43 Grade ordinary Portland cement – Specification. Bureau of Indian Standards, New Delhi, India.

54. BIS (Bureau of Indian Standards) (1999a) IS 4031(Part 2):1999 (Reaffirmed 2004). Methods of physical tests for hydraulic cement – Part 2 Determination of fineness by Blaine air permeability method. Bureau of Indian Standards, New Delhi, India.

55. BIS (Bureau of Indian Standards) (1999b) IS 9103:1999 (Reaffirmed 2004). Concrete admixtures – Specification. Bureau of Indian Standards, New Delhi, India.

56. BIS (Bureau of Indian Standards) (1999c) IS 5816:1999 (Reaffirmed 2004). Splitting tensile strength of concrete – Method of test. Bureau of Indian Standards, New Delhi, India.

57. BIS (Bureau of Indian Standards) (2000) IS 456:2000 (Reaffirmed 2005). Plain and reinforced concrete – Code of practice. Bureau of Indian Standards, New Delhi, India.

58. BIS (Bureau of Indian Standards) (2005) IS 1608:2005/ISO 6892:1998. Metallic materials – Tensile testing at ambient temperature. Bureau of Indian Standards, New Delhi, India.

59. BIS (Bureau of Indian Standards) (2008) IS 1786:2008. High strength deformed steel bars and wires for concrete reinforcement – Specification. Bureau of Indian Standards, New Delhi, India.

60. Bordelon A, Cervantes V and Roesler JR (2009) Fracture properties of concrete containing recycled concrete aggregates. *Magazine of Concrete Research* **61(9)**: 665-670.

61. Brettmann BB, Darwin D and Donahey RC (1984) *Effect of Superplasticizers on Concrete-Steel Bond Strength*. University of Kansas Center for Research, Lawrence, Kansas, SL Report No. **84-1**.

62. Brettmann BB, Darwin D and Donahey RC (1986) Bond of reinforcement to superplasticized concrete. *ACI Journal* **83(1)**: 98-107.

63. Brown CJ, Darwin D and McCabe SL (1993) *Finite Element Fracture Analysis of Steel-Concrete Bond*. University of Kansas Center for Research, Lawrence, Kansas, SM Report No. **36**.

64. BSI (1990) BS EN 812-110:1990. Testing aggregates – Methods for determination of aggregate crushing value (ACV). British Standards Institution, London, UK.

65. BSI (2002) BS 8500-1:2002. Concrete – Complementary British standard to BS EN 206-1. Part 2: Specification for constituent materials and concrete. British Standards Institution, London, UK.

66. BSI (2004) BS EN 1992-1-1:2004. Eurocode 2: Design of concrete structures – Part1-1: General rules and rules for buildings. British Standards Institution, London, UK.

67. Buck AD (1977) Recycled concrete as a source of aggregate. *ACI Journal* **74(5)**: 212-219.

68. Butler L, West JS and Tighe SL (2011) The effect of recycled concrete aggregate properties on the bond strength between RCA concrete and steel reinforcement. *Cement and Concrete Research* **41**: 1037-1049.

69. Butler L (2012) *Evaluation of recycled concrete aggregate performance in structural concrete.* PhD Thesis. Civil and Environmental Engineering Department, University of Waterloo, Waterloo, Ontario, Canada.

70. Butler L West J and Tighe S (2014) Bond of reinforcement in concrete incorporating recycled concrete aggregates. *Journal of Structural Engineering, ASCE*, Doi: 10.1061/(ASCE)ST.1943-541X.0000928.

71. Casuccio M, Torrijos MC, Giaccio G and Zerbino R (2008) Failure mechanism of recycled aggregate concrete. *Construction and Building Materials* **22**: 1500-1506.

72. CEB-FIP (1990) *CEB-FIP Model code 1990*. Thomas Telford house, London, UK.

73. Chamberlin SJ (1958) Spacing of spliced bars in beams. *ACI Journal, Proceedings* **54(8)**: 689-698.

74. Chen HJ, Yen T and Chen KH (2003) Use of building rubbles as recycled aggregates. *Cement and Concrete Research* **33**: 125-132.

75. Chidiac SE and Panesar DK (2008) Evolution of mechanical properties of concrete containing ground granulated blast furnace slag and effects on the scaling resistance test at 28 days. *Cement and Concrete Composites* 30: 63-71.

76. Chinese Standard GB 50152-92 (1992) Standard methods for testing concrete structures. Ministry of Construction, P.R China.

77. Chinn J, Ferguson PM and Thompson JN (1955) Lapped splices in reinforced concrete beams. *ACI Journal, Proceedings* **52(2)**: 201-213.

78. Choi HB and Kang KI (2008) Bond behaviour of deformed bars embedded in RAC. *Magazine of Concrete Research* **60(6)**: 399-410.

79. Chugh R and Menon D (2005) Design aids for estimation of shear in seismic design of RC beams. *The Indian Concrete Journal* **79(3)**: 22-28.

80. Clark AP (1946) Comparative bond efficiency of deformed concrete reinforcing bars. *ACI Journal* **43(4)**: 381-400.

81. Clark AP (1950) Bond of concrete reinforcing bars. *ACI Journal* **46(3)**: 161-184.

82. Collier ST (1947) Bond characteristics of commercial and prepared reinforcing bars. *ACI Journal* **43(10)**: 1125-1133.

83. Corinaldesi V (2010) Mechanical and elastic behaviour of concrete made of recycled concrete coarse aggregates. *Construction and Building Materials* **24(9)**: 1616-1620.

84. Corinaldesi V and Moriconi G (2009) Influence of mineral additions on the performance of 100 % recycled aggregate concrete. *Construction and Building Materials* **23**: 2869-2876.

85. CSA (Canadian Standards Association) (2002) CAN/CSA-S806-02: Design and construction of building components with fibre-reinforced polymers. Canadian Standards Association, Mississauga, Ontario, Canada.

86. CSA (Canadian Standards Association) (2004) CSA A23.3-04: Design of concrete structures. Canadian Standards Association, Mississauga, Ontario, Canada.

87. CSA (Canadian Standards Association) (2009) CSA A23.1-09: Concrete materials and methods of concrete construction. Canadian Standards Association, Mississauga, Ontario, Canada.

88. CSE (Centre for Science and Environment) (2014) *Construction and Demolition Waste.* Centre for Science and Environment, New Delhi, India. See http://www.cseindia.org/userfiles/Construction-and%20--demolition-waste.pdf (accessed29/01/2015).

89. CUR (Commissie voor Uitvoering van Research Ingesteld door de Betonvereniging) (1963) *Onderzoek naar de samenwerking van geprofileered staal met beton*, The Netherlands (Translation No. 112, (1964) *An Investigation of the Bond of Deformed Steel Bars with Concrete*. Cement and Concrete Association, London), Report No. **23.**

90. Darwin D (1987) Effects of Construction Practice on Concrete-Steel Bond. In *Proceedings of the Lewis H. Tuthill International Symposium on Concrete and Concrete Construction*, SP-104, (Halvorsen GT (ed.)). American Concrete Institute, Farmington Hills, MI, USA, pp. 27-56.

91. Darwin D, McCabe SL, Idun EK and Schoenekase SP (1992) Development length criteria: bars not confined by transverse reinforcement. *ACI Structural Journal* **89(6)**: 709-720.

92. Darwin D and Graham EK (1993a) Effect of deformation height and spacing on bond strength of reinforcing bars. *ACI Structural Journal* **90(6)**: 646-657.

93. Darwin D and Graham EK (1993b) *Effect of Deformation Height and Spacing on Bond Strength of Reinforcing Bars*. University of Kansas Center for Research, Lawrence, Kansas, SM Report No. **93-1**.

94. Darwin D, McCabe SL, Brown CJ and Tholen ML (1994) Fracture analysis of steel-concrete bond. In *Fracture and Damage in Quasibrittle Strcutures: Experiment, Modelling and Computer Analysis* (Bažant ZP, Bittnar Z, Jirasek M and Mazars J (eds)). E&FN Spon, London, pp. 549-556.

95. Darwin D, Tholen ML, Idun EK and Zuo J (1996) Splice strength of high relative rib area reinforcing bars. *ACI Structural Journal* **93(1)**: 95-107.

96. Deng XH (2005) Study on effect of compressive strength of recycled aggregate concrete with water cement ratio (in Chinese). *Chinese Concrete Journal* **2**: 46-48.

97. Dhir RK, Limbachiya MC and Leelawat T (1999) Suitability of recycled concrete aggregate for use in BS 5328 Designated Mixes. *Structures and Buildings* **134(3)**: 257-274.

98. Dhir RK and Paine KA (2010) Value added sustainable use of recycled and secondary aggregates in concrete. *The Indian Concrete Journal* **84(3)**: 7-26.

99. DIN (German Institute for Standardisation) (2002) DIN-4226-100:2002. Aggregates for mortar and concrete - Part 100: Recycled aggregates. (Deutsches Institut für Normung). German Institute for Standardization, Berlin, Germany.

100. Donahey RC and Darwin D (1983) *Effects of Construction Procedures on Bond in Bridge Decks*. University of Kansas Center for Research, Lawrence, Kansas, SM Report No. **7**.

101. Donahey RC and Darwin D (1985) Bond of top-cast bars in bridge decks. *ACI Journal* **82(1)**: 57-66.

102. Dosho Y (2007) Development of a sustainable concrete waste recycling system - application of recycled aggregate concrete produced by aggregate replacing method. *Journal of Advanced Concrete Technology* **5(1)**: 27-42.

103. Eligehausen R (1979) *Bond in Tensile Lapped Splices of Ribbed Bars with Straight Anchorages.* German Institute for Reinforced Concrete, Berlin, Publication 301 (in German).

104. Eligehausen R, Popov EP and Bertero VV (1983) *Local bond stress-slip relationships of deformed bars under generalized excitations*. Earthquake Engineering Research Center, University of California at Berkeley, California, Report No. UCB/EERC-82/23.

105. EPA (Environmental Protection Agency) (1998) *Characterization of Building-Related Construction and Demolition Debris in the United States.* The U.S. Environmental Protection Agency, Municipal and Industrial Solid Waste Division, Office of Solid Waste, Kansas, Report No. **EPA530-R-98-010**.

106. Esfahani MR and Rangan VB (1996) *Studies on Bond Between Concrete and Reinforcing Bars*. School of Civil Engineering, Curtin University of Technology, Perth, Western Australia, Research Report Nos. **1-96**.

107. Esfahani MR and Vijaya Rangan BV (1998a) Local bond strength of reinforcing bars in normal strength and high-strength concrete (HSC). *ACI Structural Journal* **95(2)**: 96-106.

108. Esfahani MR and Vijaya Rangan BV (1998b) Bond between normal strength and high-strength concrete (HSC) and reinforcing bars in splices in beams. *ACI Structural Journal* **95(3)**: 272-280.

109. Etxeberria M, Vazquez E, Mari A and Barra M (2007) Influence of amount of recycled coarse aggregates and production process on properties of recycled aggregate concrete. *Cement and Concrete Research* **37**: 735-742.

110. Fathifazl G, Abbas A, Razaqpur AG, Isgor OB and Foo S (2009) New mixture proportioning method for concrete made with coarse recycled concrete aggregate. *Journal of Materials in Civil Engineering* **21**: 601-611.

111. Fathifazl G, Razaqpur G, Isgor OB, Abbas A, Fournier B and Foo S (2012) Bond performance of deformed steel bars in concrete produced with coarse recycled concrete aggregate. *Canadian Journal of Civil Engineering* **39(2)**: 128-139.

112. Fergus JS (1981) Laboratory investigation and mix proportions for utilizing recycled Portland cement concrete as aggregate. In *Proceedings of the national seminar on PCC pavement recycling and rehabilitation, 27-30 September 1981.* St. Louis, Missouri, USA, Federal Highway Administration report6 FHWA-TS-82-208.

113. Ferguson PM and Thompson JN (1962) Development length for large high strength reinforcing bars in bond. *ACI Journal* **59(7)**: 887-922.

114. Ferguson PM and Thompson JN (1965) Development length for large high strength reinforcing bars. ACI Journal **62(1)**: 71-94.

115. *fib* (2000) *Bond of reinforcement in concrete*. International Federation for Structural Concrete (*fib*), Lausanne, Switzerland.

116. *fib* (2013) *fib* Model Code for Concrete Structures 2010. Ernst & Sohn, Berlin, Germany.

117. Freedonia Group (2015) *World Construction Aggregates*. See http://www.freedoniagroup.com/industry-study/2838/world-construction-aggregates.html (accessed 29/01/2015).

118. Frondistou-Yannas (1977) Waste concrete as aggregate for new concrete. *ACI Journal* **74(8)**: 373-376.

119. Gambarova PG, Rosati GP and Zasso B (1989a) Steel-to-concrete bond after concrete splitting: test results. *Materials and Structures* **22(1)**: 35-47.

120. Gambarova PG, Rosati GP and Zasso B (1989b) Steel-to-concrete bond after concrete splitting: constitutive laws and interface deterioration. *Materials and Structures* **22(5)**: 347-356.

121. Gambarova PG and Rosati GP (1996) Bond and splitting in reinforced concrete: test results on bar pullout. *Materials and Structures* **29(5)**: 267-276.

122. Gerardu JJA and Hendriks CF (1985) Recycling of road pavement materials in the Netherlands. *rijkswaterstaat communications* no. **38**, the Hague.

123. Gettu R, Bazant ZP and Martha EK (1990) Brittleness of high strength concrete. In *Proceedings of the First Materials Engineering Congress*, *ASCE,* 1990, New York, pp 976-985.

124. Girija K and Menon D (2011) Improved design guidelines for slender rectangular RC beams. In *Proceedings of the fib Symposium PRAGUE 2011 on Concrete Engineering for Excellence and Efficiency, Prague,* 8th-10th June, 2011, Vol. 1, pp 175-178.

125. Gjorv OE, Monteiro PJM and Mehta PK (1990) Effect of condensed silica fume on the steel-concrete bond. *ACI Materials Journal* **87(6)**: 573-580.

126. Gokce A, Nagataki S, Saeki T and Hisada M (2004) Freezing and thawing resistance of air-entrained concrete incorporating recycled coarse aggregate: The role of air content in demolished concrete. *Cement and Concrete Research* **34**: 799-806.

127. Gong QM and Zhao J (2007) Influence of rock brittleness on TBM penetration rate in Singapore granite. *Tunnelling and Underground Space Technology* **22**: 317-324.

128. Guo Z (1997) Strength and deformation of concrete – Experimental foundation and consecutive relationship, Beijing press –Tsinghua University (In Chinese).

129. Hamad BS, Ali AYH and Harajli MH (2005) Effect of fiber-reinforced polymer confinement on bond strength of reinforcement in beam anchorage specimens. *Journal of Composites for Construction* **9(1)**: 44-51.

130. Hamad BS and Itani MS (1998) Bond strength of reinforcement in high-performance concrete: The role of silica fume, casting position and superplasticizer dosage. *ACI Materials Journal* **95(5)**: 499-511.

131. Hamad BS and Jirsa JO (1993) Strength of epoxy-coated reinforcing bar splices confined with transverse reinforcement. *ACI Structural Journal* **90(1)**: 77-88.

132. Hansen TC and Narud H (1983) Strength of recycled concrete made from crushed concrete coarse aggregate. *Concrete International – Design and Construction* **5(1)**: 79-83.

133. Hansen TC (1986) Recycled aggregates and recycled aggregate concrete second state-of-the-art report developments 1945-1985. *Materials and Structures* **19(3)**: 201-246.

134. Harajli MH (1994) Development/splice strength of reinforcing bars embedded in plain and fiber-reinforced concrete. *ACI Structural Journal* **91(5)**: 511-520.

135. Harajli M and Abouniaj (2010) Bond performance of GFRP bars in tension: Experimental and assessment of ACI 440 guidelines. *Journal of Composites for Construction* **14(6)**: 659-668.

136. Harajli M and Al-Hajj J (2002) Bond-slip response of reinforcing bars embedded in high-strength concrete. In *Proceedings of International Symposium: Bond in concrete-From Research to Standards*. Budapest University of Technology and Economics, Budapest, Hungary.

137. Harajli MH and Salloukh KA (1997) Effect of fibers on development/splice strength of reinforcing bars in tension. *ACI Materials Journal* **94(4)**: 317-324.

138. Harajli M, Hamad B and Karam (2002) Bond-slip response of reinforcing bars embedded in plain and fiber concrete. *Journal of Materials in Civil Engineering* **14(6)**: 503-511.

139. Harajli MH, Hout M and Jalkh W (1995) Local bond stress-slip behaviour of reinforcing bars embedded in plain and fiber concrete. *ACI Materials Journal* **92(4)**: 343-354.

140. Hasaba S, Kawamura M, Toriik K and Takemoto (1981) Drying shrinkage and durability of the concrete made of recycled concrete aggregate. *Transactions of the Japan Concrete Institute* **3**: 55-60 (additional information obtained from background report in Japanese).

141. Hassan TK, Lucier GW and Rizakalla (2012) Splice strength of large diameter, high strength steel reinforcing bars. *Construction and Building Materials* **26**: 216-225.

142. Hognestad E (1951) A Study of Combined Bending and Axial Load in Reinforced Concrete Members. Engineering Experiment Station, University of Illinois, Urbana, Bulletin No. 399.

143. Hu W, Song C and Zou CY (2009) Experimental research on the mechanical properties of recycled concrete (in Chinese). *Journal of Harbin Institute of Technology* **14**: 33-36.

144. Hwang SJ, Lee YY and Lee CS (1994) Effect of silica fume on the splice strength of deformed bars of high-performance concrete. *ACI Structural Journal* 91(3): 294-302.

145. Jeanty PR, Mitchell D and Mirza MS (1988) Investigation of 'top bar' effects in beams. *ACI Journal* **85(3)**: 251-257.

146. Jirsa JO and Breen JE (1981) *Influence of Casting Position and Shear on Development and Splice Length- Design Recommendation.* Center for Transportation Research, The University of Texas at Austin, Texas, Research Report No. **242-3F**.

147. JIS (Japanese Industrial Standard) (2011) JIS A 5021:2011. Recycled aggregate for concrete-class H.

148. JIS (Japanese Industrial Standard) (2012) JIS A 5022:2012. Recycled concrete using recycled aggregate class M.

149. JIS (Japanese Industrial Standard) (2012) JIS A 5023:2012. Recycled concrete using recycled aggregate class L.

150. Johnston DW and Zia P (1982) *Bond Characteristics of Epoxy Coated Reinforcing Bars.* Federal Highway Administration, Washington, D.C., Report No. **FHWANC-82-002**.

151. Juan MS and Gutierrez PA (2009) Study on the influence of attached mortar content on the properties of recycled concrete aggregate. *Construction and Building Materials* **23**: 872-877.

152. Kaar PH, Hanson NW and Capell HT (1978) Stress-strain characteristics of high-strength concrete. In *Proceedings of the Douglas McHenry International Symposium on Concrete and Concrete Structures, SP-55, (Bresler B (ed.))*. American Concrete Institute, Farmington Hills, MI, USA, pp. 161-185.

153. Kahraman S and Altindag R (2004) A brittleness index to estimate fracture toughness. *International Journal of Rock Mechanics & Mining* **41**: 343-348.

154. Katz A (2003) Properties of concrete made with recycled aggregate from partially hydrated old concrete. *Cement and concrete research* **33**: 703-711.

155. Kawamura M, Toriik K, Takemoto K and Hasaba S (1983) Properties of recycling concrete made with aggregate obtained from demolished pavement. *Journal of the*

Society of Material Science, Japan **32(353)** (in Japanese; abstract, tables and figures in English).

156. Kim Y, Sim J and Park C (2012) Mechanical properties of recycled aggregate concrete with deformed steel re-bar. *Journal of Marine Science and Technology* **20(3)**: 274-280.

157. Kim SW and Yun HD (2013) Influence of recycled coarse aggregates on the bond behaviour of deformed bars in concrete. *Engineering Structures* **48**: 133-143.

158. Knaack AM and Kurama YC (2013) Design of concrete mixtures with recycled concrete aggregates. *ACI Material Journal* **110(5)**: 483-493.

159. Kosmatka SH, Kerkhoff B, Panarese WC, MacLeod NF and McGrath RJ (2002) *Design and control of concrete mixtures*, 7th edn. Cement Association of Canada, Ottawa, Ontario, Canada.

160. Kozul R and Darwin D (1997) *Effects of Aggregate Type, Size, and Content on Concrete Strength and Fracture Energy.* University of Kansas Center for Research, Lawrence, Kansas, SM Report No. **43**.

161. KSA (Korean Standards Association) (2010) (KS F 2441:2010) Standard test method for comparing concrete on the basis of the bond developed with reinforcing steel. Korean Standards Association, Korea.

162. KSA (Korean Standards Association) (2011) (KS F 2573:2011) Recycled aggregate for concrete. Korean Standards Association, Korea.

163. Larnach WJ (1952) Changes in bond strength caused by revibration of concrete and the vibration of reinforcement. *Magazine of Concrete Research* **10**: 17-21.

164. Li X (2007) Study on mechanical properties of recycled aggregate concrete (I)-behaviour under uniaxial compression (in Chinese). *Chinese Journal of Building Materials* **10**: 598-603.

165. Li X (2008) Recycling and reuse of waste concrete in China: Part I. Material behaviour of recycled aggregate concrete. Resources, Conservation and Recycling 53(1-2): 36-44.

166. Limbachiya MC (2010) Recycled aggregates: Production, properties and value-added sustainable applications. *Journal of Wuhan University of Technology – Materials Science Edition* **21(6)**: 1011-1016.

167. Lin YH, Tyan YY, Chang TP and Chang CY (2004) An assessment of optimal mixture for concrete made with recycled concrete aggregates. *Cement and Concrete* Research **34**: 1373-1380.

168. Liu Q, Xiao J and Sun Z (2011) Experimental study on the failure mechanism of recycled concrete. *Cement and Concrete Research* **41**: 1050-1057.

169. Luke JJ, Hamad BS, Jirsa JO and Breen JE (1981) *The Influence of Casting Position on Development and Splice Length of Reinforcing Bars*. Center for Transportation Research, Bureau of Engineering Research, University of Texas at Austin, Texas, Research Report No. **242-1**.

170. Lutz LA, Gergely P and Winter G (1966) *The Mechanics of Bond and Slip of Deformed Reinforcing Bars in Concrete*. Department of Structural Engineering, Cornell University, Ithaca, New York, Report No. **324**, pp. 711-721.

171. Lutz LA and Gergely P (1967) Mechanics of bond and slip of deformed bars in concrete. *ACI Journal* **64(11)**: 711-721.

172. MacGregor, JG (1997) *Reinforced concrete: Mechanics and design*, 3rd edn. Prentice-Hall, New Jersey, USA, pp. 290-301.

173. Malhotra VM (1976) *Use of Recycled Concrete as a New Aggregate*, Canada Centre for Mineral and Energy Technology, Ottawa, Canada, Report **76-18**.

174. Menzel CA (1952) *Effect of Settlement of Concrete on Results of Pullout Tests*. Research and Development Laboratories of the Portland Cement Association, Research Department Bulletin No. **41.**

175. Menzel CA and Woods WM (1952) *An Investigation of Bond, Anchorage and Related Factors in Reinforced Concrete Beams.* Portland Cement Association, Research Department Bulletin No. **42**.

176. Metelli G and Plizzari G (2014) Influence of the relative rib area on bond behaviour. *Magazine of Concrete Research* **66(6)**: 277-294.

177. Mohammadi Y, Singh SP and Kaushik SK (2008) Properties of steel fibrous concrete containing mixed fibres in fresh and hardened state. *Construction and Building Materials* **22**: 956-965.

178. Morohashi N, Sakurada T and Yanagibashi K (2007) Bond splitting strength of high-quality recycled coarse aggregate concrete beams. *Journal of Asian Architecture and Building Engineering*: 331-337.

179. Movassaghi R (2006) *Durability of reinforced concrete incorporating recycled concrete as aggregate*. MASc Thesis. University of Waterloo, Waterloo, Ontario, Canada.

180. Mukai T, Kikuchi M and Koizumi H (1978) *Fundamental Study on Bond Properties Between Recycled Aggregate Concrete and Steel Rebar*. Cement Association of Japan: 32nd review.

181. Nagataki S, Gokce A, Saeki T and Hisada M (2004) Assessment of recycling process induced damage sensitivity of recycled concrete aggregates. *Cement and Concrete Research* **34**: 965-971.

182. Nagataki S, Saeki T and Iida K (1998) Recycled concrete as aggregate. In *Proceedings of the CANMET/ACI International Symposium on Sustainable Development of the Cement and Concrete Industry.* Ottawa, Canada, pp 131-146.

183. Neville (1997) *Properties of concrete*, 4th edn. Prentice hall, Essex, England.

184. Nielsen CV and Glavind M (2007) Danish experience with a decade of green concrete. *Journal of Advanced Concrete Technology* **5(1)**: 3-12.

185. Nishibayashi S, Yamura K and Hayashi A (1984) Elastic-plastic properties and durability of concrete made from recycled concrete aggregate prepared by crushing concrete. *Transactions of the Japan Concrete Institute* **6**: 127-132.

186. Nixon PJ (1978) Recycled concrete as an aggregate for concrete - a review. *Materials and Structures* **11(65)**: 371-378.

187. Obla K, Kim H and Lobo C (2007) *Crushed Returned Concrete as Aggregates for New Concrete*. RMC Research and Education Foundation, Project **05-13**.

188. Obla KH and Kim H (2009) Sustainable concrete through reuse of crushed returned concrete. *Transportation research record*. *Journal of the Transportation Research Board* **2113**: 114-121.

189. Oliveria M, Barra de, and Vazquez E(1996) The influence of retained moisture in aggregates from recycling on the properties of new hardened concrete. *Waste Management* **16**: 113-117.

190. Olsen NH (1990a) Strength of Lapped Splices in High-Strength Concrete. High-Strength Concrete. In *Proceedings of the Second International Symposium,* SP-121, (Hester WT (ed.)). American Concrete Institute, Farmington Hills, MI, USA, pp. 179-193.

191. Olsen NH (1990b) *Strength of Lapped Splices in High-Strength Concrete.* Department of Structural Engineering, Technical University of Denmark, Report Series R, No. **234**.

192. Ong KCG and Ravindrarajah RS (1987) Mechanical properties and fracture energy of recycled aggregate concretes. In *Proceedings of the Sem/Rilem International Conference on Fracture of Concrete and Rock*, June 1987, Houston, Texas, pp 150-158.

193. Onuaguluchi O and Panesar DK (2014) Hardened properties of concrete mixtures containing pre-coated crumb rubber and silica fume. *Journal of Cleaner Production* **82**: 125-131.

194. Onuaguluchi O, Panesar DK and Sain M (2014) Properties of nanofibre reinforced cement composites. *Construction and Building Materials* **63**: 119-124.

195. Opera NK, Watson KM and Lafave JM (1994) Effect of increased tensile strength and toughness on reinforcing bar bond behaviour. *Cement & Concrete Composites* **16**: 129-141.

196. Orangun CO, Jirsa JO and Breen JE (1975) *The Strength of Anchored Bars: A Reevaluation of Test Data on Development Length and Splices*. Center for Highway Research, The University of Texas at Austin, Texas, Research Report No. **154-3F**.

197. Orangun CO, Jirsa JO and Breen JE (1977) A reevaluation of test data on development length and splices. *ACI Journal* **74(3)**: 114-122.

198. Padmini AK, Ratmamurthy K and Mathews MS (2009) Influence of parent concrete on the properties of recycled aggregate concrete. *Construction and Building Materials* **23**: 829-836.

199. Park R and Paulay T (1975) Reinforced concrete structures, John Wiley & Sons, New York, USA.

200. Pay AC, Canbay E and Frosch RJ (2014) Bond strength of spliced fiber-reinforced polymer reinforcement. *ACI Structural Journal* **111(2)**: 257-266.

201. Perera SVTJ and Mutsuyoshi H (2013) Shear behaviour of reinforced high-strength concrete beams. *ACI Structural Journal* **110(1)**: 43-52.

202. Pillai SU and Menon D (2010) *Reinforced concrete design*, 3rd edn. Tata McGraw Hill, New Delhi, India.

203. Poon CS, Kou SC and Lam L (2002) Use of recycled aggregates in molded concrete bricks and blocks. Construction and Building Materials 16: 281-289.

204. Poon CS, Shui ZH, Lam L, Fok H and Kou SC (2004) Influence of moisture states of natural and recycled aggregates on the slump and compressive strength of concrete. *Cement and Concrete Research* **34**: 31-36.

205. Rahal K (2007) Mechanical properties of concrete with recycled coarse aggregate. *Building and Environment* **42**: 407-415.

206. Rakshvir M and Barai SV (2006) Studies on recycled aggregates-based concrete. *Waste Management and Research* **24**: 225-233.

207. Ramalingam S and Santhanam M (2012) Environmental exposure classifications for concrete construction - A relook. *The Indian Concrete Journal* **86(5)**: 18-28.

208. Ravindrarajah RS and Tam TC (1985) Properties of concrete made with crushed concrete as coarse aggregate. *Magazine of Concrete Research* **37(130)**: 29-38.

209. Regan PE, Kennedy-Reid IL, Pullen AD and Smith DA (2005) The influence of aggregate type on the shear resistance of reinforced concrete, *The Structural Engineer*, 6 Dec.: 27-32.

210. RILEM (1983) RILEM/CEB/FIP recommendations on reinforced concrete, Bond test for reinforcement steel: 2. Pullout test. Measuring the rib pattern of re-bars. CEB News No. **73**.

211. RILEM (1992) Recycling of demolished concrete masonry, RILEM Report 6 (Hansen TC (ed)), E & FN Spon, London.

212. RILEM (1994) Specifications for concrete with recycled aggregates. *Materials and Structures* **27**: 557-559.

213. Sagoe-Crentsil KK, Brown T and Taylor AH (2001) Performance of concrete made with commercially produced coarse recycled concrete aggregate. *Cement and Concrete Research* **31**: 707-712.

214. Seara-Paz S, Gonzalez-Fonteboa B, Eiras-Lopez J and Herrador MF (2014) Bond behaviour between steel reinforcement and recycled concrete. *Materials and Structures* **47**: 323-334.

215. Shayan A and Xu A (2003) Performance and properties of structural concrete made with recycled concrete aggregate. *ACI Materials Journal* **100(5)**: 371-380.

216. Singh MP, Singh SP and Singh AP (2014) Experimental study on the strength characteristics and water permeability of hybrid steel fibre reinforced concrete. *International Scholarly Research Notices (ISRN)* **2014**: 1-10.

217. Singh SP, Singh AP and Bajaj V (2010) Strength and flexural toughness of concrete reinforced with steel-polypropylene hybrid fibres. *Asian Journal of Civil Engineering (Building and Housing)* **11(4)**: 495-507.

218. Sivakumar A and Santhanam M (2007a) Mechanical properties of high strength concrete reinforced with metallic and non-metallic fibres. *Cement and Concrete Composites* **29**: 603-608.

219. Sivakumar A and Santhanam M (2007b) A qualitative study on the plastic shrinkage cracking in high strength hybrid fibre reinforced concrete. *Cement and Concrete Composites* **29**: 575-581.

220. Smith JT (2009) *Recycled concrete aggregate - A viable aggregate source for concrete pavements*. PhD Thesis. University of Waterloo, Waterloo, Ontario, Canada.

221. Tam VWY and Tam CM (2007) Parameters for recycled aggregate and their correlation. *Waste Management and Research* **21**: 879-886.

222. Tan C, Darwin D, Tholen ML and Zuo J (1996) *Splice Strength of Epoxy-Coated High Relative Rib Area Bars*. University of Kansas Center for Research, Lawrence, Kansas, SL Report **96-2.**

223. Tepfers R (1973) *A Theory of Bond Applied to Overlapping Tensile Reinforcement Splices for Deformed Bars*. PhD Thesis. Division of concrete structures, Chalmers University of Technology, Göteborg, Sweden, Publication **73(2)**.

224. Tepfers R (1979) Cracking of concrete cover along anchored deformed bars. *Magazine of Concrete Research* 31(106): 3-12.

225. Tholen ML and Darwin D (1996) *Effects of Deformation Properties on the Bond of Reinforcing Bars*. University of Kansas Center for Research, Lawrence, Kansas, SM Report No. **42**.

226. Thompson MA, Jirsa JO, Breen JE and Meinheit DF (1975) *The Behavior of Multiple Lap Splices in Wide Sections.* Center for Highway Research, University of Texas at Austin, Texas, Research Report No. **154-1**.

227. TIFAC (Technology Information, Forecasting and Assessment Council) (2001) *Utilisation of Waste from Construction Industry*, Environment and Habitat, Code No: TMS150, Department of Science and Technology, India. See http://www.tifac.org.in/index.php?option=com_content&view=article&id=710&Itemid=205 (accessed 29/01/2015).

228. Topcu IB and Guncan NF (1995) Using waste concrete as aggregate. *Cement and Concrete Research* **25(7)**: 1385-1390.

229. Topcu IB and Sengal S (2004) Properties of concretes produced with waste concrete aggregate. *Cement and Concrete Research* **34(8)**: 1307-1312.

230. Treece RA and Jirsa JO (1989) Bond strength of epoxy-coated reinforcing rars. *ACI Materials Journal* **86(2)**: 167-174.

231. Tu TY, Chen YY and Hwang CL (2006) Properties of HPC with recycled aggregates. *Cement and Concrete Research* **36**: 943-950.

232. Untrauer RE (1965) Discussion of development length for large high strength reinforcing bars. *ACI Journal* **62(9)**: 1153-1154.

233. Untrauer RE and Warren GE (1977) Stress development of tension steel in beams. *ACI Journal* **74(8)**: 368-372.

234. Welch GB and Patten BJF (1965) Bond strength of reinforcement affected by concrete sedimentation. *ACI Journal* **62(2)**: 251-263.

235. Wight JK and Macgregor JG (2012) *Reinforced concrete mechanics and design*, 6th edn. Pearson education, New Jersey, USA.

236. Xiao J, Li J, and Zhang C (2005) Mechanical properties of recycled aggregate concrete under uniaxial loading. *Cement and Concrete Research* **35**: 1187-1194.

237. Xiao J and Falkner H (2007) Bond behaviour between recycled aggregate concrete and steel rebars. *Construction and Building Materials* **21**: 395-401.

238. Yamato T (1998) Mechanical properties, drying shrinkage and resistance to freezing and thawing of concrete using recycled aggregate. Advances in Concrete Technology. In *Proceedings of the Fourth CANMET/ACI/JCI Conference, SP-179*, (Malhotra VM (ed)), American Concrete Institute, Farmington Hills, MI, USA, pp. 105-121.

239. Zekany AJ, Neumann S, Jirsa JO and Breen JE (1981) *The Influence of Shear on Lapped Splices in Reinforced Concrete.* Center for Transportation Research, Bureau of Engineering Research, University of Texas at Austin, Texas, Research Report **242-2**.

240. Zilveti A, Sooi TK, Klingner RE, Carrasquillo RL and Jirsa JO (1985) *Effect of Superplasticizers on the Bond Behaviour of Reinforcing Steel in Concrete Members.* Center for Transportation research, Bureau of Engineering Research, University of Texas at Austin, Texas, Research Report **383-2F**.

241. Zsutty T (1985) Empirical study of bar development behavior. *Journal of Structural Engineering*, *ASCE* **111(1)**: 205-219.

242. Zuo J and Darwin D (1998) *Bond Strength of High Relative Rib Area Reinforcing Bars.* University of Kansas Center for Research, Lawrence, Kansas, SM Report No. **46**.

243. Zuo J and Darwin D (2000) Splice strength of conventional and high relative rib area bars in normal and high-strength concrete. *ACI Structural Journal* 97(4): 630-641.

Appendix A

MOMENT-CURVATURE ANALYSIS OF THE BEAM SECTIONS

A typical moment curvature analysis calculation is presented for the design section located in the splice region. The section details relevant to the computations are shown in Figure A1. The experimental results of the reinforcing bar are tabulated in Table A1.

Beam ID: AS12R0-1

The material properties for the section are:

Concrete cylinder compressive strength, $f_c^{'}$ = 36.91 MPa

Elastics modulus for reinforcement bars, E_s = 2 x 10^5 MPa

Yield stress for reinforcing bars, f_y = 532 MPa

Ultimate tensile strength of steel, f_{su} = 616 MPa

Clear cover to the reinforcement bars, c = 15 mm

Diameter of the reinforcement bars, d_b = 12 mm

The idealised stress-strain curve for concrete has been adopted as per Figure A2. The idealised stress-strain curve for steel, shown in Figure A3 has been adopted for the reinforcing bars.

(1) CRACKING

Transform the composite section to all concrete section

E_c = modulus of elasticity of concrete

$$E_c = 4700\sqrt{f_c^{'}} = 4700\sqrt{36.91} = 28554.19\,MPa \qquad \text{(ACI 318-11)}$$

n = modular ratio

$$n = \frac{E_s}{E_c} = \frac{2\times10^5}{4700\sqrt{36.91}} = 7$$

A_b = Area of reinforcing steel

$$A_b = \frac{\pi \times d_b^2}{4} = 2 \times \left(\frac{\pi \times 12^2}{4} \right) = 226.19\, mm^2$$

Locate the neutral axis of the section

$$C_T = \frac{\left[(b\,h)\frac{h}{2} \right] + (n-1)\,A_b \left[h - \left(c + \frac{d_b}{2} \right) \right]}{(b\,h) + (n-1)\,A_b}$$

$$C_T = \frac{\left[(110 \times 225)\frac{225}{2} \right] + (7-1)\,226.19 \left[225 - \left(15 + \frac{12}{2} \right) \right]}{(110 \times 225) + [(7-1) \times 226.19]}$$

$$C_T = 117.26\, mm$$

Therefore $C_B = h - C_T = 225 - 117.26 = 107.74$ mm

Find the moment of inertia of the transformed section, I_{TR}

$$I_{TR} = \left[\frac{b\,h^3}{12} + b\,h \left(\frac{h}{2} - C_T \right)^2 \right] + I_{BAR} + (n-1)\,A_b \left(C_B - \left(c + \frac{d_b}{2} \right) \right)^2$$

I_{BAR} <<< and hence is neglected

$$I_{TR} = \left[\frac{110 \times 225^3}{12} + (110 \times 225) \left(\frac{225}{2} - 117.26 \right)^2 \right] + (7-1)\,226.19 \left(107.74 - \left(15 + \frac{12}{2} \right) \right)^2$$

$$I_{TR} = 1.152 \times 10^8\ mm^4$$

Modulus of rupture of concrete, $f_{cr} = 0.62 \times \lambda \times \sqrt{f_c'} = 0.62 \times 1 \times \sqrt{36.91} = 3.77\, MPa$

(ACI 318-11)

(For normal weight concrete, $\lambda = 1$)

Cracking moment, $M_{cr} = \frac{f_{cr}\, I_{TR}}{C_B} = \frac{3.77 \times 1.152 \times 10^8}{107.74} = 4.03 \times 10^6\ Nmm$

Curvature, $\varphi_{cr} = \frac{M_{cr}}{E_c\, I_{TR}} = \frac{4.03 \times 10^6}{4700\sqrt{36.91} \times 1.152 \times 10^8} = 1.225 \times 10^{-6}\ mm^{-1}$

Stress in concrete, $\varepsilon_{cm} = \varphi\, kd = 1.225 \times 10^{-6} \times 117.26 = 0.00014$

From strain compatibility

$$\frac{\varepsilon_{cm}}{kd} = \frac{\varepsilon_s}{d - kd}$$

Strain in reinforcement bars,

$$\varepsilon_s = \varepsilon_{cm}\left[\frac{d}{kd} - 1\right] = 0.00014\left[\frac{204}{117.26} - 1\right] = 0.104 \times 10^{-3}$$

M_{cr} = 4.03 kNm, φ_{cr} = 1.225 x 10^{-9} m^{-1}, ε_s = 0.104 x 10^{-3}

(2) MAXIMUM CONCRETE STRAIN, $\varepsilon_{cm} = 0.0005 \quad (0 < \varepsilon_{cm} < \varepsilon_o = 0.002)$

$$\alpha = \frac{\varepsilon_{cm}}{\varepsilon_o} = \frac{0.0005}{0.002} = 0.25$$

Stress block coefficients K_1, K_2 and K_3 suggested by Kaar *et al*. (1978)

For $\quad 0 \le \varepsilon_{cm} \le \varepsilon_o$

$$K_1 = \alpha - \frac{1}{3}\alpha^2$$

$$K_2 = \frac{\frac{1}{3} - \frac{1}{12}\alpha}{1 - \frac{1}{3}\alpha}$$

$$K_3 = 1.0$$

Therefore the stress block coefficients are K_1 = 0.229, K_2 = 0.3409, K_3 = 1.0

From strain compatibility

$$\frac{\varepsilon_{cm}}{kd} = \frac{\varepsilon_s}{d - kd}$$

Strain in reinforcement bars, $\varepsilon_s = 0.0005\left[\frac{204}{kd} - 1\right]$

Tensile strain in concrete corresponding to modulus of rupture,

$$\varepsilon_r = \frac{f_{cr}}{E_c} = \frac{3.77}{4700\sqrt{36.91}} = 1.32 \times 10^{-4}$$

From similar triangles,

$$\frac{\varepsilon_{cm}}{kd} = \frac{\varepsilon_r}{x}$$

$$x = \left(\frac{1.32 \times 10^{-4}}{0.0005}\right) kd$$

$$x = 0.264\, kd$$

By a process of trial and error, the neutral axis depth which satisfies the equilibrium conditions is estimated. The ultimate moment of resistance of the section and the corresponding curvatures are then worked out.

Trail 1

Try kd = 60 mm

$$x = 0.264\, kd = 0.264 \times 60 = 15.84\, mm$$

$$\varepsilon_s = 0.0005\left[\frac{204}{kd} - 1\right] = 0.0005\left[\frac{204}{60} - 1\right] = 1.2 \times 10^{-3}$$

Stress in reinforcement bars, $f_s = \varepsilon_s\, E_s = 1.2 \times 10^{-3} \times 2 \times 10^5 = 240\, MPa$

Force in concrete in compression,

$$C_c = K_1\, K_3\, f_c^{'}\, b\, kd = 0.229 \times 1 \times 36.91 \times 110 \times 60 = 55.77 \times 10^3\ N$$

Force in concrete in tension,

$$T_c = \frac{1}{2} f_{cr}\, b\, x = 0.5 \times 3.77 \times 110 \times 15.84 = 3.28 \times 10^3\ N$$

Force in steel, $T_s = A_b\, f_s = 226.19 \times 240 = 54.29 \times 10^3\ N$

Total force in compression, $C_c \neq$ Total force in tension, $T = T_c + T_s$

$55.77 \times 10^3 \neq 57.57 \times 10^3$

Revise the depth of neutral axis

Trail 2

Try kd = 60.83 mm

$$x = 0.264\,kd = 0.264 \times 60.83 = 116.06\,mm$$

$$\varepsilon_s = 0.0005\left[\frac{204}{kd} - 1\right] = 0.0005\left[\frac{204}{60.83} - 1\right] = 1.177 \times 10^{-3}$$

Stress in reinforcement bars, $f_s = \varepsilon_s\, E_s = 1.177 \times 10^{-3} \times 2 \times 10^5 = 235.4\,MPa$

Force in concrete in compression,

$$C_c = K_1\, K_3\, f_c^{'}\, b\, kd = 0.229 \times 1 \times 36.91 \times 110 \times 60.83 = 56.56 \times 10^3\ N$$

Force in concrete in tension,

$$T_c = \frac{1}{2} f_{cr}\, b\, x = 0.5 \times 3.77 \times 110 \times 16.06 = 3.33 \times 10^3\ N$$

Force in steel, $T_s = A_b\, f_s = 226.19 \times 235.4 = 53.24 \times 10^3\ N$

Total force in compression, C_c = Total force in tension, $T = T_c + T_s$

$56.56 \times 10^3 = 56.57 \times 10^3$

Selected depth of neutral axis is appropriate

Ultimate moment of resistance of the section can be evaluated using the following equation

$$M = C_c\left(d - K_2\, kd\right) - T_c\left(d - kd - \frac{2\,x}{3}\right)$$

$$M = \left[56.56 \times 10^3\left(204 - 0.3409 \times 60.83\right)\right] - \left[3.33 \times 10^3\left(204 - 60.83 - \frac{2 \times 16.06}{3}\right)\right]$$

$M = 9.92 \times 10^6$ Nmm

Curvature, $\varphi = \frac{\varepsilon_{cm}}{kd} = \frac{0.0005}{60.83} = 8.22 \times 10^{-6}\ mm^{-1}$

$M_{0.0005} = 9.92$ kNm, $\varphi_{0.0005} = 8.22 \times 10^{-9}\ m^{-1}$, $\varepsilon_s = 1.177 \times 10^{-3}$

(3) YIELD POINT

Contribution of concrete in tension is small and can be neglected.

$$\varepsilon_s = \varepsilon_y = \frac{f_y}{E_s} = \frac{532}{2\times10^5} = 2.66\times10^{-3}$$

From similar triangles

$$\frac{\varepsilon_{cm}}{kd} = \frac{\varepsilon_s}{d-kd}$$

$$\varepsilon_{cm} = \left(\frac{kd}{d-kd}\right)\varepsilon_s$$

By a process of trial and error, the neutral axis depth which satisfies the equilibrium conditions is estimated.

Trail 1

Try kd = 57 mm

$$\varepsilon_{cm} = \left(\frac{57}{204-57}\right)\times 2.66\times10^{-3} = 1.031\times10^{-3}$$

$$\alpha = \frac{\varepsilon_{cm}}{\varepsilon_o} = \frac{1.031\times10^{-3}}{0.002} = 0.516$$

Stress block coefficients K_1, K_2 and K_3 suggested by Kaar *et al*. (1978)

For $0 \le \varepsilon_{cm} \le \varepsilon_o$

$$K_1 = \alpha - \frac{1}{3}\alpha^2$$

$$K_2 = \frac{\frac{1}{3} - \frac{1}{12}\alpha}{1-\frac{1}{3}\alpha}$$

$$K_3 = 1.0$$

Therefore the stress block coefficients are K_1 = 0.4271, K_2 = 0.3506, K_3 = 1.0

Force in concrete in compression,

$$C_c = K_1 K_3 f_c^{'} b\, kd = 0.4271 \times 1 \times 36.91 \times 110 \times 57 = 98.84 \times 10^3 \; N$$

Force in steel, $T_s = A_b f_y = 226.19 \times 532 = 120.33 \times 10^3 \; N$

Total force in compression, $C_c \neq$ Total force in tension, $T = T_c + T_s$

$98.84 \times 10^3 \neq 120.33 \times 10^3$

Revise the depth of neutral axis

Trail 2

Try kd = 62.65 mm

$$\varepsilon_{cm} = \left(\frac{62.65}{204 - 62.65} \right) \times 2.66 \times 10^{-3} = 1.179 \times 10^{-3}$$

$$\alpha = \frac{\varepsilon_{cm}}{\varepsilon_o} = \frac{1.179 \times 10^{-3}}{0.002} = 0.5895$$

Therefore the stress block coefficients are $K_1 = 0.473$, $K_2 = 0.354$, $K_3 = 1.0$

Force in concrete in compression,

$$C_c = K_1 K_3 f_c^{'} b\, kd = 0.473 \times 1 \times 36.91 \times 110 \times 62.65 = 120.31 \times 10^3 \; N$$

Force in steel, $T_s = A_b f_y = 226.19 \times 532 = 120.33 \times 10^3 \; N$

Total force in compression, C_c = Total force in tension, $T = T_c + T_s$

$120.31 \times 10^3 \neq 120.33 \times 10^3$

Selected depth of neutral axis is appropriate

Ultimate moment of resistance of the section can be evaluated using the following equation

$$M = C_c \left(d - K_2 \, kd \right)$$

$$M = 120.31 \times 10^3 \left(204 - 0.354 \times 62.65 \right)$$

$M = 21.88 \times 10^6$ Nmm

Curvature, $\varphi = \frac{\varepsilon_{cm}}{kd} = \frac{1.179 \times 10^{-3}}{62.65} = 18.82 \times 10^{-6}\ mm^{-1}$

M_{yield} = 21.88 kNm, φ_{yield} = 18.82 x 10^{-9} m^{-1}, ε_s = 2.66 x 10^{-3}

(4) MAXIMUM CONCRETE STRAIN, $\varepsilon_{cm} = 0.002$

From equilibrium condition

Total force in compression, C_c = Total force in tension, T_s

$$K_1 K_3 f_c^{'} b\, kd = A_b f_s$$

$$f_s = \frac{K_1 K_3 f_c^{'} b\, kd}{A_b}$$

From similar triangles

$$\frac{kd}{\varepsilon_{cm}} = \frac{d}{\varepsilon_{cm} + \varepsilon_s}$$

$$kd = \left(\frac{\varepsilon_{cm}}{\varepsilon_{cm} + \varepsilon_s} \right) d$$

Hence, $f_s = \frac{K_1 K_3 f_c^{'}}{A_b} \left(\frac{\varepsilon_{cm}}{\varepsilon_{cm} + \varepsilon_s} \right) d$

or, $f_s = \frac{K_1 K_3 f_c^{'}}{\rho} \left(\frac{\varepsilon_{cm}}{\varepsilon_{cm} + \varepsilon_s} \right)$ (Equation A1)

where $\rho = \frac{A_b}{b\, d}$ is defined as the reinforcement ratio.

Equation A1 satisfies strain compatibility and equilibrium conditions. If the above relation for f_s in which the variable ε_s for given ε_{cm} is plotted over the idealised stress-strain plot (Figure A3) for the reinforcing bars, then the intersection will yield the unknown ε_s and thus f_s. Then the neutral axis depth *kd*, can be evaluated from the equation:

$$A_b f_s = K_1 K_3 f_c^{'} b\, kd$$

Ultimate moment of resistance *M*, can be calculated from the equation:

$$M = A_b f_s (d - K_2\, kd)$$

Curvature φ, as usual, can be found from the equation: $\varphi = \frac{\varepsilon_{cm}}{kd}$

For the present case, $\rho = \frac{A_b}{b\,d} = \frac{226.19}{110 \times 204} = 10.08 \times 10^{-3}$

For maximum concrete strain, $\varepsilon_{cm} = 0.002$

$$\alpha = \frac{\varepsilon_{cm}}{\varepsilon_o} = \frac{0.002}{0.002} = 1$$

Therefore the stress block coefficients are K_1 = 0.667, K_2 = 0.375, K_3 = 1.0
Hence Equation A1 reduces to

$$f_s = \frac{0.667 \times 1 \times 36.91}{10.08 \times 10^{-3}} \left(\frac{0.002}{0.002 + \varepsilon_s} \right)$$

$$f_s = \frac{4.8847}{0.002 + \varepsilon_s} \qquad \text{(Equation A2)}$$

In Figure A4, Equation A2 is superimposed graphically on the idealised strain curve for the reinforcement bar. Figure A4 indicates that ε_s lies in the strain hardening portion and the value of ε_s for the given maximum concrete strain $(\varepsilon_{cm} = 0.002)$ as determined from the intersection of the plots, is equal to 7.183 x 10^{-3} and the corresponding stress f_s is equal to 532 MPa.

Hence, $kd = \frac{A_b\, f_s}{K_1\, K_3\, f_c^{'}\, b} = \frac{226.19 \times 532}{0.667 \times 1 \times 36.91 \times 110} = 44.43\, mm$

$$M = A_b\, f_s\, (d - K_2\, kd) = 226.19 \times 532\, [204 - (0.375 \times 44.43)] = 22.54 \times 10^6\ Nmm$$

$$\varphi = \frac{\varepsilon_{cm}}{kd} = \frac{0.002}{44.43} = 45.01 \times 10^{-6}\ mm^{-1}$$

$M_{0.002}$ = 22.54 kNm, $\varphi_{0.002}$ = 45.01 x 10^{-9} m^{-1}, ε_s = 7.183 x 10^{-3}

(5) MAXIMUM CONCRETE STRAIN, $\varepsilon_{cm} = 0.003$

Stress block coefficients K_1, K_2 and K_3 suggested by Kaar *et al*. (1978)

For $\varepsilon_{cm} > \varepsilon_o$

$$K_1 = \frac{1}{\varepsilon_{cm}}\left[\varepsilon_{cm} - \frac{\varepsilon_o}{3} - \frac{Z}{2}\left(\varepsilon_{cm} - \varepsilon_o\right)^2\right]$$

$$K_2 = 1 - \frac{1}{C_5}\left[\frac{5}{12}C_1\,\varepsilon_o + C_4\left(C_1 + \frac{C_2}{2\,\varepsilon_{cm}}\right) + C_3\left(C_1 + \frac{C_2}{3\,\varepsilon_{cm}}\right)\right]$$

$$K_3 = 1$$

where $C_1 = \dfrac{\varepsilon_o}{\varepsilon_{cm}}$

$$C_2 = \varepsilon_{cm} - \varepsilon_o$$

$$C_3 = \frac{1}{2}Z\,C_2^2$$

$$C_4 = C_2 - Z\,C_2^2$$

$$C_5 = \varepsilon_{cm} - \frac{1}{3}\varepsilon_o - C_3$$

$$Z = 150$$

Therefore the stress block coefficients are K_1 = 0.753, K_2 = 0.415, K_3 = 1.0

Hence Equation A1 reduces to

$$f_s = \frac{0.753 \times 1 \times 36.91}{10.08 \times 10^{-3}}\left(\frac{0.003}{0.003 + \varepsilon_s}\right)$$

$$f_s = \frac{8.27}{0.003 + \varepsilon_s} \qquad \text{(Equation A3)}$$

In Figure A4, Equation A3 is superimposed graphically on the idealised strain curve for the reinforcement bar. Figure A4 indicates that ε_s lies in the strain hardening portion and the value of ε_s for the given maximum concrete strain $(\varepsilon_{cm} = 0.003)$ as determined from the intersection of the plots, is equal to 12.55 x 10^{-3} and the corresponding stress f_s is equal to 532 MPa.

Hence, $kd = \dfrac{A_b\,f_s}{K_1\,K_3\,f_c^{'}\,b} = \dfrac{226.19 \times 532}{0.753 \times 1 \times 36.91 \times 110} = 39.36\,mm$

$$M = A_b\, f_s\, (d - K_2\, kd) = 226.19 \times 532\,[204 - (0.415 \times 39.36)] = 22.58 \times 10^6\ Nmm$$

$$\varphi = \frac{\varepsilon_{cm}}{kd} = \frac{0.003}{39.36} = 76.22 \times 10^{-6}\ mm^{-1}$$

$M_{0.003}$ = 22.58 kNm, $\varphi_{0.003}$ = 76.22 x 10^{-9} m^{-1}, ε_s = 12.55 x 10^{-3}

The moments, curvatures and the strains at the specified points are summarised in Table A2. Graphical representation of moment-curvature and moment-strain are illustrated in Figures A5 and A6 respectively. From Figure A6, for the known experimental moment, the corresponding steel strain is calculated. The stress in steel is then calculated by multiplying the steel strain with the modulus of elasticity of the steel.

Table A1 Experimental results of the reinforcing bars

Parameter	Unit	Bar Diameter	
		12 mm	**20 mm**
E_s	MPa	2 x 10^5	2 x 10^5
E_{sh}	MPa	2014.38	1692.97
f_y	MPa	532	588
f_{su}	MPa	616	691
ε_y	mm/mm	0.00295	0.00273
ε_{sh}	mm/mm	0.026	0.02474
ε_{su}	mm/mm	0.0677	0.08558

Table A2 Moments, curvatures and strains for the reinforced concrete section

Sl. No.	**Specified point (In terms of maximum concrete strain ε_{cm}, or otherwise)**	**Moment, M (kNm)**	**Curvature, φ (m^{-1})**	**Strain in steel, ε_s (mm/mm)**
1	First crack	4.03	1.225 x 10^{-9}	0.104 x 10^{-3}
2	$\varepsilon_{cm} = 0.0005$	9.92	8.22 x 10^{-9}	1.177 x 10^{-3}
3	Yield	21.88	18.82 x 10^{-9}	2.66 x x10^{-3}
4	$\varepsilon_{cm} = 0.002$	22.54	45.01 x 10^{-9}	7.183 x 10^{-3}
5	$\varepsilon_{cm} = 0.003$	22.58	76.22 x 10^{-9}	12.55 x 10^{-3}

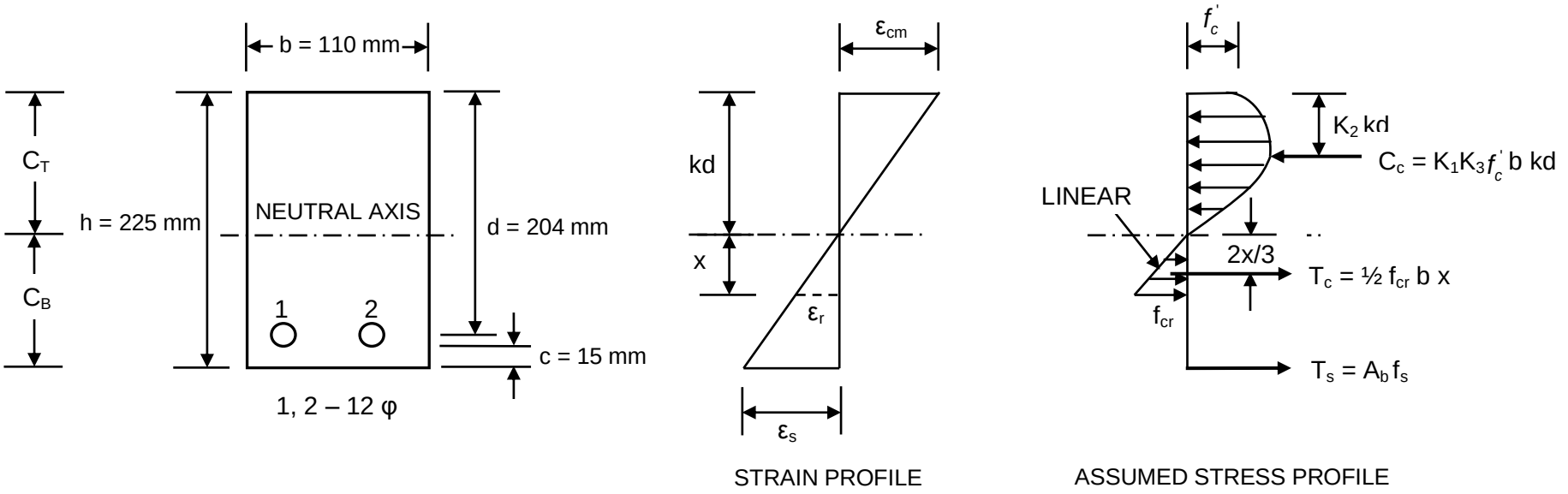

Figure A1 Reinforced concrete section

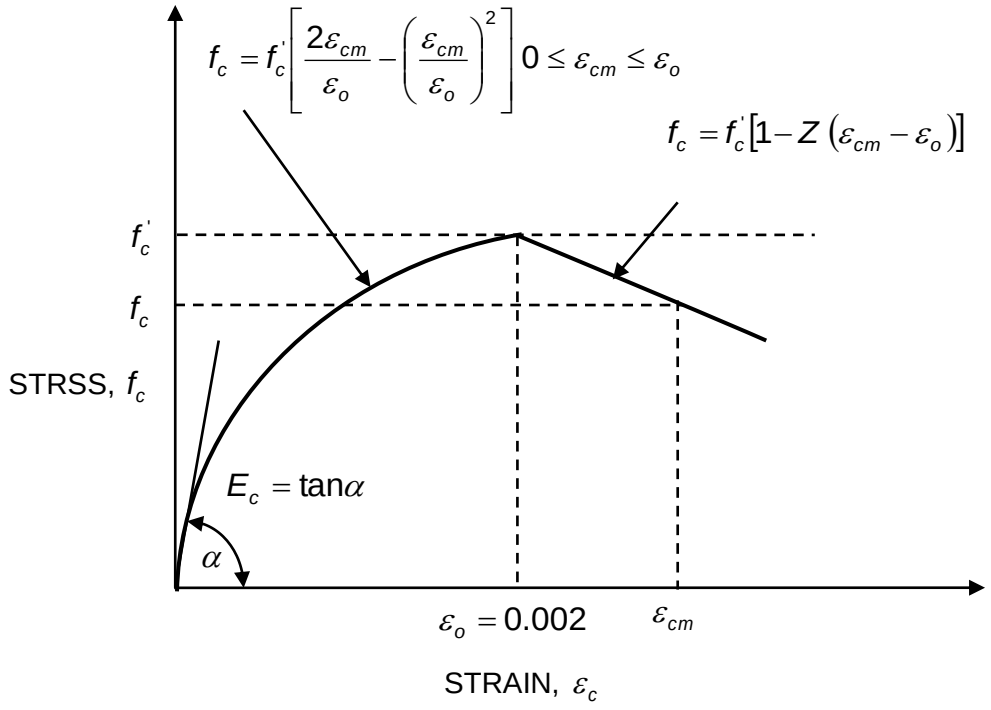

Figure A2 Idealised stress-strain curve for concrete (Hognestad, 1951)

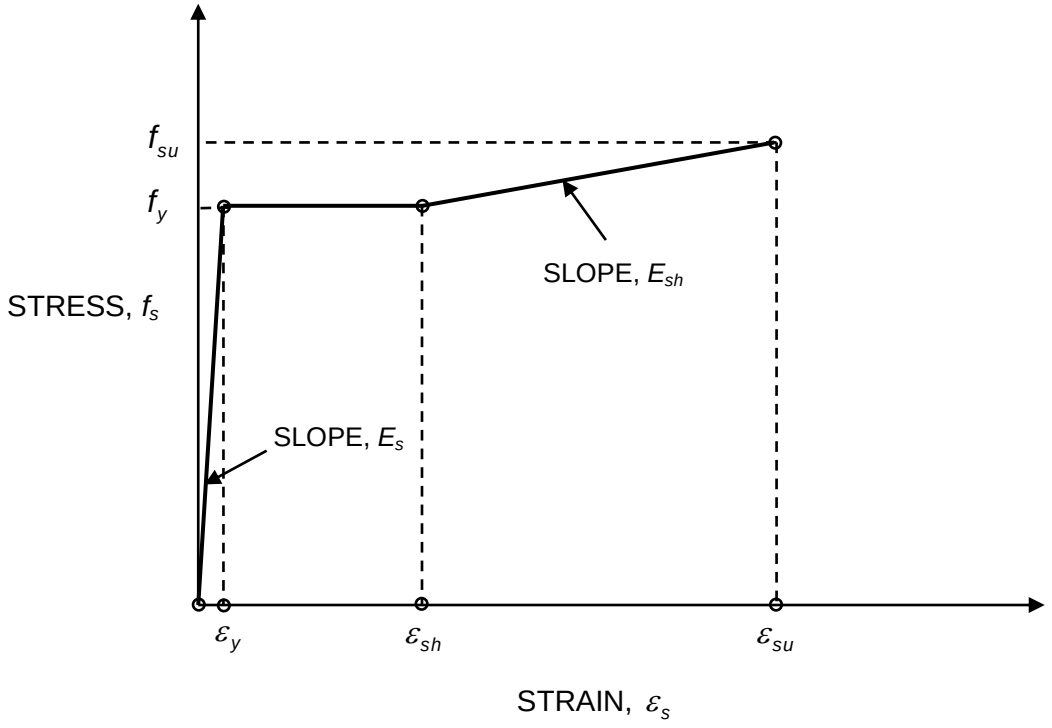

Figure A3 Idealised stress-strain curve for steel (Park and Paulay, 1975)

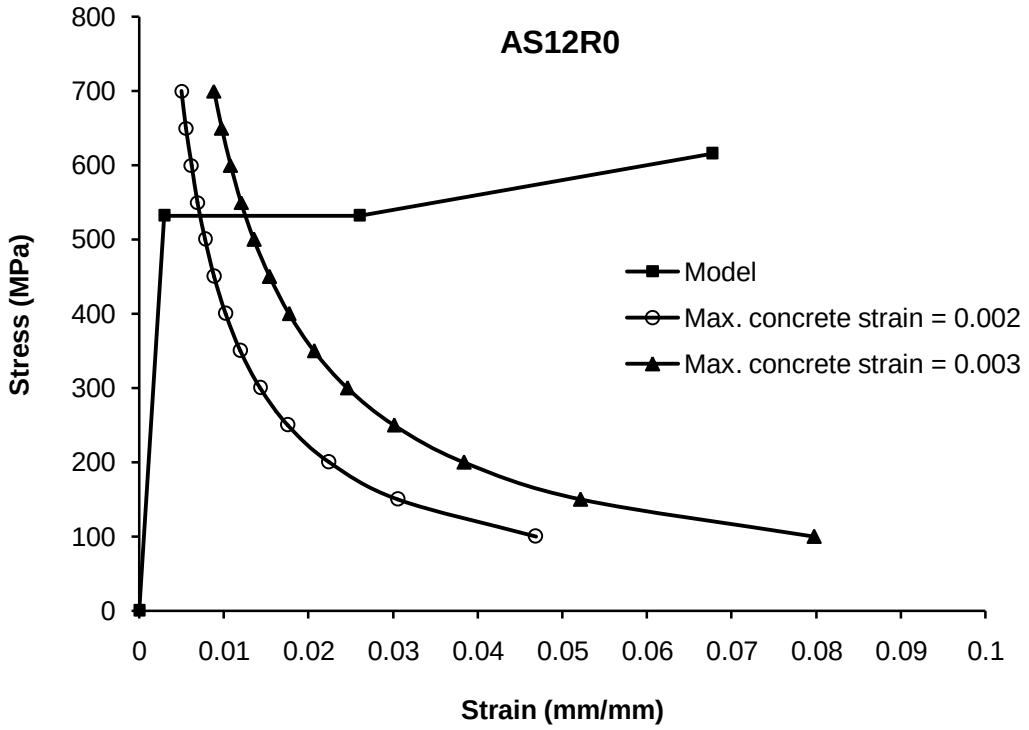

Figure A4 Stress-strain plots for the reinforcing bar

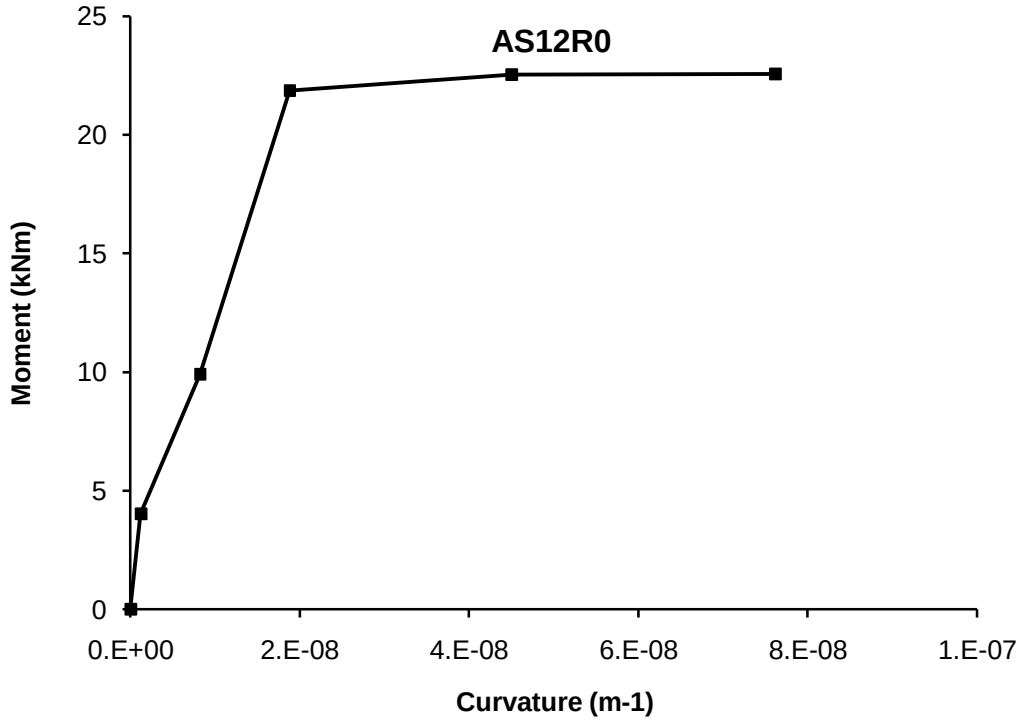

Figure A5 Moment-curvature plot for the reinforced concrete section

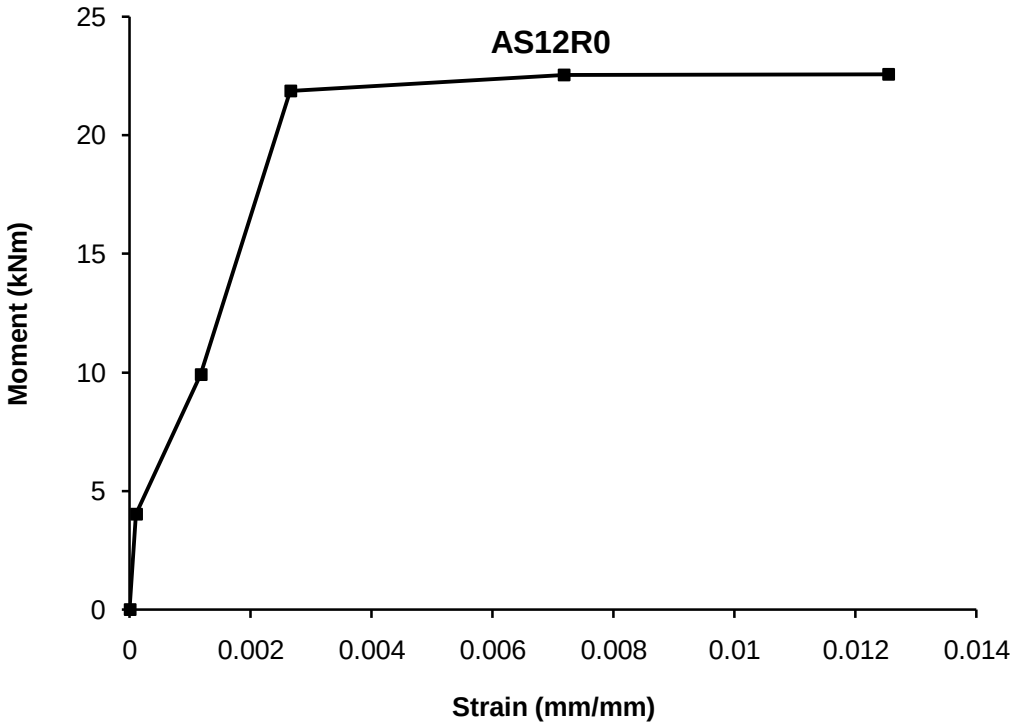

Figure A6 Moment-strain plot for the reinforced concrete section

PUBLICATIONS

A. JOURNALS

1. Prince MJR and Singh B (2013) Bond behaviour of deformed steel bars embedded in recycled aggregate concrete. ***Construction and Building Materials*** **49**: 852-862.

2. Prince MJR and Singh B (2014) Bond behaviour between recycled aggregate concrete and deformed steel bars. ***Materials and Structures*** **47**: 503-516.

3. Prince MJR and Singh B (2014) Investigation of bond behaviour between recycled aggregate concrete and deformed steel bars. ***Structural Concrete*** **15(2)**: 154-168.

4. Prince MJR and Singh B (2014) Bond behaviour between recycled aggregate concrete and deformed steel bars. ***Journal of Structural Engineering****, S.E.R.C.* **41(2)**: 132-143.

5. Prince MJR and Singh B (2014) Bond strength of deformed steel bars in high-strength recycled aggregate concrete. ***Materials and Structures*** DOI: 10.1617/s11527-014-0452-y.

6. Prince MJR and Singh B (2015) Bond behaviour of normal- and high-strength recycled aggregate concrete. ***Structural Concrete*** **16(1)**: 56-70.

7. Prince MJR and Singh B. Pullout behaviour of deformed steel bars in high-strength recycled aggregate concrete. ***ICE Construction Materials*** DOI: 10.1680/coma.14.00026.

B. DISCUSSIONS

1. Prince MJR and Singh B (2013) Behaviour of lap-spliced plain steel bars. Discussion on paper by M. Nazmul Hassan and Lisa R. Feldman. ***ACI Structural Journal*** **110(1)**: 157-160.

C. CONFERENCES

1. Prince MJR and Singh B (2013) Bond strength evaluation of recycled aggregate concrete using a pullout test. In *Proceedings of the International UKIERI Concrete Congress, Innovations in Concrete Construction,* 5-8 March 2013, NIT Jalandhar, India, pp 1821-1841.